University of Salerno

Department of Chemistry and Biology "Adolfo Zambelli"

PhD Doctoral Program in Chemistry

XIV CYCLE NEW SERIES

PhD Thesis

"New Insights into Peptoids' Chemistry: Synthesis, Characterization and Properties"

Tutor:
Prof. *Francesco De Riccardis*

Co-Tutor:
Prof. *Irene Izzo*

Coordinator:
Prof. *Gaetano Guerra*

PhD Student:
Alessandra Meli

Matr. 8880700203

ACADEMIC YEAR 2014-2015

TABLE OF CONTENTS

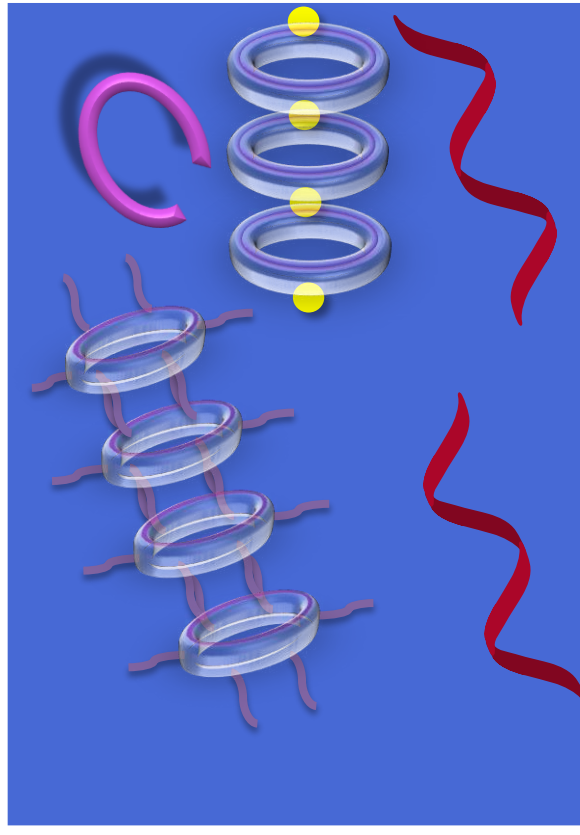

CHAPTER 1

Introduction

1

1.1 THE ADVENT OF PEPTOIDS

The concept of peptidomimetics deeps its roots mainly in the work of Ariëns between the 70s and 80s.[1] He was intrigued by the possibility to translate bioactive peptides into correspondingly active small non-peptide compounds.

Peptides play a central role in biological systems; nevertheless, they suffer from metabolic lability and systemic transport problems. Ariëns foresaw that bridging the gap between peptides and non-peptides could have opened new and interesting outlooks in the field of drug design.[1a] Indeed, he suggested some perspectives in design of compounds mimicking the biological activity of natural peptides but structurally diverse from them, and he designated such analogues with the term peptoids.

This definition was then borrowed by Horwell *et al.* for describing the analogues of cholecystokinin-(30-33) as probes for central nervous system cholecystokinin receptors, so it was still referring to a vast class of compounds biologically resembling natural peptides.

It was just in 1992 that the term peptoids gained a narrow sense, when Bartlett and co-workers addressed it to a specific family of oligomers of *N*-substituted glycines.[2] They are based on an unnatural repetitive unit that, respect to the parent peptide, swaps the amide hydrogen atom for the α-carbon side chain, making the peptoid backbone achiral (**Figure 1.1**).

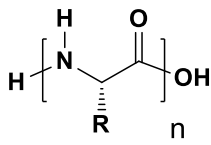

1.1

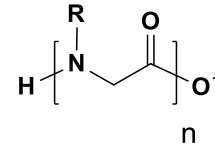

1.2

Figure 1. 1. Generic structures of peptide (**1.1**) and peptoid (**1.2**).

Even though peptides and peptoids are structural isomers, the echo of such difference is impressive.

Being related to peptides, they are compatible with biological environments, but the abiotic character of these molecules can confer protection from proteolytic degradation and allow high cellular uptake, offering a wide variety of biological applications.

Peptoids can exist in a much bigger conformational state with respect to peptides, since they can adopt low energy conformations with either *cis* and *trans* amide bonds, as depicted in the Ramachandran-type plots.[2] Furthermore, the lack of amide hydrogens removes intramolecular hydrogen bond networks and the stabilization of secondary structures as in peptides.[2] All those peculiar features make the peptoid main chain extremely flexible.

Another important attribute to take into account for the development of new structures alternative to natural compounds is the synthetic route for preparing them. The synthesis should be easy, scalable, automatable and versatile, allowing the introduction of a wide variety of functional groups to build large libraries of analogues to test. Peptoids' chemistry offers this advantage as well since their first introduction.

Bartlett and co-workers first prepared the monomer in solution, then achieved the fast oligomerization on solid-phase.[2] In the same year, Zuckermann *et al.* introduced a completely automated solid-phase method for the synthesis of peptoids, general

and versatile to incorporate different side-chain substituents.[3] This relies on the two-step-assembly of the monomer unit directly on solid-phase from two submonomers; bromoacetic acid and the desired primary amine (**Scheme 1.1**). Iterating the cycles of coupling/amination, the peptoid chain grows on solid-phase, to be detached when the desired length is reached.

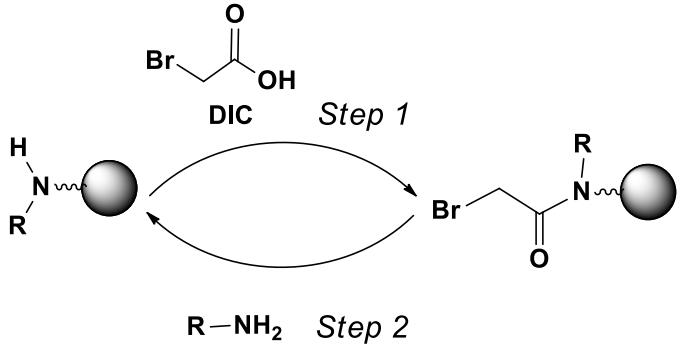

Scheme 1. 1. General synthetic scheme for the solid-phase assembly of peptoids.

The introduction of submonomer solid-phase peptoids synthesis allowed for the rapid diffusion and deep investigation of this class of peptides mimics. After more than twenty years since their development, peptoids are still a hot topic in many fields. With such versatile and efficient tool in our hands, we can count on exciting leads for drug design as well as for engineering biocompatible materials.

1.2 CONFORMATIONAL CONTROL

One of the very first properties of the newborn peptoids studied by researchers was their folding into secondary structures.

Due to the flexibility of the backbone, peptoids are not structurally well organized and defined. The advantage is that they can be forced into helical, loop and turn motifs in a controlled fashion.

The proper choice of the side chains to incorporate into the peptoid sequence restricts the backbone conformations and achieves control on the secondary structure.

For example, molecular mechanics calculations on the octamer of (S)-*N*-(1-phenylethyl) glycine (**1.3**, **Figure 1.2**) suggested that the introduction of bulky chiral side chains causes steric interactions and charge-charge repulsion with backbone carbonyls, which are the driving force for peptoid helical secondary structure.[4] As polyproline type I helix, peptoid helix has all *cis*-amide bonds, a right-handed screw sense, and three residues per turn (**Figure 1.2**).[4]

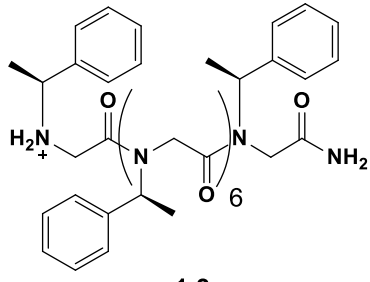

1.3

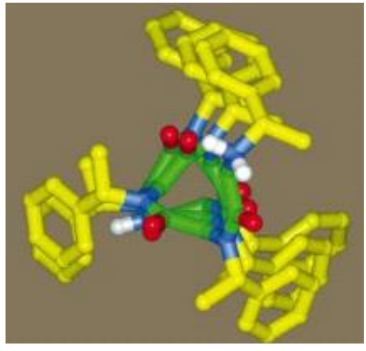

Figure 1. 2. Octamer of (S)-*N*-(1-phenylethyl) glycine (**1.3**) and its molecular mechanic model showing the predicted helical conformation. The *N* terminus is free and the *C* terminus is amidated.

Later on, studies on several peptoid oligomers containing chemically diverse side chains, performed by circular dichroism (CD) spectroscopy, NMR spectroscopy, and X-ray crystallography, attempted to highlight the rules of predictability for helix conformations. The results of those efforts point out the importance of different parameters, such as; the content of aromatic and aliphatic residues,[5] the peptoidic chain length,[5a-c] the chirality of the side chains,[5a, 5b, 5d] and the electronic and steric features of the groups appended to the backbone.[6]

When all chiral, aromatic side chains are present in the peptoid, this can stabilize the helical structure even as short as a pentamer.[5a, 5b] Hexameric oligomers, on the other hand, require at least 50% chiral, aromatic residues for the formation of the helix,[5c] but this percentage is intended to fall with the increasing of chain length beyond 12-15 residues.[5a, 5c, 5d] Surprisingly, a *N*-(1-cyclohexylethyl) glycine pentamer showed a helix with *cis* amide bonds at solid state, as revealed by X-ray crystallography.[5d] However, its weak CD spectrum indicated a less ordered and stable helical fold, in agreement with the results previously reported.

The use of chiral side chains can afford a preferred handedness in peptoid helices, and the corresponding enantiomers can invert the screw-sense.[5a, 5b, 5d] Nevertheless, the content of 33% achiral residues in a dodecamer peptoid did not disrupt the helical profile; hence, the chirality can be propagated even in the presence of achiral units.[5a]

In addition, carbonyl oxygen-carbonyl amide and carbonyl-aromatic n→π* interactions are hypothesized to play a role in peptoids folding promoting the isomerization between the *cis* and *trans* geometry of the amide bonds.[6a] The first one requires an orbital overlap that can be satisfied just in *trans*-amide, whereas the other one stabilizes the *cis*-amide (**A** and **B, Figure 1.3**).

It has been demonstrated that a careful selection of the side chains can tune the n→π* interactions and so the geometry of the amide bonds. ^{1}H-NMR examination on a series of compounds incorporating different *N*-side chains and various functional groups-capped *C*-terminal carbonyl proved that $n\rightarrow\pi^{*}_{Am}$ interactions can be enhanced by *N*-cyclohexyl chains and *C*-terminal methyl esters.[6a]

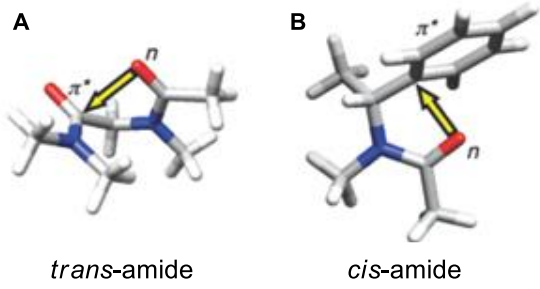

Figure 1. 3. Three-dimensional representations of $n \rightarrow \pi^*_{Am}$ (**A**) and $n \rightarrow \pi^*_{Ar}$ interactions (**B**).

The strength of such interaction can stabilize and increase the content of *trans*-amide rotamers in solution. Likewise, *N*-aryl side chains exerts control over peptoid bond geometry and enforce the *trans* conformation due to repulsive interactions between the aromatic ring and the amide oxygen in the *cis* geometry.[6b, 6c] Computational studies on *N*-(phenyl) glycine hexamer (**1.4**, **Figure 1.4**) showed the formation of extended helices, containing repeating *trans* amide bonds and resembling the polyproline type II helix.[6b]

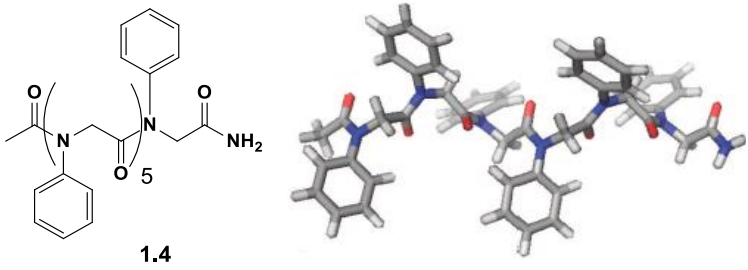

Figure 1. 4. Hexamer of *N*-(phenyl) glycine (**1.4**) and its molecular mechanic model showing the predicted helical conformation.

Amide rotamer equilibria can be influenced and shifted towards *trans* conformations also by *N*-hydroxy[7] and *N*-alkoxy[8] side chains. The ability to induce a high extent of order derives from the oxygen atom that, directly bound to the amide nitrogen, exerts steric and stereoelectronic effects directing the side chain away from the amide oxygen.

Further studies on the relationship between monomer sequence and secondary structures led to the discovery of an interesting new three-dimensional architecture, the threated loop (**Figure 1.5**).[9] The nonamer of *N*-(S)-(1-phenylethyl) glycine, unlike its analogues ranging from 6- to 15-mer that displayed the expected helical conformation, showed an unusual folded unit triggered by multiple intramolecular hydrogen bonds between the terminal NH_2^+ group and the backbone carbonyl groups of residues 5, 7 and 9. The bonding with the ninth unit, together with the interaction between the capping amide group and the carbonyl from residue 2, are fundamental to close the loop. The non-covalent interactions inducing the threated loop have a precise disposition that explains why such conformation is unique and peculiar for the nonamer peptoid.

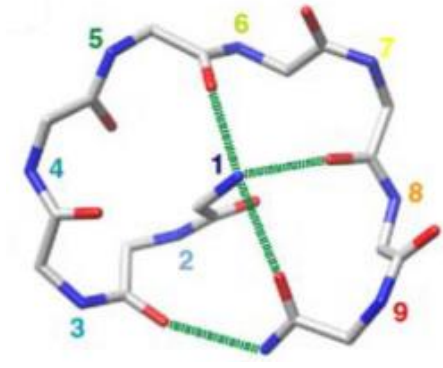

Figure 1. 5. Solution structure of the nonamer of N-(S)-(1-phenylethyl) glycine showing the peptoid threated loop. The dashed green lines denote hydrogen-bonding interactions.

The design of novel peptoid structural motifs always requires innovative tools since, unlike peptides, the peptoid backbone lacks almost completely of hydrogen-bonding donors, fundamental in the stabilization of several secondary structures.

Cyclization of linear peptoids is also an effective strategy to increase structural rigidity and so their conformational order.[10]

It has been recently demonstrated that linear peptoids of different chain length and composition, incorporating exclusively *N*-alkyl side chains, can efficiently undergo head-to-tail condensation reaction in the presence of the common coupling agents, to form macrocyclic compounds ranging from 4- to 20-mer.[10] As for peptide chemistry, this is a tool to further enforce peptoids biostability, resulting more resistant to proteolysis lacking of free *N* and *C* termini.[11] Cyclopeptoids showed higher conformational order with respect to their linear counterparts; hence, the macrocyclization reaction resulted to be a covalent constrain that, in the hexamer and octamer macrocycles (**A** and **B**, **Figure 1.6**), led to a folding resembling peptide β-turn, as revealed by their crystal structures. This result is of outmost importance in the development of bioactive peptidomimetics. Macrocyclic structures are indeed recurring in many natural and pharmaceutical compounds and cyclic peptides have improved stability and pharmacokinetics compared to their linear precursors.[12] However, peptides macrocyclization reaction may proceed in low yield, to due the preferred *trans* geometry of the peptide bond.[13] On the other hand, peptoids can easily interconvert between the *cis* and *trans* conformations of the amide bond, being susceptible to turn structures and assisting smoothly rapid macrocyclization. Indeed, as showed in **Figure 1.6**, each cyclic peptoid contains a mixture of *cis* and *trans* amide bonds, accommodating two consecutive *cis* amides that reside in the correspondence of the tight turn regions.

In addition, it has been shown that the incorporation of two *trans* amide-inducing *N*-aryl side chains into a cyclic peptoid hexamer, at the positions (*i* and *i* + 3), showed to mimic the same conformation pattern (-*cis*-*cis*-*trans*-*cis*-*cis*-*trans*-)$_{cyclic}$ found in the hexamer of **Figure 1.6A**.[6b]

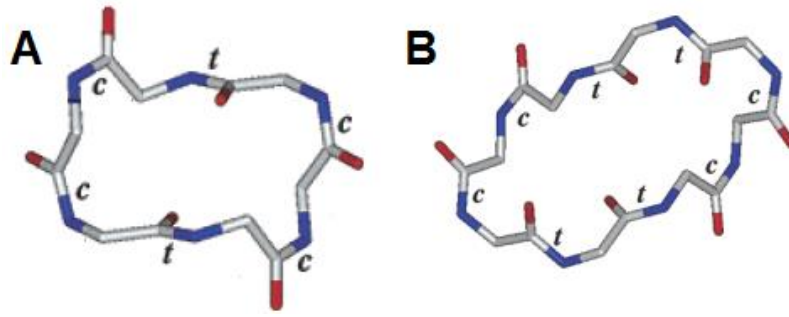

Figure 1. 6. X-ray crystal structure of cyclic peptoid hexamer (**A**) and octamer (**B**) backbone. Side chains are omitted for clarity.

As expected, the *N*-aryl side chains displayed the *trans* geometry, whereas *cis* amides were preferred along the turn regions. Similarly, many other cyclic hexapeptoids, comprising different typology of side chains, yielded crystal structures with the same sequence of amide bond conformations *cctcct*.[14] These studies provide some criteria of predictability of the backbone structural architecture. Indeed, blind-structure predictions correctly suggested the *cis/trans* pattern also for a bigger-size cyclic peptoid.[15] The crystal structure of the nonamer composed of (S)-*N*-(1-phenylethyl) glycine units exhibited a *cccctcccct* motif, with several significant deviations from amide planarity.

A further degree of constrain is achieved in peptoid backbone with macrocyclization of short oligomers. For example, tetrameric cyclic peptoids present a typical *ctct* core geometry and the comparison of the amide backbone structure reveal a similar overall rectangular shape.[14, 16] This peculiar structure is retained also in solution, as showed by NMR analysis, and it confirms the strength of the added constrain and the high degree of conformation order in small-size peptoid ring.[17]

Additional stabilization of peptoid structures and generation of high-ordered conformations is accomplished by metal coordination.[18]

In the specific case of cyclic peptoids, our group demonstrated the binding affinity of hexameric and octameric oligomers towards Li^+, Na^+, K^+, Sr^{2+}, and Gd^{3+}.[17, 19]

The cyclic hexamers of *N*-benzyloxyethyl glycine and *N*-methoxyethyl glycine (**1.5** and **1.6**, **Figure 1.7**) showed conformational disorder in solution as result of several conformers slowly equilibrating on the NMR time scale.[17, 19b]

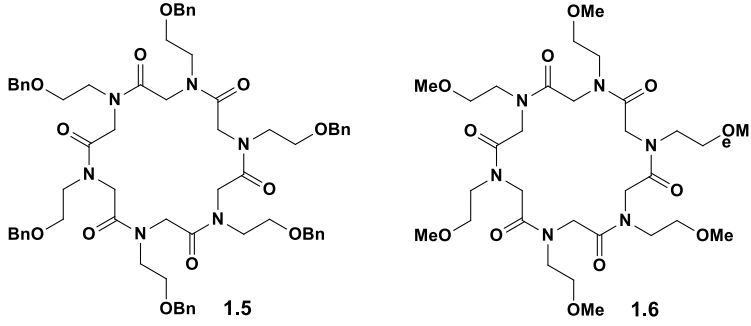

Figure 1. 7. Structures of cyclic hexapeptoids of *N*-benzyloxyethyl glycine (**1.5**) and *N*-methoxyethyl glycine (**1.6**).

In both cases, upon addition of sodium picrate, the coalescence of the NMR signals demonstrated the formation of a new chemical species in solution with an S_6-symmetry axis. Interestingly, the cyclic hexamer **1.5** yielded needle-like crystals as a 2:3 complex with strontium picrate.[17] The analysis showed unique *all-trans* amides because of the ion coordination (**Figure 1.8**).

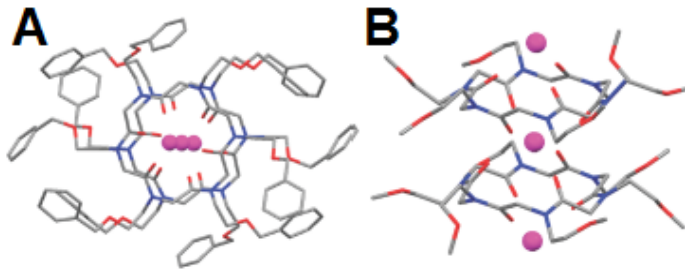

Figure 1. 8. Top view (**A**) and side view (**B**) of X-ray crystal structure of **1.5**$_2$*[Sr(Picr)$_2$]$_3$.

Cyclopeptoid **1.6** was instead crystallized both in the free and Na^+-complexed forms.[19d] A direct comparison of the two crystal structures was possible. The typical *cctcct* amide bonds pattern arose in the free form (**A**, **Figure 1.9**), while the sodium complex showed a different peptoid backbone conformation with *all*-trans amide geometries (**B**, **Figure 1.9**).

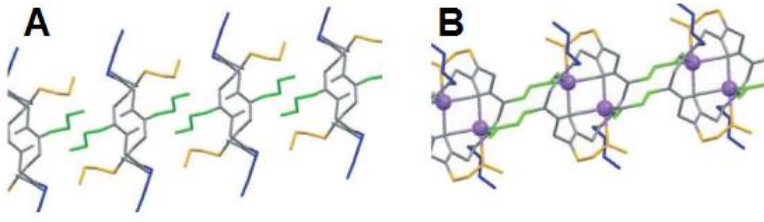

Figure 1. 9. Columnar arrangement of the cyclic hexapeptoid *N*-methoxyethyl glycine (**1.6**) in the free (**A**) and sodium coordinated form (**B**).

It is worth to note that in the presence of the cation, **1.6** formed a 1D coordination polymer, preserving the columnar arrangement of the free form.[14]

The examples showed herein prove that the toolbox for controlling the folding of the "rebel" peptoidic backbone is progressively expanding. The theoretical calculations to predict the structural conformations of peptoids are becoming extremely precise and the discoveries achieved so far highlight the tricks for

accomplishing the desired secondary structures and high-ordered conformations. The degree of control that we gained over peptoids is of utmost importance to make such foldamers unique and valuable peptidomimetics.

1.3 THE IMPORTANCE OF PEPTOIDS: PROPERTIES AND APPLICATIONS

The pace of progress since peptoids discovery is breathtaking. The rational criteria for the *de novo* design of stable structured peptoids and a better understanding of their properties expanded their potential biological applications as biomimetic materials.

The metal binding ability, for example, was crucial for generating cation transport systems,[19a] potential MRI probes,[19c] and efficient phase transfer catalysts.[19b, 20]

Peptoids folding into helix have been applied as antimicrobial compounds[21] as well as biomimetic catalysts.[22]

Helical peptoid oligomers were demonstrated to act as enantioselective catalyst when an achiral catalytic center is attached to it. The helical scaffold, with its intrinsic screw-sense, provide the asymmetric environment that transfer the chiral information to the substrate.

Maayan *et al*. tried oxidative transformations of 1-phenylethanol with right- and left-handed helices on which TEMPO (2,2,6,6-tetramethylpiperidine-1-oxyl) was placed as a catalyst (**Figure 1.10**).[22a] The oligomer length and the position of TEMPO was varied in order to find the parameters for the best catalytic activity.

This idea was further extended to create cooperative catalytic systems.[22b]

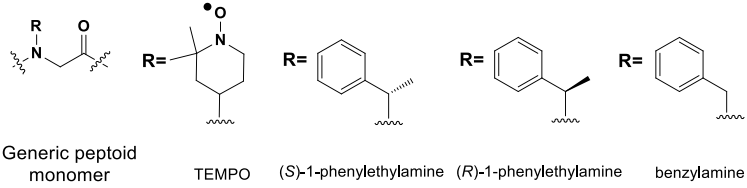

Figure 1. 10. Monomeric units used in the design of catalytic peptoids

These are featured by a transition metal catalyst and an organocatalyst in proximity to each other, creating a confined catalytic pocket. Phenanthroline-copper and TEMPO were installed onto the peptoid-helix scaffold, allowing for the oxidation of primary alcohols in 0.1% loading (**Figure 1.11**).

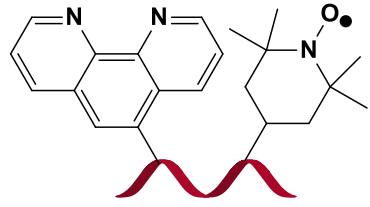

Figure 1. 11. Intramolecular cooperative catalytic system.

Antimicrobial peptoids recall the main features of natural antimicrobial peptides (AMPs). These are usually amphipathic secondary structures, such as α-helical, β-hairpin, extended, or loop structures). The cationic region serves to discriminate between the bacterial negatively charged cell membranes and the mammalian neutral ones, whereas the hydrophobic portion should mediate the mechanism of interaction and lysis of bacteria. Following those features, a library of linear peptoids of different chain length and charge, achieved by the introduction of *N*-(4-aminobutyl) and *N*-(2-carboxyethyl) side chains (**1.7** and **1.8**, **Figure 1.12**), was synthesized and evaluated against Gram-negative and Gram-positive bacterial strains.[21b]

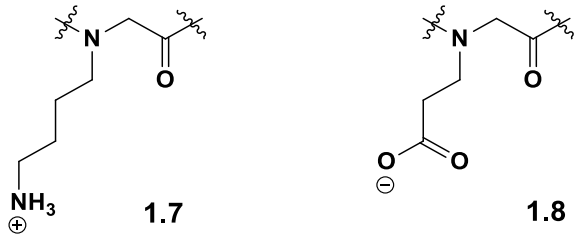

Figure 1. 12. Peptoid monomer charged side chains structures.

Remarkably, a stronger helical structure and an increased hydrophobicity led to greater hemolytic activity. On the other hand, good antibiotic activity was displayed with overall cationic charge of 3+ at least and moderated hydrophobicity.

Cyclic peptoids, recapitulating the features of natural AMPs, were also synthesized in order to evaluate their antimicrobial activity and selectivity.[23] The activity against Gram-negative and Gram-positive bacteria increased with the presence of charged amino groups and, comparing cyclic peptoids with their linear precursors, macrocyclization resulted to enhance microbial activity. Furthermore, these peptoids showed a high selectivity without affecting human erythrocytes.

The results obtained were a clear evidence that macrocyclic peptoids are promising candidate for the development of novel antimicrobial compound. The interest of the researchers in such field is due to the higher resistance of bacterial pathogens to conventional antibiotic. Hence, more amphiphilic cyclic peptoids were synthesized and tested against the methicillin-resistant *Staphylococcus aureus* (MRSA).[24] The compounds showed potent antimicrobial activity and non-hemolytic activity, and may act through a pore formation mechanism on the bacterial cell surface, as showed by scanning electron microscopy (SEM) images of untreated *S. Aureus* and cell treated with different concentration of cyclic peptoids. Such

mechanism of action, in which MRSA is a primary target, has recently been demonstrated.[25] SEM images elucidated that treatment with antimicrobial peptoids induces membrane pore formation but such activity is attenuated when osmoprotective polymers (polyethylene glycol) are added.

One of the very first properties of peptoids to have been explored was molecular recognition. Zuckermann and co-workers evaluated the affinity binding of peptoid dimers and trimers to G-protein-coupled receptors.[26] The importance to inhibit protein-protein interaction is the potential application of peptoid as pharmaceutical agent or chemical tool to shed light on the mechanism of biomolecular interaction.

Recently, linear and cyclic peptoids were prepared to study their inhibitory activity towards amyloid-β (Aβ), involved in the onset of Alzheimer disease.[27] They were designed inspired to the binding motif of the apolipoprotein E (ApoE) that interacts with Aβ, introducing on the nitrogen atom the aminoacidic side chains found in that sequence. *In vivo* experiments are in course to evaluate their ability to block the interactions between ApoE and Aβ and to compare the pharmacokinetics properties of cyclic peptoids with respect to their linear counterparts. The comparison between the macrocyclic and linear compounds related to their properties as protein ligands will give new elements to discuss about which one can be consider a drug lead.

In this context, Kodadek published a comparison of linear and macrocyclic compound libraries as a source of protein ligands, highlighting the advantage of macrocyclization, especially for the cyclic hexamers over their linear counterparts.[28]

The properties and applications presented herein are just few of the many that peptoids exhibit.[29] However, those examples

aim to point out the versatility of such class of compounds, which can be finely tuned to achieve the desired behavior. Peptoids are just a powerful weapon in the hand of the scientists who understand their unlimited potentials in the vast scenario of chemistry.

1.4 AIM OF THE THESIS

Peptoid chemistry is a source of inspiration itself. The control we can exert on the structures of such compounds pushes us to go further on in the exploration of new architectures trying to find out if there is a limit to our imagination.

The aim of my PhD thesis is to contribute to such research and to enrich the realm of peptoids with novel compounds and new insight into their behavior and properties investigating potential applications.

Chapter 2 describes the synthesis of extended cyclic arylopeptoids. The idea is to stretch the peptoid backbone by inserting a benzylic unit. The result is the development of compounds with cavities, tested as cationic transporters to elucidate how the ring size and the introduction of aromatic units could influence the ion affinity and transportation mechanisms.

Chapter 3 concerns the synthesis of two cyclic hexapeptoids designed for the complexation of gadolinium ion. Our attempt is to enhance the affinity for the lanthanide and to study the relaxation properties of the complex, in order to develop effective and safe contrast agents.

Chapter 4 shows the generation of the first example of cyclopeptoid-based iminosugar click-clusters with unprecedented valences. Starting from the synthesis of the cyclopeptoid central

scaffold, I describe the route to high molecular weight compounds, tested as inhibitors of a class of glycosidases.

Chapter 5 is focused on the crystal engineer. A library of hexameric cyclopeptoids has been synthesized to study the role of the side chains in the solid state self-assembly and to disclose which interactions are fundamental for the packing of these molecules.

The *fil rouge* through the thesis is the synthesis of linear and cyclic peptoids. Once prepared, the destiny of those compounds was completely different. They entered in diverse fields of chemistry and added a small piece of knowledge with their unique properties. Such heterogeneity gave me the chance to deeply understand the variety of potential applications of cyclopeptoids and to appreciate the tools I had in my hands.

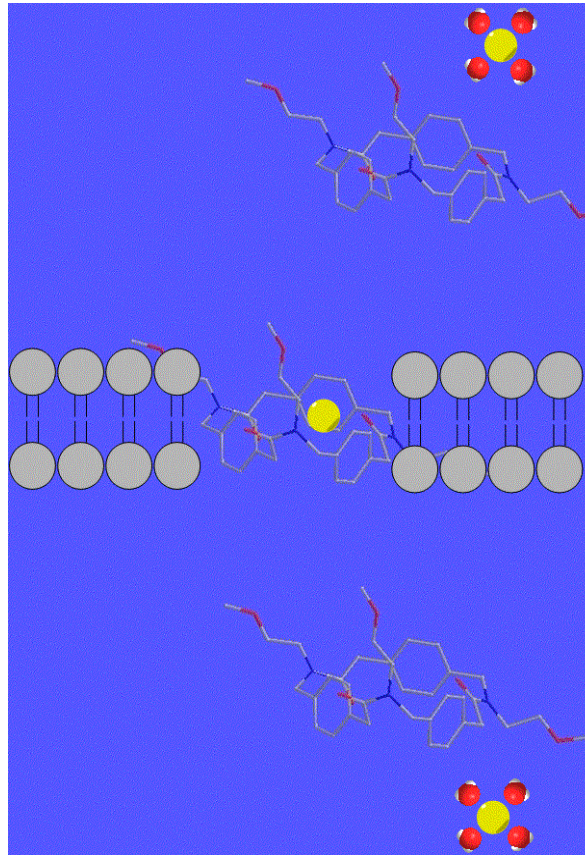

CHAPTER 2

Synthesis And Ion-Transport Properties Of Extended Arylopeptoids

2

2.1 INTRODUCTION

Sight, hearing, taste, smell, touch and dreaming are the five (plus one) senses that make us just us.

Behind our perception of the entire world around, there is a complex sensory system coordinated by an even more intricate nervous system. Excitation and electrical signal production in neurons are physiological processes that involve the flow of ions across the insulating cell membranes.[30] The continuous transportation of ions into and out of cells is thus critical for many of life's processes.[31]

The elaborate design of the cytoplasmic membrane provides 6transport devices that were highly refined during the course of evolution.[30, 32] Nature made them up to overcome the energy barrier the membrane presents to ion crossing.[31] Outside the membrane, ions are stabilized by polar water molecule, but they lose such hydration energy when crossing the lipid bilayer getting into the oily environment inside the membrane.[31]

Pore, channels and carriers mediate fast traffic of ions stabilizing the dehydrated species and acting in lipid bilayers.[33]

Ion transporters exhibit selectivity not only for certain charged species but also for the membranes in which they function.[32] Such evolved system ensures the effectivity of the proper cellular activities, *e.g.,* maintenance of biological homeostasis (essential for differentiation, proliferations and apoptosis of cells), electric signal transmission and energy conversion. [34]

The general molecular understanding of the variety of ion transporters and the elucidation of their mechanism of action could

lead to the fundamental “structure-activity” relationship. This is a powerful tool in the hands of chemists and molecular biologists, because it allows them to tailor the functions of ion transporters and to access such a structural diversity to overtake the biological limitations.

The challenge is to look up at Nature and try to mimic the perfect gears that move the carousel of life.

2.1.1 Ion Transporters At Work

High-resolution crystal structures and functional experiments on ion transporters have helped the investigation on a structural and functional level.

Studies on chloride channel families (ClC),[35] cation-selective channels such as gramicidin,[36] bacterial K^+ channel called KcsA from *Streptomyces lividans*,[37] and K^+ carriers such as valinomycine,[38] elucidated their architectures, shapes and organization within the cell membrane.

Natural ion channels are both peptidic channel and large protein complexes, whereas carriers are typically cyclic polypeptide.

To mediate the flow of ions across the membrane, ion channels create a passageway spanning the thickness of the membrane bilayer, which is about 4 nm, or creating aqueous cavities in the middle of the transmembrane portion of the channel (**Figure 2.1**).[30-31] They open a pore through the lipid bilayer that has the important property of the selective permeability; its size dictates the maximum size of ions allowed to pass through its length. Ion channels conduct specific ions at high rates ($>10^6$ ions per second) and finally conduction is turned on and off by a gating mechanism, that is a simple pore opening/closing, regulated by an external stimulus such as ligand binding or membrane voltage.

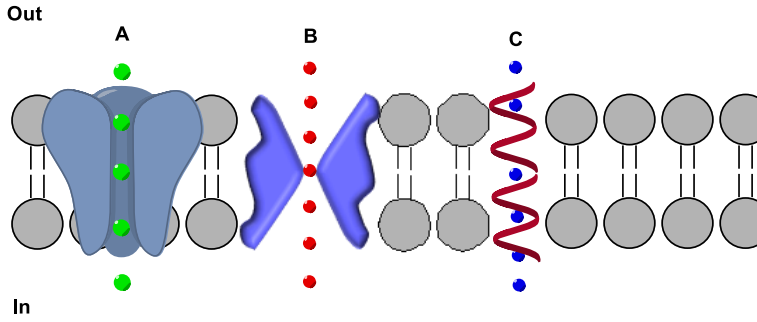

Figure 2.1. Overall architecture of ion channels. (A) KcsA K^+ channel has a wide water-filled pore in the middle of the transmembrane portion of the channel and a selectivity filter K^+ ions (green spheres). (B) ClC has ha double funnel-shaped structure leading to a narrow pore that selectivity filters the anions (red spheres). (C) Gramidicine is a pentadecapeptide with a β-helix secondary structure that arranges in a head-to-head helical dimer forming tubular channels for the passage of alkali metals (blue spheres).

Natural ion carriers regulate ions traffic on the basis of transport mechanisms which differ from ion channels for kinetic criteria.[30] They are often described as "molecular ferryboat" (**Figure 2.2**).[32]

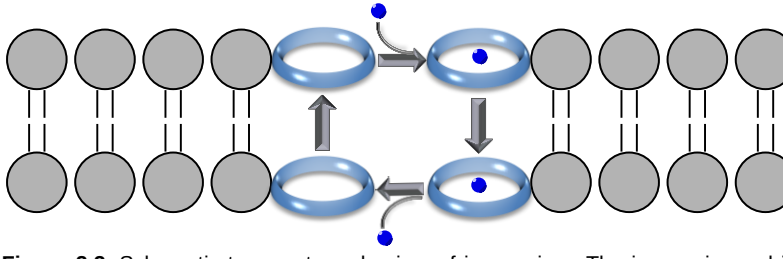

Figure 2.2. Schematic transport mechanism of ion carriers. The ion carrier and its cargo (green sphere) move together through the membrane.

In this analogy, the membrane can be seen as the river and the two aqueous phases, intracellular and extracellular media, as the opposite shores.[39] Firstly, the carrier binds to a specific ion, selectively and reversibly, forming a metal ion complex that is lipid soluble. Therefore, they move together, allowing the ion to pass through the hydrophobic region of the bilayer. When the complex arrives at the other membrane interface, the ion is released and the

ionophore crosses again the membrane. The rate of passage of ions is of 10^4 ions per second, thus much slower than through open channels. [38-39]

The above-mentioned systems are the two broad mechanisms for transmembrane transport of ions.

Nevertheless, the chemical details beyond the designation of the channel-forming mechanism remain unclear and more insights are needed to shed light on how the ion or substrate reaches the binding sites within transmembrane domains.

Knowing the structure of an ion channel or an ion carrier, however, is the starting point to understand the principles of selective ion transport in terms of the architecture and detailed chemistry of the ion conduction pathway.

It is now clear that the essential and basic ability of membrane-spanning and amphiphilicity are needed.[40] Amphiphilic structures present a hydrophobic region moiety, for solubility in the bilayer environment and branching interactions with the membrane, plus charged head groups in the metal-coordinating midsection.[41] Such inner surface should present weak regions of electron density, such as hard oxygen containing ethers and esters or aromatic groups to capture and transport small cations, or hydrogen bond donor groups to stabilize anions.

Ion transport through membranes is definitely a supramolecular function.[42] Hydrogen bonding, hydrophobic interactions, ion pairing, π,π-interactions and cation–π interactions are the five standard non-covalent interactions of supramolecular chemistry for stabilizing the self-assembly of functional architectures and the flow of ions. As such, the transporter has to be preorganized in order to attain the perfect complementarity with a certain guest. The binding process will be selective and effective if the match

between the binding site and the size of the ion is achieved and its preferred coordination geometry is respected.

With these features in mind, it is possible to provide a structural and functional paradigm that shows the basic design criteria for artificial ion transporters.

2.1.2 Mimicking Nature And Beyond: Synthetic Ion Transporters

The design of Nature-inspired synthetic ion transporters that reproduce natural motifs is of utmost importance for their contribution in the fields of both biomedicine and technology. Non-natural antibacterial and anticancer,[32] catalyst [43] and sensors,[44] are just some of the many applications such systems could find in the vast scenario of scientific research. Furthermore, developing synthetic ion transporters would mean generating chemical models to probe different aspects of ionophores and to gain a greater understanding of the chemical mechanism of transporters functions.

Extensive research has been devoted to mimic natural ionophores and thereby design and prepare synthetic compounds that have comparable properties exhibiting channel or carrier behavior.

Nature stimulated the creativity of chemists, who went well beyond the observation of reality. Following their imagination, they produced an arsenal of artificial ion transporters featured by modification of naturally occurring motifs from proteins and peptides or totally new structures.[45] Ranging from steroid-based to calix[4]arene-based ionophores, passing through sugar-based or crown ethers ionophores and metal-organic transmembrane nanopores, numerous examples of synthetic systems forming artificial ion transporters are reported in the literature (**Figure 2.3**).

Although the impressive expansion of structural diversity, it is remarkable that all of these compounds, differing in their chemical structure, show quite similar ionophoric behaviors. Indeed, their common feature is the ensemble of supramolecular interactions, which is at the basis of ion transport. Furthermore, beside this standard “chemical code”, there are more “exotic” interactions, such as anion-π and halogen bonding interactions,[46] which expand the landscape of synthetic transport system.

The major contribution of such intriguing and exciting investigation is the conceptual innovation and the motivation to realize more and highly creative examples for broadening the realm of ion transportation systems.

The introduction of new types of transporters, exhibiting refined motifs and fascinating architectures, was a real source of inspiration to us. We took on the challenge to give our contribution to such topic and a possible breakthrough on the design of new synthetic transport system.

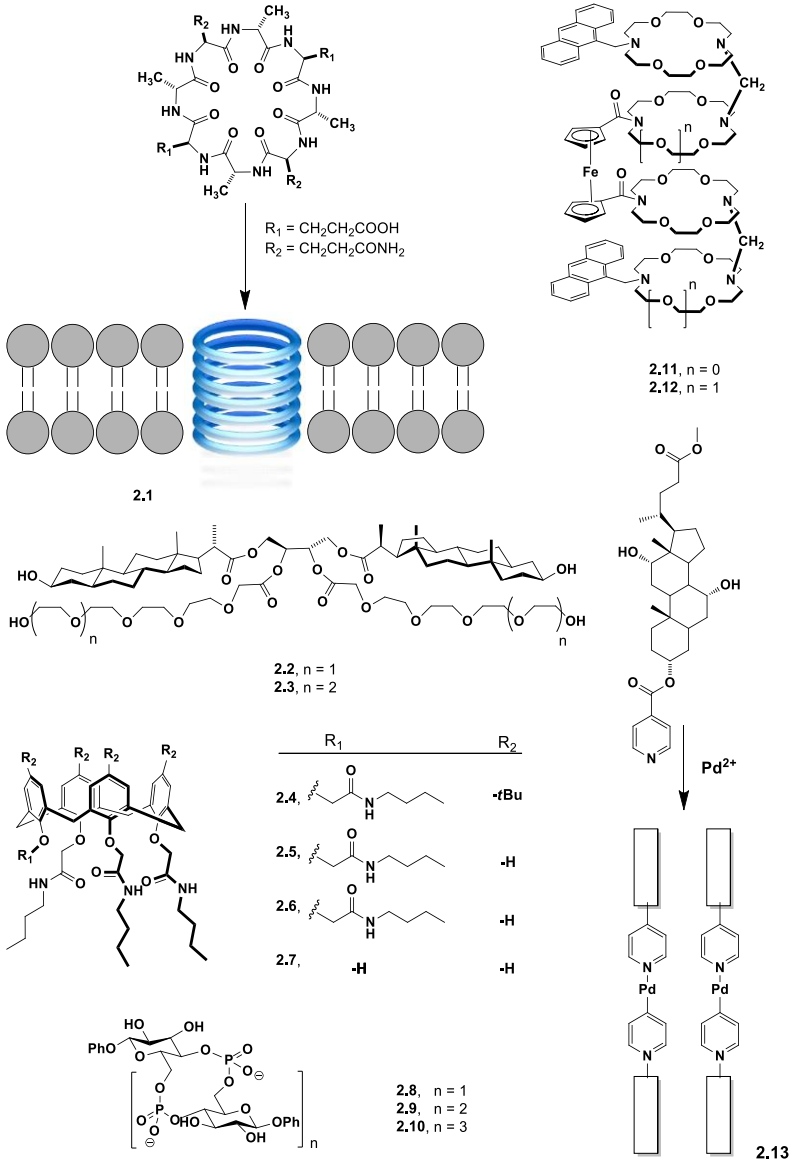

Figure 2.3. Recent synthetic transport systems: self-assembled cyclopeptide nanotube **2.1**, dimeric steroid derivatives **2.2** and **2.3,** cone-shaped calixarenes **2.4**–**2.7**, cyclic oligosaccharides named CyPLOS **2.8**–**2.10**, crown ether oligomers **2.11** and **2.12**, and metal–organic scaffold based on Pd-gated cholate bundle **2.13**. [32-33, 38, 41, 47]

2.2 AIM OF THE WORK: SYNTHESIS AND ION TRANSPORT ACTIVITY OF EXTENDED CYCLIC ARYLOPEPTOIDS.

2.2.1 Introduction

Peptoids have been broadly applied to complex metal ions. [17, 19c, 48] Upon coordination, they are usually able to form well-defined folded architectures. The conformation triggered by the ion complexation defines their specific properties and activities.

Our group showed that cyclopeptoids can be tested for cation transport activity (**2.14-2.17**, **Figure 2.4**). [19a]

Macrolactamization restricts peptoids conformations, so that they result quite preorganized as required for ion complexation. The carbonyl ligands are the binding sites in the cyclopeptoids cavity, whose dimension can be varied to accommodate ions of different size.

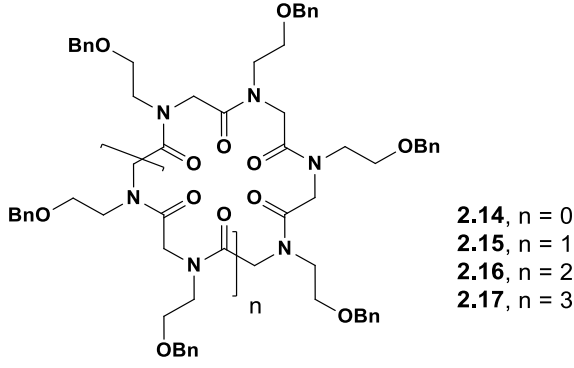

Figure 2.4. Cyclopeptoids tested for cation transport activity.

The flexible eighteen-membered *N*-benzyloxyethyl macrocycle **2.15** showed to strongly bind small cations such as Li^+, Na^+ and K^+, whereas the expanded cyclopeptoids **2.16** and **2.17** preferred larger cations from the first group alkali metals. In

particular, **2.15** transported Na^+ with high selectivity, and the octamer macrocycle **2.16** showed Cs+> Rb+> K+ selectivity, both acting as unimolecular ion carriers. The extreme macrocycles **2.14** and **2.17**, either too small or too floppy, were both inactive.

Encouraged by those results and inspired by the family of synthetic macrocycles of *N*-alkylated para-cyclophanamides (**2.18**, **Figure 2.5**), that have been shown to act as selective hosts, we decided to develop a new group of cyclopeptoids that incorporates aromatic units into the peptoidic backbone.

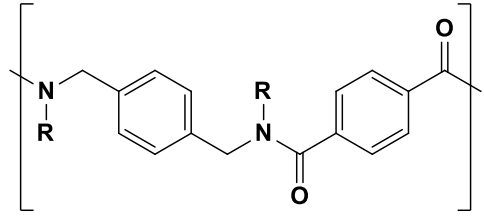

2.18

Figure 2.5. *N*-alkylated *para*-cyclophanamides.

In the design of the reported macrocycles, the methoxyethyl side chain was chosen for its ability to increase the amphiphilicity of the molecule and optimize its water/lipid partition.

As result of our efforts, here it is reported the synthesis of two cyclic oligomeric *N*-substituted aminomethyl benzylamides: the cyclotrimeric oligoamide **2.19** and cyclotetrameric **2.20** (**Figure 2.6**).

The *N*-alkylated *para*-aminomethyl benzylamides fall in the class of "arylopeptoids", extensively studied by the group of Hjelmgaard and Faure who synthesized and characterized linear and cyclic *ortho*- *meta*- and *para*- *N*-alkylated aminomethyl benzamides.[49-33] They demonstrated that the amide group of the arylopeptoid backbone may exist as a *cis/trans* mixture which may be controlled by proper choice of side chains.[49c, 49d]

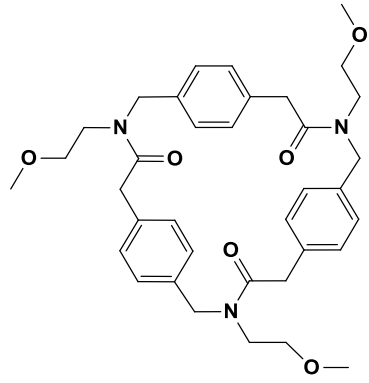

2.19

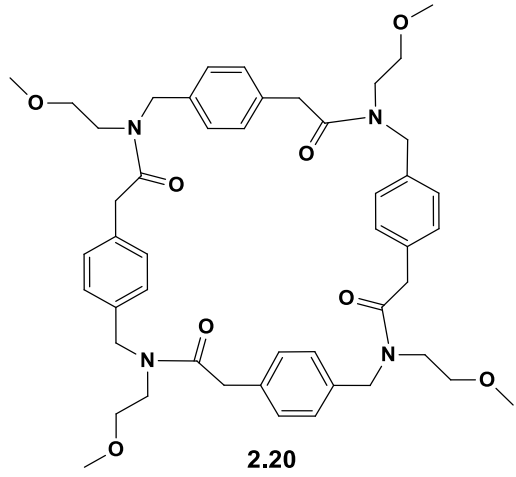

2.20

Figure 2.6. Cyclic oligomeric *N*-substituted aminomethyl benzylamides **2.19** and **2.20**.

The *cis-trans* isomerism facilitated the head-to-tail macrocyclization for the *ortho*- and *meta*- derivatives but not the *para*-series of the trimeric arylopeptoids (**2.21** and **2.22**, **Figure 2.7**).[49b] The aromatic core skeleton may represent a rigidified motif that, combined with the *para*-substitution pattern, hampered the macrocyclization reaction.

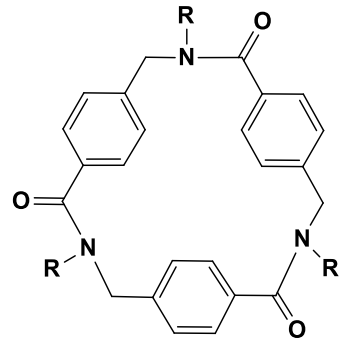

2.21, R = Et
2.22, R = *i*-Pr

Figure 2.7. *para*-Series of properly *N*-substituted arylopeptoids.

With this in mind, we thought to extend the backbone with a methylene unit that may give much more freedom to the carbon skeleton, so facilitating the termini condensation and the generation of new and interesting structures. Indeed, they provide a hydrophobic core and large internal cavities, easily sizeable by means of the synthetic protocol, which may be examined from the host-guest chemistry viewpoint. The guest recognition may become effective through non-covalent interactions at the binding site *via* the *n* carbonyl lone pairs and aromatic π cloud. The binding behavior of the macrocycles may arise through an induced-fit mechanism originating from the intrinsic flexible character of the peptoid backbone.

Figure 2.8 displays possible conformations of cyclooligomers **2.19** and **2.20** in the presence of the sodium cation. The structural analysis shows that the 24-membered ring **2.19** has a C_3-symmetry and perfectly encircle the sodium cation through cation-π stabilizing interaction, whereas the 32-membered ring **2.20** seems too big to comfortably accommodate it.

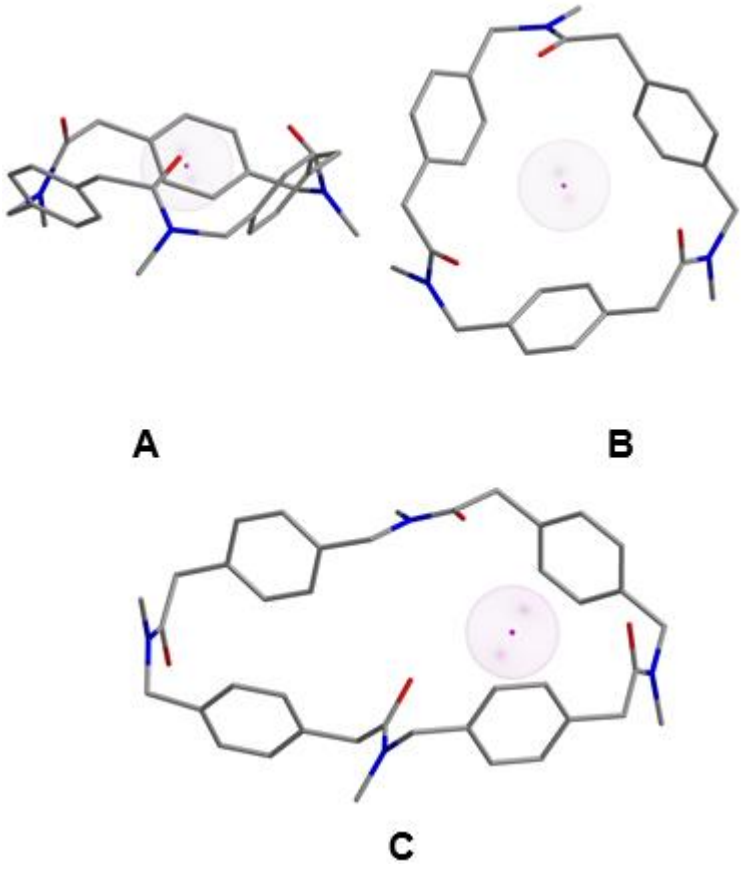

Figure 2.8. Structures showing the Na^+ complex of compounds **2.19** (A: side view; B: top view) and **2.20** (side view) in their *trans* peptoid bond conformations. For simplicity's sake, the N-linked side chain is reported as $–CH_3$. Hydrogen atoms have been omitted for clarity. Atom type: C gray, N blue, O red, Na magenta. (Chem 3D plus output).

The backbone structure of arylopeptoids still retains the favorable characteristic of peptoids: they are accessible through the "submonomer" approach.[49c]

Nevertheless, arylopeptoids synthesis results more demanding with respect to the peptoid counterpart. The benzyl group is much less reactive than the bromoacetate, the substitution

reaction is substrate depending and the growing aromatic chain suffer from poor solubility.[49a, 49d]

For those reasons, there is plenty of synthetic methods in the literature, both on solid phase as well as in solution, highly refined and tuned according to the specific substrates applied.[49a, 49c-e, 50]

2.2.2 Results And Discussions

We have developed a new and facile synthetic approach to construct the first *N*-substituted aminomethyl benzylamide oligomers, in order to have ample variety of chemical structures.

Our first attempt was to study the feasibility of solid-phase synthesis. We chose the 2-chlorotrityl resin as solid support and *p*-bromomethyl benzylic acid as building block, applying the standard conditions of the submonomer approach.[2] The instability of the building block under basic conditions and the sterically hindered solid support led to a complex mixture of products as revealed by HPLC analysis. Having excluded the use of such method, we thought to bring together the advantages of the solution and solid-phase synthesis.

The method we optimized could be described as a "submonomer" approach in solution followed by a monomer solid-phase synthesis. Indeed, the displacement reaction was realized in solution, whereas the subsequent acylation on the less reactive secondary amide and growth of the oligoamide chain were performed on solid-phase.

We started the synthesis of the Fmoc-protected arylopeptoid building-block with the radical bromination of the commercially available *p*-tolylacetic acid in presence of NBS (**Scheme 2.1**). Such procedure was inspired by the one reported for the *m*-isomer [51] to avoid the use of the toxic Br_2 described for the bromination of the *p*-

tolylacetic acid.[52] The esterification of the free carboxyl group of the 4-(bromomethyl)phenylacetate (**2.24**) was carried out following a well-known methylation procedure [53] to give the protected methyl ester (**2.25**). The methyl 4-(bromomethyl)phenylacetate was then subjected to the amination reaction in the presence of an excess methoxyethylamine. Excess amine and a very slow addition of the substrate to its solution are mandatory to prevent polyalkylation of methoxyethylamine.

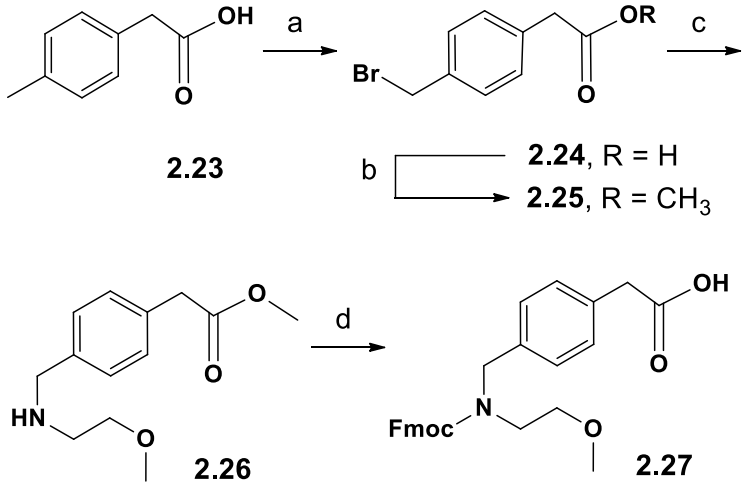

Scheme 2.1: Synthesis of monomer **2.27**. Reagents and conditions. (a) N-bromosuccinimide, benzoyl peroxide (40%); CCl_4 (b) methanol, chlorotrimethylsilane (97%); (c) methoxyethylamine, DMF (98%); (d) i) $LiOH \cdot H_2O$, 1,4-dioxane; ii) $NaHCO_3$, Fmoc-Cl, 44% yield.

The subsequent hydrolysis of the methyl 2-(4-((2-methoxyethylamino)methyl)phenyl) acetate (**2.26**), in the presence of lithium hydroxide, was followed by the protection of its free amino group as 9-fluorenylmethoxycarbonyl (Fmoc) derivative.

The overall yield of the monomer **2.27**, ready for the solid-phase oligomerization, was 17%.

The Fmoc protected **2.27** was then oligomerized on the 2-chlorotrityl chloride resin (**Scheme 2.2**).

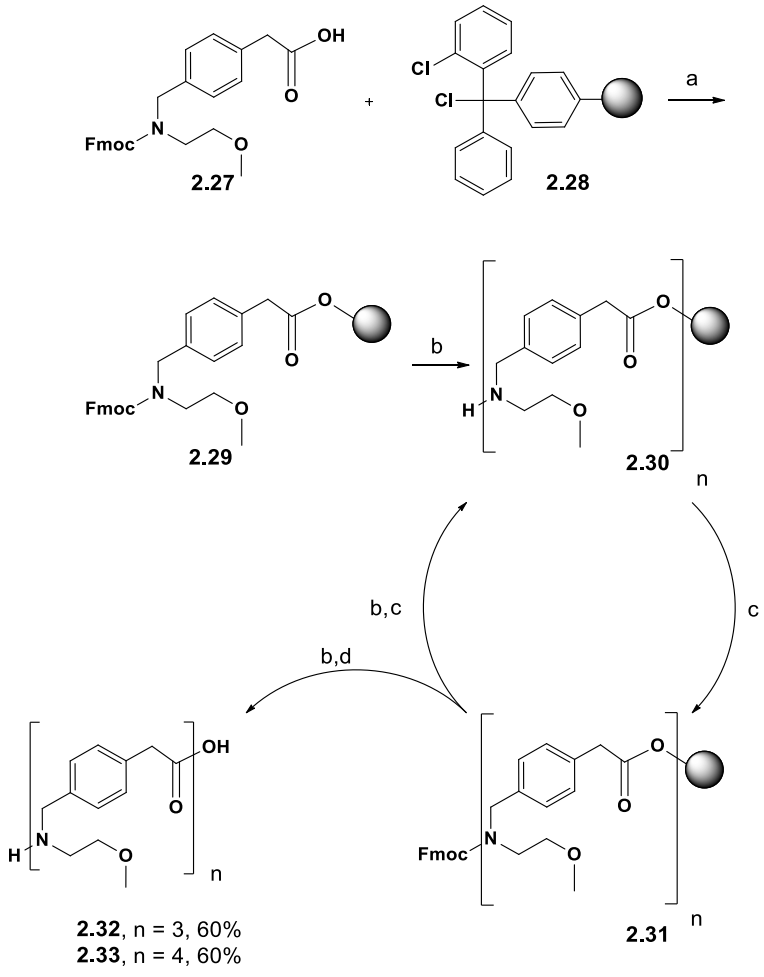

Scheme 2.2: Synthesis of trimer and tetramer *N*-substituted aminomethyl benzylamides **2.32** and **2.33**, respectively. Reagents and conditions. (a) i) **2.27** (0.67 equiv., 0.2 M), DIPEA (4.0 equiv.), CH_2Cl_2, 90 min.; ii) DCM/MeOH/DIPEA (17:2:1), 15 min.; (b) Piperidine/DMF (1:4) (2 x 1 min, 2 x 5 min); (c) **2.27** (3.0 equiv, 0.3 M), HATU (3.0 equiv.), DIPEA (6.0 equiv.), DMF, 1 h; (d) HFIP/DCM (1:4) solution (2 x 30 min). Overall yields of the crude residues **2.32** and **2.33**: 60%.

Loading onto the resin was realized in the presence of DIPEA and the subsequent capping, in order to terminate the excess of reactive positions, was performed using a mixture of DCM/MeOH/DIPEA (17:2:1). The elongation of the desired arylopeptoid chain was accomplished by iterative deprotection-coupling cycles. The detachment of the Fmoc- protective group was carried out with piperidine (25% in dry DMF) and the free amine was then coupled with the HATU-activated monomer **2.27** in the presence of DIPEA as the base. The yields per coupling were excellent (>99%, based on the chloranil test) and gave the linear trimeric and tetrameric *N*-substituted aminomethyl benzylamides **2.32** and **2.33** respectively, once detached from the acid labile resin with hexafluoroisopropanol (HFIP) (20% in dry DCM).

The crude intermediates **2.32** and **2.33** were cyclized in high dilution conditions ($2.0 \cdot 10^{-3}$ M) with the assistance of HATU and DIPEA (**Scheme 2.3**), affording the expected targets **2.19** and **2.20** in good yields (>90%, RP-HPLC analysis). This exciting result suggests that the addition of an extra- methylene unit into the arylopeptoid backbone strongly favours the direct macrocyclization.

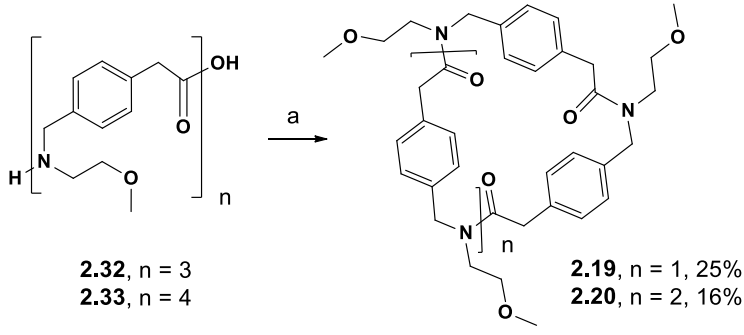

2.32, n = 3
2.33, n = 4

2.19, n = 1, 25%
2.20, n = 2, 16%

Scheme 2.3: Synthesis of macrocyclic arylopeptoids **2.19** and **2.20**. Reagents and conditions. (a) **2.32** and **2.33** (1.0 equiv., $2.0 \cdot 10^{-3}$ M), HATU (4.0 equiv.), DIPEA (6.0 equiv.), DMF, 24 h. Overall yields of **2.19** and **2.20**: 25% and 16% respectively.

The complexity of the *r.t.* ^{1}H-NMR spectra recorded for both the cyclic "benzylopeptoids" demonstrated the slow exchange of multiple conformations on the NMR time scale. This result was expected due to the relative flexibility of the backbone skeleton and the *cis-trans* isomerism of the amide bonds. However, our attempt was to understand whether a preferred conformation could emerge in solution decreasing the acquisition temperature at 268 K. Again, ^{1}H-NMR spectra with broad signals indicated the presence of several conformers in equilibrium at NMR time scale. The cyclotrimer **2.19** was further analyzed *via* ^{1}H-NMR recording the spectrum at 263 K. Also in this case no discernible pattern was observed. This outcome is in contrast with the one obtained by the group of Faure and Hjelmgaard for the *meta*- and *orto*- cyclotrimers carrying ethyl side chains.[49b] This result suggests that **2.19** is much more flexible and has much more conformational freedom in solution thanks to the extra methylene unit and the *para*- substitution.

Furthermore, differently from the parents peptoids,[14, 17, 19-20] the *N*-substituted aminomethyl benzylamide cyclic trimer **2.19** and tetramer **2.20** did not yield any ordered conformation in the presence of cationic guests.

The ion transport activities of the benzylopeptoids **2.19** and **2.20** were evaluated by the group of Prof. Tecilla at the University of Trieste. The ionophoric activities of compound **2.19** and **2.20** and the determination of their anion/cation selectivity were investigated by means of the HPTS assay.[54] HPTS is the 8-Hydroxypyrene-1,3,6-Trisulfonic Acid, a sensory fluorescent dye with a pK_a ~7.3, primarily used as a pH indicator in the near-neutral range. Its working mechanism is one excitation maximum at 405 nm decreasing with pH and another one at 450 nm increasing with increasing pH. When the fluorescent dye is entrapped in vesicles, of large unilamellar

liposomes (100 nm diameter) with a 95:5 egg phosphatidylcholine (EYPC) and egg phosphatidylglycerol (EYPG) lipid composition prepared in HEPES buffer at pH 7.0 containing 100 mM NaCl, it can detect the downfall of 0.6 units transmembrane pH gradient by external addition of NaOH and so the ability of synthetic ion transporters to dissipate it (HEPES = 4-(2-hydroxyethyl)piperazine-1-ethanesulfonic acid). Indeed, if a base is applied in the extravesicular compartment, the synthetic ion transporter can mediate the increase of intravesicular pH by facilitating either proton efflux or OH^- influx. To compensate the charge translocation, there will be either a cation influx or an anion efflux depending on the cases. The four possible overall processes are H^+/Na^+ antiport, OH^-/Cl^- antiport, H^+/Cl^- symport and Na^+/OH^- symport. Hence, the increase in HPTS emission with time after the ion transporter addition can help detecting the preferred ion exchange process. The ionophoric activity of the cyclic peptoids is reported in **Figure 2.9**.

Figure 2.9a shows that compound **2.19** promotes the pH gradient collapse across the phospholipid membrane and its activity increases by increasing the ionophore concentration. On the contrary, **2.20** is inactive and the kinetic trace recorded at 2% concentration of peptoid is almost superimposed to that obtained in the absence of any ionophore (control). **Figure 2.9b** reports the first-order rate constants (k_{obs}, s^{-1}) for the transport process whose kinetic traces were recorded for different concentrations of **2.19**. Such linear behaviour indicates that the species responsible for the transport process is monomeric.

Furthermore, by changing the cation and the anion present in solution,[55] the HPTS assay revealed ion selectivity.

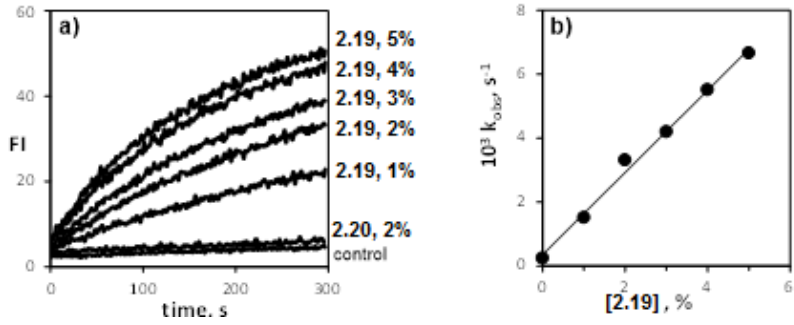

Figure 2.9. a) Normalized fluorescence change in HPTS emission as a function of time after base pulse to 95:5 EYPC/EYPG vesicles containing **2.19**, **2.20** and without additives (control) at 25 °C. b) Dependence of the observed rate constant for the transport process (k_{obs}, s^{-1}) vs concentration of compound **19**. The concentration of peptoids is indicated in the Figure and is given in percent with respect to the total concentration of lipids (0.17 mM).

In particular, for cation selectivity the liposome suspension was prepared as described above but using 100 mM MCl (M= Li+, Na+, K+, Rb+, Cs+) as added salt and the corresponding MOH base for the pH pulse. **Figure 2.10a** reports the variation of the observed rate constants for the transport process (k_{obs}, s^{-1}) as function of the concentration of peptoid **2.19** obtained in the experiments with the different cations. For all the cations investigated a unified transport mechanism was envisioned, since all the kinetic profiles are linear. The same rate of transport was revealed for Na^+, K^+, Rb^+. However, the selectivity is low and only slightly more efficiently than Li^+ and Cs^+. On the contrary, compound **2.20** did not show any activity regardless the cation present in solution. Anion selectivity of compound **2.19** was also investigated. Figure **2.10b** shows the result obtained in the presence of 3% concentration of compound **2.19** and using 100 mM NaX (X= Cl^-, Br^-, I^-, $ClO4^-$) as added salt and NaOH base for the pH pulse. Also in this case the selectivity observed is

low. Halides are better transported that perchlorate and, among halides, the more lipophilic iodide is the faster anion transported.

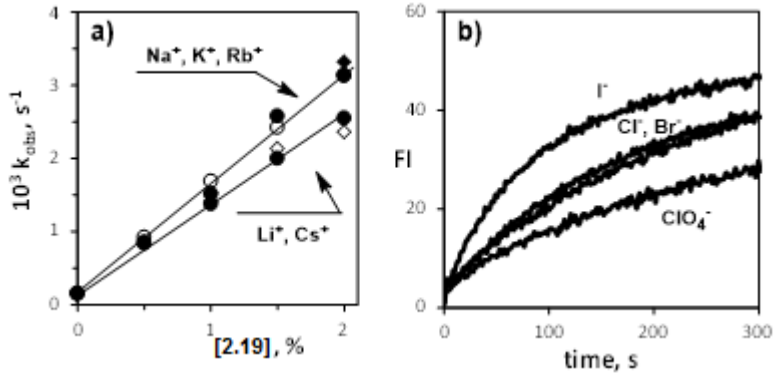

Figure 2.10: a) Cation selectivity: dependence of the observed rate constant for the transport process (k_{obs}, s^{-1}) *vs* concentration of compound **2.19** in the HPTS assay using 100 mM MCl (M= Li^+, Na^+, K^+, Rb^+, Cs^+) as added salt and the corresponding MOH base for the pH pulse. b) Anion selectivity: normalized fluorescence change in HPTS emission as a function of time after base pulse with NaOH to 95:5 EYPC/EYPG liposomes containing compound 19 (3%) and using 100 mM NaX (X= Cl^-, Br^-, I^-, ClO_4^-) as added salt. The concentration of peptoid is given in percent with respect to the total concentration of lipids (0.17 mM).

The outcome of the experiments performed clearly indicates that the two examined macrocycles have different ion transport activities. The cyclic peptoid **2.19** is able to transport cations across a phospholipid membrane in response to a pH gradient, whereas **2.20** does not show any transport ability. Such different behaviour can be explained on the basis of the different macrocycles' size that strongly influences the cation capture/transport. In addition to this, the observation that the active species involved in the transport is a monomer, enforces the hypothesis of a carrier mechanism, in analogy to that demonstrated for related glycine base α-cyclopeptoids.[19a] Nevertheless, the cyclic arylopeptoids show lower selectivity and activity with respect to the parent cyclopeptoids. A possible explanation relies in the lower number of efficient cation-

binding carbonyl groups (6 in the α-cyclopeptoid versus 3 in **2.19**) and a more rigid, less adaptive structure. Thus, the arylopeptoid is not able to "wrap" around the cation and the binding is weaker and less size specific. Despite of that, the slight selectivity of compound **2.19** towards the mid-size alkaline cations (Na^+, K^+, Rb^+) respect to the smaller Li^+ and the larger Cs^+ may be the starting point for optimization of the system in the next future. Finally, the observed selectivity among anions with the more lipophilic iodide better transported suggests that the cation is translocated across the membrane together with its counteranion in a symport carrier mechanism in which MX is exchanged with MOH thus resulting in the observed pH gradient discharge.

2.3 CONCLUSION

A new class of arylopeptoids has been designed, synthesized and characterized in order to explore their binding properties towards the first group alkali metal and their ion transport activities. The reported structures, based on the *N*-aminomethylphenylacetyl spacer, have an extended carbon skeleton with respect to the parent arylopeptoids described in the literature so far. The *para*-substituted cyclic trimer and tetramer have been efficiently synthesized by means of a mixed in-solution/ on-solid phase synthetic approach. The difficult alkylation steps of the primary amine were conveniently carried out in solution using 4-(bromomethyl)phenylacetate and, upon amine Fmoc-protection, the desired building block was isolated and oligomerized on 2-chlorotrytil chloride resin. This methodology afforded the linear precursor of the target compounds in an efficient manner. Finally, they underwent macrocyclization in high dilution conditions, leading to the cyclic

arylopeptoids. This studies show that the extra methylene units in the aromatic carbon skeleton provide a certain degree of conformational freedom, facilitating the termini condensation despite the *para*-substitution pattern and the rigid aromatic units.

The ^{1}H-NMR spectra recorded either at room temperature as well as at 268K and 263K, showed the absence of well-defined conformations in solutions.

The cyclic trimer and tetramer extended arylopeptoids were finally subjected to ion transport studies, demonstrating not only a dependence on the size and the charge of the cavity, but also on the flexibility of the structure. The cyclic tetramer inner cavity is too large to selective accommodate any ion, whereas the cyclic trimer is slightly active towards the mid-size alkaline cations (Na^+, K^+, Rb^+), preferably transported with the iodide counterion, showing a symport carrier mechanism.

The results of our efforts contributed to the realm of synthetic ion transporters with two new structures, accessible through a versatile synthetic methodology. Despite their modest ionophoric activity, they lead to important hints for a better understanding of the structure/activity relationship and the ion transport mechanism.

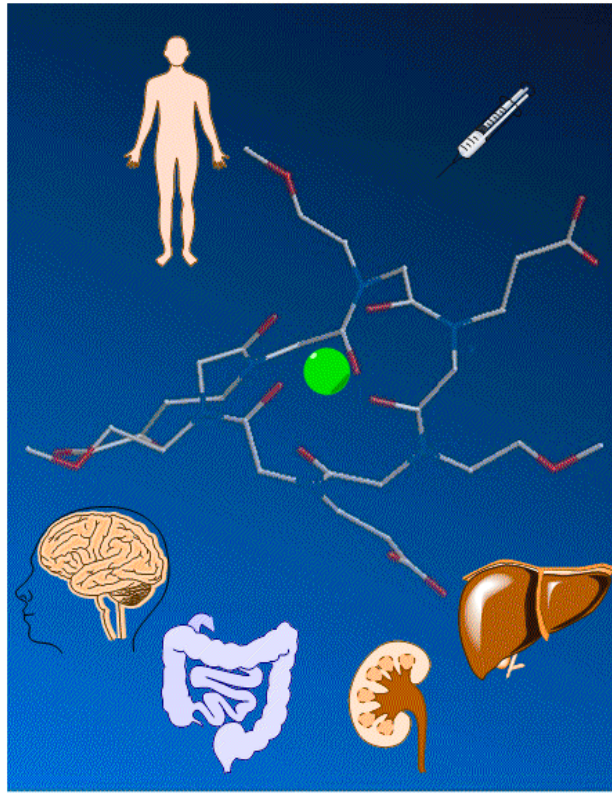

CHAPTER 3

Cyclic Hexapeptoids As Potential MRI Probes: Design, Synthesis And Evaluation Of Relaxometric Properties

3

3.1 INTRODUCTION

The medical need to explore deep inside the human body from the outside led to enormous advances in clinical diagnosis. Increasing research activities are providing new opportunities for visualization and characterization of soft, hydrated tissues to discriminate between healthy and diseased ones.

A very large contribution to the field is from magnetic resonance imaging (MRI) that, since its introduction in the early 1980s, has been growing very fast.[56] Its deep tissue penetration and ability to acquire high-resolution images in any plane, without exposing the patient to ionizing radiation as in X-Ray analysis, made it a routinely used diagnostic tool in hospitals worldwide. The detection and evaluation of biochemical, biomechanical, or structural pathological changes in tissue is a revolutionary tool for early diagnosis and interventions that can considerably slow or reverse the progression of the disease.[57]

Over the years, MRI has achieved a number of successes to become the technique of choice for the study of several diseases, in particular tumors.[58]

The brain can be deeply scanned for the detection of intracranial tumors, structural vascular anomalies (aneurysms and vascular malformations) and ischemia or heart attacks, white matter lesions in the brain such as the plaques found in multiple sclerosis or Alzheimer's disease and congenital diseases.[56, 59] Other areas of the body can also be imaged by the optimal choice of MRI parameters. MRI can be applied to the facial bone, the structures below the face, the neck and the cervical spine.[56] Furthermore, it is an extremely

effective technique for evaluating the musculoskeletal system and pelvic anatomy (*e.g.* the uterus).[56-57] Finally, the use of MRI has also been extended to the diagnosis of chest and intra-abdominal disease, limited in the past because peristaltic motion significantly degraded the quality of images.[56, 60]

The intensive investigation in this research area hardly changed and broadened the spectrum of clinical MRI examinations during the last decade.

In his paper from 1983, three years after MRI emerged, Richard Henderson wrote "*NMR* (in former times this is how they referred to MRI) *is a significant new imaging modality, the importance of which is only beginning to be realized*".[61]

Now, his words sound more like a prediction of the actual broad applications of MRI.

3.1.1 Description Of MRI

The experimental foundations of MRI lay on the NMR spectroscopy basis.[60c, 61-62]

Since its discovery in 1942, NMR has been used for elucidating the structure of organic molecules, but just in 1971 its medical value was realized.[61]

NMR application to produce medical images was obtained tuning it on hydrogen nuclei resonances, since the human body is 75% water molecules and its distribution is known to be altered by many pathological states.[62] Indeed, the strength of the MRI signal depends primarily on the density of the protons in the tissue; the greater the density, the stronger the signal. Furthermore, signal intensity in MRI stems from two parameters defined in the basic principles of NMR that are the relaxation times T_1 and T_2. They describe the time for the net macroscopic magnetization of proton

spins to relax back to its equilibrium value in the longitudinal Z axis and transverse XY plane respectively, after a radio-frequency pulse has been applied. T_1 and T_2 are strongly influenced by the viscosity or rigidity of a tissue. Hence, there can be dramatic differences in relaxation times between the tissues and so a major contrast between them, giving a high or low signal that results in a bright or dark image. For example, pathology is usually associated with both prolonged T_1 and T_2.[61] In general, signal tends to increase with the decrease of T_1 and so with the increasing of the longitudinal relaxation rate of water protons in the tissue, because the steady-state magnetization along the Z axis is greater yielding brighter images.[60b, 60c] On the other hand, they decrease with the decrease of T_2, and so with the increasing of the transverse rate, since this diminishes its availability for detection, appearing as darker images.[60b, 60c] Moreover, pulse sequences can emphasize changes either in T_1 or in T_2, in order to manipulate the MRI response and so the imaging. The former are referred to as T_1-weighted, and the other as T_2-weighted scans.[60b]

Finally, also the apparatus needed for MRI is inspired to the technology developed for NMR spectroscopy.[61-62] Indeed, MRI system requires a magnet for applying the static magnetic field, large enough for accepting the human body, a radio-frequency coil to generate the pulse and detect the free induction decay signal and finally a computer to process it. This applies the Fourier transformation to yield a one-dimensional projection of signal amplitude and then a series of such projections can be reconstructed into two-dimensional images of NMR signal intensity.[61]

3.1.2 Contrast Agents For MRI: Gd^{3+} Complexes

Under normal conditions, MRI provides impressive images that reproduce anatomy in high resolution. Nevertheless, in order to

indicate the status of organ function or physiological information, a greater image contrast is required.[60c] To further enhance it, a contrast agent (CA) can be administered to patients prior to scanning.[60c, 63]

Contrast agents are a new class of pharmaceuticals comprising complexes of paramagnetic transition and lanthanide metal ions.[60c, 61-63] Their mode of action is to increase the relaxation rate of water proton spins in the immediate surroundings of the tissue in which they localize, via dipolar interactions and in dependence on their concentration. The result is a change in signal intensity so enhancing the image contrast. This is the only effect that can be observed, because CAs are not directly visualized in the image.

Depending on the nature of the contrast agents as well as the applied magnetic field, they are able to decrease both T_1 and T_2 to different extents.[60b] CAs can thus be classified into two general categories; positive, those that predominantly reduce T_1, and negative, those that only mostly affect T_2.[64] The choice of the proper CA is generally oriented towards the positives, in order to obtain an intense signal in short times, since the percentage change in longitudinal relaxation rate in tissue is much greater than that in the transverse.[60b, 64]

Ranging from Fe^{3+} oxide nanoparticles to metal complexes of Mn^{2+}, Eu^{2+} and Gd^{3+}, many different types of CA have been investigated.

Gadolinium based contrast agents have been found to be the most useful ones. Due to its seven unpaired electrons combined with the ability of decreasing T_1 and T_2 by roughly similar amounts, that allows the best visualization mapping T_1-weighted images, Gd^{3+} ions induce the largest effect in signal enhancement.[60b, 63] Furthermore, there is another important electronic reason that explains such well

performing behavior. Gd^{3+} has a symmetric ground state electronic structure and couples a large magnetic moment with a long electron spin relaxation time. A much slower electronic relaxation rate makes Gd^{3+} electrons more closely in tune with water proton frequency, so that they can feel much better the effect of ions that gives rise to relaxivity.[60b, 65]

Despite all the advantages of Gd^{3+} application in MRI, this cannot be injected as free ion, due to its high toxicity even at low doses (10-20 μmol Kg^{-1}).[64] Indeed, having a size approximating Ca^{2+} but with a higher charge, it can favorably displace endogenous calcium ion and block its binding sites, leading to inhibition of peptides and enzymes functions and disruption of Ca^{2+}-required signaling.[60b, 63, 65-66]

For the exposed reasons, Gd^{3+}-based contrast agents have to be finely designed and developed in order to meet stability, non-toxicity and specific tissue localization requirements. The efforts for reaching those targets and making such CA of effective diagnostic value produced an active research area that joined together chemical, physical, and biological sciences and brought them into diagnostic medicine.

Nowadays, it is known that it is necessary to use ion organic ligands that tightly bind a single gadolinium ion forming very stable chelates with the lanthanide.[64, 66] If the proper ligands are chosen, they remain chelated to the metal ion that is kind of buried in a molecular cage with no chance to bind to donor groups in proteins and enzymes.[60b] Hence, the complex can be viewed as an inert species that acts as an intact drug molecule.[60b]

The most stable complexes have been developed exploiting the high affinity shown by Gd^{3+} towards cyclic or linear polyaminocarboxylate ligands, in which nitrogen and oxygen donor

atoms are the binding sites that coordinate the metal center.[63-64] **Figure 3.1** shows the six complexes approved as CAs for clinical use. Gd-DTPA (Magnevist® **3.1**, **Figure 3.1**) was the first MRI-CA to have been commercially available and opened the way to the design and synthesis of several derivatives.[63-64]

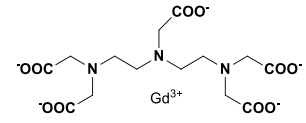

Gd-DTPA **3.1**
Magnevist®: Schering AG, Germany

Gd-DOTA **3.2**
Dotarem®: Guerbet SA, France

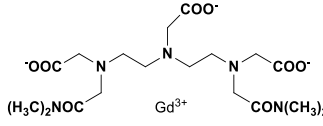

Gd-DTPA-BMA **3.3**
Omniscan®: GE Health, USA

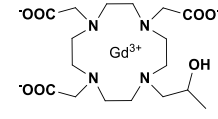

Gd-HPDO3A **3.4**
Prohance®: Bracco Imaging, Italy

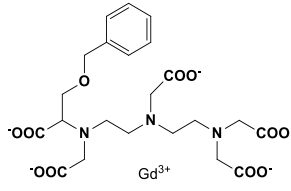

Gd-BOPTA **3.5**
Multihance®: Bracco Imaging, Italy

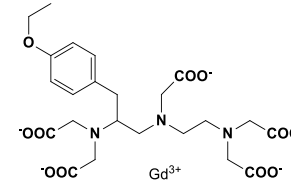

Gd-EOB-DTPA **3.6**
Eovist®: Schering AG, Germany

Figure 3.1. Gd^{3+}-based MRI contrast agents currently used in the clinical practice.

The cyclic analogue of DTPA ligand is DOTA, whose Gd^{3+} complex was commercialized as Dotarem® (**3.2**, **Figure 3.1**) right after the diffusion of Magnevist®.

Later, two new neutral complexes became soon available; Gd-DTPA-BMA (Omniscan®, GE Health, USA) and Gd-HPDO3A (Prohance®, Bracco Imaging, Italy) (**3.3** and **3.4**, **Figure 3.1**).

The feature that joins **3.1**-**3.4** is their high hydrophilicity that blocks the access to the cells.[60b] After administration *via* intravascular injection, these compounds equilibrate quickly between plasma and interstitial spaces (spaces between cells) across the walls of capillaries, to be finally excreted from the kidney with half-lives of about 1.6 h. [63]

With the aim of altering the pharmacokinetics and the biodistribution of these CAs, designed as specifically targeted agents, an aromatic substituent was introduced on the carbon backbone of the DTPA ligand, so generating two new derivatives; Gd-EOB-DTPA (Eovist, Schering AG, Germany) and Gd-BOPTA (Multihance®, Bracco Imaging, Italy) (**3.5** and **3.6**, **Figure 3.1**).[64] Those are able to target the hepatobiliary system and act as a liver imaging agent for the indication and evaluation of hepatic lesions.[63]

A common feature to all of these commercially available Gd-based MRI-contrast agents is the choice of ligands, that consist of 8 donor atoms.[63, 66] Such design allows the chelate to leave an open coordination site just for one water molecule that will directly interact with the 9-coordinate gadolinium ion in the inner-sphere.[63, 66] In the second sphere, there will be the water molecules hydrogen-bonded to the ligand, while all the others comprise the outer sphere and the solvent, called bulk water. The fast exchange between the inner-sphere water molecule and the bulk water affect the relaxation process of all protons present in the region in which the CA distributes and contributes to increase the observed longitudinal relaxation rate.

The advantageous electronic features that make Gd^{3+} the metal of choice for the synthesis and application of MRI-CA are complemented by another property, ideal for fast water exchange; the ionic radius.[63] Being in the middle of the 4f row of the periodic table, it can easily fluctuate between higher coordination numbers (9), typical for the early lanthanides, and lower coordination numbers (8), as for the late lanthanides. Moreover, the hindrance of the chosen ligand can also influence the water exchange and so the relaxation process.

Detailed studies on the ligand features led to the design and synthesis of a number of them, able to wrap around Gd^{3+} yielding kinetically and thermodynamically stable chelates *in vivo* that induce dramatic variation of the water proton relaxation rates, thus providing innovative probes for MRI applications.

3.2 Aim Of The Work: Gadolinium-Binding Cyclic Hexapeptoids: Synthesis And Relaxometric Properties.

3.2.1 Introduction

The chemistry of Gadolinium complexes is a rapidly growing field of research, motivated by the extraordinary fascinating properties of these compounds as potential contrast agents for MRI investigations. This interest has led to the synthesis of several example of Gd^{3+} complexes characterized by the presence of a variety of functionalized scaffolds or nanoparticles.[58c] Ranging from dendrimers,[67] polymers,[68] and supramolecular aggregates,[69] to peptides,[58a, 58e, 70] peptidomimetics,[19c, 71] lipids,[58d] sugars[72] and proteins,[73] all of them containing stabilized Gd^{3+} ions, multiple environments have been studied to find optimization of the relaxivity

and unique applications in medical diagnosis. More specifically, the last ones were mainly conjugated to Gd^{3+} chelates, comprising polyaminopolycarboxylate ligands, as vectors to deliver the contrast agent to the targeting sites, so increasing their specificity.

Based on the original DOTA and DTPA frameworks for chelation, and on the natural Ca-binding proteins that commonly present a loop made by 12 amino acids bearing side chains with oxygen donors, innovative systems have emerged as effective Gd^{3+} ligands.

A huge work with peptides has prompted interesting structures able to stably encapsulate the ion and dramatically increase relaxivity.

Interesting examples are the *de novo* designed gadolinium metallopeptides **3.7** and **3.8** showed in **Figure 3.2**.

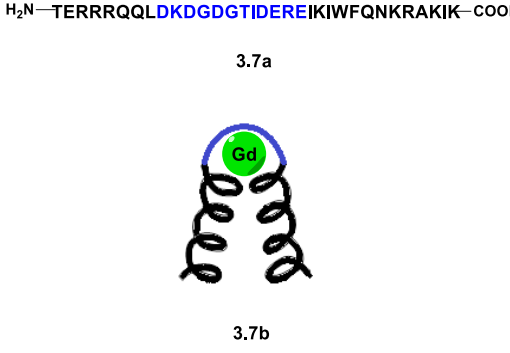

Figure 3.2. 3.7A. Sequence of P3W, with Gd-binding site highlighted in blue;[70b] **3.7B**. Folded structure of metallopeptide with Gd-chelate embedded within the binding moiety;[70b] **3.8**. Schematic representation of the cyclodecapeptide PA. Only the side chains of the aspartic and glutamic acids have been represented.[70a]

3.7 (**Figure 3.2**) is the 33-mer peptide called P3W, featured by a helix-turn-helix structure; α-helicity is found to increase the Gd^{3+} binding.[70b]

3.8 (**Figure 3.2**) is a new cyclodecapeptide that acts as a tetrapodal ligand. It incorporates two prolylglycine sequences as β-

turn inducers and two aspartic acids and glutamic acids with acidic carboxyl side chains for cation complexation. The ligand is preorganized, with the four carboxyl groups oriented on the upper face to coordinate the Gd^{3+} ions.

Peptides have been most widely used for building effective MRI contrast agents. However, they suffer from enzymatic degradation by protease and peptidase activity, hence being poorly biostable and bioavailable *in vivo.*

To overcome this problem, recently peptidomimetics have gained interest in such research field due to their higher stability with respect to their parent peptides.[74]

Peptoids are slowly emerging as supporting ligands in the complexation of Gd^{3+}, and the few examples in the literature show that they can either act as transporter systems[71a] or target specific moiety,[71b] either as chelating agents.[19c]

Our group contributed to the development of peptoid-based MRI probes introducing the gadolinium-binding cyclic hexapeptoid **3.9** showed in **Figure 3.3.**[19c]

The molecular design chosen for the ligand was dictated by several factors that we thought could positively influence the complexation of Gd^{3+}.

Cyclic peptoids demonstrated to be preorganized and flexible enough to selective complex different metal ions depending on the size of their cavity. Hexameric structures showed the highest affinity towards Na^{+} cation,[17, 19a, 19b, 19d] therefore, considering the comparable ionic radii of sodium (1.02 Å) and gadolinium (0.94 Å), we envisioned a stable Gd-coordination by the proposed cyclic hexapeptoid. Furthermore, water soluble and polar carboxylic acid side chains were incorporated into the peptoid backbone given their well-known Gd^{3+} complexing ability.

The strong enhancement of water proton longitudinal relaxation upon Gd^{3+} coordination by **3.9**, revealed its useful properties as contrast agent and its potential application in MRI. Such chelate also represents the first example of water soluble Gd-coordinating hexadentated cyclopeptoid.

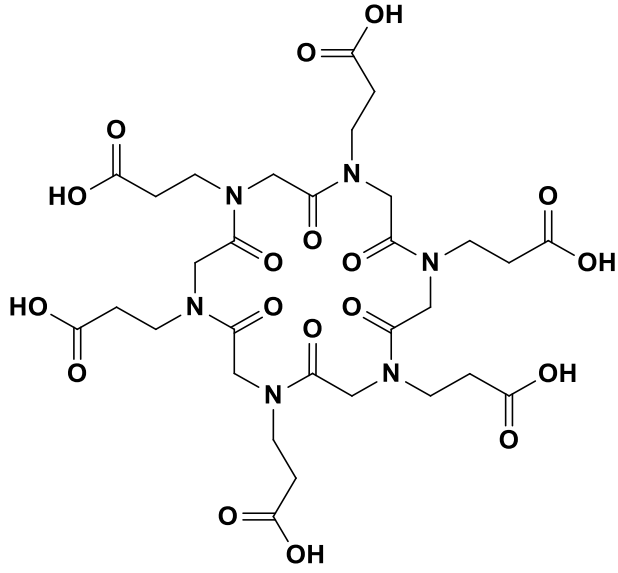

3.9

Figure 3.3. Structure of cyclic hexapeptoid with six carboxyl side chains.

Fascinated and encouraged by those results, we designed two more cyclic hexapeptoids (**3.10** and **3.11**, **Figure 3.4**), differing in the chemical composition of the side chains and the backbone.

Our aim was to study how the decoration of the carbon backbone core could affect the Gd-binding abilities and the longitudinal relaxation rate of water protons.

In the design of both compounds **3.10** and **3.11**, we decided to keep three carboxyl functionalities and to alternate them with three methoxyethyl amine and three proline residues respectively. The

ether-bearing arms alter the polarity and the content of oxygen in the ligand **3.10** so, given the high Gd^{3+} oxophilicity, they could influence the complexation process. The proline units in the ligand **3.11**, on the other hand, were thought to favor the chelate formation with Gd^{3+}, due to the enanced selectivity, observed for cyclopeptoids containing proline units,[19d] to coordinate Na^{+} cation.

The outcome of the following experiments will tell us the role exerted by the side chains, also providing a deeper understanding of the overall complexation process.

With the aim of expanding the vast platform of peptoids and giving new insights into their not-so-far explored applications as MRI-probes, we successfully synthesized cyclic hexapeptoids **3.10** and **3.11**.

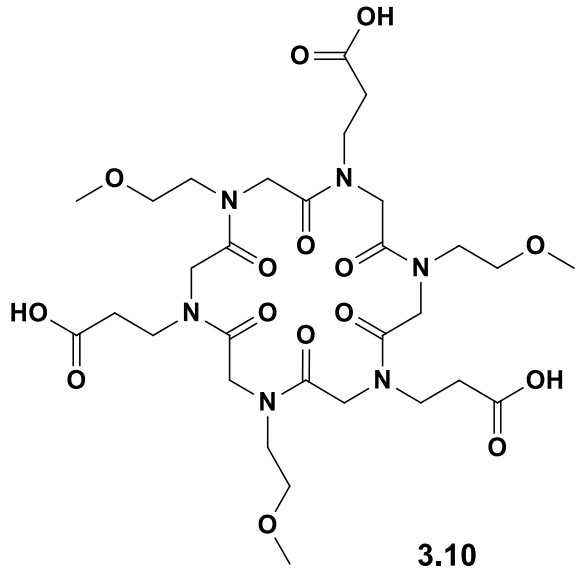

3.10

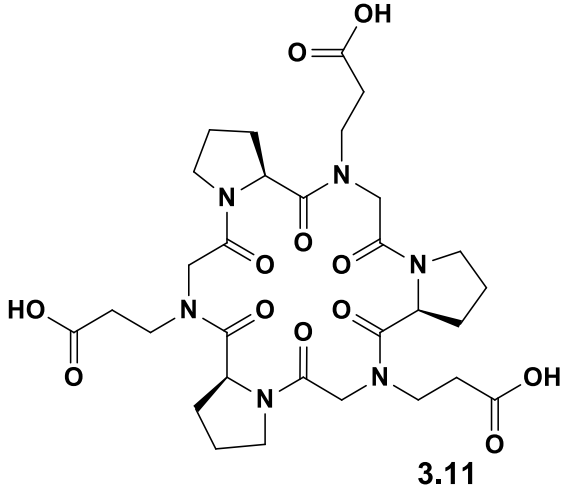

3.11

Figure 3.4. Structures of the cyclic hexapeptoids **3.10** and **3.11**.

3.2.2 Results And Discussion

Cyclic peptoids **3.10** and **3.11** were synthesized on solid-phase through two different methods. The synthetic strategy applied for **3.10** was the mixed "submonomer/monomer" approach, whereas **3.11** was obtained *via* the monomeric one.

The common feature was the introduction of three carboxyl arms, accomplished by the coupling of the *N*-fluorenylmethoxycarbonyl,*N*'-carboxymethyl-β-alanine *t*-butyl ester building block **3.15**.

This was easily synthesized in solution through two different synthetic procedures.

Our first attempt was to reproduce a well-known method that we previously used in the synthesis of **3.9** (**Figure 3.3**). As shown in the **Scheme 3.1**, this consisted in two main steps.

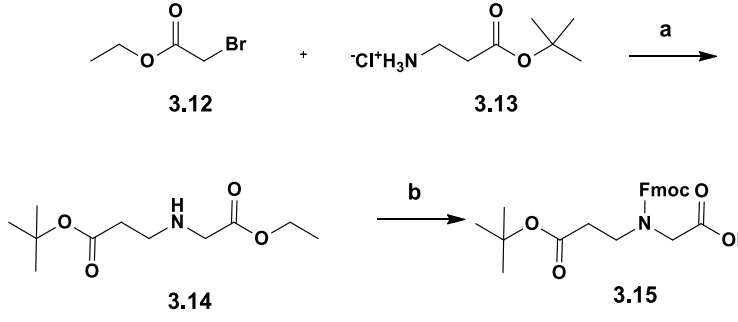

Scheme 3. 1. Synthesis of *N*-fluorenylmethoxycarbonyl,*N'*-carboxymethyl-β-alanine *t*-butyl ester **3.15**. Regents and conditions; (**a**) DIPEA, dry DMF, 18 h, r.t.; (**b**) i) LiOH, H_2O/1,4-dioxane (1:1), 0 °C, 3h; ii) $NaHCO_3$, Fmoc-Cl, r.t., 18 h, 57%, three steps.

First, we performed the *N*-alkylation of the β-alanine *t*-butyl ester hydrochloride **3.13** with ethyl bromoacetate **3.12** in the presence of DIPEA. Then, compound **3.14** underwent the one-pot hydrolysis of the ethyl ester and protection of the amino group with 9-fluorenylmethoxycarbonyl chloride (Fmoc-Cl) to yield the desired

building-block **3.15**. This was incorporated on solid-phase after flash chromatography purification on silica gel.

The need of a second procedure was due to the mismatch of this method with the scale-up of the building-block **3.15**. When 10 g of β-alanine *t*-butyl ester hydrochloride **3.13** were used, the step of hydrolysis dramatically failed, as revealed by ^{1}H-NMR that still showed the ethyl group pattern. Hence, we thought to protect the carboxylic acid as methyl ester, which requires milder conditions for removal.

The development of the new synthetic strategy started with the study of a known facile method for the *N*-alkylation of various glycines *via* aza-Michael addition with acrylate derivatives[75]. This is reported as an effective route to the alkylation of several amino acids and, in our case, avoided the use of the expensive β-alanine *t*-butyl ester hydrochloride **3.13**.

Scheme 3.2 shows the synthetic procedure for the scale-up to 5.0 g of *N*-fluorenylmethoxycarbonyl,*N*'-carboxymethyl-β-alanine *t*-butyl ester building block **3.15**.

Starting with the glycine methyl ester hydrochloride **3.16**, this was first treated with sodium carbonate in a mixture of H_2O/brine in order to obtain the methyl glycinate **3.17**. That was a very delicate step, since **3.17** is relatively volatile. Indeed, this was extracted with DCM that was then just in part evaporated under controlled pressure. ^{1}H-NMR signals integration provided the amount of product obtained, so it could undergo the next step. Methyl glycinate **3.17** was added to *t*-butyl acrylate **3.18** in the aza-Michael reaction, and then **3.19** was efficiently demethylated and protected on the amino group as Fmoc-derivative. The modified procedure for the synthesis of *N*-fluorenylmethoxycarbonyl,*N*'-carboxymethyl-β-alanine t-butyl ester **3.15** perfectly suited the needs for the scale-up. **3.15** was purified by

flash chromatography on silica gel and then used for the solid phase synthesis of the two oligomers **3.10** and **3.11**.

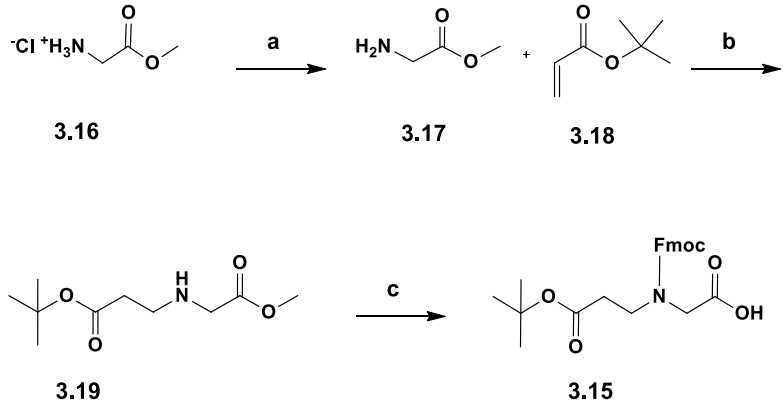

Scheme 3. 2. Scale-up synthesis of *N*-fluorenylmethoxycarbonyl,*N'*-carboxymethyl-β-alanine *t*-butyl ester **3.15**. Regents and conditions; (**a**) Na_2CO_3 8% in H_2O/brine; (**b**) MeOH, *o.n*, 50°C; (**c**) i) LiOH, H_2O/1,4-dioxane (1:1), 0 °C, 3h; ii) $NaHCO_3$, Fmoc-Cl, r.t., 18 h, 46%, three steps.

The on-resin oligomerization was accomplished through a mixed "submonomer/monomer" and a "monomer" approach, giving the linear *N*-*t*-butoxycarbonylethyl/*N*-methoxyethyl glycine oligomer **3.20** and *N*-*t*-butoxycarbonylethyl/*N*-prolyl glycine oligomer **3.21** (**Figure 3.5**).

The overall oligomerization process on solid-phase is illustrated in **Scheme 3.3.**

The building-block **3.15** was loaded on the solid support 2-chlorotrityl chloride resin **3.22**, and the unreacted sites were capped with a solution of DCM/MeOH/DIPEA to avoid the growth of shorter oligomers. The Fmoc protecting group was removed under basic conditions, and the coupling of the free amine was accomplished in

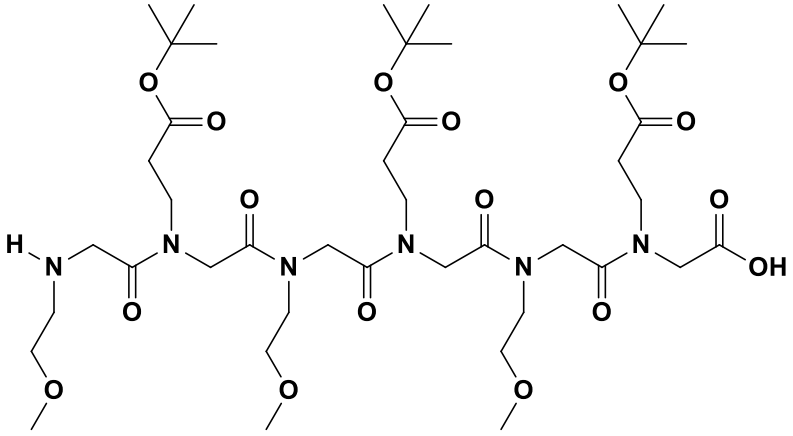

3.20

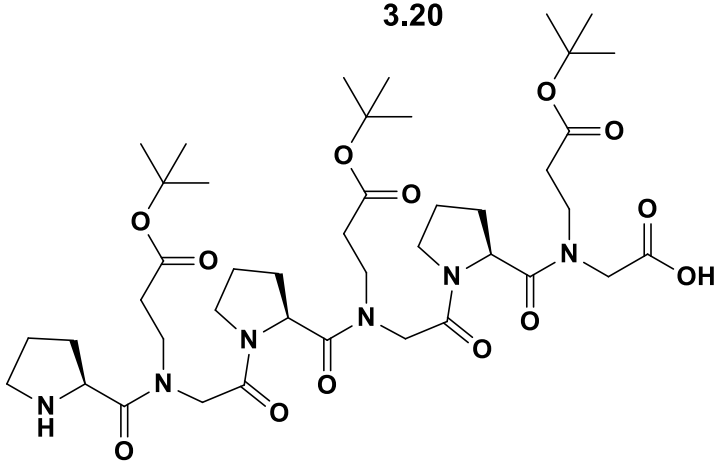

3.21

Figure 3. 5. Linear precursors **3.20** and **3.21**.

the presence of DIC for the bromoacetic acid or HATU/DIPEA for the proline residue, with average coupling yields >98%.

In the submonomeric approach the subsequent step was the displacement with methoxyethylamine, hence the formation of the *N*-alkylated glycine on solid-phase (left side of **Scheme 3.3**). On the other hand, the monomeric approach required the deprotection of the

amine group to set it free for the next coupling (right side of **Scheme 3.3**). This allowed us to install the building-block **3.15** in both the growing chains through the assistance of HATU. The cycles of deprotection/coupling/amination/coupling (submonomeric approach) and deprotection/coupling (monomeric approach) were reiterated until the desired length of the peptoids was reached (n = 3). The linear peptoids **3.20** and **3.21** were then cleaved from the resin under acidic conditions and utilized in the next step without further purification.

3.20 and **3.21** were efficiently cyclized under high dilution conditions ($3.0 \cdot 10^{-3}$ M) in the presence of HATU to give the protected cyclic peptoids **3.24** and **3.25** (**Figure 3.6**) in good yields (purity >85%, RP-HPLC analysis). The cyclic hexapeptoid **3.24** was purified by flash chromatography on demetallated silica gel, in order to avoid undesired complexations with the cations present in the common silica gel, whereas **3.25** was purified by C_{18} semi-preparative RP-HPLC.

The protected cyclic precursors were then liberated by the *t*-butyl groups with trifluoroacetic acid and *m*-cresol, as cation scavenger, to afford the target compounds **3.10** and **3.11**.

The complexity of the r.t. ^{1}H-NMR spectrum recorded for the cyclic precursors **3.24** and **3.25** and the target compounds **3.10** and **3.11** demonstrated the slow equilibrium of multiple conformations on the NMR time scale. Spectroscopic studies were performed in order to establish their Na^+ cation propensities (as a prelude to the studies on their Gd-binding properties).

The addition of an excess amount of sodium picrate to solution of **3.24**, **3.25**, **3.10** and **3.11,** induced the formation of complexes with remarkably simplified ^{1}H-NMR spectra.

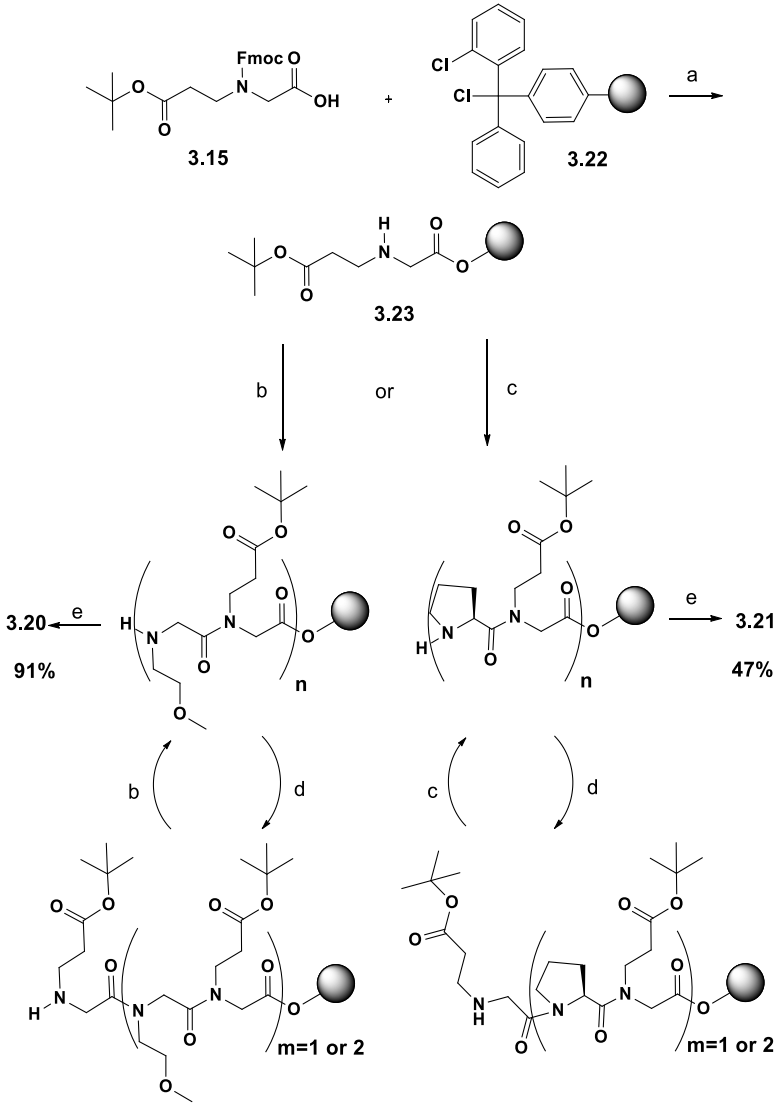

Scheme 3. 3. Solid-phase synthesis of **3.20** and **3.21**. Reagents and conditions; (**a**) i) DIPEA in dry DCM, 1.5 h; ii) DCM/MeOH/DIPEA (17:2:1), 15 min; iii) Piperidine 20% in DMF; (**b**) i) bromoacetic acid/DIC (10:11 equiv.) in dry DMF, 40 min; ii) methoxyethylamine (10 equiv.) in dry DMF, 30 min; (**c**) i) Fmoc-Pro-OH/HATU/DIPEA (4:4:8 equiv.) in dry DMF, 1 h Pro^2, 2 h Pro^4 and Pro^6; ii) Piperidine 20% in DMF; (**d**) i) **3.15**/HATU/DIPEA (4:4:8 equiv.) in dry DMF, 1 h; ii) Piperidine 20% in DMF; (**e**) HFIP 20% in dry DCM (2 x 30 min).

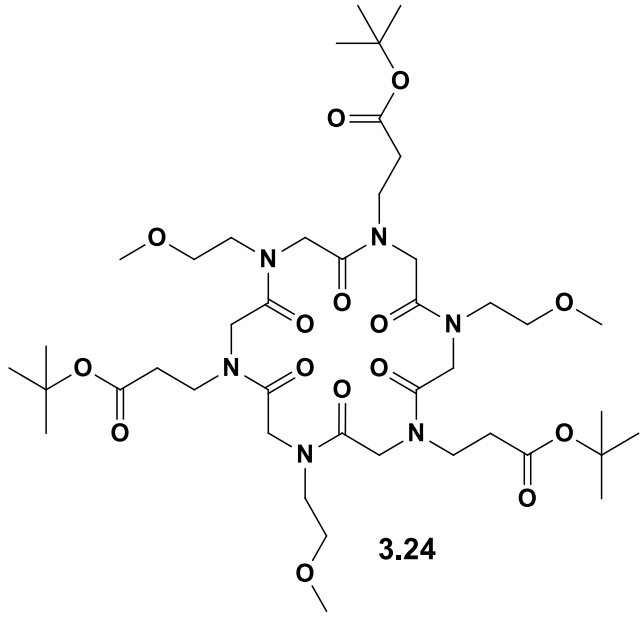

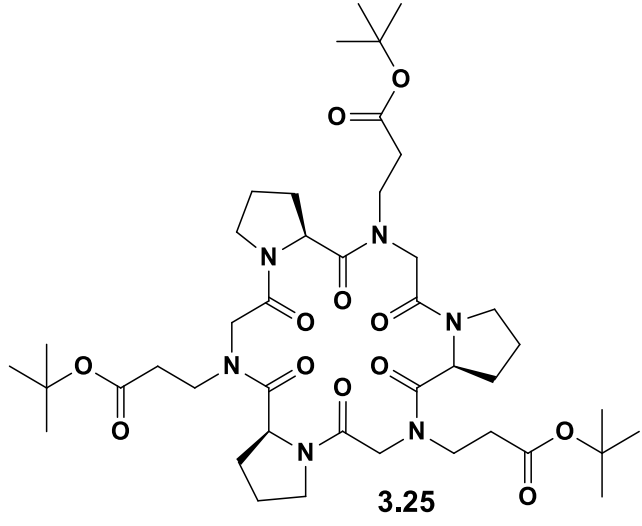

Figure 3. 6. Structures of cyclic precursors **3.24** and **3.25.**

Figure 3.7 and **3.8** show a comparison between the free forms and the Na-complexes of **3.24** and **3.10** respectively, through their ^{1}H-NMR spectra.

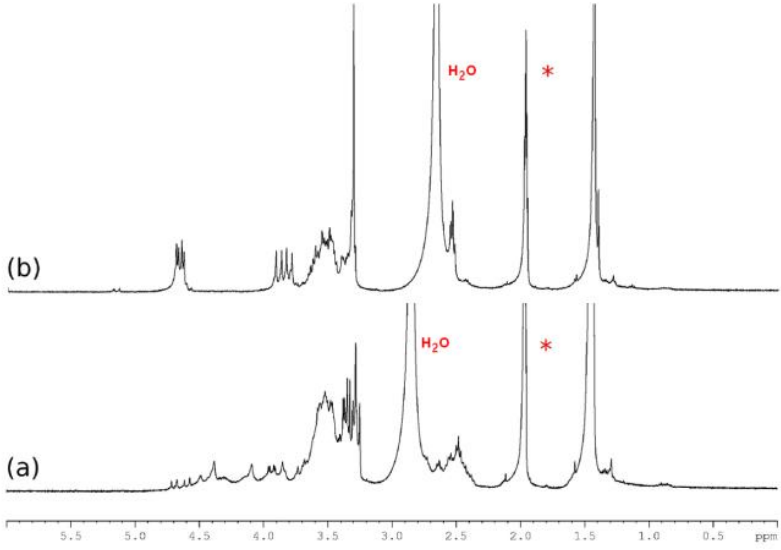

Figure 3. 7. ^{1}H-NMR spectra of free **3.24** (**a**) ($CD_3CN/CDCl_3$ 9:1 solution, [24]=4.0 mM, 400.13 MHz) and (**b**) in the presence of 6.0 eq. of sodium picrate. Residual solvent peaks are labelled with *.

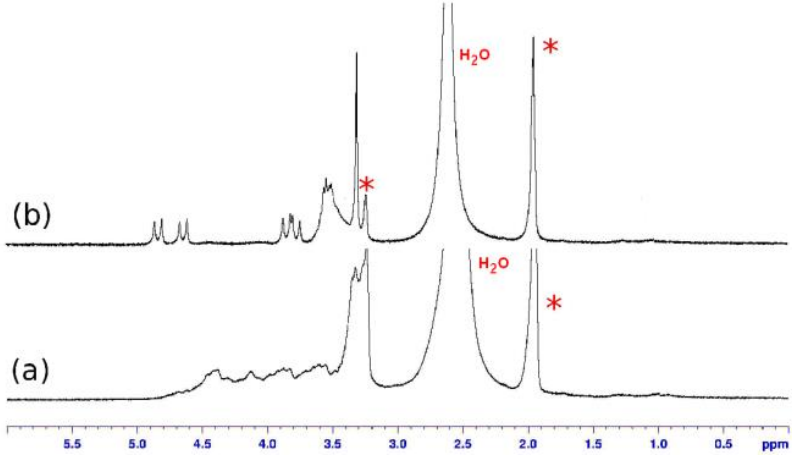

Figure 3. 8. ^{1}H-NMR spectra of free **3.10** (**a**) ($CD_3CN/CDCl_3$ 9:1 solution, [10]=4.0 mM, 400.13 MHz) and (**b**) in the presence of 6.0 eq. of sodium picrate. Residual solvent peaks are labelled with *.

The same information is given in **Figure 3.9** and **3.10** for **3.25** and **3.11** respectively. In particular, it was evident the formation of 3-fold symmetric species for all the complexes.

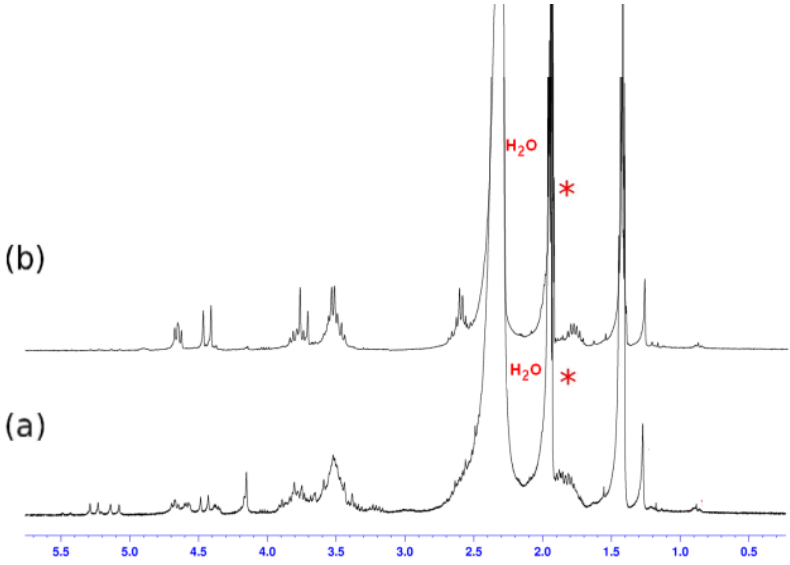

Figure 3. 9. ^{1}H-NMR spectra of free **3.25** (**a**) ($CD_3CN/CDCl_3$ 9:1 solution, [25]=4.0 mM, 400.13 MHz) and (**b**) in the presence of 6.0 eq. of sodium picrate. Residual solvent peaks are labelled with *.

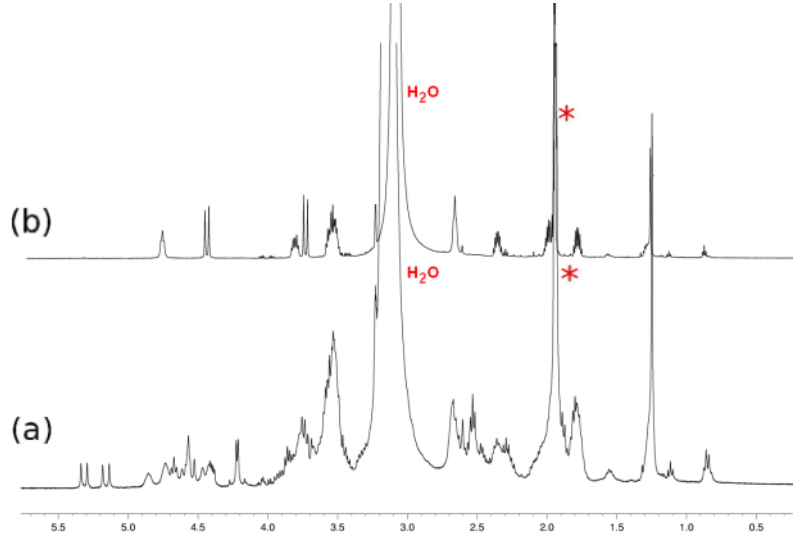

Figure 3. 10. ^{1}H-NMR spectra of free **3.11** (**a**) ($CD_3CN/CDCl_3$ 9:1 solution, [11]=4.0 mM, 400.13 MHz) and (**b**) in the presence of 6.0 eq. of sodium picrate. Residual solvent peaks are labelled with *.

The next steps were the formation of Gd^{3+} chelates and the characterization of their possible relaxometric properties, performed by Dott. Gianolio at the University of Turin.

Structural and dynamic information on the Gd^{3+} complexes can be obtained from relaxometric studies on their aqueous solutions. Such investigation consists in the measurement of water proton relaxation times, since those depend on the interaction of water molecules in the inner and outer coordination sphere of the paramagnetic Gd^{3+} complexes. For these reason, the observed relaxation enhancement of the bulk water protons is directly correlated to structural and dynamic properties of the Gd^{3+} complexes.

To start this study, first it was evaluated the complex formation through the relaxometric titration of a given quantity of ligand with increasing amounts of $GdCl_3$.

Surprisingly, the cyclic peptoid **3.11** did not show complexation ability towards Gd^{3+}. This result was unexpected and disappointing and made us doubting also about the properties of the cyclic peptoid **3.10**. Luckily, this resulted to effectively chelate the Gd^{3+} ion. Hence, it was possible to follow the formation of the complex by measuring the observed relaxation rate ($R_1^{obs}=1/T_1^{obs}$) at 20 MHz (Proton Larmor Frequency) and 25°C, of solutions of ligand **3.10** as a function of increasing concentrations of added $GdCl_3$ (**Figure 3.11**). A straight line is obtained which slope is the relaxivity (r_{1p}) of the readily formed Gd-**3.10** complex (equation 1):

$$R_1^{obs} = R_{1W} + r_{1p}\,[\text{Gd-CP}] \qquad (1)$$

Where R_{1W} is the diamagnetic contribution of pure water (0.38).

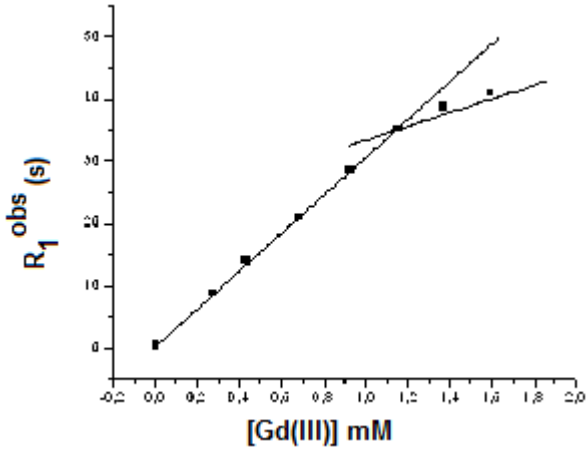

Figure 3. 11. Relaxometric titration of ligand **3.10** with Gd^{3+} ion (20 MHz, 25°C, neutral pH).

After the ligand saturation point, when the added $Gd^{3+}$is in excess with respect to the ligand, the slope of the line changes to follow the relaxivity of the free Gd^{3+} aqua ion (r_{1p}=12.98 $mM^{-1}s^{-1}$ at 20 MHz and 25°C). From this experiment, relaxivity value of 27.2 $mM^{-1}s^{-1}$ was determined for Gd-**3.10**. Such parameter is proportional to the efficiency of the paramagnetic complex acting as relaxation agent. The extracted value is significantly higher than those reported for the commercially available Gd^{3+} complexes, that range between 4 and 6 $mM^{-1}s^{-1}$.

The next experiment was performed in order to estimate the stability constant for the Gd-**3.10** complex. This consisted in a relaxometric procedure measuring the observed relaxation rate of Gd-**3.10** solution, upon addition of increasing concentration of EDTA. EDTA is a Gd^{3+} ligand with a known K_f (5.01×10^{17}) and competes with **3.10** for the complexation. Indeed, there was a decrease in the observed relaxation rate due to the transfer of the Gd^{3+} ion from ligand **3.10** to EDTA ligand (**Figure 3.12**). By knowing the stability constant of Gd-EDTA and the relaxivities of the Gd-complexes (Gd-

3.10 and Gd-EDTA) it is possible to fit these experimental data in order to extract the value of the unknown K_f for Gd-**3.10**. The value found was $3.65\times10^{14}\pm1.04\times10^{14}$.

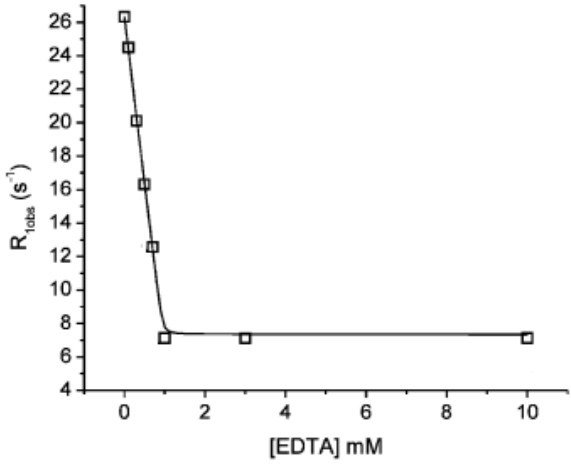

Figure 3.12. Variation of the observed longitudinal relaxation rate of solutions of Gd-**3.10 (**0.954 mM) as a function of the addition of increasing concentrations of EDTA. Measures were carried out at 25°C, 20 MHz and neutral pH.

Furthermore, we measured how the relaxivity changed when a magnetic field, varying over a range corresponding to proton Larmor frequencies, was applied. Reporting the relaxivity values as a function of the proton Larmor frequencies on a logarithmic scale, we obtained a profile called NMRD (nuclear magnetic relaxation dispersion) (**Figure 3.13**).

Table 3.1 shows all the parameters involved in the relaxation processes, and they were extracted by fitting of the experimental data with the equations that describe the paramagnetic relaxation theory; the Solomon-Bloembergen-Morgan equations. The values of the parameters involved in the electronic relaxation (Δ^2 and τ_v) are very similar to those reported for the Gd^{3+} complexes.

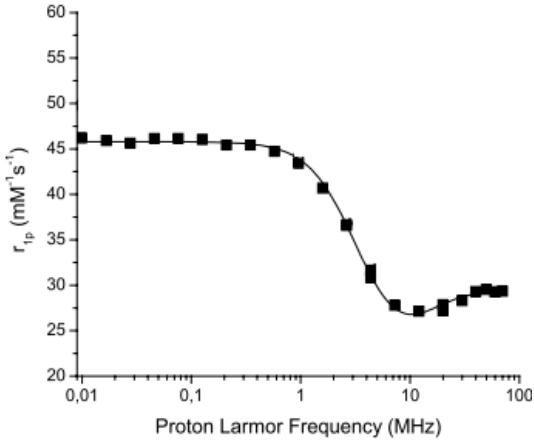

Figure 3. 13. *1/T_1* NMRD profiles of Gd-**10,** recorded at 25 °C in PBS buffer (pH 7.4). The data refer to 1 mM concentration of the paramagnetic complex.

The value of the reorientational correlation time (τ_R) depend on the volumetric and dimensional features of the chelates; the bigger the system, the slower the reorientation. Increased relaxivity in the magnetic fields in the range of 20-60 MHz are caused by slowed reorientational motion.

Finally, the values obtained for q and q_{ass} account for the coordination of water in the chelate. Three molecules are directly coordinated to the Gd^{3+} ion in the inner sphere and fifteen in the second sphere, proximal to the ion through hydrogen bonds.

It is worth noting that Gd-**3.10** showed the same value of q and the other determinants of the observed relaxivities of cyclopeptoid **3.9** (**Figure 3.3**).[19c] Our aim was to highlight the role of the side chains in the formation of the chelate, and giving a better understanding of the parameters that can affect the process of chelation.

	Δ^2 (s^{-2})[b]	τ_v[c]	τ_R[d]	τ_m[e] (s)	q[f]	q_{ass}[g]
Gd-**10**	$2.7x10^{19}$	22.5	22.6	$1x10^{-8}$	3	15

Table 3.1. Main relaxometric parameters derived from fitting of NMRD profiles reported in Figure 3.13. [a]

[a] On carrying out the fitting procedure, some parameters were fixed to reasonable values; rGd-H (distance between Gd and protons of the inner sphere water molecule)=3.1 Å; a (distance of minimum approach of solvent water molecules to Gd ion)=3.8 Å; D (solvent diffusion coefficient)=$2.2x10^{-5}cm^2s^{-1}$. [b] Squared mean transient zero-field splitting (ZFS) energy. [c] Correlation time for the collision-related modulation of the ZFS Hamiltonian. [d] Reorientational correlation time. [e] Exchange life-time of the coordinated water molecule (fixed). [f] Number of inner sphere water molecules. [g] Number of second sphere water molecules.

The results obtained are extremely exciting, suggesting that the two ligands, **3.9** and **3.10**, coordinate the metal in a similar way. Hence, we can state that the arms of cyclopeptoid do not seem to be involved in the binding process, since they are not part of the coordination sphere of Gd^{3+}. The six oxygen atoms from the six endocyclic carbonyl groups are the ones thought to capture the oxophilic Gd^{3+} in a TTP geometry (tricapped trigonal prismatic) that leaves three binding site for three molecules of water, which complete the 9-coordination.

The rationale behind Gd^{3+} complexation from cyclic peptoids herein proposed is also in line with the result obtained for the compound **3.11**: the need of all the oxygen donors from the inner cavity implies a huge flexibility of the peptoidic backbone, so they could catch Gd^{3+} ion respecting its preferred coordination geometry.

It has been demonstrated that cyclic peptoids comprising proline residues are more constrained than the others are, since proline favours the *cis* geometry of the amide bond, reducing the conformational freedom typical of the peptoids. The degree of preorganization induced by proline residues in the cyclic peptoids

could advantage the coordination of Na^+ ion, but it is evident that this is not the case of Gd^{3+}. The structure of **3.11** is too rigid to attain the conformation ideal for Gd^{3+} chelation.

3.3 CONCLUSION

Intrigued by the several properties and applications of cyclopeptoids, we proposed two new structures, **3.10** and **3.11**, for the production of next generation MRI contrast agents.

Studying an almost unexplored field for peptoids, we envisioned the chelation of Gd^{3+} *via* such innovative ligands, in order to enhance the relaxation rate of water protons and hence the MRI signal.

Experiments on the Gd^{3+} binding affinity and relaxometric properties of the complexes not only revealed their behavior and potential application in the clinical practice, but also shed light on the factors playing in the chelation process.

The high activity showed by **3.10** was comparable to the result obtained for the compound **3.9**, which differs in the chemical composition of the side chains. On the other hand, the more rigid **3.11** did not display Gd^{3+} coordination. It seems that a crucial factor in the formation of the metallocyclopeptoid in the presence of Gd^{3+} is the flexibility of the backbone.

The research and development of safe and specific contrast media is always increasing, with the ultimate goal of enhancing the power of MRI even further, getting rid of painful, invasive procedures for the benefit and wellness of the patients.

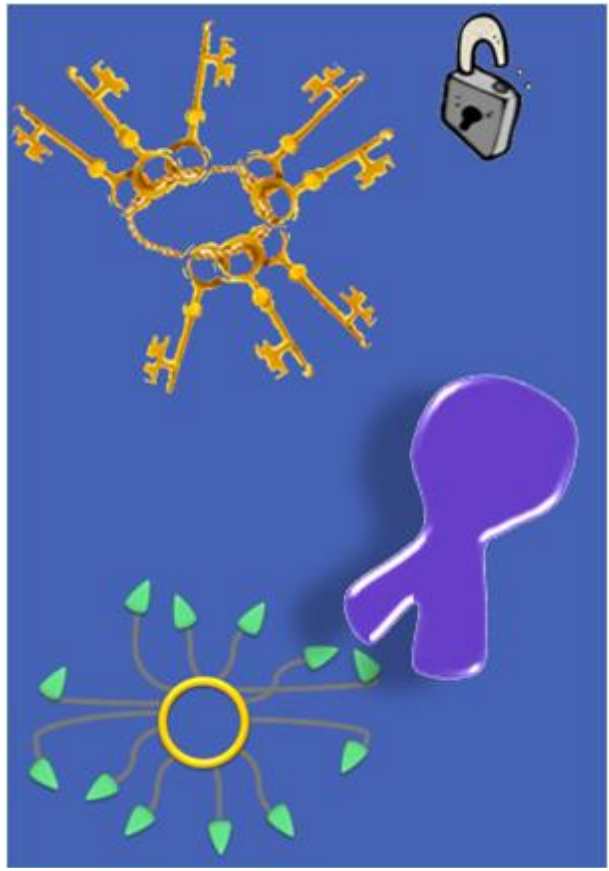

CHAPTER 4

Synthesis And Inhibitory Activity Evaluation Of The First Example Of Cyclopeptoid-Based Iminosugar Click-Clusters

4

4.1 INTRODUCTION

Glycoconjugates play fundamental roles in the cell physiology and are pivotal metabolites in health and disease states.[76] For that reason, the enzymes involved in the biosynthesis and degradation of glycosidic bonds have gained increasing attention.[77]

Intracellular glycosyltransferases and glycosidases, act in a very precise and controlled fashion, with specificity directed towards each of the different sugar linkages and functions depending on their intracellular compartmentalization.[76a, 77-78]

Once glycosylation patterns are altered, the normal expression, metabolism and functions of the organisms can be permanently altered.[76a, 77] Lysosomal storage diseases (LSDs),[78a] type II diabetes,[76a] bacterial and viral infections,[76a] immune responses[76a] as well as metastasis of tumor cells[76a, 77-78] are all related to structure modifications of the carbohydrates of glycoconjugates and so to the activity of defective glycosidases.

A proper control of glycosidases activities could be a way to restore their normal catalytic behavior and so could represent a potential treatment of carbohydrate-related diseases.[76a, 77] This could be achieved by the application of small agents able to bind at glycosidases catalytic site and act as glycosidases inhibitors.

4.1.1 Glycosidases Inhibitors

X-ray crystal structures of carbohydrates-glycosidases complexes provided mechanistic insights into glycosidic bond hydrolysis.[76b, 79] Crystallographic studies indicated the existence of a short-lived transition state possessing substantial oxocarbenium

character (**Figure 4.1**).[79b, 80] Under these conditions, the substrate is distorted from its typical chair conformation and the anomeric carbon possesses trigonal character.

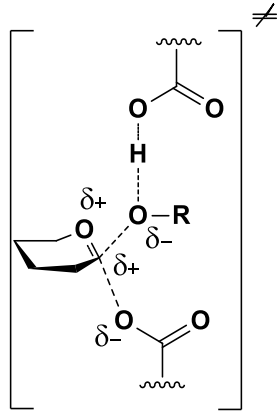

Figure 4. 1. Transition state of enzymatic hydrolysis of glycosidases.

A good glycosidases inhibitor shows the highest affinity for the enzyme and, according to Pauling postulate, this is likely to mimic the structure of the transition state.[81]

This hint led to the generation of therapeutically valuable inhibitors, designed incorporating one or more features, such as charge or geometry, which resemble the ones from the transition state.

Alongside with chemically synthesized sugar mimics, many natural occurring products have been isolated, inhibiting glycosidases and sometimes showing therapeutic potential.[76a, 77, 80] Nojirimycin (NJ, **4.1**, **Figure 4.2**) was the first natural sugar mimic to have been isolated from *Streptomyces* strains in 1966.[82] NJ is an iminosugar, also called azasugar, a cyclic sugar where a nitrogen atom has replaced the ring oxygen atom. Its structural studies led to the synthesis of the derivative deoxynojirimycin (DNJ, **4.2**, **Figure 4.2**), later shown to occur naturally.[83]

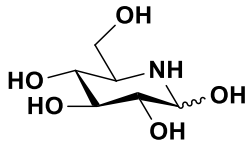

NJ, **4.1**

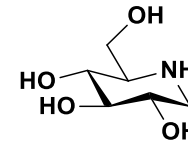

DNJ, **4.2**

Figure 4. 2. Structures of iminosugars NJ (**4.1**) and DNJ (**4.2**)

As a result, iminosugars were further investigated for the treatment of carbohydrates-related diseases. The structures of NJ and DNJ served as templates for the design and synthesis of different glycoside derivatives as promising candidates in glycosidases inhibition.

A growing number of natural and unnatural analogues of these compounds have been reported and some of them emerged on the market as powerful drugs. Glyset®, the *N*-hydroxyethyl-1-deoxynojirimycin (**4.3**, **Figure 4.3**), is in use for the treatment of type II diabetes.[84] Zavesca®, the analog possessing an *N*-butyl group (**4.4**, **Figure 4.3**), has already been approved to tackle the symptoms of type I Gaucher disease[85] and is under evaluation in clinical trials for cystic fibrosis.[86]

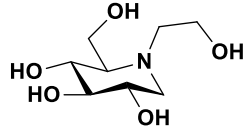

Glyset®, Pfizer, **4.3**

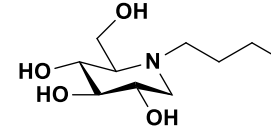

Zavesca®, Actelion, **4.4**

Figure 4. 3. Structures of Glyset (**4.3**), and Zavesca (**4.4**).

Gaucher disease is the most severe lysosomal-storage disorder (LSD) and it is caused by a deficiency of glucosylceramide β-glucosidase, also called β-glucocerebrosidase, (GCase), the enzyme responsible for glucosylceramide (GlcCer) hydrolysis to

release ceramide and glucose.[87] The mutant GCase results in a misfolded structure, which does not pass the “quality control” mechanism of the endoplasmic reticulum, being partially or completely disrupted in there. This mechanism leads to an accumulation of undegraded (GlcCer) in lysosomes, leading to symptoms such as bone pains, skeletal lesions, anemia, liver or spleen damage.[88]

Aware of the onset of Gaucher disease, scientists developed three different therapeutic approaches in the last twenty years.

The first successful treatment was the enzyme replacement therapy (ERT), consisting in the administration of a recombinant form of GCase.[89] However, the drawbacks of ERT are the high cost and the availability just for non-neurophatic type 1-Gaucher disease. Recently, two novel strategies arose in this field: the substrate reduction therapy (SRT) and the pharmacological chaperone therapy (PCT).[90] In SRT, inhibitors of GlcCer synthase reduce the synthesis of glycosphingolipids to decrease their influx into the lysosomes. Zavesca® (**4.4**, **Figure 4.3**) is an implementation of this therapy being the first oral treatment for a lysosomal disease. Despite its efficacy, large doses are required, which led to side effects, such as abdominal pain, and its use is recommended only for adults with type1 Gaucher disease. In this context, PCT emerged as a promising therapeutic option. The concept at the basis of PCT is that competitive GCse inhibitors are capable to restore the catalytic activity of the defective enzymes. When binding the active site, they alter or stabilize the three-dimensional architecture of misfolded mutant enzymes and so induce their proper conformation. This prevents their degradation in the ER and allows trafficking to lysosomes, where GCse will exert their normal activity. Hence, PCT benefits of specificity, targeting directly the cause of LSDs, and of a

small-molecule-based approach, that implies oral bioavailability and the potential to cross the blood-brain-barrier.

Cystic fibrosis is not a LDS but rather a genetic disease. However, it is related to a mutant protein, the Phe508del-cystic fibrosis transmembrane conductance regulator (CFTR), degraded by the ER quality control. The result is a reduced chloride and sodium transport across membranes that in the lungs generates dehydration and abnormal formation of thick mucus.[91] *N*-Bu DNJ is among those small molecules demonstrated to act as CFTR correctors by overcoming the processing defect of the mutant protein, hence of interest in pharmacological therapy as alternative to heart or lung transplantation, which to date is the only cure available for CF.[86, 92]

4.1.2 Multivalent Effect

Despite many efforts, to date just few rational design criteria are available for improving the chaperon activity of a potent PC and no clue is known for the design of CFTR correctors as well. Consequently, more studies must be done in order to achieve sufficient levels of residual cellular activity enhancement and shed light on the mechanism of action of PC and iminosugar-based CFTR correctors.

Since 1999, an intense research activity on iminosugar derivatives has enriched the field of glycoscience thanks to the group of Prof. Compain.[93] Compain and coworkers are investigating new therapeutic approaches for Gaucher disease as well as for cystic fibrosis.

With the aim of identifying new CFTR correctors[94] and overcoming the obstacles to therapeutic application of pharmacological chaperones, getting closer to species displaying

enhanced activity, Compain's group recently investigated the potential of multivalency.[95]

Multivalency is a common concept in glycoscience, since many recognition events are mediated by the interaction between a receptor and a matching ligand present in multiple copies on a central scaffold. For example, multimeric carbohydrate-binding proteins, such as lectins, show affinity enhancement on a valence-corrected basis, when matching with multivalent ligands. This binding mechanism is known as clustering and the consequent binding potency enhancement is the multivalent effect.[96]

At first glance, this approach might look odd applied to glycosidases, since these enzymes usually possess a single substrate-binding site. Indeed, the effect of multivalency on glycosidases inhibition does not involve clustering but rather statistical rebinding. This mechanism can be explained in terms of a bunch of keys opening one lock.[95] The "bunch" of iminosugars provides a high local ligand concentration that should favor the recapture mechanism by the glycosidase. An additional sliding mechanism of iminosugar in the enzyme active site guarantees an increasing of the life-time of the multivalent ligand–enzyme complex, thereby leading to higher binding affinities.

It is worth noting that the biological activity of the multivalent ligand depends not only on the moiety that binds the receptor, but also on the scaffold.[95] This is relevant since it influences the overall architecture of the multivalent system, defining its shape, orientation, flexibility, size, and valency; hence its mechanism of action.

To understand which structural features could have a significant effect on the biological activity and so how to design synthetic multivalent ligands, our group has entered the field of

glycoscience examining the role of several scaffolds on the multivalent effect.

4.2 AIM OF THE WORK: SYNTHESIS OF THE FIRST EXAMPLE OF IMINOSUGAR-CYCLOPEPTOID CLICK-CLUSTERS

4.2.1. Introduction

Enzyme inhibition is an emerging approach in the treatment of carbohydrate-related diseases and multivalency is gaining growing interest for enhancing the inhibition potency of weak or poorly selective inhibitors.

In parallel, the synthetic methodology for generating multivalent inhibitors is also rapidly expanding. The most valuable approach is the use of click-chemistry that allows a facile and rapid functionalization of the central scaffold with the selected ligand. The clicking bioconjugation technique has enabled the preparation of several multivalent inhibitors, subsequently submitted to the biological evaluation of their activity.

The proof-of-concept of multivalent effect from multivalent inhibitors has been demonstrated, ranging from modest to high values depending on the scaffold features.

Figure 4.4 shows the structures of iminosugar clusters that gave the best results and inspired our work.

The dodecavalent DNJ cluster **4.5**, based on a compact spherical fullerene C_{60} building block, led for the first time to strong affinity enhancements of the inhibitory potency for Jack bean α-mannosidase, approximately 2150-fold relative to the corresponding monomer.[97] Right afterwards, β-cyclodextrin-based DNJ clusters were evaluated against Jack bean α-mannosidase.[98] Increasing

either the valency (21) either the linker alkyl chain length (C_9) enabled to reach the highest multivalent effect, as found for **4.8**, which had 9900-fold enhancement compared to the monovalent iminsugars. Tetravalent click-clusters based on porphyrin (**4.9**)[99] and calix[4]arene (**4.10** and **4.11**) with the same linker length (C_3) and ligand motif (DNJ) were also studied.[108] Their comparison provided the opportunity to evaluate the binding properties of multivalent systems with different scaffolds but identical valency and linker length.

In this context, the results obtained pointed out the importance of the spatial ligand orientation and the rigidity of the central scaffold, given the higher multivalent effect obtained with the rigid porphirine core (800-fold enhancement relative to the corresponding monomer against 20-fold and 267-fold for **4.10** and **4.11** respectively).

Regarding the study of multivalency on CFTR correction activity enhancement, significant results were obtained for the trivalent iminosugars **4.12** and **4.13**, providing the first evidence of multivalent effect as therapeutic potential in cystic fibrosis.[94] The compound with the longest spacer arm (C_9) demonstrated to have an EC_{50} value of 0.5 μM, hence to be up to 1000-fold stronger than the monovalent model (EC_{50} = 458 μM) and 225-fold more potent than the clinical candidate *N*-Bu DNJ (EC_{50} = 112 μM). Being a submicromolar CFTR corrector, it points out that a lower valency highly enhances the CFTR correction activity.

With these features in mind, we envisioned a new class of iminosugar clusters showing ascending valences and diverse spatial ligand orientation. It is worth to note that such systems should also possess the properties desired for biological application.

Hence, our attention was directed to cyclic peptoids, which appeared as the optimal scaffolds for the design and synthesis of innovative iminosugar clusters with improved performances.

Peptoids are easy to prepare and benefit of enhanced proteolytic stability and cellular up-take over the parent peptides.[2] Due to these advantages, they have been widely applied for the synthesis of molecules of biological interest, also entering the field of glycoscience as candidates for new therapeutics.[100] However, just few example of cyclic peptoids have been reported in such context and no iminosugar-cyclopeptoid cluster has ever been described before.[101]

Our aim is to further explore the application of cyclic peptoids for building potentially bioactive glycoconjugates, and to evaluate the role of the scaffold architecture on multivalent effect, highlighting the structure-activity relationship and unveiling the secret for reaching the highest multivalent effect.

Hence, herein we report the first example of cyclopeptoid-based iminosugar click-clusters.

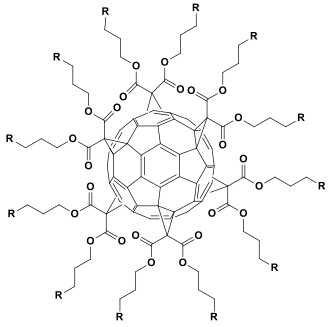

4.5, n=6

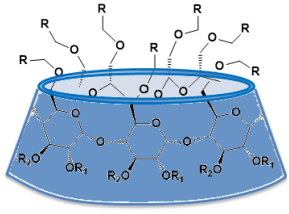

7-valent clusters **14-valent clusters**

4.6a, R_1=R_2=Me, n=6 **4.7a**, R_1=CH_2R, R_2=H, n=6
4.6b, R_1=R_2=Me, n=9 **4.7b**, R_1=CH_2R, R_2=H, n=9

21-valent cluster

4.8, R_1=R_2=Me, R=R_3

R= 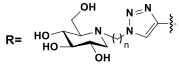

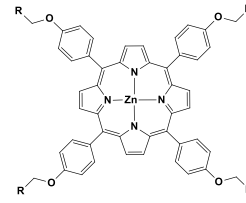

4.9, n=3

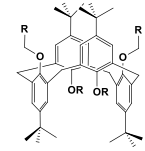

4.10, n=3

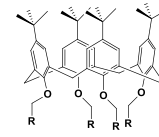

4.11, n=3

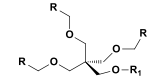

4.12, R_1=H, n=6 **4.14**, R_1=R, n=6
4.13, R_1=H, n=9 **4.15**, R_1=R, n=9

R_3= 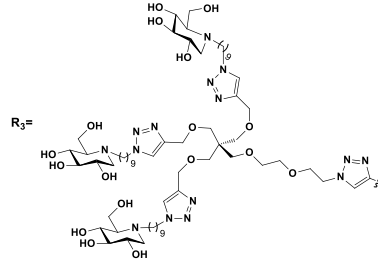

Figure 4. 4. Structures of iminosugar clusters active towards Jack bean α-mannosidase (**4.5**-**4.11**) and Phe508del-CFTR (**4.12**-**4.15**).

4.2.2. Results and Discussions

The assembly of the multivalent glycoconjugates was performed by using a convergent approach. This involved the attachment of azido-functionalized carbohydrates DNJ onto the cyclic peptoid scaffolds through copper(I)-catalyzed azide-alkyne cycloaddition reaction (CuAAC).[102] The choice of DNJ as peripheral ligand is due to its own inhibitory activity and therapeutic value; the majority of the glycoclusters reported in the literature is indeed decorated with DNJ binding motifs. This also means that conjugating the same carbohydrate probes to the cyclic peptoids could allow a comparison with the other systems already described.

The synthesis started with the assembly of the cyclic peptoids. These were designed with appended propargyl groups, which make them “clickable” to undergo the click chemistry with the azido-DNJ derivatives.[103]

The library of the scaffolds synthesized is showed in **Figure 4.5**.

The linear precursors were obtained by the efficient solid phase sub-monomer approach elaborated by Zuckerman *et al.* for the preparation of peptoids.[2] This method allowed for the rapid synthesis of various oligomers of valences ranging from two up to sixteen. **Scheme 4.1** shows the synthetic strategy, relying on the use of 2-chlorotrityl chloride resin as solid support on which the peptoid chain was elongated. In the first step, bromoacetic acid (**4.25**) was loaded onto a 2-CTC (**4.26**) through an ester linkage. Each monomer was then built directly on the resin through a two-step sequence that was iteratively repeated until the desired oligomer length was reached. Amination with suitable primary amines displaced the bromine and installed the desired *N*-alkyl side chain. We introduced *N*-propargyl amines for the synthesis of the scaffolds all

propargylated (**4.17**-**4.24**, **Figure 4.5**) and *N*-propargyl amines alternated with *N*-methoxyehtyl amines for the divalent one (**4.16**, **Figure 4.5**). Once on solid phase, the free amine was coupled with bromoacetic acid with the assistance of *N,N*-diisopropylcarbodiimide (DIC). The reactions of amination and acylation were carried out in the presence of an excess of reagents (10 equivalents) and accomplished in 30 and 40 min respectively. The success of each coupling step was confirmed *via* the colorimetric analysis of chloranil test and the growing of the peptoidic chain was monitored by means of HPLC-ESI of the crude products upon mini-cleavage. After the completion of the synthesis, the oligomers were cleaved from the resin using a 20% solution of hexafluoroisopropanol (HFIP) in DCM.

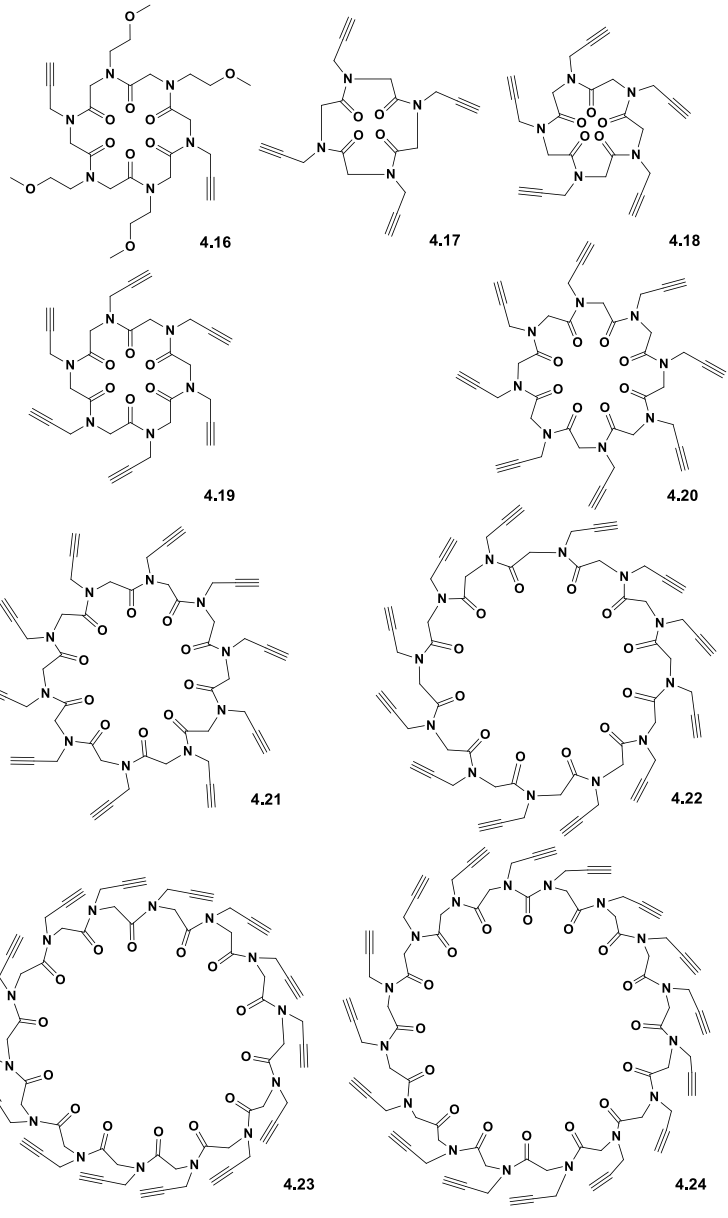

Figure 4. 5. Library of cyclopeptoid scaffolds **4.16**-**4.24**.

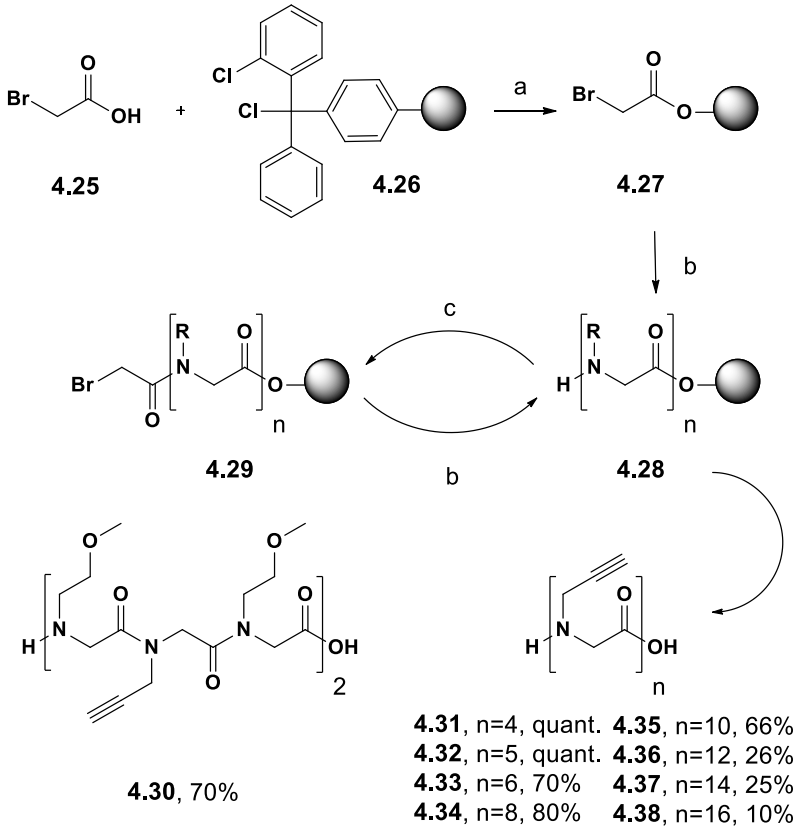

Scheme 4. 1. Sub-monomer approach for the synthesis of precursors of cyclopeptoids **4.16-4.24**: (**a**) DIPEA, in dry DCM, 1.5h; (**b**) propargylamine or methoxyethyl amine when needed (10 equiv) in dry DMF, 30 min; (**c**) bromoacetic acid/DIC (10:11 equiv.) in dry DMF, 40 min; (**d**) HFIP 20% in dry DCM (2 x 30 min).

N-substituted glycine oligomers comprising 4 to 16 monomers were synthesized manually in high to good yield and crude purity, estimated by analytical reversed-phase HPLC, to range from 95% to 60% largely depending upon oligomer length (**Figure 4.6**, **Table 4.1**). The preparation of longer structured molecules logically presents some synthetic challenges.[104] The coupling efficiency tends to decrease slightly at the increasing of the chain length due to conformational and solubility issues.

Peptoid oligomer	Oligomer length	Purity %
4.30	6	>95
4.31	4	>95
4.32	5	>95
4.33	6	>95
4.34	8	82
4.35	10	72
4.36	12	70
4.37	14	65
4.38	16	60

Table 4. 1. Purity of crude products **4.30-4.38** determined by analytical RP-HPLC.

However, the submonomer approach is a useful and powerful method to overcome such drawbacks and to access longer oligomers in good purity.[2]

Without further purifications, all linear products underwent head-to-tail cyclization in solution. Under high dilution conditions (3.0×10^{-3} M) and in the presence of the efficient coupling agent HATU, macrocyclization proceeded smoothly to give the cyclic compounds **4.16**-**4.24**. Furthermore, a syringe pump[105] was used to slowly add the linear peptoide precursor and so avoiding the side reactions of dimerization or cyclodimerization that may accompany the

cyclization of peptoids. After purification, compounds **4.16**-**4.24** were recovered in 31%, 35%, 20%, 31%, 32%, 12%, 10%, 8%, 5% overall yield respectively.

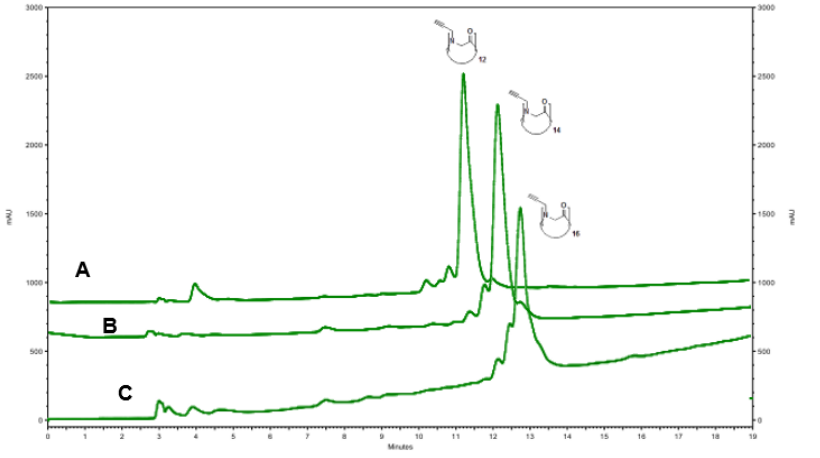

Figure 4. 6. Analytical HPLC traces of crude peptoid synthesis products: trace **A**, 12-mer **4.36**; trace **B**, 14-mer **4.37**; and trace **C**, 16-mer **4.38**. Traces **A** and **B** are vertically offset for clarity.

All the cyclic oligomers, except the tetramer **4.17**, showed complex room temperature ^{1}H-NMR spectra, suggesting the contemporary presence of several conformers in slow exchange on the NMR time scale. Cyclotetrapeptoid **4.17** provided simplified NMR spectra with two independent resonance peak patterns both in the ^{1}H- and in the ^{13}C-NMR spectra. This result invokes the presence of a center of symmetry in the molecule and a *ctct* amide sequence as indicated by the values Δδ of diastereotopic intra-annular proton doublets: Δδ (a) 1.67 ppm, (b) 0.07 ppm, respectively (**Figure 4.7**). Such well-defined shape and the rigid conformation of the amide backbone structure are in agreement with the other cyclotetrapeptoids described in the literature.[14, 16-17]

Furthermore, it is worth to note that the big size rings are so flexible that from 4- to 16-mer cyclopeptoids, ^{1}H-NMR peaks broaden

progressively. Hence, the spectra from 10- to 16-mer cyclopeptoids yielded three broad patterns belonging to the alkynyl protons, around 2.5 ppm, and the methylene units, either from the side chains either from the backbone, that overlap in the region between 4.6 and 4.0 ppm (**Figure 4.8** and **4.9**).

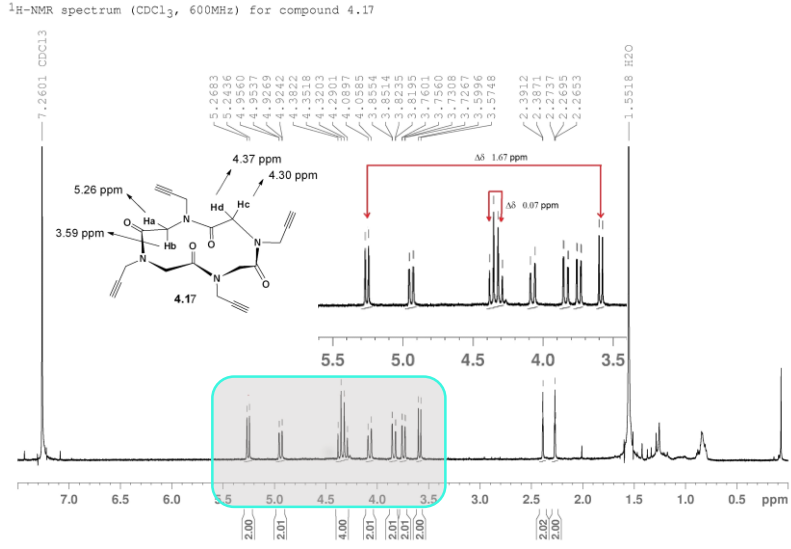

Figure 4. 7. [1]H-NMR for compound **4.17**.

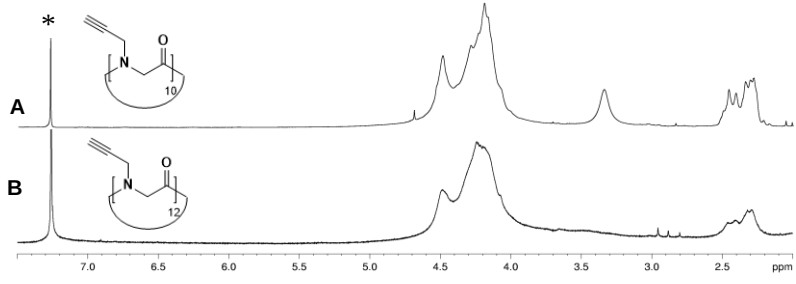

Figure 4. 8. Zoom in [1]H-NMR spectrum of: (**A**) compound **4.35** (400 MHz, $CDCl_3$) and (**B**) **4.36** (300 MHz, $CDCl_3$). * Residual solvent peak for $CDCl_3$.

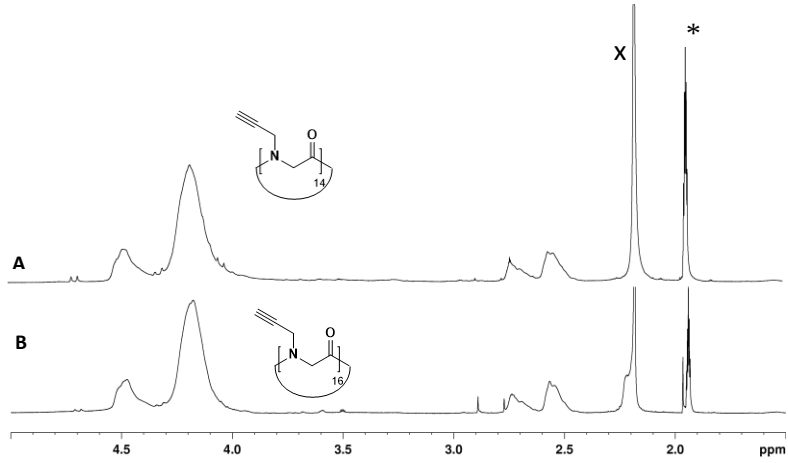

Figure 4. 9. Partial ^{1}H-NMR spectrum of (**A**) compound **4.37** (600 MHz, CD_3CN) and (**B**) **4.38** (600 MHz, CD_3CN). * Residual solvent peak for CD_3CN, X for H_2O.

With the platform of clickable cyclic peptoids in our hands, we were ready to perform the functionalization with *N*-alkyl derivatives of DNJ.

This last synthetic stage and the evaluation of the inhibitory activity were carried out in collaboration with the group of Prof. Compain at the University of Strasbourg.

I have been visiting his laboratory in Strasbourg for a short period, to take part in the preparation of the azide-armed *N*-hexyl and *N*-nonyl DNJ ligands and the DNJ-clusters based on compounds **4.19**.

The synthetic strategy applied was the one recently developed and optimized by Compain and coworkers.[94, 98, 106] The first step was the synthesis of the peracetylated azide-armed *N*-hexyl and *N*-nonyl DNJ derivatives **4.43a** and **4.43b** from the preformed **4.41** (**Scheme 4.2**).[97] First, the azidobromoalkanes **4.40** were obtained through the nucleophilic substitution with sodium azide on the dibromoalkanes **4.39**.

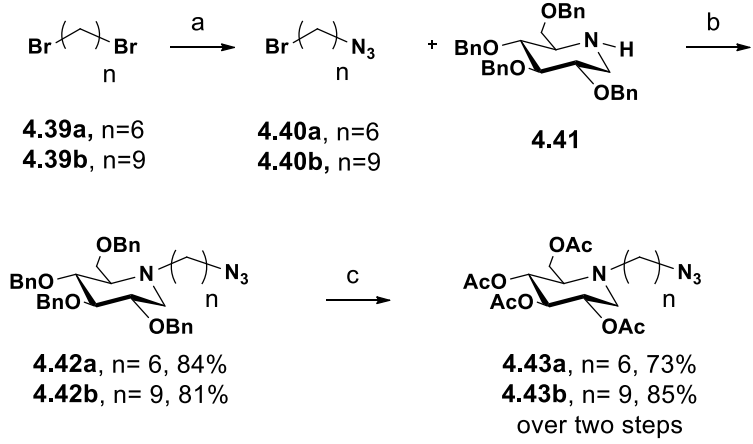

Scheme 4. 2. Synthesis of *N*-alkyl DNJ **4.43a** and **4.43b**. Reagents and conditions: (**a**) NaN_3, DMSO, overnight; (**b**) K_2CO_3, CH_3CN, MW, 150°C; (**c**) **i**. BCl_3, CH_2Cl_2, -60°C to 0°C; **ii**. Ac_2O, pyridine, DMAP cat.

The crude compounds were purified on flash chromatography, to remove the undesired dialkylation side products, and the pure azidobromoalkanes were thus dissolved in acetonitrile with the iminosugars **4.41.** The resulting solution was heated in a microwave reactor at 150°C for 4 h, giving the expected products **4.42** in yields up to 81%. The microwave-assisted alkylation of the rather unreactive endocyclic amine **4.41** is a huge improvement with respect to the method previously reported and allows for much better yields.[98a] The way to the synthesis of the peracetylated iminosugars required the selective cleavage of the benzyl protecting groups affording the azidopiperidinols, which were readily peracetylated to provide compounds **4.43**.

At this stage of synthesis, we were ready to perform the multiconjugaton reaction that enabled the attachment of peracetylated azido iminosugars **4.43** onto polyalkyne scaffolds **4.16** and **4.19**-**4.21**[107] by microwave-assisted CuAAC reaction (**Scheme 4.3**). The desired DNJ clusters **4.44** and **4.46-4.48** were obtained in good to high yield, ranging from 69% to 95%.

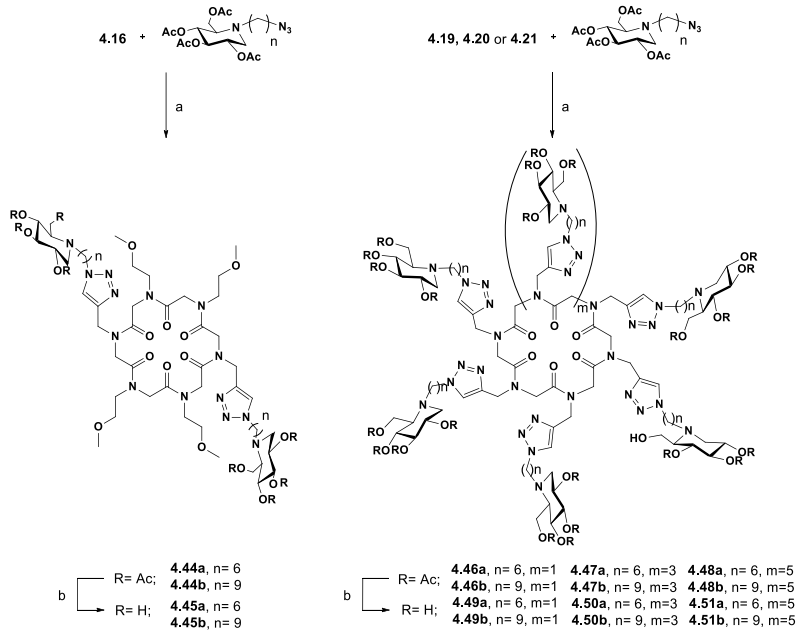

Scheme 4. 3. Synthesis of DNJ clusters **4.45** and **4.49-4.51**. Reagents and conditions: (**a**) $CuSO_4 \cdot 5H_2O$ cat., sodium ascorbate, DMF/H_2O (5:1), MW, 80 °C, 3 h; (**b**) Amberlite IRA 400 (OH^-), MeOH/H_2O (1:1), 40 °C. Overall yields from compounds **4.16** and **4.19**-**4.21**: **4.45a** 73%; **4.45b** 94%; **4.49a** 95%**; 4.49b** 83%; **4.50a** 69%; **4.50b** 80%; **4.51a** 70%; **4.51b** 80%.

^{1}H-NMR spectra recorded at room temperature for such compounds showed interesting pieces of information on their conformation in solution. The hexavalent and decavalent clusters **4.46** and **4.48** yielded complex NMR patterns, as a result of the simultaneous presence of several conformers in solution slowly equilibrating on the NMR time scale. This outcome is in agreement with the conformational disorder highlighted for the scaffolds and for other cyclic peptoids described in the literature. On the other hand, the octavalent clusters **4.47** showed simplified ^{1}H-NMR spectra. A possible explanation could be the chelation of Na^+ upon the CuAAC reaction in the presence of sodium ascorbate. Interestingly, the divalent clusters **4.44** presented just a partial conformational

disorder, as a sign of a predominant conformation in solution and the minor presence of exchanging conformers. Upon addition of excess of sodium picrate to **4.44a** and **4.46a**, the ^{1}H-NMR spectra showed the coalescence of signals, indicating that the metal chelation triggered the formation of a sodium complex with a 2-fold and 6-fold symmetry respectively (**Figure 4.10** and **4.11**).

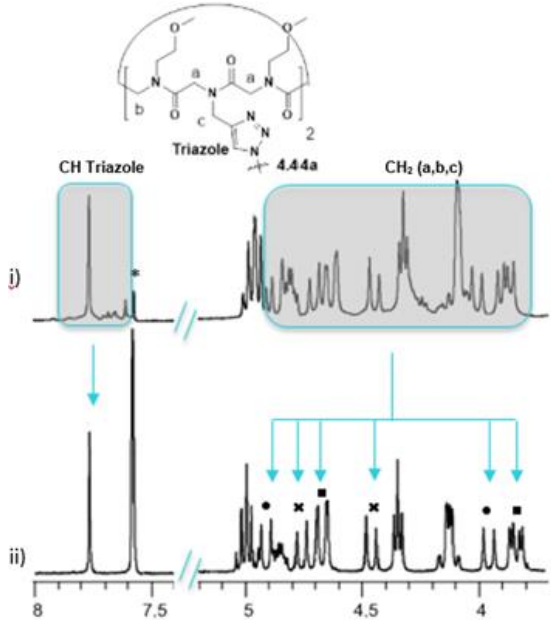

Figure 4. 10. i) Partial ^{1}H-NMR spectrum (400 MHz, $CD_3CN/CDCl_3$ 9:1) of compound **4.44a**; **ii**) Partial ^{1}H-NMR spectrum (400 MHz, $CD_3CN/CDCl_3$ 9:1) of compound **4.44a** with sodium picrate (11 equiv). * Residual solvent peak for $CDCl_3$. •, X and ■ are assigned to protons a or b or c.

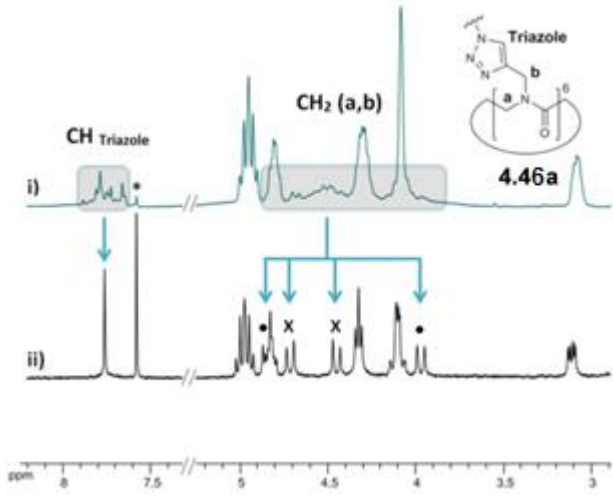

Figure 4. 11. i) Partial ^{1}H-NMR spectrum (400 MHz, $CD_3CN/CDCl_3$ 9:1) of compound **4.46a**; **ii**) Partial ^{1}H-NMR spectrum (400 MHz, $CD_3CN/CDCl_3$ 9:1) of compound **4.46a** with sodium picrate (11 equiv). * Residual solvent peak for $CDCl_3$. • and X are assigned to protons a or b.

Products **4.44** and **4.46-4.48** underwent the subsequent O-deacetylation on an anion exchange Amberlite IRA-400 (OH^-) resin, to afford the final deprotected iminosugar clusters **4.45** and **4.49**-**4.51** in quantitative yield (**Scheme 4.3**).

The eight cyclopeptoid-based iminosugar click-clusters underwent biological evaluation to address the importance of the scaffold architecture on multivalent effect for correcting protein-folding disorders such as Gaucher disease and cystic fibrosis.

The divalent compounds **4.45** were shipped to Dr. C. Norez lab where they were tested as CFTR correctors. Indeed, it has been demonstrated that the highest activity enhancement can be obtained with systems of lower valency.[94] Concentration-dependent correction by multivalent iminosugars was determined treating CFKM4 cells for 2 h with 100 µM of compounds. Then, Phe508del-CFTR activity was assessed with the iodide effluxes technique in the presence of a stimulating cocktail of CFTR activators made of forskoline (10 µM)

plus genistein (30 μM). The responses yielded the EC_{50} values reported in **Table 4.2**, together with the EC_{50} values for *N*-Bu DNJ (**4.4**, **Figure 4.3**), as a reference compound with regard to its therapeutic potential and their monovalent analogues, included as model controls (**4.52**, **Figure 4.12**).

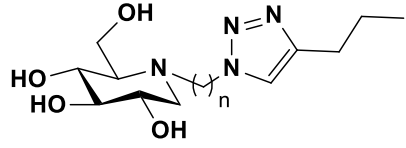

4.52a, n=6
4.52b, n=9

Figure 4. 12. Model control of monovalent iminosugars.

Entry	Iminosugar	Valency	Spacer lenght	EC_{50} [μM]
1	**4.4**[94]	**1**	**-**	**112**
2	**4.45a**	**2**	**C6**	**91**
3	**4.45b**	**2**	**C9**	**82**
4	**4.52a**[94]	**1**	**C6**	**12**
5	**4.52b**[94]	**1**	**C9**	**458**

Table 4. 2. Corrector efficiency for multivalent iminosugars and their monovalent analogues.

The divalent iminosugars (entries 2 and 3) were comparable to the clinical candidate *N*-Bu DNJ (entry 1) and the different alkyl spacer lengths C_6 and C_9 had no significant impact on EC_{50} values. Furthermore, the C_6-armed divalent iminosugar **4.45a** resulted

weaker than the corresponding monovalent model (entry 4) whereas, the compound with the longest spacer arm (C_9) **4.45b**, was slightly more efficient than its monovalent counterpart (entry 5). Even though the CFTR-correction gained with the trivalent iminosugar **4.12a** (**Figure 4.4**) are still the strongest, cyclopeptoid-based iminosugar click-clusters are anyway a step forward in the field of therapeutic treatment for cystic fibrosis. Indeed, they demonstrate that multivalency is an effective tool for enhancing CFTR-correction activity and such scaffolds are a valuable platform of compounds to explore the role of key structural parameters, such as valency, ligand topology, and alkyl spacer length, on the biological activity for the identification of molecules capable of rescue of functional CFTR in cystic fibrosis. New insights, more hints and a better understanding of the concept of multivalent design will come after the preparation and biological evaluation of the tetra and pentavalent iminosugar click-clusters based on cyclopeptoids **4.17** and **4.18** (**Figure 4.5**).

To further study the inhibitory multivalent effect of DNJ clusters to defective glycosidases of therapeutic interest, compounds **4.49**-**4.51** (**Scheme 4.3**) were subjected to inhibition assay by Prof. C. Tarnus in her lab in Mulhouse.[107]

Jack bean α-mannosidase was the enzyme against which the best multivalent effects in glycosidase inhibition were collected so far. Hence, to add one more piece to such intriguing puzzle, the hexa-, octa- and decavalent iminosugars were tested as inhibitors of such peculiar enzyme. **Table 4.3** reports the values of the constant inhibition K_i, which reflects the inhibitory activity of the multivalent cluster, the relative inhibition potency *rp*, which defines the inhibitory activity of the multivalent cluster with respect to the analogue monovalent model, so giving an idea of the enhancement of the inhibitory activity obtained, and the relative inhibition potency per

number of iminosugar units *rp/n*, which mathematically estabilishes the multivalent effect as a normalized parameter. The related monovalent controls **4.52** are also shown in the table for comparative purposes.

Entry	Iminosugar	Valency	Spacer Length	K_i [μM]	*rp*	rp/n
1	**4.49a**	**6**	**C6**	**65 ± 24**	**4.9**	**0.8**
2	**4.49b**	**6**	**C9**	**11 ± 1**	**17**	**2.8**
3	**4.50a**	**8**	**C6**	**21 ± 2**	**15**	**1.9**
4	**4.50b**	**8**	**C9**	**8 ± 3**	**23**	**2.9**
5	**4.51a**	**10**	**C6**	**15 ± 10**	**21**	**2.1**
6	**4.51b**	**10**	**C9**	**5 ± 1**	**38**	**3.8**
7	**4.52a**	**1**	**C6**	**322**	**-**	**-**
8	**4.52b**	**1**	**C9**	**188**	**-**	**-**

Table 4. 3. Relative inhibition potency, multivalent effect and inhibitory activity (Ki, μM) against jack bean α-mannosidase of cyclopeptoid-based clusters **4.49**-**4.51** and their monovalent control models **4.52**.

A careful analysis of the data reported in the table reveals that all the cyclopeptoids tested show a significant multivalent effect (*rp/n* > 1), a part from the hexavalent ligand bearing the C_6 alkyl spacer (entry 1). Furthermore, also in this case, the C_9 alkyl-armed DNJ clusters resulted in a higher inhibition potency, with the best performance being obtained with the decavalent ligand and the C_9 linker (entry 6, *rp/n* = 3.8). Despite the encouraging activities found for such compounds, they are still less potent than the clusters based

on β-cyclodextrins. Recalling the inhibitory potency and the multivalent effect found for the two heptavalent β-CD **4.6a** and **4.6b** (**Figure 4.4**), the value of K_i was 7.7 and 0.36 μM, which leads to a *rp/n* of 6.0 and 75 respectively.[98a] Hence, cyclopeptoid-based iminosugar click-clusters **4.49**-**4.51** were 2- to 31-fold less potent than their analogues with the same alkyl spacer but different inner core. A possible explanation to those results could rely in the different ligand spatial orientation as consequence of the structural features of the central scaffold. Indeed, it has been demonstrated that the rigidity of the scaffold is beneficial in achieving higher multivalent effects.[97, 99] Our multivalent systems could be not rigid enough to raise the inhibitory potencies due to the intrinsic flexibility of the cyclopeptoid backbone. However, even though they are not the best α-mannosidase inhibitors, the evaluation of their activities further highlights the role of the scaffold architecture on binding affinity enhancements. In addition, this outcome clearly points out that an increase both in the valency and in the linker length favours the inhibition potencies of cyclopeptoid-based iminosugar clusters. This hint, together with the improved biostability and bioavailability of cyclic peptoids, their easy synthesis, the simple functionalization by CuAAC reactions and the facile access to scaffolds with increased valency, indicates that they are a valuable and promising tool for the construction of multivalent ligands with improved performances. Their advantages pushed us to further investigate the application of such new systems into the α-mannosidase inhibition. Hence, we developed the second generation of cyclopeptoid-based iminosugar click-clusters.

The six cyclopeptoids **4.19-4.24** (**Figure 4.5**) incorporating six to sixteen propargyl side chains were chosen as the central scaffolds. The alkynyl termini underwent CuAAC reaction in the

presence of the azido-armed tripode **4.53** that enabled to expand the valency by three and to create elegant and branched molecular structures (**Scheme 4.4**). Once again, DNJ iminosugars were chosen as peripheral ligands, attached through a C_9 alkyl linker, since the clusters comprising these structural elements showed the largest inhibitory multivalent effects.

18- to 48-valent DNJ clusters **4.60**-**4.65** were obtained in two steps. First, the microwave assisted derivatization of the propargyl side chains with the trivalent ligands afforded peracetylated DNJ clusters **4.54**-**4.59** in 32 to 77% yields. Then, the *O*-deacetylation with basic anion exchange resin gave the final deprotected cyclopeptoid-iminosugar conjugates in good yield.

The second generation of cyclopeptoids iminosugar click-clusters were ready to be evaluated as inhibitors of Jack bean α-mannosidase, the glycosidase with the largest responses to multivalent inhibitor presentation to date.

Table 4.4 shows the corresponding inhibition constants (*Ki*) as well as relative inhibition potency (*rp*) and the multivalent effect (*rp/n*) of multivalent ligands **4.60**-**4.65**. For comparative purposes, **4.52b** was included as structurally related monovalent control.

Comparing the inhibitory multivalent effect of the decavalent cluster **4.51b** (entry 6, **Table 4.3**), the last component of the first generation synthesized, with the value found for the 18-valent cluster **4.60** (entry 2, **Table 4.4**), the first member of the second generation of iminosugar ligands, an increase of one order of magnitude was gained (*rp/n* from 3.8 to 74). Hence, the addition of eight DNJ units to the cyclopeptoid core was beneficial for dramatic improvement in binding enhancements.

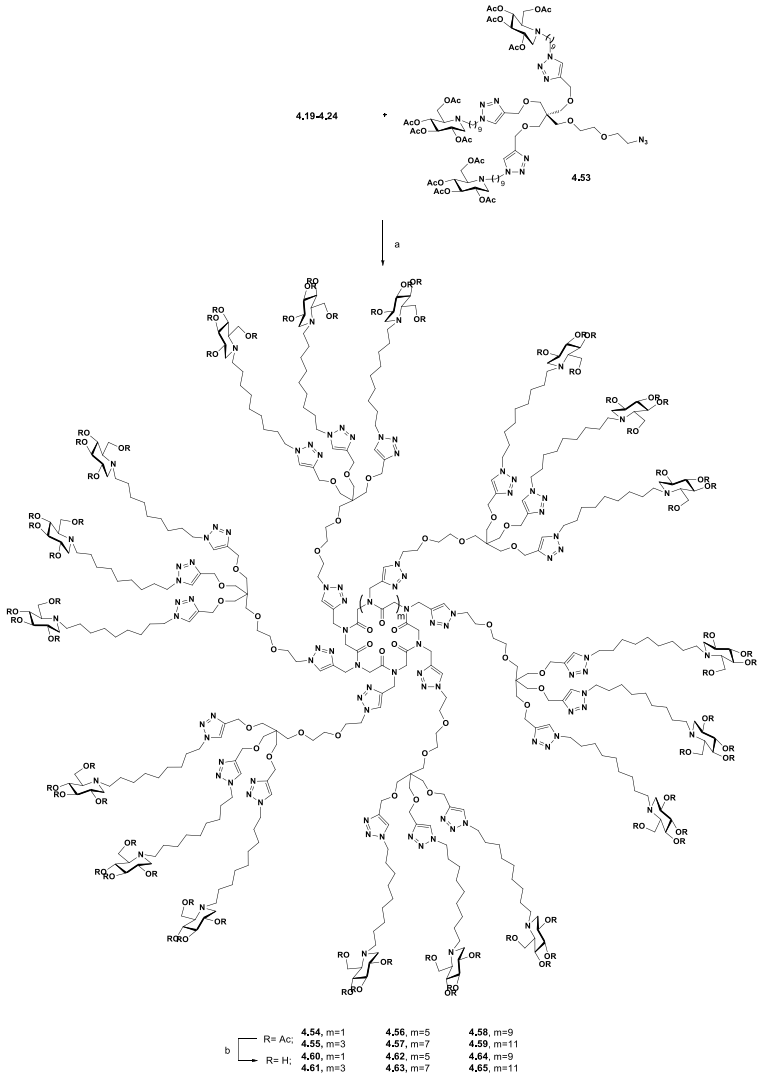

Scheme 4. 4. Synthesis of DNJ clusters **4.60-4.65**. Reagents and conditions: (**a**) $CuSO_4 \cdot 5H_2O$ cat., sodium ascorbate, DMF/H_2O (5:1), MW, 80 °C or 90°C, 3 h; **4.54** 75%; **4.55** 73%; **4.56** 53%; **4.57** 70%; **4.58** 77%; **4.59** 32%; (**b**) Amberlite IRA 400 (OH^-), MeOH/H_2O (1:1), 40 °C. Overall yields from compounds **4.19**-**4.24**: **4.60** 66%; **4.61** 56%; **4.62** 53%**; 4.63** 40%; **4.64** 62%; **4.65** 28%.

However, for a better understanding of the multivalent effect, two more compounds were synthesized.

To determine the minimum number of DNJ units to generate a significant binding enhancement, a 14-valent iminosugar **4.67** was prepared (**Scheme 4.5**).

To evaluate the influence of the cyclic nature of the peptoid scaffold on the multivalent effect, cluster **4.70**, the acyclic analogue of **4.63**, was synthesized by clicking the tripode **4.53** on the linear peptoid **4.68** previously obtained on solid-phase (**Scheme 4.6**).

Switching from a cyclic to a linear peptoid scaffold resulted detrimental to α-mannosidase inhibition, as reflected by rp/n values reduced by one order of magnitude (entry 6, **Table 4.4**).

Concerning the evaluation of **4.67** binding potency, this revealed that an increment of just four DNJ units, from 10 to 14 in **4.51b** and **4.67** respectively, led the multivalent effect to raise of two orders of magnitude (entry 7, **Table 4.3** and entry 1 **Table 4.4**). It is interesting to note that, from 14- to 18-valent iminosugar, there is a slight decrease of inhibitory activity. This result is probably to address to the ligand special orientation presented by the 14- and 6-mer cyclopeptoid. However, it was noteworthy to follow an outstand increase of *rp/n* moving from 18- to 36-valent iminosugars (**4.60**-**4.63**, entries 2-5 **Table 4.4**). **4.63** led to a remarkable relative inhibition potency, ca. 171000-fold stronger than the one displayed by the corresponding monovalent analogue **4.52b** (entry 9, **Table 4.4**). Comparing such value with the multivalent effect showed by 21-valent β-cyclodextrin (**4.8**, **Figure 4.4**, *rp/n* = 610), we can state to have reached a new record with the highest inhibitory activity ever reported in the field of glycosidases inhibition. This result also means that the multivalent effect has touched a plateau, since no enhancement of inhibitory potency is observed further increasing the valency to 42 and 46 (compounds **4.64** and **4.65**, entries 7 and 8).

Entry	Iminosugar	Valency	K_i [μM]	*rp*	rp/n
1	**4.67**	**14**	**0.126 ± 0.014**	**1492**	**107**
2	**4.60**	**18**	**0.142 ± 0.017**	**1324**	**74**
3	**4.61**	**24**	**0.037 ± 0.012**	**5081**	**212**
4	**4.62**	**30**	**0.0099 ± 0.0028**	**18990**	**633**
5	**4.63**	**36**	**0.0011 ± 0.0004**	**170909**	**4747**
6	**4.70**	**36**	**0.011± 0.005**	**17090**	**474**
7	**4.64**	**42**	**0.0015 ± 0.0003**	**125333**	**2984**
8	**4.65**	**46**	**0.0011 ± 0.00007**	**170909**	**3560**
9	**4.52b**	**1**	**188**	**-**	**-**

Table 4. 4. Relative inhibition potency, multivalent effect and inhibitory activity (Ki, μM) against jack bean α-mannosidase of cyclopeptoid-based clusters **4.60-4.65**, **4.67, 4.70** and their monovalent control model **4.52b**.

Collecting all the multivalent effect values registered for the first and the second generation of cyclopeptoid-based iminosugar click-clusters and plotting them versus the valency of the corresponding compounds, it is interesting to highlight an exponential increase of *rp/n* that goes to the top with the 36-valent iminosugar to decrease again with the next clusters (**Figure 4.13**).

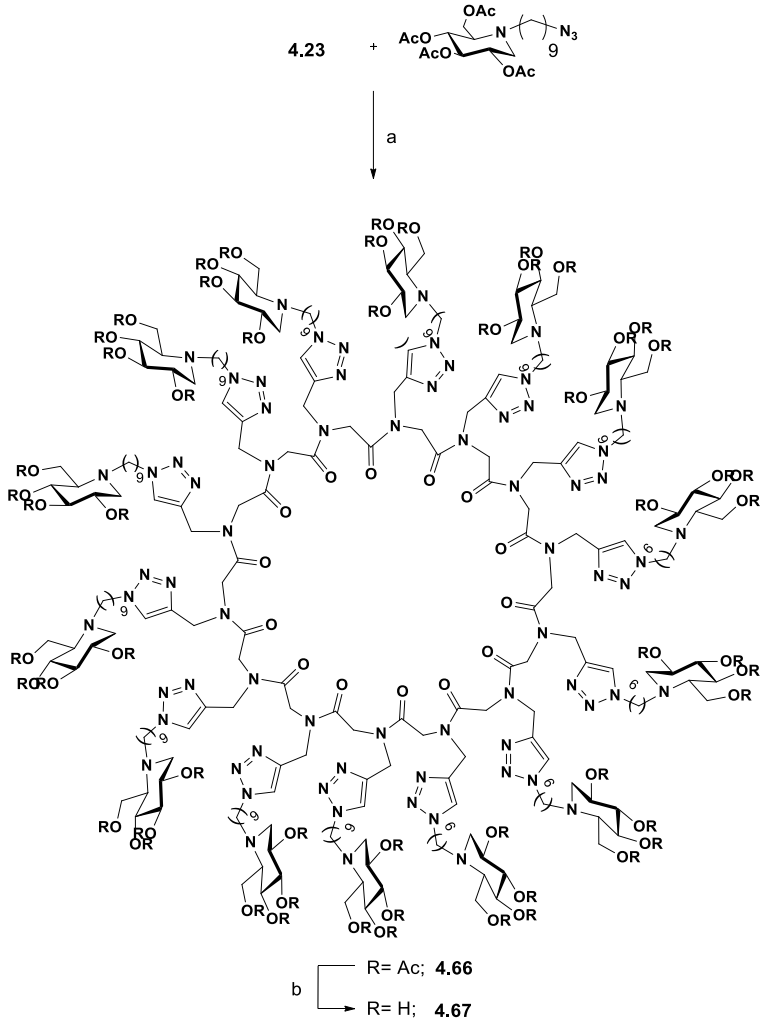

Scheme 4. 5. Synthesis of DNJ cluster **4.67**. Reagents and conditions: (**a**) $CuSO_4 * 5H_2O$ cat., sodium ascorbate, DMF/H_2O (5:1), MW, 80 °C, 3 h; **4.66** 53%; (**b**) Amberlite IRA 400 (OH^-), MeOH/H_2O (1:1), 40 °C. Overall yield from compound **4.23**: **4.67** 45%

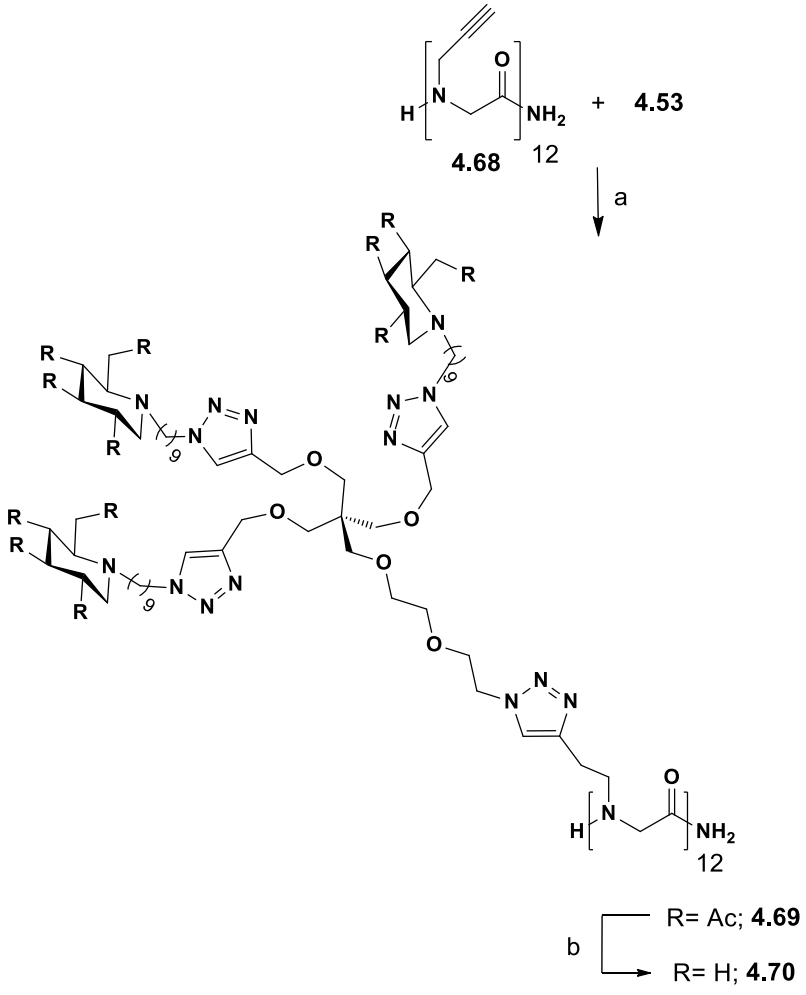

Scheme 4. 6. Synthesis of DNJ cluster **4.70**. Reagents and conditions: (**a**) $CuSO_4 \cdot 5H_2O$ cat., sodium ascorbate, DMF/H_2O (5:1), MW, 80 °C, 3 h; **4.69** 88%; (**b**) Amberlite IRA 400 (OH^-), MeOH/H_2O (1:1), 40 °C. Overall yield from compound **4.68**: **4.70** 88%

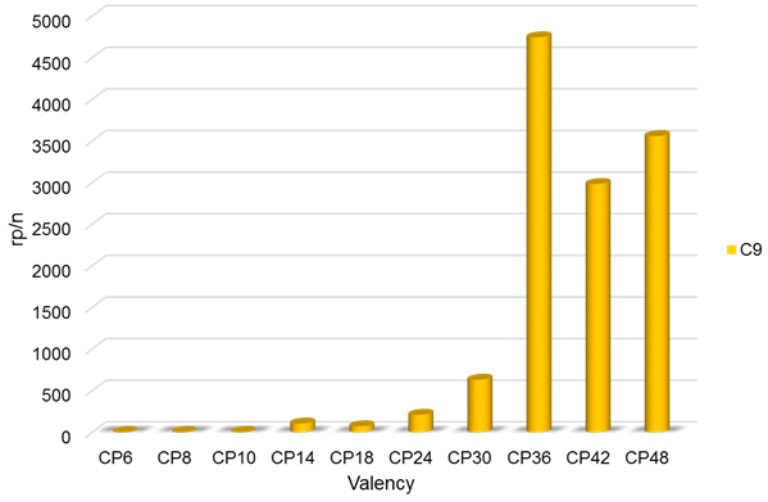

Figure 4. 13. Relative inhibition potency/DNJ units *vs.* valency of cyclopeptoid (CP) based iminosugar click-clusters.

The achievement of a plateau in the multivalent effect broke a new record in Jack Bean α-mannosidase inhibition. Nevertheless, the operating binding mode of such multivalent ligands still remains unclear. To shed light on their mode of action in order to construct a rule for developing new and powerful inhibitors, we studied the interactions of Jack Bean α-mannosidase and the 36-valent cluster **4.63**, for which the highest multivalent effects are reported.

Jack Bean α-mannosidase is a high-molecular-weight metalloenzyme $(LH)_2$ of 230 kDa. It can be defined as a homodimer comprising two heterodimeric subunits (LH for Light and Heavy chains) of around 49 (L) and 66 kDa (H). Recently, it has been suggested that each subunit has a binding site, being catalytically active in the dimeric structure.

Since several binding modes can be possible with the multivalent iminosugars, electron microscopy (EM) with negative staining was performed by Dr. Birck at the Structural Biology

Platform, IGBMC in Illkirch (France) to obtain high-resolution images of the enzyme alone and in the presence of **4.63**, hence providing receptor/ligand interactions on nanometric scale.

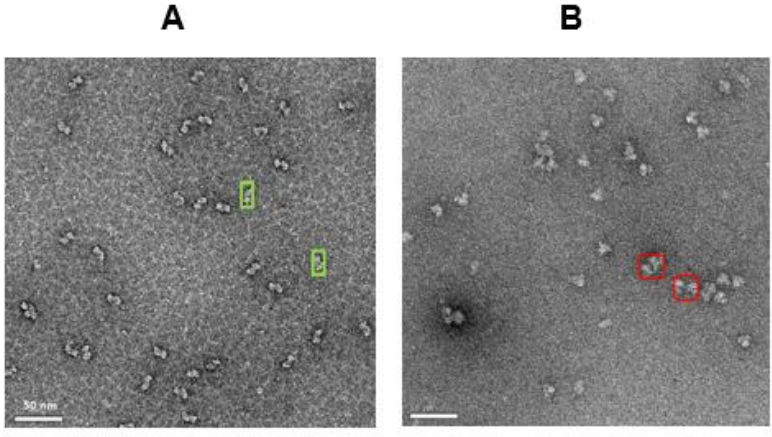

Figure 4. 14. EM pictures of Jack Bean α-mannosidase (**A**) and Jack Bean α-mannosidase interacting with 4.63 (**B**) - scale bars = 50 nm.

Figure 4.14A shows an image of mannosidase alone. The green frame contains clear clusters of ~10x20 nm matching the size of two Jack Bean α-mannosidase molecules in a $2x(LH)_2$ complex. The enzyme, incubated with the multivalent cluster at a concentration in the same range than the one used for the inhibition assays (5 µg/ml), produced several disparate arrangements. In **Figure 4.14B** different assemblies can be seen, such as some in the red frame of size ~ 20x20 that may correspond to the interaction of one inhibitor with two tetramers $(LH)_2$.

Analytical Ultracentrifugation Sedimentation Velocity (AUC-SV) experiments performed by Dr. A. Podjarny at the Institut de Génétique et de Biologie Moléculaire et Cellulaire in Illkirch (France) confirmed this hypothesis. AUS-SV measures the rate of movement of solutes in high centrifugal fields, and enables the quantitative analysis of macromolecules in solution to define the size, shape and

interactions of macromolecules. One common application of this method is to determine the sedimentation coefficient distribution c(s) of macromolecules. Since it is related to the buoyant molar mass M, the unequivocal deterrnination of M is possible from sedimentation velocity experiments. **Figure 4.15** shows the sedimentation coefficient distribution plot for Jack Bean α-mannosidase (in magenta) and for the Jack Bean α-mannosidase:**4.63** complex (in blue). Peaks in the distribution belong to certain oligomers and may identify their molecular mass. For Jack Bean α-mannosidase alone (magenta curve), the main species sedimented at 9.3 S corresponding to the tetramer $(LH)_2$ with a molar mass estimate of 210 kDa. A minor peak at 13.4 S also appears in the c(s) plot, indicating species with a molar mass estimate of 377 kDa which may correspond to the association of two Jack Bean α-mannosidase molecules in a $2x(LH)_2$ complex. The blue curve indicates the binding of Jack Bean α-mannosidase to **4.63** and shows the broadening of sedimentation coefficient distribution. This exhibites maxima at about 14 S suggesting the reversible formation of a 2:1 tetramer$(LH)_2$:inhibitor complex in dynamic equilibrium with other species.

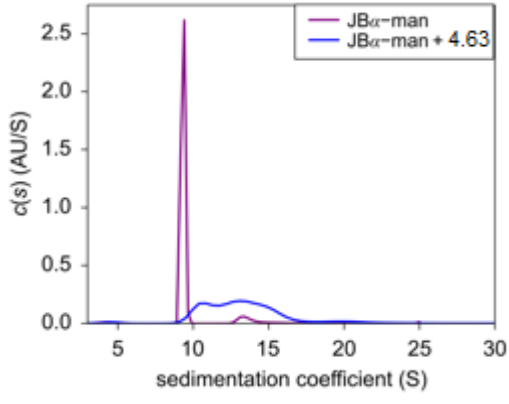

Figure 4. 15. AUC-SV experiments: sedimentation coefficient distribution plot for Jack Bean α-mannosidase (in magenta) and for the Jack Bean α-mannosidase-4.63 complex (in blue).

Finally, a third method was applied to get complete insight into the binding mode of multivalent iminosugars.

Dr. N-T. Nguyen-Huynh at the Laboratoire de Spectrométrie de Masse des Interactions et des Systèmes (University of Strasbourg) performed electrospray mass spectrometry (ESI-MS) on the native enzyme before (**Figure 4.16A**) and after the addition of the inhibitor **4.63** (MW = 17,4 kDa) (**Figure 4.13B**). In both cases there were identified three different multi-charged ions patterns. **Figure 4.16A** reveals the molecular mass of the primal heterodimer LH (MW = 121.3 kDa), the tetramer $(LH)_2$ (MW = 242.3 kDa) and the association of two tetramers $(LH)_2$ (MW = 484.9 kDa), respectively. **Figure 4.16B** shows two enzyme:inhibitor complex with two different stoichiometries; 1:1 (MW = 259.9 kDa) and 2:1 (MW = 501.9 kDa).

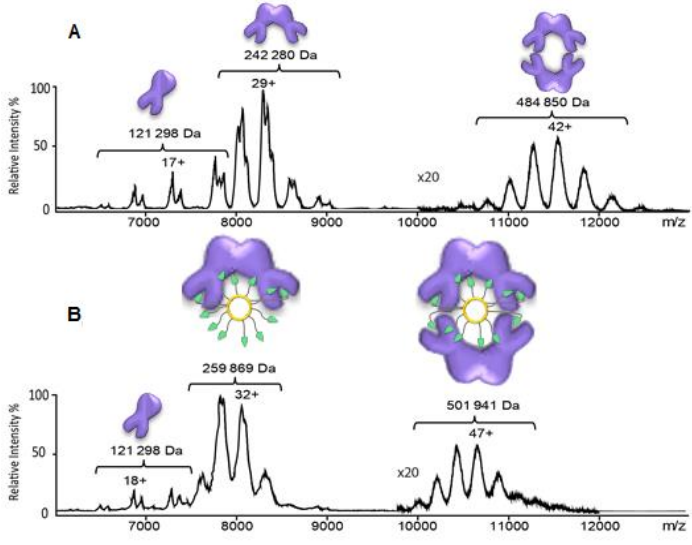

Figure 4. 16. Native ESI-MS spectra for (**A**) Jack Bean α-mannosidase and (b) Jack Bean α-mannosidase interacting with **4.63**. Multi-charged ions patterns are labelled with the corresponding enzyme and enzyme-inhibitor complexes.

The experiments performed on Jack Bean α-mannosidase and the multivalent iminosugar **4.63** gave a series of complementary pieces of information that we put together to finally have an overall picture of the mechanism behind multivalent inhibition. The 36-valent cyclopeptoid-based iminosugar click-cluster provides the optimal number of ligands and allows for the ideal spatial orientation of the iminosugar moieties to bind a first molecule of Jack Bean α-mannosidase and then cross-link a second one allowing for the stabilization of a 2:1 tetramer $(LH)_2$-inhibitor chelate complex (**Figure 4.17**). Reversible active-site specific interactions with the iminosugars but also protein-protein interactions between two tetramers interplay in the formation of the enzyme-inhibitor complex. It is worth to note that the architectural features of the scaffold, such as its size, valency and flexibility, revealed to be crucial in shifting the equilibrium of the different species in solution towards the formation of the complex.

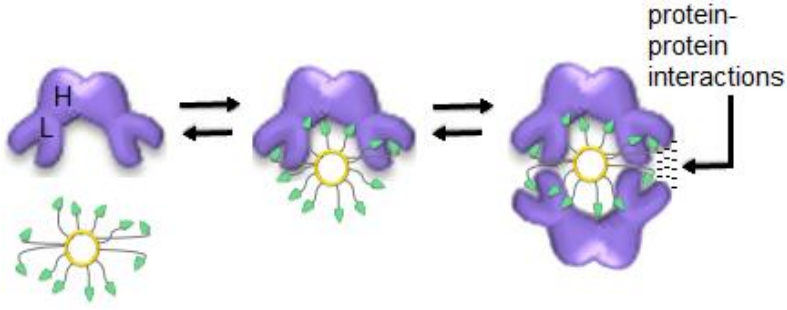

Figure 4. 17. Cartoon representation of the equilibrium between the free forms of the inhibitor **4.63** and the Jack Bean α-mannosidase with the chelate complexes $(LH)_2$-inhibitor.

4.3 CONCLUSION

A library of propargylated cyclopeptoids **4.16-4.24** (**Figure 4.5**) has been synthesized on solid-phase *via* the submonomer approach. This powerful method allowed for an easy access to longer chains (12- to 16-mer) that underwent the macrocyclization reaction to afford the largest cyclopeptoids size ever described.

The platform of cyclopeptoids was then decorated with hexyl- and nonyl-azide armed DNJ ligands *via* the efficient CuAAC reaction, to yield the first example of cyclopeptoid-based iminosugar click-clusters.

The first generation of such compounds presented 2 to ten copies of the DNJ iminosugar ligands, installed on the 6- to 10-mer cyclopeptoid scaffolds. The divalent compound was tested as CFTR corrector, resulting as powerful as the structures previously reported. The 6- to 10-valent compounds were evaluated as inhibitor of Jack Bean α-mannosidase. Despite the considerable multivalent effect registered, they resulted weak inhibitors of the enzyme studied. However, they highlighted the importance of the high valency and the longer C_9 alkyl spacer as structural element to enhance the binding potency.

The second generation of cyclopeptoid-based iminosugar click-clusters was synthesized incorporating a DNJ tripode with nonyl spacer arms on 6- to 16-mer scaffolds, accessing valency never reached before. The 36-valent cluster showed the best multivalent effect and broke the record previously won by 21-valent β-cyclodextrine.

Experiments of EM, AUC-SV and ESI-MS revealed its mechanism of action. The flexible and long-armed DNJ cluster is

able to accommodate two mannosidase molecules and bridge four active-sites to form very tight sandwich-type complexes.

The importance of this outcome is providing a rational behind the binding of the multivalent inhibitors and an explanation to the multivalent effect. This claims the key architectural features for designing and developing new structures able to rise the inhibition potency and to find application as therapeutic compounds in protein-misfolded diseases.

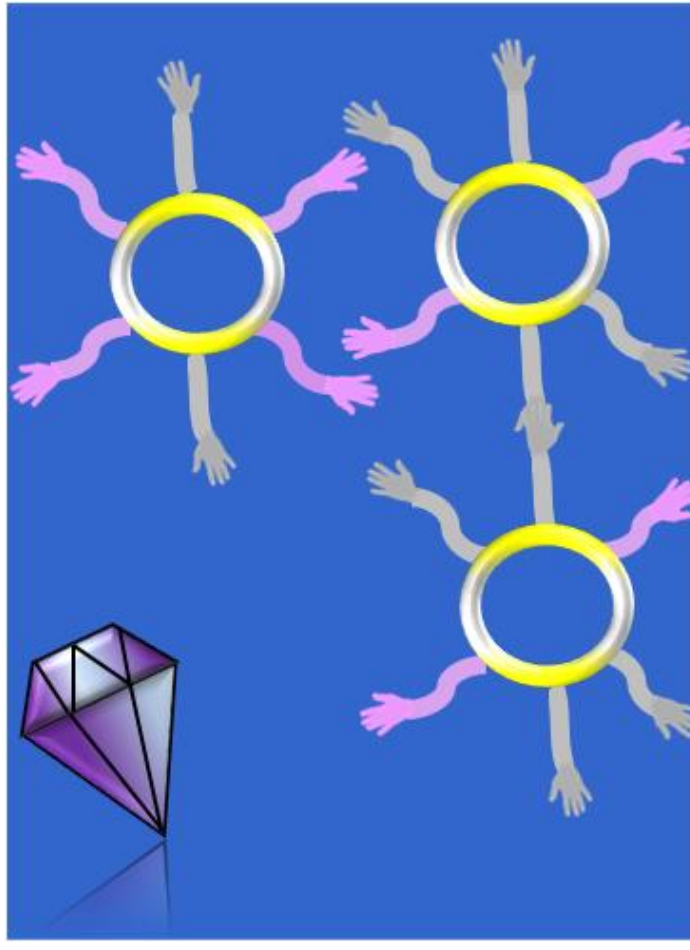

CHAPTER 5

The Role Of Side Chains In The Solid-State Assembly Of Cyclic Hexapeptoids

5

5.1 INTRODUCTION

Since the advent of peptoids, researchers started to play around with their structures and to explore the enormous structural diversity exploiting the malleability of the backbone.

Many complementary methodologies are employed in the structural characterization of peptoids, most of all circular dichroism spectrophotometry (CD), NMR spectroscopy and X-ray crystallography.[108] However, due to the *cis*/*trans* isomerism of the peptoid bonds,[2] a peptoid made of *n* monomers gives rise to 2^{n-1} equilibrating configurational isomers in solution, or 2^2 if the *N*-terminal amino group is capped and acetylated.[109] Hence, it is extremely difficult to go through their NMR spectra,[110] which appear of tough interpretation even if a covalent constrain as macrolactamization is applied.[10, 16-17, 19, 49b]

For that reason, crystallization of peptoids is highly auspicable, in order to freeze a preferred conformation and to attain their structural characterization. In this respect, X-ray crystallography ranks over the other “devices of curiosity”.

5.1.1. Solid State Assembly Of Cyclic Peptoids

As stated in the paragraph 1.3, cyclopeptoids have shown to be extremely interesting for the various properties displayed and their potential applications.

The elucidation of their structure is fundamental to gain a deep understanding of the structure-activity relationship, in order to get more hints for the *de novo* design of folded and active compounds. X-ray crystallography is of first aid in reaching this target, which is also central in the crystal-engineering field.

Very recently, our group presented a survey on the solid-state assembly of cyclic peptoids with the aim to recapitulate their main features, hence to shed light on the interactions that interplay in their arrangement.[14] Eighteen compounds, both homo- and heterooligomers, have been studied and classified depending on their ring size, ranging from 3- to 10-mers.

It is remarkable that the side chains have a primary role in defining the solid-state arrangement of the cyclopeptoids. Indeed, the removal of the amide proton implies the exclusion of NH···OC hydrogen bonding from the structural interactions and renders the backbone conformation almost identical within the same-size-ring family. It means that there is a recurrent sequence of geometry of the amide bonds (**Table 5.1**), and this was also confirmed in the crystal structures of small cyclopeptoids synthesized later on.[16] Furthermore, it is worth to note that hexameric cyclopeptoids pass from a *cctcct* to an *all-trans* configuration upon metal complexation.[17, 19d]

Weak but extended interactions, such as inter-annular CH···OC hy and CH···π for compounds including pi systems (aromatic side chains, triple bonds and so on…) chains, vicariate the stronger NH···OC interactions.

No. of Residues	Sequence
3	***ccc***
4	***ctct***
5	***ccctt***
6	***cctcct; all-trans for M complex***

7	***ccccttt***
8	***ccttcctt***
9	***cccctccct***
10	***cccttccctt***

Table 5. 1. Pattern of *cis* (*c*) and *trans* (*t*) amide bonds configuration in the crystal structures of cyclic peptoids.

CH···OC hydrogen bonds involve the methylene hydrogen from one molecule's peptoid backbone and the carbonyl oxygen from another neighboring molecule. Such interactions support side-by-side and face-to-face arrangement that provides a columnar assembly of the macrocyclic compounds. For example, cyclotetra-*N*-benzyloxyethyl glycine (**5.1**, **Figure 5.1**) forms columns thanks to the interaction between two methylene hydrogen atoms and two *trans* carbonyl oxygen atoms (**A**, **Figure 5.1**).[17]

Benzyloxyethyl side chains, extending horizontally with respect to the plane occupied by the cyclopeptoid, contribute to the overall assembly. CH_{ar}···O and CH_2···pi interactions stabilize the staking of the macrocycles, while CH_2···OC and CH_{ar}···pi bonding provide side-by-side intertubular contacts.

A comparison of **5.1** (**Figure 5.1**) with cyclotetrasarcosyl[17] **5.2** (**Figure 5.2**) clearly highlights the importance of side chains and how they can influence the assembly. Indeed, while benzyloxyethyl side chains promotes a columnar arrangement, methyl side chains hampers such disposition of the macrocycles.

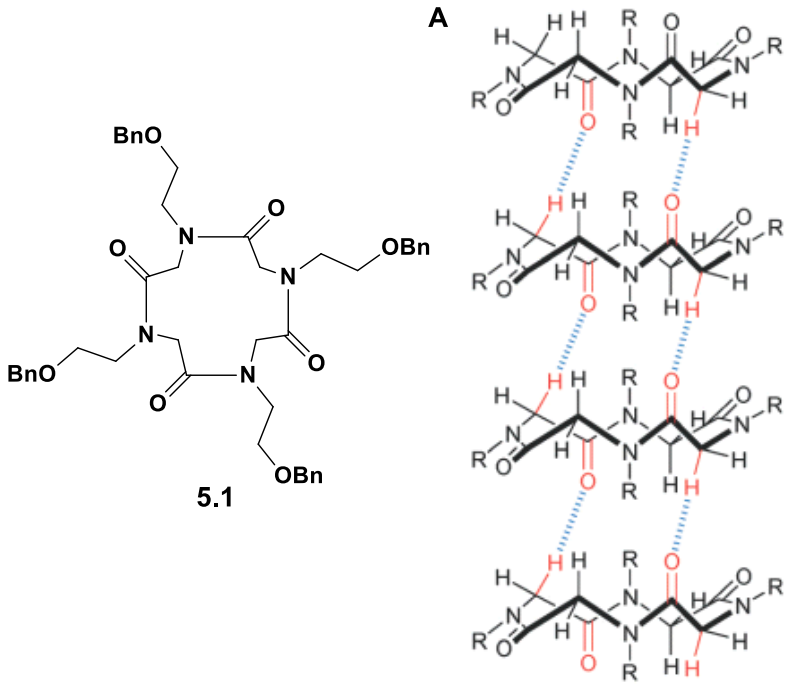

Figure 5. 1. Cyclotetra-*N*-benzyloxyethyl glycine **(5.1**) and its tubular assembly (**A**). Benzyloxyethyl side chains are omitted for clarity.

Crystal structure of **5.2** shows weak CH···OC hydrogen bonding involving the methyl hydrogen atoms from the side chains and the oxygen of the carbonyl groups (**A**, **Figure 5.2**). Such interactions bring the two molecules perpendicularly to each other and so determine a T-shape arrangement. T-shape arrangement often occurs with methyl and benzyl side chains, which can compete with CH···OC inter-annular hydrogen bonds.

On the other hand, methoxyethyl side chains showed to promote a different arrangement, acting as pillars in the cyclohexa-*N*-methoxyethyl glycine (**1.6**, **Figure 1.7**).[19d] The long side chains, protruding vertically with respect to the plane defined by the macrocycle, provide the CH_2···OC interactions with the backbone

carbonyl groups and with the other side chains that guarantee the columnar arrangement.

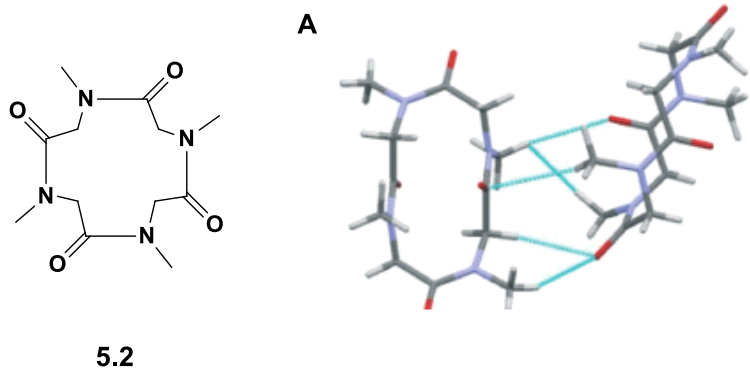

5.2

Figure 5. 2. Cyclotetrasarcosyl (**5.2**) and the T-shaped arrangement of two adjacent molecules in the crystal structure (**A**).

Methoxyethyl side chains promote the same assembly also in the cyclic octamer **5.3** (**Figure 5.3**), by means of CH_{ar}···OC hydrogen bonding and CH_3···pi interactions with the aromatic ring from the benzylic groups (**A**, **Figure 5.3**).[10]

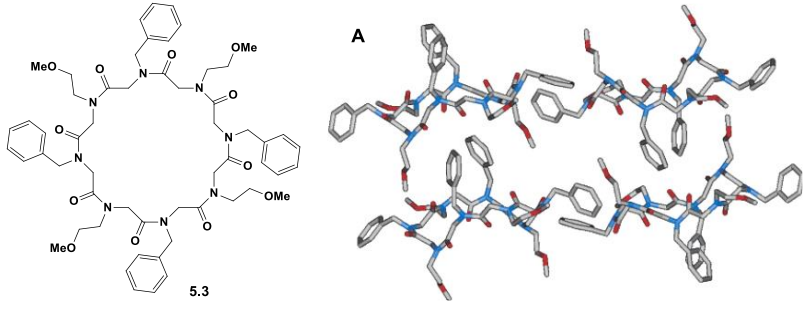

5.3

Figure 5. 3. Side view of crystal packing of cyclo-(*N*pm-*N*me)$_4$ (**5.3**) and the tubular arrangement (**A**).

Propargyl side chains have demonstrated to act as pillars as well, stabilizing the columnar architecture. The cyclic octamer **5.4** (**Figure 5.4**) stacks by means of CH···pi interactions (**A**, **Figure 5.4**) and methoxyehtyl side chains

provide additional interactions binding cyclopeptoids molecules side-by-side.[111] **Figure 5.4B** is the top view of the crystal packing and shows the inner cavity in which water molecules are located. They do not have any structural role, since dehydrated crystals yielded the same arrangement via single crystal to single crystal transformation. Just empty hollows were left once water had gone.

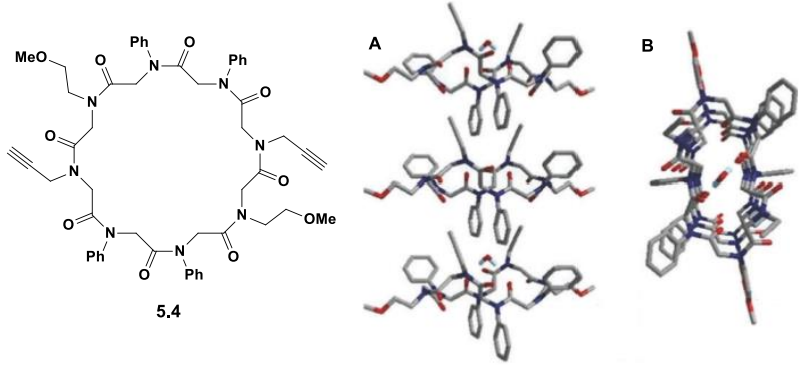

Figure 5. 4. Cyclo-(*N*pa-*N*me-*N*ph-*N*ph)$_2$ (**5.4**) and its tubular assembly (**A**). The view from the top shows water moleculers into the hollow (**B**).

Those last examples not only make clear the function of side chains but also the influence of the ring size. Bigger the macrocycle, higher is the probability to set a columnar arrangement. Smaller rings, on the other hand, favor T-shape interactions. Finally, it is quite usual to find the crystallization solvent included in the structure. Sometimes this has a structural role and contribute to the asset of the solid state, not so often this is uninfluential and can be safely removed without damaging the crystal.[111]

5.1.2. Hirshfeld surface

Between the 80s and the 90s, Desiraju claimed the role of crystal engineering and indicated to scientists the direction to achieve a fruitful molecular crystal analyzing.[112]

Crystal engineering aims to design novel materials with specific chemical and physical properties. As we have previously underlined, this is possible looking closely at the crystal structures, visualizing the molecule in its entirety and trying to unveil all the intermolecular interactions that simultaneously contribute to the packing.

An overall view of the factors that interplay in the solid-state assembly should be desirable, and the quantification of each interaction would be extremely helpful in comparing similar crystal structures.

To follow such guidelines, Spackman borrowed the "stockholder partitioning" scheme from Hirshfeld (1977),[113] and generated surfaces that he named after him in his honor. Hirshfeld surfaces show the partitioning of molecular crystals electron densities into molecular fragments, providing an immediate visualization of the molecular packing.[114] Mathematically, such surfaces can be defined as a weighting function $w_A(r)$ for a particular molecule A in a crystal:

$$w_A(\boldsymbol{r}) = \sum_{i\,\epsilon\,molecule\,A} \rho_i^{at}(\boldsymbol{r}) \,/\, \sum_{i\,\epsilon\,crystal} \rho_i^{at}(\boldsymbol{r}) = \rho_{promolecule}(\boldsymbol{r}) / \rho_{procrystal}(\boldsymbol{r})$$

$\rho_i^{at}(r)$ are spherically-averaged electron densities of the various atoms *i* in the molecule A. The numerator is a sum over the electron densities of the atomic fragments in the molecule A (called promolecule) and the denominator is an analogous sum over the crystal (called procrystal). Since the atomic electron densities are sharply peaked near the nuclei and decay exponentially, $w_A(r)$ is a continuous function with $0<w_A(r)<1$, being 1.0 at molecule A, and zero at distances far from it. This can be plotted, for example, for a

benzene molecule in the crystal (**Figure 5.5**). The contours of $w_A(r)$ surround the molecule and are closely spaced in the proximity of the van der Waals surface.

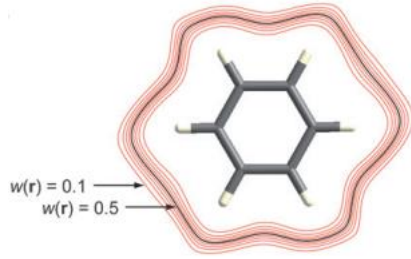

Figure 5. 5. Contours of $w_A(r)$ surrounding a benzene molecule in the crystal.

The isosurface defined by $w_A(r) = 0.5$ is the Hirshfeld surface and envelops the molecule, defining the volume of space where the promolecule is in the maximum proximity of neighboring molecules. Furthermore, because of the nature of the weight function, the volumes never overlap.

The Hirshfeld surface of a given compound can be generated by the program CrystalExplorer,[115] once the crystal structure has been solved and well-characterized and any disorder present had been modeled.

The properties of the Hirshfeld surface are a series of functions that embody information of intermolecular contacts. They are summarized in **Table 5.2**.[114b]

As any other surface, Hirshfeld surface has two local principal curvature, k_1 and k_2, that define shape index ***S*** and curvedness ***C***. Shape index on the Hirshfeld surface identifies complementary hollows and bumps where two molecular surfaces touch one another, displaying them in red and blue respectively (**A**, **Figure 5.6**). Curvedness indicates flat regions and positive large curvature as green areas separated by dark blue edges (**B**, **Figure**

5.6). ***S*** and ***C*** are useful to identify the packing mode and how neighboring molecules interact.

Function	Symbol and definition	Mapping range
distance from a point on the surface to the nearest nucleus **outside** the surface	d_e	red (short distances) through green to blue (long distances)
distance from a point on the surface to the nearest nucleus **inside** the surface	d_i	red (short distances) through green to blue (long distances)
shape index, *S*, a measure of ''which'' shape, defined in terms of principal curvatures k_1 and k_2	$S=\frac{2}{\pi}\ arctg\ (\frac{k1+k2}{k1-k2})$	-1.0 (concave) through 0.0 (minimal surface) to +1.0 (convex)
curvedness, *C*, a measure of ''how much'' shape defined in terms of principal curvatures k_1 and k_2	$C=\frac{2}{\pi}\ ln\sqrt{k_1^2+{k_2^2}/{2}}$	-4.0 (flat) through 0.0 (unit sphere) to +0.4 (singular)
normalized contact distance, defined in terms of d_e, d_i and the vdW radii of the atoms	$d_{norm}=\frac{di-r_i^{vdW}}{r_i^{vdW}}+\frac{de-r_e^{vdW}}{r_e^{vdW}}$	red (distances shorter than sum of vdW radii) through white to blue (distances longer than sum of vdW radii)

Table 5. 2. Functions of distance and curvature mapped on Hirshfeld surfaces.

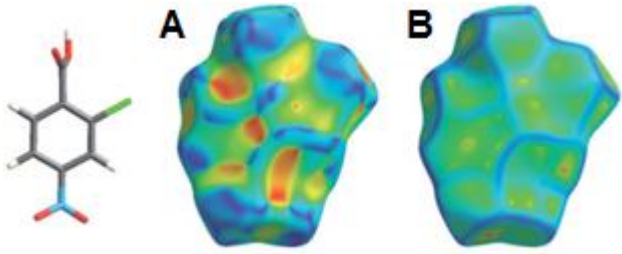

Figure 5. 6. Front view of the Hirshfeld surface for 2-chloro-4-nitrobenzoic acid, mapped with shape index (**A**) and curvedness (**B**).

Functions of distance, d_e and d_i represent the distance from a point on the surface to the nearest nucleus outside and inside the surface respectively. They can be plotted one versus the other providing a 2D map called Hirshfeld fingerprints (**A** and **B**, **Figure 5.7**). The color of the pixel indicates the density of contacts; ranging from blue through green to red, we pass from few to many points. Moreover, this is a useful tool to display long-distance and short-distance contacts. The appearance of a pair of spikes at the bottom left of the plot (short d_i and d_e, the upper one associated with the donor atom, the lower one with the acceptor), and the pattern of diffuse points in between these spikes occurs only for cyclic hydrogen bonds (**A**, **Figure 5.7**). An interesting feature is also the red region near the center of the map that shows the π-π staking between the planar rings (**B**, **Figure 5.7**).

A combination of both d_e and d_i, each normalized by the vdW radius of the specific atoms involved in the close contact to the surface, generates the contact distance d_{norm}.

The advantage of introducing this function is to visualize close contacts to large atoms like Br or I, as well as contacts to H, C or C, discriminating the different size of atoms, that d_e and d_i alone cannot appreciate.

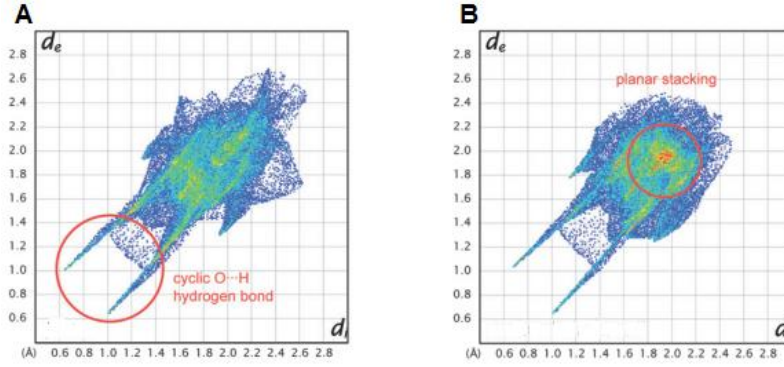

Figure 5. 7. Hirshfeld fingerprint for 2-chloro-4-nitrobenzoic acid showing hydrogen bonding (**A**) and planar staking interactions (**B**).

Figure 5.8 shows d_{norm} mapped on the Hirshfeld surface of 2-chloro-4-nitrobenzoic acid. The red spots on the large blue surface show contacts shorter than the vdW separation.

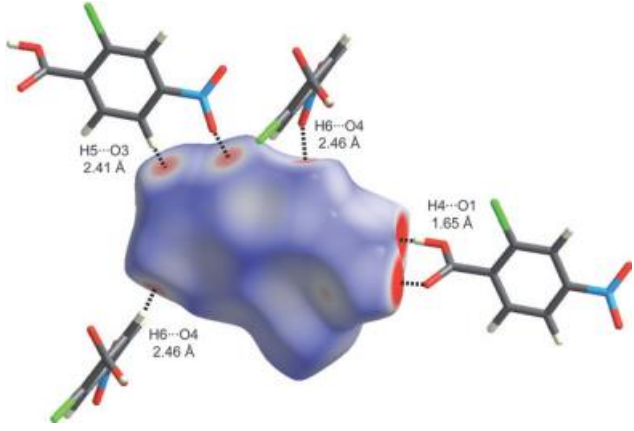

Figure 5. 8. d_{norm} mapped on the Hirshfeld surface of 2-chloro-4-nitrobenzoic acid.

The introduction of Hirshfeld surfaces and Hirshfeld fingerprints is one more tool in the kit of crystallographers, fundamental to complete the structural analysis of a molecule at the solid state. Making use of the mapping and interpreting their meaning

is of primary importance in describing the packing and considering simultaneously all the interactions that contribute to the assembly.

Bearing those lessons in mind, we exploited the potential of the Hirshfeld method and we provided a detailed analysis of our cyclic peptoids of interest, emphasizing the contacts that arise according to the side chains installed.

5.2 AIM OF THE WORK: SYNTHESIS AND CHARACTERIZATION OF A LIBRARY OF CYCLIC HEXAPEPTOIDS WITH METHOXYETHYL AND PROPARGYL SIDE CHAINS

5.2.1 Introduction

Cyclic peptoids proved to assembly at the solid state in a very elegant fashion. The examples described in the literature also demonstrated that a certain degree of predictability emerges when peculiar side chains are introduced into the peptoidic backbone.

Comparing the crystal structures of the cyclic hexamer of *N*-methoxyethyl glycine[19d] **1.6** (**A**, **Figure 5.9**) with the octamers cyclo-(*N*pm-*N*me)$_4$[10] **5.3** (**B**, **Figure 5.9**) and cyclo-(*N*pa-*N*me-*N*ph-*N*ph)$_2$[111] **5.4** (**C**, **Figure 5.9**), it is possible to highlight the role of the methoxyehtyl and propargyl side chains in the packing. Methoxyethyl side chains in **1.6** and **5.3** and propargyl side chains in **5.4** stretch vertically with respect to the plane occupied by the macrocycle and exert a pillar function in the columnar arrangement. In addition, for **1.6** and **5.4**, methoxyehtyl side chains, extending horizontally, provide side-by-side interactions that promote the intertubular contacts.

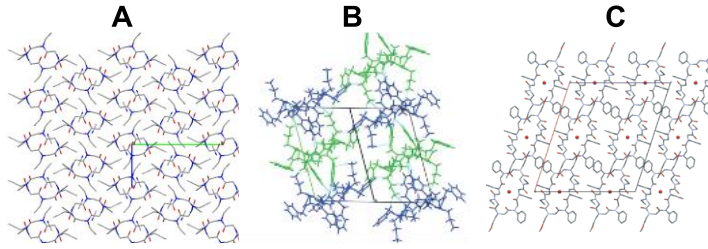

Figure 5. 9. Crystal packing of **1.6** (**A**), **5.3** (**B**) and **5.4** (**C**)**.**

Remarkably, in the presence of propargyl side chains, the methoxyethyl ones give up to their pillar role and assume another structural function.

Fascinated and intrigued by the role-playing game of those two diverse side chains in the cyclopeptoids, we decided to synthesize new compounds to study their influence on the solid-state assembly. Furthermore, applying the Hirshfeld surface method and the Hirshfeld fingerprint analysis, we aimed to highlight and quantify the different supramolecular interactions of those side chains. This information is an important concept of practical use in crystal engineering and indicates the best direction to follow in the crystal design.[116]

We started investigating the complementary partner of **1.6**, which is the cyclic hexamer of *N*-propargyl glycine (**4.19**, **Figure 5.10**). Afterwards, we thought to mix up the methoxyethyl and propargyl side chains, and we considered the symmetric cyclic hexamer with two propargyl and four methoxyethyl side chains (**4.16**, **Figure 5.10**). Encouraged by the interesting properties it showed at the solid-state, we synthesized a library of analogues. We started from **4.16**, progressively swapping the positions of one methoxyethyl with the adjacent propargyl side chain (**5.5** and **5.6**, **Figure 5.10**). Then, we synthesized its “specular” compound, featuring 4 propargyl and 2 methoxyethyl side chains (**5.7**, **Figure 5.10**), and afterwards

we moved one methoxyethyl side chain next to the other one (**5.8**, **Figure 5.10**). Finally, we ended up with the mono methoxyethylated cyclic hexapeptoid analogue (**5.9**, **Figure 5.10**).

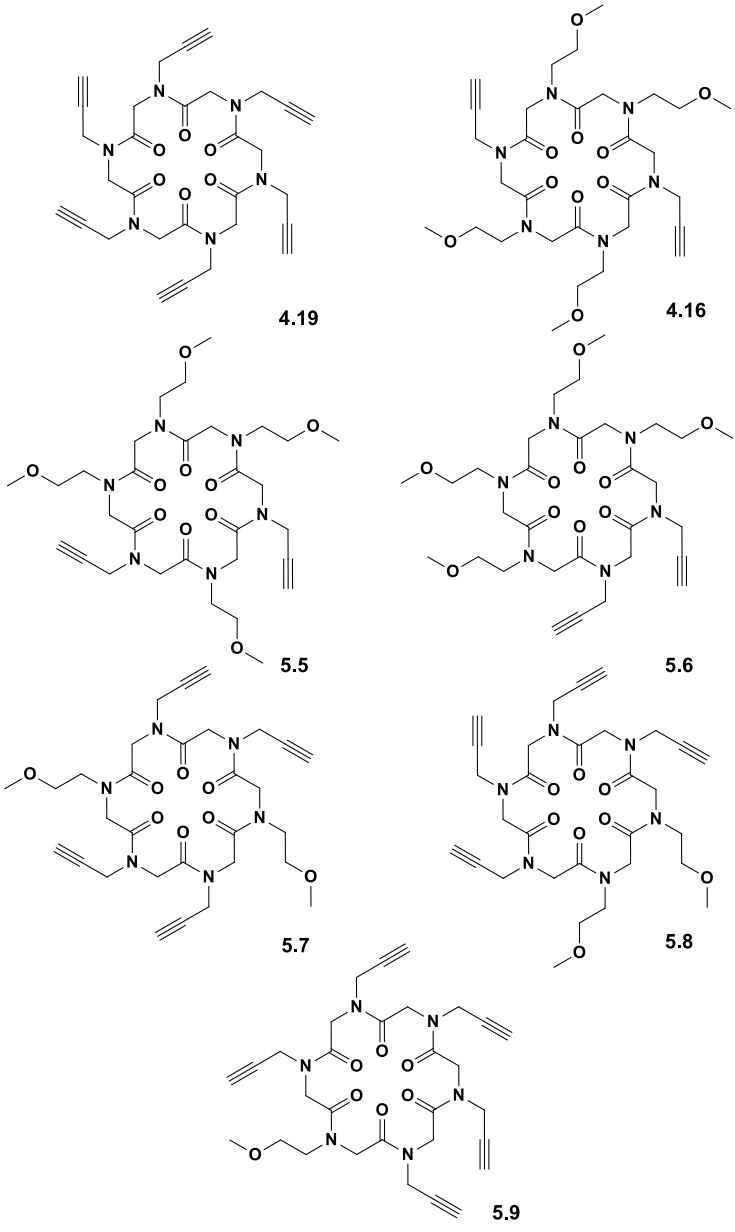

Figure 5. 10. Library of cyclic hexapeptoids **4.16**, **4.19** and **5.5-5.9**.

5.2.2 Results and Discussions

The synthesis of the linear precursors of **4.16** and **4.19** has been described in the **Scheme 4.1**, followed by the explanation of the cyclization conditions.

Analogously, the linear precursors of **5.5**-**5.9** were prepared on solid phase by means of the sub monomeric approach (**Scheme 5.1**).

Once the solid-phase synthesis of the desired linear oligomers was accomplished, **5.15**-**5.19** were detached from the acid labile 2-CTC resin under mild acidic conditions. They were collected in good yield, ranging from 59% to 97%, and in good purity, as evaluated via HPLC-PDA analysis. The crude products were rinsed with toluene and underwent to the macrocyclization reaction without further purification.

Since HATU was used as coupling agent in the previous head-to-tail condensations showing good performances, this was once again of assistance for the preparation of the cyclic compounds **5.5**-**5.9**. Hence, the linear peptoid precursors **5.15**-**5.19** were dissolved in dry DMF and slowly add, by means of a syringe pump[105], to a solution of HATU (4.0 equiv.) and DIPEA (6.2 equiv.) in dry DMF under high dilution conditions (3.0×10^{-3} M) and inert atmosphere. The macrocyclization proceeded smoothly to give the desired cyclic peptoids. After purification, compounds **5.5**-**5.9** were recovered in 56%, 70%, 37%, 57%, 86%, overall yield respectively.

With the library of cyclic peptoids in our hands, we were ready to explore their solid-state assembly properties.

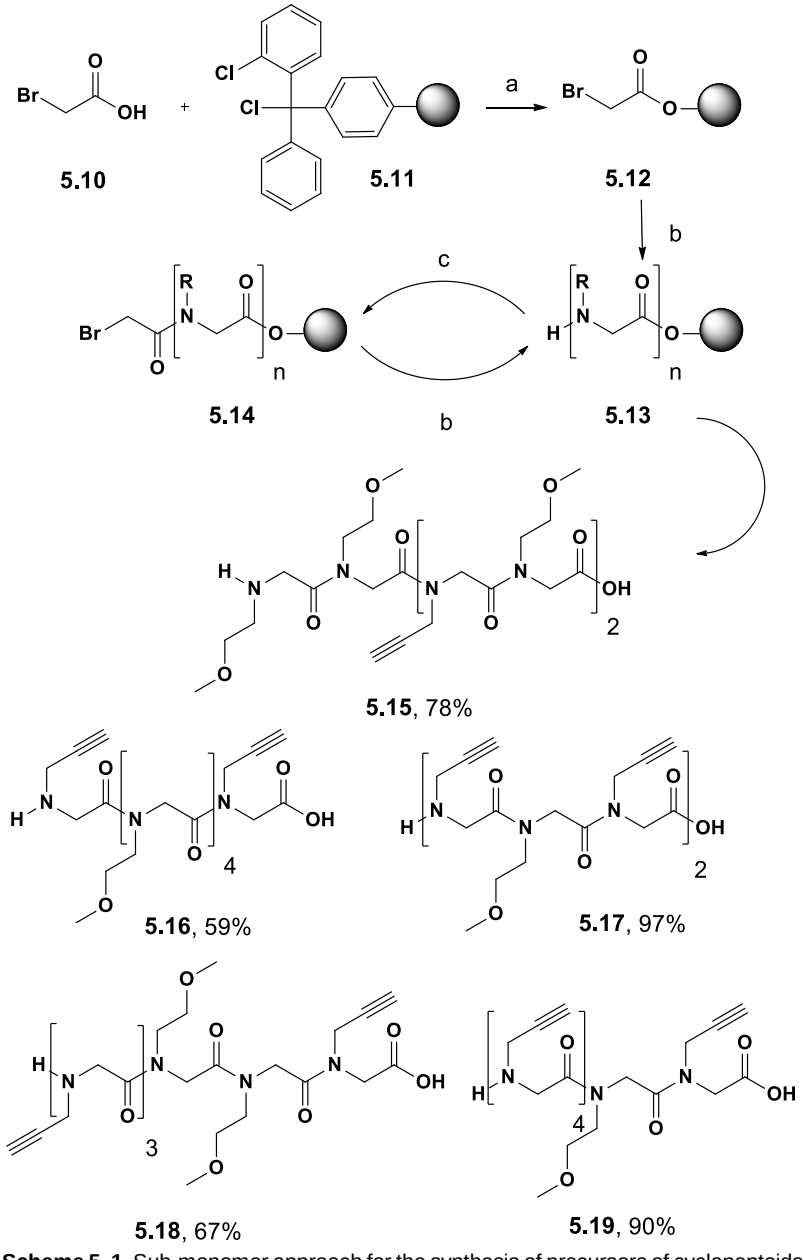

Scheme 5. 1. Sub-monomer approach for the synthesis of precursors of cyclopeptoids **5.5**-**5.9**: (a) DIPEA, in dry DCM, 1.5h; (b) propargylamine or methoxyethyl amine when needed (10 equiv) in dry DMF, 30 min; (c) bromoacetic acid/DIC (10:11 equiv.) in dry DMF, 40 min; (d) HFIP 20% in dry DCM (2 x 30 min).

The all propargylated cyclohexapeptoid **4.19** (Figure **5.10**) was crystallized by slow evaporation in hot acetonitrile (50°C) cooling down until room temperature.[117]

Colorless prism-shaped crystals were obtained, whose dimension, smaller than 0.1 mm, required synchrotron X-rays. European synchrotron radiation facility (ESRF) provided high-quality X-ray diffraction data from single crystal analysis and a high-resolution crystal structure was obtained (**Figure 5.11**).

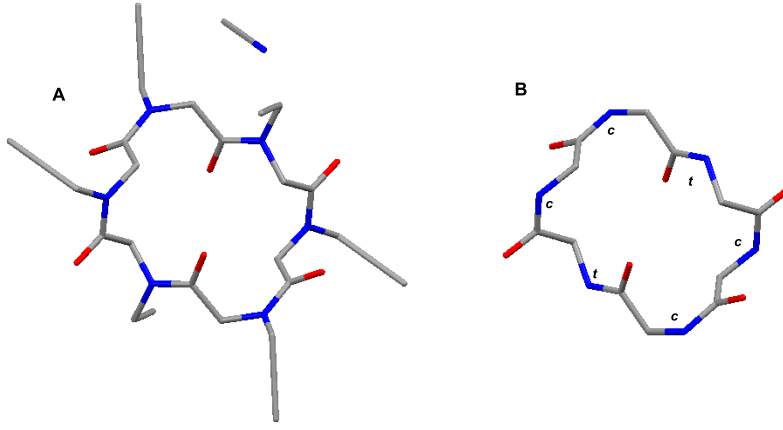

Figure 5. 11. Crystal structure of cyclic peptoid hexamer **4.19** showing: (**A**) the directions of the side chains and the presence of a molecule of acetonitrile and (**B**) the backbone. c - cis, t – trans.

The unit cell contains two macrocycles with the same conformation and four molecules of acetonitrile. As all the other cyclic hexapeptoids described,[14] **4.19** has an overall rectangular form with four *cis* amide bonds at the turn and two *trans* amide bonds along the skeleton on the opposite sides.

Figure 5.12 shows the packing of **4.19** along the cell axis. It is interesting to note that the all propargylated cyclic hexapeptoid, unlike the all methoxyethylated one, has two side chains extending

vertically from the backbone on the opposite face and providing the columnar arrangement.

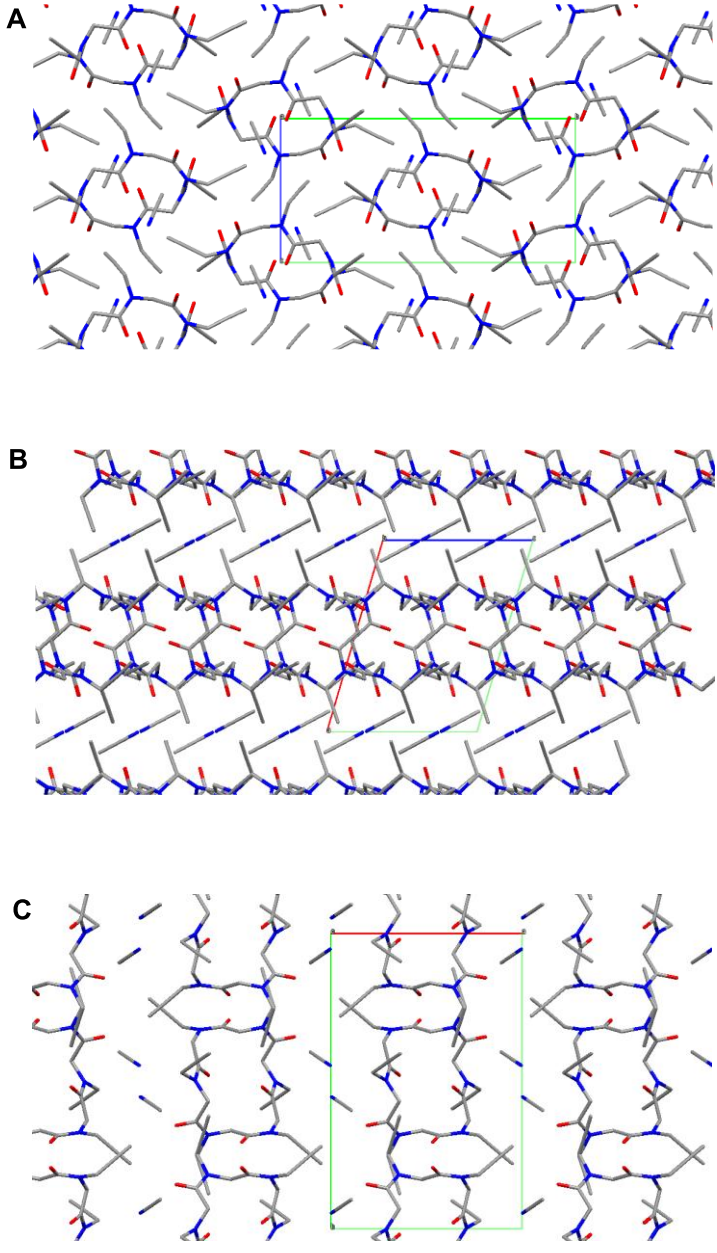

Figure 5. 12. Packing of **4.19** along the cell axis *a* (**A**), *b* (**B**) and *c* (**C**)

The other four protrude horizontally with respect the plane occupied by the macrocycle and enable lateral packing. Two of them, at the opposite corners of the macrocycle, interact with other two side chains from the adjacent macrocycle, with is rotated by 180° with res respect to the former and translated by *a*/2. The other two side chains, not only interact with the side chains from the neighbor molecule, but can also interdigitate in the cavity created by two contiguous macrocycles in the column. Finally, rows of cyclic peptoids are separated by rows of acetonitrile molecules, creating a layered structure made by cyclic peptoids alternating with guest molecules.

The calculation of d_{norm} mapped on the Hirshfeld surface, provides a clearer image of the macrocycle **4.19** and shows the interactions with the surroundings (**Figure 5.13**). It is possible to immediately appreciate the volume and the shape of **4.19**, as well as the short-distance contacts (shorter than the sum of vdW radii) depicted as red spots on the surface. Those correspond to the CH···OC contacts between the backbone carbonyl oxygen atoms and the propargyl side chain methine hydrogen atoms. Such contribution is quite important to the crystal packing and counts just shy of the H···H contacts between the side chains, as the Hirshfeld fingerprint fragmentations reveal.

The Hirshfeld fingerprint analysis reveals the significant contribution of C···H contacts between the side chains (32,1%) apart from O···H (20.7%) and H···H contacts (34,9%) (**Figure 5.14**).

Furthermore, it enables a direct comparison with the all-methoxyethylated analogue **1.6**.[14] In this case, the major contribution derives from H···H contacts (67.5%), which appear in a central green-blue wide spike that also indicates the closest ones at 2.15 Å, corresponding to contacts among methylene hydrogen atoms of

adjacent columns. In addition, O···H contacts significantly contribute to the total interactions in the crystal (30.3%), whereas C···H poorly participate to the packing (1.3%). Finally, it is worth noting the compactness of the relative packing. The fingerprint of the macrocycle **4.19** extends up to 2.6 Å, the one of **1.6** stays in the limit of 2.4 Å, indicating that this last has a more compact packing, as result of the major contribution from the stronger O···H and H···H contacts.

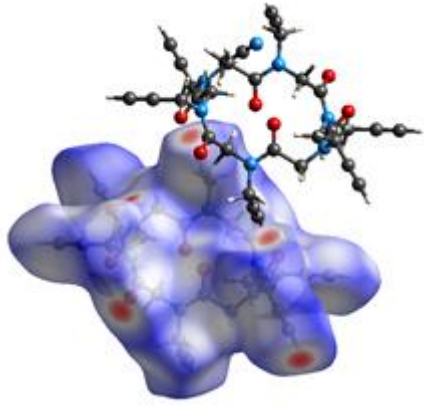

Figure 5. 13. Normalized contact distances d_{norm} mapped on the Hirshfeld surface of macrocycle **4.19**.

Having exchanged the methoxyethyl side chains with the propargyl ones has unaffected the columnar assembly at the solid state, even though the mode of forming the column has varied. The macrocycles **4.19** pile up thanks to two vertical side chains, whereas four of them provide the side-by-side assembly. The packing results less compact and acetonitrile, which is the crystallization solvent, can be host in the structure.

This interesting result prompted us to further investigate the role of methoxyethyl and propargyl side chains in cyclic hexapeptoids. We were wondering what could have happened

mixing the typology of side chains in the same macrocycle, and to satisfy our curiosity we considered the compound **4.16**.[117-118]

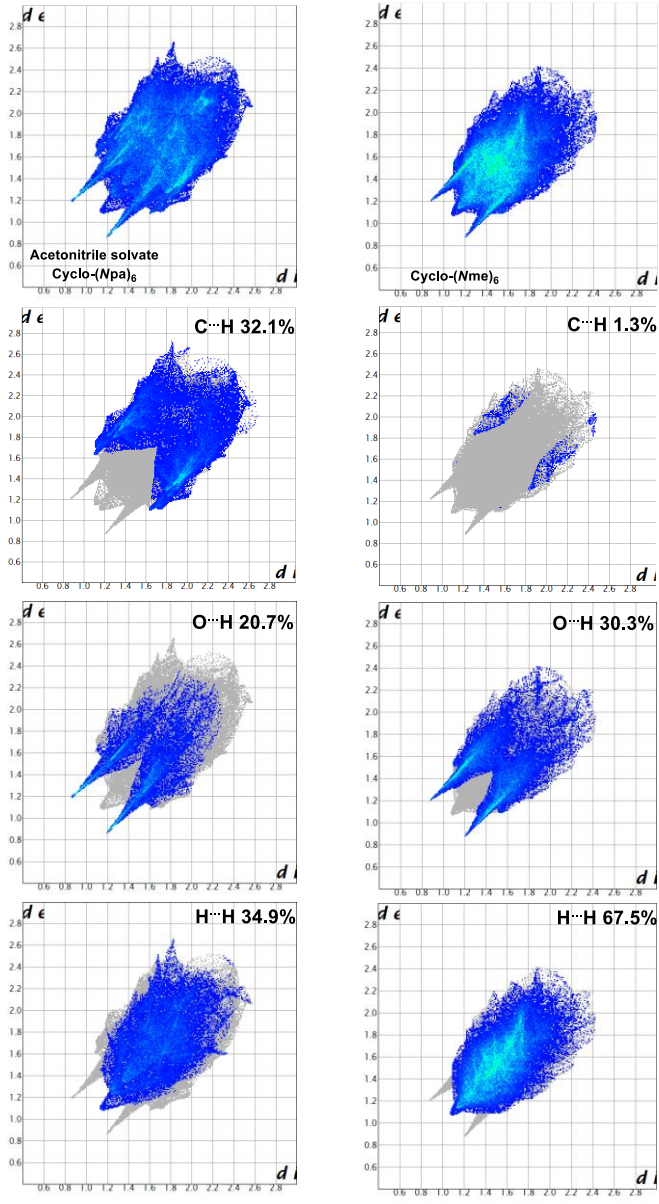

Figure 5. 14. Comparison of full fingerprint plots and decomposed fingerprint plots into O···H, C···H and H···H intermolecular interactions respectively for cyclo-(*N*pa)$_6$ (**4.19**) acetonitrile solvate, and cyclo-(*N*me)$_6$ (**1.6**).

Cyclo-(*N*pa-*N*me$_2$)$_2$ was crystallized by slow evaporation in hot acetonitrile (50°C) cooling down until room temperature. Transparent crystals were obtained and underwent X-rays analysis to yield the structure showed in **Figure 5.15**. Also in this case, the macrocycle presents an overall rectangular shape with the amide bonds configuration pattern *cctcct*. The *cis* geometries are in the correspondence of two methoxyethyl and two propargyl side chain and accommodate the backbone turn. They are situated on the opposing face of the macrocycle, according to the inversion center that is in the molecule.

The unit cell of the crystal is composed of one macrocycle and four molecules of acetonitrile (**Figure 5.16**).

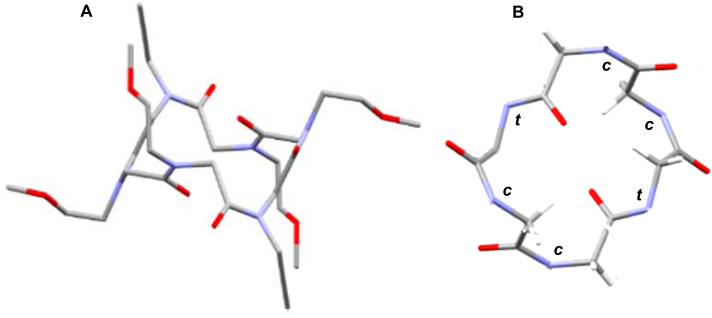

Figure 5. 15. Crystal structure of cyclic peptoid hexamer **4.16** showing: (**A**) the directions of the side chains and (**B**) the backbone. *c - cis, t – trans.*

For each cyclic peptoid molecule, the more apolar propargyl groups, stretching up vertically, provide the columnar arrangement. This is stabilized by the CH···OC hydrogen bonding between the alkynyl hydrogen atoms and the carbonyl oxygen atoms from the macrocycles above and below. The more hydrophilic methoxyethyl side groups on the *cis* bonds extends horizontally with respect to the plane occupied by the macrocycle. Protruding laterally, they enable lateral packing between rows of cyclic peptoids through side-by-side

CH···OC interactions. The vertical methoxyethyl side chains point up and down in the cavity between two contiguous macrocycles in the column and interact with molecules of acetonitrile. The solvent also interacts with the peptoidic backbone and other molecules of acetonitrile. **Figure 5.16A** shows the packing along the *a* axis and highlights rows of cyclic peptoids running in parallel, and molecules of acetonitrile that insert between them.

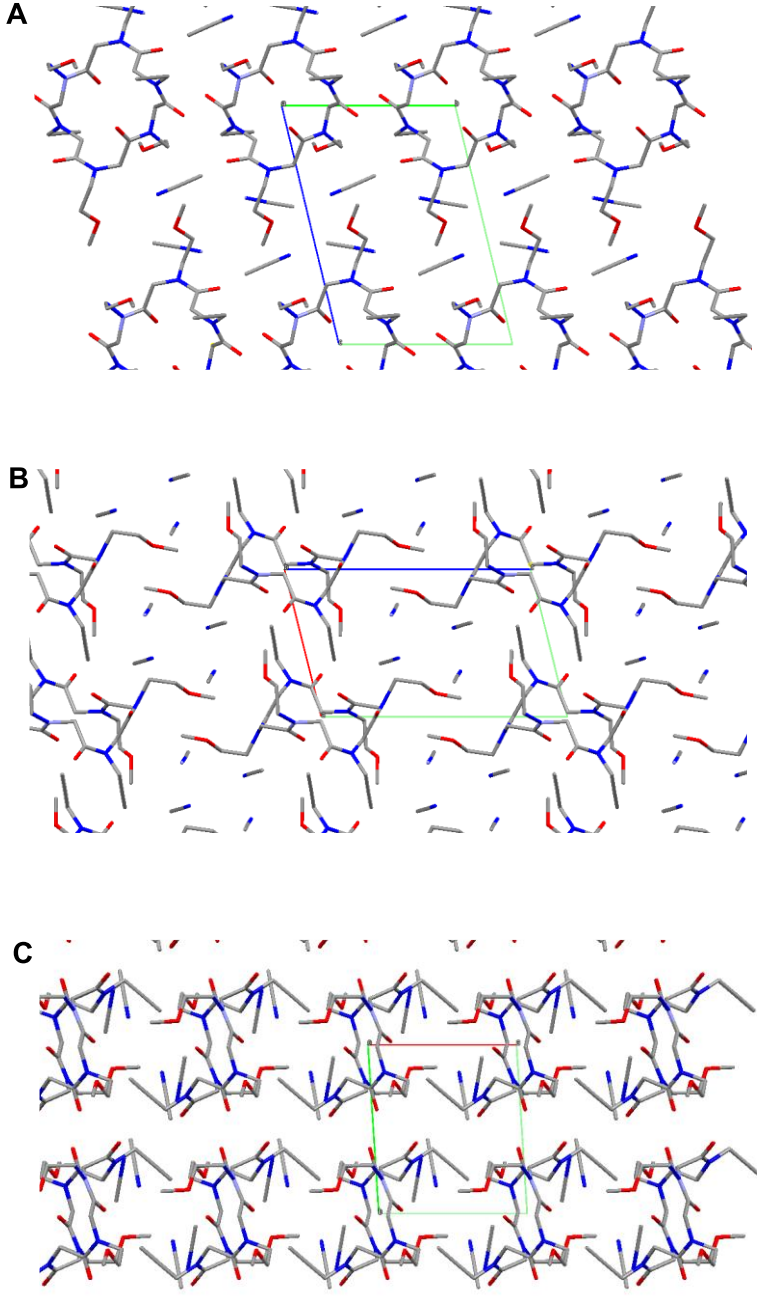

Figure 5. 16. Packing of **4.16** along the cell axis *a* (**A**), *b* (**B**) and *c* (**C**) showing hydrogen bonding.

It is interesting to note that, as for compound **5.4**,[111] when propargyl side chains come into play, they are the ones who promote the columnar assembly via CH···OC hydrogen bonding. The presence of the methoxyethyl side chains guarantees intercolumnar contacts. All the interactions can be better displayed on the Hirshfeld surface mapping d_{norm} (**Figure 5.17**). The red spots highlight the short contacts CH···OC within two macrocycles within a column.

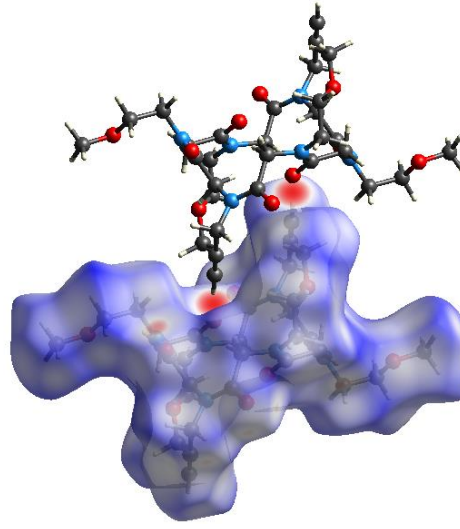

Figure 5. 17. Normalized contact distances d_{norm} mapped on the Hirshfeld surface of macrocycle **4.16**.

Those remarks pushed us to move on in such investigation. Hence, we decided to consider first the cyclic peptoid **5.7** from the library in **Figure 5.10**, given its analogy with compound **4.16**. Indeed, with respect to **4.16**, it keeps two methoxyethyl groups at opposite positions on the cyclic peptoid core but it has a higher content of propargyl side chains.

Compound **5.7** was dissolved in hot acetonitrile and, slowly cooling the solution, it crystalized as white blocky and flat-plate crystals (**Figure 5.18**).

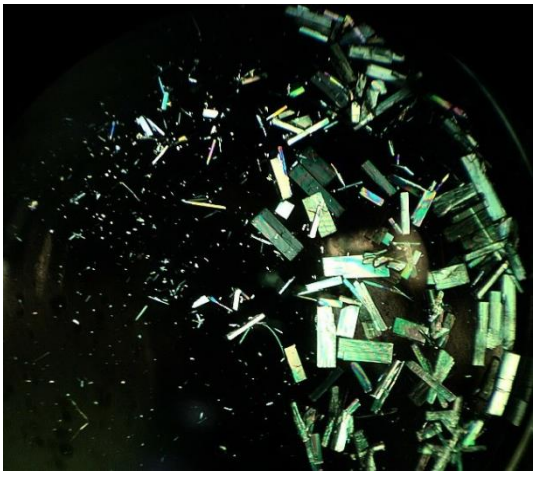

Figure 5. 18. Crystals of **5.7**. View from the microscope.

X-ray crystallography revealed a solvate structure with acetonitrile. The macrocycle has a crystallographic inversion center and the cyclic peptoidic backbone once again presents the amide bonds sequence *cctcct* with slightly distorted bond angles (**Figure 5.19**). The *cis* geometries are in the correspondence of the four propargyl side chains and accommodate the backbone turn. Two of them extend horizontally in the equatorial directions, while the methoxyethyl, together with the remaining propargyl side chains, point vertically up and down with respect to the macrocycle plane (**Figure 5.20**). The alkynyl hydrogen atoms from the vertical propargyl side chains of the cyclic peptoid are involved in hydrogen bonding with the carboxyl oxygen atoms from the macrocycles above and below. Those CO···HC interactions provide a columnar arrangement along the shortest c axis, similarly to the analogue **4.16**. Furthermore, methoxyethyl side chains do not contribute to CO···HC contacts, but rather to CH-pi interactions between both methylene and methyl hydrogen atoms, and the vertical propargyl group of the next cyclopeptoid molecule.

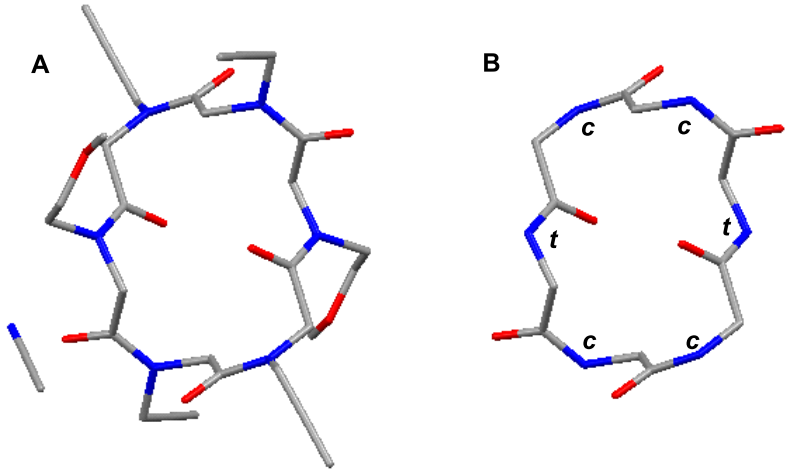

Figure 5. 19. Crystal structure of cyclic peptoid hexamer **5.7** showing: (**A**) the directions of the side chains and one molecule of acetonitrile and (**B**) the backbone. *c - cis, t – trans.*

The horizontal propargyl side chains enable lateral packing. Indeed, the methylene atoms act as H donors towards the triple bond pi system from the vertical propargyl side chains of the next cyclopeptoid molecules via CH-pi interactions.

Acetonitrile molecules sit in the space between the cyclopeptoids rows, forming channels parallel to the *c* axis and alternating with cyclopeptoids. CH-pi interactions (N≡C···HC) between acetonitrile molecules link them together, whereas they poorly interact with cyclopeptoid molecules by means of the methyl hydrogen atoms to one carbonyl oxygen atom (CO···HC) and to the equatorial propargyl triple bond (C≡C···HC).

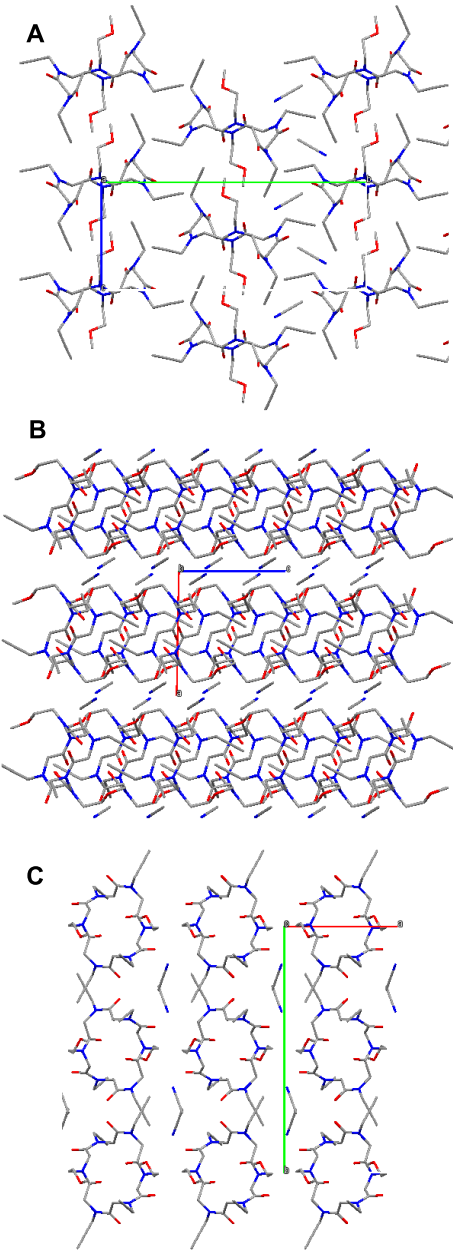

Figure 5. 20. Packing of **5.7** along the cell axis *a* (**A**), *b* (**B**) and *c* (**C**). Crystal structures includes acetonitrile molecules.

The Hirshfeld surface displaying d_{norm} for the compound **5.7** reveals the red spots in the correspondence of the short CH···CO interactions, involving the vertical propargyl side chains and the carbonyl oxygen atom (**Figure 5.21**).

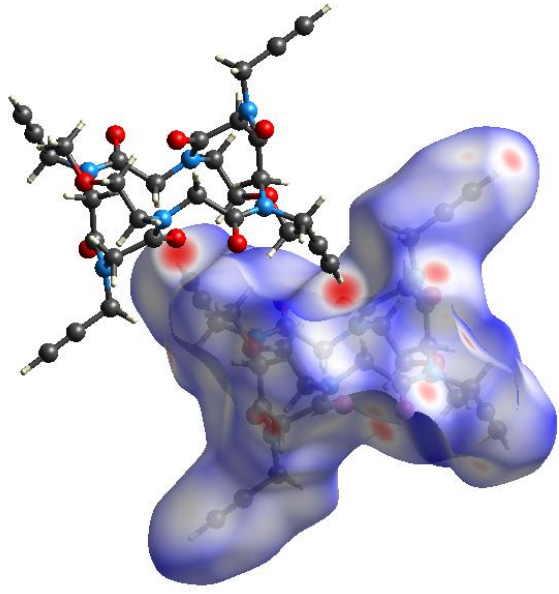

Figure 5. 21. Normalized contact distances dnorm mapped on the Hirshfeld surface of macrocycle **5.9.**

The Hirshfeld fingerprint analysis provides the quantitative contribution of each type of interaction to the packing and enable for a comparison between the two parental structures from **4.16** and **5.9**. Both the structures are acetonitrile solvate, but the first shows a more compact packing than the second one, as evidenced by its fingerprint extending in the limit of 2.3 Å. Indeed, it has a higher frequency of short-distance contacts that are indicated by the light blue-colored pixel in the fingerprint breakdown for H···H interactions. Those arise mainly from the methoxyethyl side chains interdigitating within the columns of cyclic peptoids.

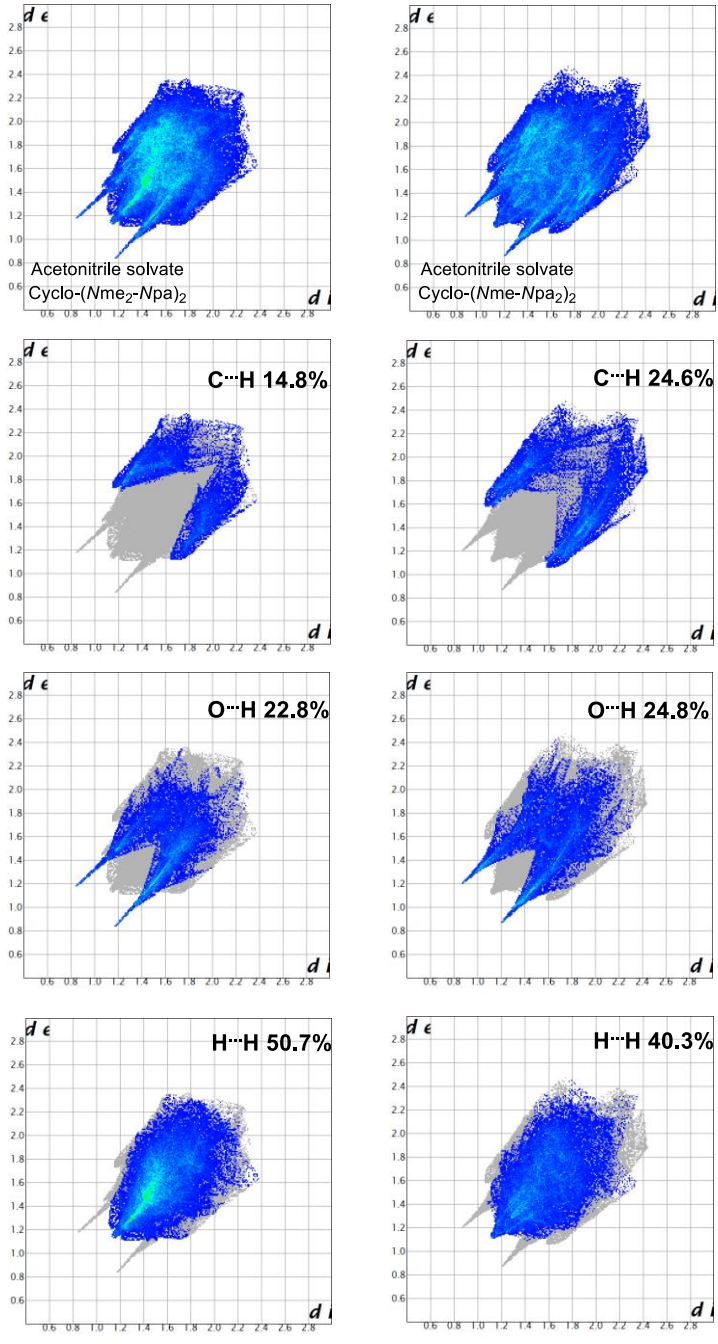

Figure 5. 22. Hirshfeld fingerprints for compound **4.16** and **5.9**.

Remarkably, in both cases we evidence the same contribution from O···C hydrogen bonding, visible as two spikes in the fingerprint plot and counting for 22.8% and 24.8%. This confirms that the shortest interactions, fundamental for the columnar assembly, are a common feature in this compounds and can be addressed just to two propargyl side chains pointing up and down with respect to the plane of the macrocycle. C···H interactions poorly contribute to the crystal packing. They can be ascribed to the CH-pi interactions with the triple bond from the propargyl side chains and appear as lateral wings in the fingerprint breakdown. Having two more propargyl groups in the compound **5.9** is evidenced also by the higher percentage of such contacts in the structure (24.6% vs 14.8%).

5.3 CONCLUSION

Cyclic peptoids have been demonstrated to be extremely interesting to study by means of X-ray crystallography.

The flexibility of the peptoidic backbone renders the role of the side chains of primary importance in defining cyclic peptoid structure at the solid state.

Our aim was to gain a deep understating of side chains structural function, in order to get control over the conformation of such peptidomimetics and achieving the desired folding properties.

To pursue our interest, we synthesized a library of cyclic hexapeptoids comprising methoxyethyl and propargyl side chains. We varied their relative content and positioning along the peptoidic backbone to shed light on their respective role in the assembly.

From comparison X-ray crystal structures and making use of the Hirshfeld surfaces and fingerprints, we could grasp cyclic peptoids structural features.

Both of the side chains tend to promote a columnar assembly, in which the macrocycles stack on the top of each other. The columns form rows, which are alternated with molecules of acetonitrile entering into the structure.

Independently from the total number of propargyl side chains in the cyclic hexapeptoids, just two of them are involved in the vertical assembly that gives rise to the columnar assembly. Two methoxyethyl side chains, on the other hand, extend horizontally in the plane of the macrocycle and provide side-by-side interactions, which stabilize the intercolumnar assembly. The last two side chains are of assistance, and can occupy either a vertical either a horizontal orientation. Depending on them and their interactions, the packing can result more or less compact.

This result is extremely exciting and opens up new frontiers of investigation. Being able to manipulate the assistant side chains orientation within the same crystal would lead to materials featured by dynamicity. We managed to control the backbone conformation and side chains orientation creating columnar assemblies. Now it is time to add a further degree of control to in the search of new and unexplored properties and application of this class of peptidomimetics.

CHAPTER 6

Conclusion

6

6.1 CONCLUDING REMARKS

Our journey into the realm of peptoids ends up here.

Chasing new structures and properties, we contributed to the development of novel compounds that displayed interesting features and potential applications.

We managed to synthesize a new class of “arylopeptoids”, by the insertion of an aromatic ring and a methylene unit into the peptoidic backbone (Chapter 2). Tested as ion transporters, the cyclic tetramer resulted to be too large to selective accommodate any ion, whereas the cyclic trimer is slightly active towards the mid-size alkaline cations (Na^+, K^+, Rb^+), preferably transported with the iodide counterion, showing a symport carrier mechanism.

Exploiting the ion complexation properties of cyclic peptoids, we synthesized two hexamers with three carboxyethyl side chains each, to promote the formation of Gd^{3+}-complex as MRI-probes (Chapter 3). Binding studies revealed the importance of the structural flexibility of the host on its complexation ability. When carboxyethyl side chains are alternated with methoxyethyl side chains, the cyclic peptoid coordinates Gd^{3+} and displays good relaxometric properties, but if proline residues are introduced, the structure results too rigid to complex.

The versatility of peptoids enable us to explore the field of glycoscience as well. A library of cyclic peptoids, ranging from 4-mer to 16-mer, with appended propargyl groups was synthesized and underwent click chemistry DNJ azido-derivatives (Chapter 4). This is the first example of cyclopeptoid-based iminosugar click-clusters, that showed acitivity towards α-mannosidases inhibition and the

highest multivalent effect in the correspondence of the 36-valent ligand.

This impressive outcome is the result of the modular synthetic approach of peptoids that enables for the insertion of an unlimited numbers and types of side chains.

Taking advantage of such feature, we synthesized a library of cyclic hexapeptoids with methoxyethyl and propargyl side chains, varying in the relative content and positions (Chapter 5). Studying their role in the solid-state assembly of cyclic hexapeptoids, they showed to promote a columnar arrangement in which the propargyl groups are the pillars and the methoxyethyl chains provide intercolumnar interactions and side-by-side contacts.

The vast properties of peptoids and their versatility of use clearly emerge within the chapters of the thesis.

The results obtained contribute to a better understanding of their structural features, providing tools to finely tune their properties in order to further expand their potential applications. Moreover, new and challenging questions arose along with these studies. Finding the right answer will be the task of the future science to broaden the knowledge and expand the horizons of the realm of the peptoids.

CHAPTER 7

Experimental Section

7

7.1 GENERAL PROCEDURES

Starting materials and reagents purchased from commercial suppliers were generally used without purification unless otherwise mentioned. All the linear peptoids were synthesized in solid phase. Solid phase syntheses were undertaken manually in polypropylene syringes fitted with two polyethylene filter discs. All solvents and soluble reagents were removed by suction. Washings between coupling and displacement steps were carried out with DMF (3 × 1 min) and DCM (3 × 1 min) using 4 mL solvent/g resin for each wash. The coupling efficiency was followed by chloranil colorimetric test. Each treatment was carried out in orbital shakers. Reaction temperatures were measured externally; reactions were monitored by TLC on Merck silica gel plates (0.25 mm) and visualized by UV light or by spraying with ninhydrin solution. Flash chromatography was performed on Merck silica gel 60 (particle size: 0.040-0.063 mm) and the solvents employed were of analytical grade. HPLC analysis were performed on a JASCO LC-NET II/ADC and a Thermo Scientific instruments. The first one comprises a JASCO Model PU-2089 Plus Pump and a JASCO MD-2010 Plus UV-vis multiple wavelength detector set at 220 nm, the second one a Finnigan Surveyor LC Pump Plus and a Finnigan Surveyor UV/Vis Plus Detector set at 220 nm. The columns used were C_{18} reversed-phase analytical and semipreparative columns (Waters, Bondapak, 10 μ m, 125 Å, 3.9 mm × 300 mm and 7.8 × 300 mm, respectively) run with linear gradients of ACN (0.1% TFA) into H2O (0.1% TFA) over 30 min, at a flow rate of 1.0 mL/min for the analytical runs and 2.0 mL/min for the semipreparative ones. High resolution ESI-MS spectra were recorded on a Q-Star Applied Biosystem mass

spectrometer. ESI-MS analysis in positive ion mode was performed using a Finnigan LCQ Deca ion trap mass spectrometer (ThermoFinnigan, San Josè, CA, USA) and the mass spectra were acquired and processed using the Xcalibur software provided by Thermo Finnigan. Samples were dissolved in 1:1 CH_3OH/H_2O, 0.1 % formic acid, and infused in the ESI source by using a syringe pump; the flow rate was 5 µl/min. The capillary voltage was set at 4.0 V, the spray voltage at 5 kV, and the tube lens offset at -40 V. The capillary temperature was 220 °C. Data were acquired in MS1 and MSn scanning modes. Zoom scan was used in these experiments. High-resolution ESI-MS spectra were recorded on a Q-Star Applied Biosystem mass spectrometer.

NMR spectra were recorded on a Bruker DRX 600 (^1H at 600.13 MHz, ^{13}C at 150.90 MHz), Bruker DRX 400 (^1H at 400.13 MHz, ^{13}C at 100.03 MHz), Bruker DRX 300 (^1H at 300.1 MHz, ^{13}C at 75.5 MHz) and Bruker DRX 250 (^1H at 250.0 MHz, ^{13}C at 62.5 MHz). Chemical shifts (δ) are reported in ppm relative to the residual solvent peak ($CHCl_3$, δ = 7.26; $^{13}CDCl_3$, δ = 77.0; CD_2HCN , δ = 1.94; $^{13}CD_3CN$, δ = 1.32) and the multiplicity of each signal is designated by the following abbreviations: s, singlet; d, doublet; t, triplet; m, multiplet; bs, broad singlet. Coupling constants (*J*) are quoted in Hertz. DEPT and COSY experiments completed the full assignment of each signal. Purity of all products described herein has been determined by HPLC-PDA analysis at 220 nm.

7.2 COMPOUNDS FROM CHAPTER 2

7.2.1. Synthesis and Characterization

Compound 2.24

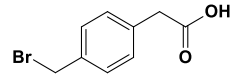

2.24

p-Tolylacetic acid (3.0 g, 20 mmol), *N*-bromosuccinimide (3.7 g, 21 mmol) and benzoylperoxide (0.10 g, 0.41 mmol) were dissolved in 150 ml of CCl_4. The mixture was refluxed for 15 h and filtered hot. The filtrate was concentrated *in vacuo*. The solid was rinsed with cold CCl_4 to give **2.24** as a white amorphous solid with variable amounts of succinimide. Crude **2.24** (1.82 g, 40%, based on ^{1}H NMR analysis) underwent the subsequent step without further purification.

^{1}H NMR: (300 MHz, $CDCl_3$) δ: 7.30 (2H, d, *J* 8.0 Hz, Ar), 7.27 (2H, d, *J* 8.0 Hz, Ar), 4.48 (2H, s, C*H*$_2$Br), 3.66 (2H, s, C*H*$_2$COOH).

ESI-MS (positive, m/z): 229.0 m/z (100, $[M + H]^+$), 231.0 m/z (98, $[M + H]^+$).

Compound 2.25

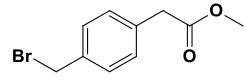

2.25

To a solution of 4-(bromomethyl)phenylacetic acid (1.8 g, 7.9 mmol) in MeOH (20 mL) was added trimethylsilyl chloride (1.6 mmol, 0.20 mL), and the mixture was stirred for 5 h. The solvent was removed *in vacuo* and the residue was dissolved in again dissolved in MeOH (20 mL) and finally concentrated to give **2.25** as a thick oil (1.87 g, 97%).

^{1}H NMR: (250 MHz, $CDCl_3$) δ: 7.35 (2H, d, *J* 8.0 Hz, Ar), 7.25 (2H, d, *J* 8.0 Hz, Ar), 4.47 (2H, s, C*H*$_2$-Br), 3.69 (3H, s,

COOC<u>*H*</u>$_3$), 3.62 (2H, s, C<u>*H*</u>$_2$COOCH$_3$). ^{13}C NMR: (62.5 MHz, $CDCl_3$) δ: 171.6 (<u>*C*</u>OOCH$_3$), 136.5 (<u>*C*</u>CH$_2$Br), 134.2 (<u>*C*</u>CH$_2$CO), 129.6, (<u>*C*</u>H x 2) 129.2 (<u>*C*</u>H x 2), 52.0 (COO<u>*C*</u>H$_3$), 40.7(<u>*C*</u>H$_2$CO), 33.1 (<u>*C*</u>H$_2$Br).

ESI-MS: 243.0 m/z (100, $[M + H]^+$), 245.0 m/z (98, $[M + H]^+$).

Compound 2.26

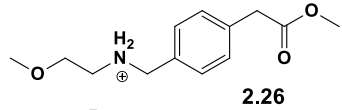

2.26

To a solution of methoxyethyl amine (3.3 mL, 38 mmol) in dry DMF (4.0 mL) was slowly added (20 minutes) a solution of 4-(bromomethyl)phenylacetate **2.25** (1.9 g, 7.7 mmol) in dry DMF (40 mL). After the addition, the mixture was stirred for 2 h. The solvent was removed in vacuo to give the crude product **2.26** as a pale yellow oil (2.40 g, 98%), which was used in the next step without further purification.

^{1}H NMR: (250 MHz, $CDCl_3$) δ: 7.59 (2H, d, *J* 8.0 Hz, Ar), 7.29 (2H, d, *J* 8.0 Hz, Ar), 6.31 (2H, bs, N<u>*H*</u>$_2^+$), 4.20 (2H, s, CC<u>*H*</u>$_2$-NH$_2^+$), 3.78 (2H, t, *J* 6.0 Hz, C<u>*H*</u>$_2$OCH$_3$), 3.68 (3H, s, COOC<u>*H*</u>$_3$), 3.60 (2H, s, C<u>*H*</u>$_2$COOH), 3.38 (3H, s, C<u>*H*</u>$_2$OC<u>*H*</u>$_3$), 3.07 (2H, t, *J* 6.0 Hz, C<u>*H*</u>$_2$NH$_2^+$). ^{13}C NMR: (62.5 MHz, $CDCl_3$) δ: 171.8 (<u>*C*</u>OOCH$_3$), 135.3 (<u>*C*</u>CH$_2$CO), 130.8 (<u>*C*</u>H x 2), 130.0 (<u>*C*</u>H x 2), 129.4 (<u>*C*</u>CH$_2$NH$_2^+$), 67.5(CH$_2$O<u>*C*</u>H$_3$), 59.0 (CH$_2$O<u>*C*</u>H$_3$), 52.1 (COO<u>*C*</u>H$_3$), 51.0 (C<u>*C*</u>H$_2$NH$_2^+$), 45.4 (CCH$_2$NH$_2^+$<u>*C*</u>H$_2$), 40.6 (C<u>*C*</u>H$_2$CO).

ESI-MS: 238.5 m/z (100, $[M + H]^+$).

Compound 2.27

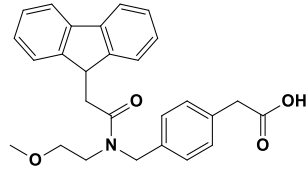

2.27

To a stirred solution of crude **2.26** (2.4 g, 7.6 mmol) in 1,4-dioxane (30 mL) at 0 °C, $LiOH•H_2O$ (0.79 g, 19 mmol) in H_2O (30 mL) was added. After two hours, $NaHCO_3$ (1.3 g, 15 mmol) and Fmoc-Cl (2.9 g, 11 mmol) were added. The reaction mixture was stirred overnight. Subsequently, $KHSO_4$ was added (until pH=3) and the mixture was concentrated in vacuo to remove the excess of 1,4-dioxane. CH_2Cl_2 (100 mL) was added to the mixture and the aqueous layer was extracted with CH_2Cl_2 (three times). The combined organic phases were dried over $MgSO_4$, filtered and the solvent evaporated *in vacuo* to give a crude material (4.4 g, yellow amorphous oil). The residue was purified by flash chromatography (CH_2Cl_2/CH_3OH, from: 100/0 to 95/05, 0.1% AcOH) to give **2.27** (1.48 g, 44%).

^{1}H NMR: (400 MHz, $CDCl_3$, mixture of rotamers) δ: 7.85-7.02 (12H, m, Ar and Ar[Fmoc]), 4.63 (1H, d, *J* 6.6 Hz, C*H*$_2$[Fmoc] rot. a), 4.54-4.47 (3H, m, C*H*$_2$[Fmoc] rot. b, CC*H*$_2$N rot. a and rot. b), 4.26 (0.55H, t, *J* 6.6 Hz,C*H*[Fmoc] rot. a), 4.21 (0.45H, t, *J* 6.6 Hz, C*H*[Fmoc] rot. b), 3.65 (1H, s, C*H*$_2$-COOH rot. a), 3.63 (1H, s, C*H*$_2$COOH rot. b), 3.52 (0.98H, t, *J* 5.3 Hz, C*H*$_2$$OCH_3$ rot. a), 3.45 (1.02H, t, *J* 5.3 Hz, NC*H*$_2$ rot. a), 3.32 (2H, m, C*H*$_2$$OCH_3$ and NC*H*$_2$ rot. b), 3.20 (1.54 H, s, OC*H*$_3$ rot. a), 3.17 (1.46 H, s, OC*H*$_3$ rot. b). ^{13}C NMR: (100 MHz, $CDCl_3$, mixture of rotamers) δ: 176.7 (*C*OOH), 156.5 (*C*O[Fmoc] rot. a), 156.3 (*C*O[Fmoc] rot. b), 143.9 (*C*[Fmoc] rot. a), 143.8 (*C*[Fmoc] rot. b), 141.3 (*C*[Fmoc] rot. a), 141.2 (*C*[Fmoc] rot. b), 136.6, (*C*[Ar]), 132.4 (*C*[Ar] rot. a), 132.3 (*C*[Ar] rot. b), 130.0 (*C*H[Ar] rot. a), 129.9 (*C*H[Ar] rot. b), 129.4, (*C*H[Ar]), 127.9 (*C*H[Fmoc] rot. a), 127.5 (*C*H[Fmoc] rot. a), 127.2 (*C*H[Fmoc] rot. b), 127.0 (*C*H[Fmoc] rot. a), 126.9 (*C*H[Fmoc] rot. b), 124.7 (*C*H_2[Fmoc] rot. a), 124.6 (*C*H_2[Fmoc] rot. b), 120.0 (*C*H[Fmoc] rot. b), 70.8 (*C*H_2[Fmoc] rot. a), 70.6 (*C*H_2[Fmoc] rot. b), 67.3 (*C*$H_2$$OCH_3$ rot. a), 66.9 (*C*$H_2$$OCH_3$ rot. b), 58.6 (CH_2O*C*H_3 rot. a), 58.5 (CH_2O*C*H_3 rot.

b), 51.0 (C<u>C</u>H$_2$N rot. a), 50.8 (C<u>C</u>H$_2$N rot. b), 47.3 (<u>C</u>H[Fmoc] rot. a), 47.1 (<u>C</u>H[Fmoc] rot. b), 46.5 (N<u>C</u>H$_2$ rot. a), 45.6 (N<u>C</u>H$_2$ rot. b), 40.6 (<u>C</u>H$_2$COOH).

ESI-MS: 446.3 m/z (100, $[M + H]^+$), 468.1 m/z (71, $[M + Na]^+$), 484.1 m/z (98, $[M + K]^+$).

Linear peptoids 2.32 and 2.33

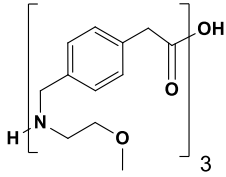

2.32

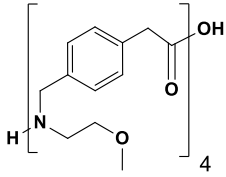

2.33

Linear oligomeric *N*-substituted aminomethyl benzylamides **2.32** and **2.33** were synthesized using a monomer solid-phase approach. In a typical synthesis, 2-chlorotrityl chloride resin (α-dichlorobenzhydryl-polystyrene cross-linked with 1% DVB; 100 – 200 mesh; 1.5 mmol g-1, 0.10 g, 0.15 mmol) was swollen in dry CH_2Cl_2 (1 mL) for 45 min and washed twice with dry DMF (1 mL) and dry DCM (1 mL). The first monomer **2.27** was loaded on the resin with the following protocol; 0.67 equiv of **2.27** (90.0 mg, 0.20 mmol) and 4.0 equiv of DIPEA (140 µL, 0.80 mmol) were dissolved in dry CH_2Cl_2 (1 mL) and the solution was added onto the resin. The resulting mixture was shaken on a shaker platform for 90 min at room temperature, and then rinsed with CH_2Cl_2 (3 × 1 min) and DMF (3 × 1 min). To terminate the excess of reactive positions, the resin was incubated with 1 mL of a capping solution; DCM/MeOH/DIPEA (17:2:1) and the reaction was shaken for 15 more min. Then, the solvents were removed by suction, and the resin washed with DCM (3 × 1 min), DMF (3 × 1 min) and DCM (3 × 1 min). The oligomer elongation was realized alternating deprotection and coupling steps, until the desired length was accomplished. The

Fmoc-deprotection treatment was carried out with Piperidine/DMF (1:4) (2 x 1 min, 2 x 5 min) and the subsequent coupling with 3.0 equiv of **2.27** (133 mg, 0.30 mmol), 3.0 equiv of HATU (110 mg, 0.3 mmol) and 6.0 equiv of DIPEA (104 µL, 0.60 mmol) in dry DMF (1 h). The resulting deprotected linear oligomer was cleaved using a HFIP/DCM (1:4) solution (2 x 30 min) and then washed with DCM. The resin was then filtered away and the combined filtrates were concentrated *in vacuo*. The final products were dissolved in 50% acetonitrile in HPLC grade water and analyzed by RP-HPLC [purity >90% for **2.32** and **2.33**; conditions: 5 → 100% A in 30 min for the all oligomers (A, 0.1% TFA in acetonitrile, B, 0.1% TFA in water); flow: 1 mL min− 1, 220 nm]. The linear oligomers were subjected to the cyclization reaction without further purification.

2.32: 60% (crude residue); ES-MS: 634.3 m/z $[M + H]^+$; t_R : 11.9 min.

2.33: 60% (crude residue); ES-MS: 839.4 m/z $[M + H]^+$; t_R : 13.6 min.

Compounds 2.19 and 2.20

A solution of the linear oligomers **2.32** and **2.33** (0.060 mmol), previously co-evaporated three times with toluene, was prepared under nitrogen in dry DMF (4 mL). The mixture was dropwise added to a stirred solution of HATU (90 mg, 0.24 mmol) and DIPEA (64 µL, 0.37 mmol) in dry DMF (16 mL) by a syringe pump in 12 h, at room temperature in anhydrous atmosphere. After 24 h the resulting mixture was concentrated *in vacuo*, diluted with CH_2Cl_2 (50 mL), and washed with a solution of HCl (1.0 M, 25 mL). The water layer was further extracted with CH_2Cl_2 (2 × 50 mL) and the combined organic phases were washed with water (100 mL), dried over anhydrous $MgSO_4$, filtered and concentrated *in vacuo.* The cyclic products were dissolved in 50% acetonitrile and HPLC grade

water and analyzed by RP-HPLC [purity >95% for oligomers **2.19** and **2.20**, conditions: 5% – 100% A in 30 min for the two cyclopeptoids (A, 0.1% TFA in acetonitrile, B, 0.1% TFA in water); flow: 1 mL min^{-1}, 220 nm]. The crude residue **2.19** was purified by flash chromatography on a C18 silica gel, conditions: 20% – 60% A [(A, 0.1% TFA in acetonitrile, B, 0.1% TFA in water); while **2.20** by precipitation in ethyl acetate.

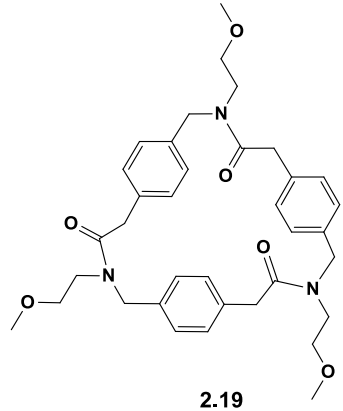

2.19

Compound **1.19**: 25%; pale yellow amorphous solid; t_R: 13.3 min (see general information for the conditions).

^{1}H NMR: (600 MHz, CD_3CN, mixture of rotamers) δ : 7.31 (1H, d, *J* 7.4 Hz, Ar), 7.28 (9H, m, Ar), 6.90 (2H, d, *J* 7.4 Hz, Ar), 4.76-4.53 (6H, m, ArC*H*$_2$N), 3.84-3.32 (18H, m, COC*H*$_2$Ar, NC*H*$_2$CH$_2$OCH$_3$, NCH$_2$C*H*$_2$OCH$_3$), 3.29-3.20 (9H,mm, NCH$_2$CH$_2$OC*H*$_3$). ^{13}C NMR: (150 MHz, CD_3CN, mixture of rotamers, broad signals) δ: 172.8, 172.6, 172.5, 172.3, 172.1, 138.1, 137.7, 137.6, 137.4, 137.3, 137.0, 136.9, 136.2, 135.8, 135.6, 135.4, 130.5, 130.3, 130.2, 129.9, 129.8, 129.5, 129.4, 129.1, 128.9, 128.8, 128.7, 128.5, 127.6, 127.4, 127.3, 127.1, 71.7, 71.4, 71.2, 71.0, 70.8, 70.7, 70.5, 70.4, 70.1, 70.0, 59.1, 59.0, 58.9, 58.8, 58.6, 58.5, 49.2, 49.0, 48.9, 48.7, 48.6, 48.5, 48.4, 48.3, 48.0, 47.9, 47.8, 41.2, 41.0, 40.8, 40.7, 40.6, 40.5, 40.4, 40.3, 30.7, 30.6, 30.3, 30.1.

ESI-MS: 616.6 m/z (100, $[M + H]^+$), 638.7 m/z (93, $[M + Na]^+$) and 654.6 m/z (20, $[M + K]^+$).

ESI-HR MS: $[M + H]^+$ m/z 616.3356 (calcd for $C_{36}H_{46}N_3O_6$ 616.3387).

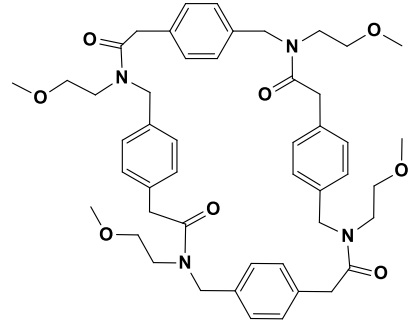

2.20

Compound **2.20**: 16%; white amorphous solid; t_R: 14.7 min (see general information for the conditions).

^{1}H NMR: (600 MHz, $CDCl_3$, mixture of rotamers) δ: 7.33-6.70 (16H, m, Ar), 4.57-3.06 (44H, m, ArC$\underline{H_2}$N, COC$\underline{H_2}$Ar, NC$\underline{H_2}$CH$_2$OCH$_3$, NCH$_2$C$\underline{H_2}$OCH$_3$, NCH$_2$CH$_2$OC$\underline{H_3}$). ^{13}C-NMR: (150 MHz, $CDCl_3$, mixture of rotamers, broad signals) δ : 171.8, 171.5, 136.1, 135.5, 134.9, 134.7, 134.6, 134.4, 134.1, 133.9, 129.9, 129.6, 129.4, 129.3, 129.2, 129.1, 129.0, 128.6, 128.5, 128.4, 128.3, 128.1, 128.0, 127.9, 127.8, 127.7, 127.6, 126.8, 126.7, 126.5, 126.4, 126.3, 71.0, 70.4, 60.4, 59.2, 58.8, 52.8, 52.4, 52.2, 48.4, 48.0, 47.8, 47.5, 47.0, 46.7, 46.4, 46.1, 46.0, 45.7, 40.8, 40.5, 40.3, 40.2, 40.0.

ESI-MS: 821.4 m/z (39, $[M + H]^+$), and 430.3 (100, $[M + H + K]^{2+}$).

ESI-HR MS: $[M + H]^+$ m/z 821.4530 (calcd for $C_{48}H_{61}N_4O_8$ 821.4489);

7.3 COMPOUNDS FROM CHAPTER 3

7.3.1. Synthesis and Characterization

Compound 3.14

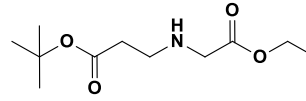

3.14

To a stirred solution of the commercially available *tert*-butyl 3-aminopropanoate hydrochloride **3.13** (3.00 g, 16.5 mmol) and DIPEA (5.74 mL, 33.0 mmol) in DMF dry (15.0 mL), ethyl bromoacetate (0.915 mL, 8.25 mmol) was slowly added. The reaction mixture was stirred overnight, concentrated *in vacuo* to remove the excess of DMF, dissolved in CH_2Cl_2 (100 mL) and washed with brine solution. The aqueous layer was extracted three times with CH_2Cl_2. The combined organic phases were dried over $MgSO_4$, filtered and the solvent evaporated in vacuo to give crude **3.14** (2.4 g, yellow amorphous solid), which was used in the next step without further purification.

^{1}H NMR: (300.1 MHz, CDCl 3) δ: 4.27 (2H, q, *J* 7.1 Hz, $CH_3C\underline{H_2}$), 3.65 (2H, s, $OCC\underline{H_2}NH$), 3.09 (2H, t, *J* 7.0 Hz, $NHC\underline{H_2}CH_2CO$), 2.74 (2H, t, *J* 7.0 Hz, $NHCH_2C\underline{H_2}CO$), 1.47 (9H, s, $C(C\underline{H_3})_3$), 1.31 (3H, t, *J* 7.1 Hz, $C\underline{H_3}CH_2$); ^{13}C NMR: (75.5 MHz, CDCl 3) δ: 170.8 ($\underline{C}OOC(CH_3)_3$), 168.9 ($\underline{C}OOCH_2CH_3$), 81.4 ($\underline{C}(CH_3)_3$), 61.7 ($\underline{C}H_2CH_3$), 49.1 ($NH\underline{C}H_2CO$), 44.3 ($NH\underline{C}H_2CH_2$), 33.5 ($NHCH_2\underline{C}H_2$), 28.0 ($C(\underline{C}H_3)_3$), 14.0 ($CH_2\underline{C}H_3$).

Compound 3.15

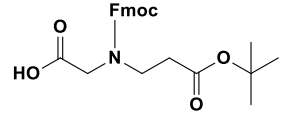

3.15

Method a. Synthesis from 3.14

To a stirred solution of crude **3.14** (2.40 g) in 1,4-dioxane (30.0 mL) at 0 °C, $LiOH•H_2O$ (0.932 g, 22.2 mmol) in H_2O (30.0 mL) was added. After two hours, $NaHCO_3$ (1.52 g, 18.1 mmol) and Fmoc-Cl (3.20 g, 10.4 mmol) were added. The reaction mixture was stirred overnight. Subsequently, $KHSO_4$ was added (until pH=3) and the mixture was concentrated *in vacuo* to remove the excess of 1,4-dioxane and dissolved in CH_2Cl_2 (100 mL). The aqueous layer was extracted with CH_2Cl_2 (three times). The combined organic phases were dried over $MgSO_4$, filtered and the solvent evaporated *in vacuo* to give a crude material (4.00 g, yellow amorphous solid). The residue was purified by flash chromatography (CH_2Cl_2 /CH_3OH, from: 100/0 to 98/02, 0.1% AcOH) to give **3.15** (2.28 g, 65% three steps).

Method b. Synthesis from 3.19

To a stirred solution of crude **3.19** (5.32 g) in 1,4-dioxane (82.0 mL) at 0 °C, $LiOH•H_2O$ (2.56 g, 61.1 mmol) in H_2O (82.0 mL) was added. After two hours, $NaHCO_3$ (4.5 g, 53.7 mmol) and Fmoc-Cl (9.5 g, 36.6 mmol) were added. The reaction mixture was stirred overnight. Subsequently, $KHSO_4$ was added (until pH=3) and the mixture was concentrated *in vacuo* to remove the excess of 1,4-dioxane and dissolved in CH_2Cl_2 (250 mL). The aqueous layer was extracted with CH_2Cl_2 (three times). The combined organic phases were dried over $MgSO_4$, filtered and the solvent evaporated

in vacuo to give a crude material (8.30 g, yellow amorphous solid). The residue was purified by flash chromatography (CH_2Cl_2 /CH_3OH, from: 100/0 to 98/02, 0.1% AcOH) to give **3.15** (4.74 g, 50% three steps).

^1H NMR: (400.13 MHz, $CDCl_3$, mixture of two rotamers) δ: 7.78 (1.1H, d, *J* 7.3 Hz, Ar-H[Fmoc] rot. a), 7.73 (0.9H, d, *J* 7.3 Hz, Ar-H[Fmoc] rot. b), 7.60 (1.1H, d, *J* 7.3 Hz, Ar-H[Fmoc] rot. a), 7.53 (0.9H, d, *J* 7.3 Hz, Ar-H[Fmoc] rot. b), 7.19-7.44 (4H, m, Ar-H[Fmoc]), 4.54 (1.1H, d, *J* 6.0 Hz, C$\underline{H_2}$CH[Fmoc] rot. a), 4.44 (0.9H, d, *J* 6.3 Hz, C$\underline{H_2}$CH[Fmoc] rot. b), 4.28 (0.55H, t, *J* 6.0 Hz, $CH_2C\underline{H}$[Fmoc] rot. a), 4.20 (0.45H, t, *J* 6.0 Hz, $CH_2C\underline{H}$[Fmoc] rot. b), 4.13 (1.1H, s, OCC$\underline{H_2}$N rot. a), 4.05 (0.9H, s, OCC$\underline{H_2}$N rot. b), 3.58 (0.9H, t, J 6.0 Hz, NC$\underline{H_2}CH_2CO$ rot. b), 3.45 (1.1H, t, *J* 6.4 Hz, NC$\underline{H_2}CH_2CO$ rot. a), 2.58 (0.9H, t, *J* 6.0 Hz, $NCH_2C\underline{H_2}CO$ rot. b), 2.32 (1.1H, t, *J* 6.4 Hz, $NCH_2C\underline{H_2}CO$ rot. a), 1.46 (4.95H, s, C(C$\underline{H_3}$)$_3$ rot. a), 1.44 (4.05H, s, C(C$\underline{H_3}$)$_3$ rot. b); ^{13}C NMR: (62.89 MHz, $CDCl_3$, mixture of two rotamers) δ: 174.1 ($\underline{C}$OOH rot. a), 173.9 ($\underline{C}$OOH rot. b),171.5 ($\underline{C}$OOC rot. a), 171.0 ($\underline{C}$OOC rot. b),156.2 ($\underline{C}$O[Fmoc] rot. a), 155.7 ($\underline{C}$O[Fmoc] rot. b), 143.5 ($\underline{C}$[Fmoc] rot. a and rot.b), 141.1 ($\underline{C}$[Fmoc] rot. a), 141.0 ($\underline{C}$[Fmoc] rot. b), 127.5 ($\underline{C}$[Fmoc] rot. a), 127.4 ($\underline{C}$[Fmoc] rot. b), 127.0 ($\underline{C}$[Fmoc] rot. a), 126.9 ($\underline{C}$[Fmoc] rot. b), 124.6 ($\underline{C}$[Fmoc] rot. a and rot.b),119.7 ($\underline{C}$[Fmoc] rot. a),119.6 ($\underline{C}$[Fmoc] rot. b), 80.9 ($\underline{C}(CH_3)_3$ rot. a and rot.b), 67.6 ($\underline{C}H_2$[Fmoc] rot. a), 67.5 ($\underline{C}H_2$[Fmoc] rot. b), 49.9 ($\underline{C}H_2COOH$ rot. a), 49.6 ($\underline{C}H_2COOH$ rot. b), 46.9 ($\underline{C}$H[Fmoc] rot. a), 46.8 ($\underline{C}$H[Fmoc] rot. b), 45.0 ($N\underline{C}H_2CH_2$ rot. a), 44.3 ($N\underline{C}H_2CH_2$ rot. b), 34.5 0 ($NCH_2\underline{C}H_2$ rot. a), 34.3 ($N\underline{C}H_2CH_2$ rot. b), 27.8 (C($\underline{C}H_3$)$_3$ rot. a), 27.7 (C($\underline{C}H_3$)$_3$ rot. b).

HRMS (ES) $[M+H]^+$, $_{m/z}$ found 426.1932. C 26 H 32 $NO6^+$ requires 426.1911.

Compound 3.17

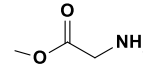

3.17

To **3.16** (5.00 g), 8% Na_2CO_3 (6.70 g) in H_2O/brine (80 mL) were added under stirring, to obtain a homogeneous solution. The reaction mixture was extracted three times with CH_2Cl_2 (150 mL) and the combined organic phases were dried over $MgSO_4$ and filtrated. To prevent the loss of **3.17**, the solvent partially evaporated *in vacuo* and **3.16** was obtained as a yellow oil (6.84 g, 95%, based on ^{1}H NMR analysis).

^{1}H NMR: (400 MHz, MeOD) δ: 3.72 (3H, s, C$\underline{H}_3$O), 3.37 (2H, s, COC$\underline{H}_2$NH$_2$).

Compound 3.19

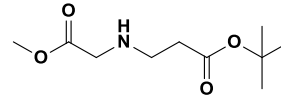

3.19

To a stirred solution of crude **3.17** (5.84 g, 65.0 mmol) in MeOH (70.0 mL), *tert*-butyl acrylate **3.18** was added (4.70 mL, 32.5 mmol). The reaction mixture was refluxed overnight at 50°C. After 15 hours, it was rinsed with toluene (2 x 50.0 mL) and the solvent was evaporated *in vacuo* to give **3.19** (5.30 g, 75%).

^{1}H NMR: (400 MHz, MeOD) δ: 3.72 (3H, s, C$\underline{H}_3$O), 3.40 (2H, s, C$\underline{H}_2$COOCH$_3$), 2.81 (2H, t, *J* 6.7 Hz, NHC$\underline{H}_2$CH$_2$CO), 2.44 (2H, t, *J* 6.7 Hz, NHCH$_2$C$\underline{H}_2$CO), 1.46 (9H, s, OC(C$\underline{H}_3$)$_3$).^{13}C NMR: (100 MHz, MeOD) δ: 173.3 (C$\underline{O}$OC(CH$_3$)$_3$), 172.9 (C$\underline{O}$OCH$_3$), 81.5 (CO$\underline{C}$(CH$_3$)$_3$), 52.2 (C$\underline{H}_3$O), 50.8 (C$\underline{H}_2$COOCH$_3$), 45.5 (NH$\underline{C}$H$_2$CH$_2$CO), 36.2 (NHCH$_2$C$\underline{H}_2$CO), 28.4 (C(C$\underline{H}_3$)$_3$).

Linear peptoid 3.20 ("monomer/submonomer" approach)

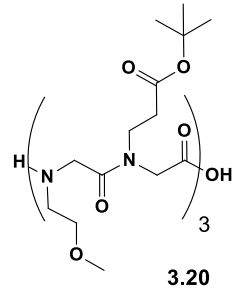

3.20

Linear peptoid **3.20** was synthesized using a "monomer/submonomer" solid-phase approach. In a typical synthesis, 2-chlorotrityl chloride resin (α-dichlorobenzhydryl-polystyrene cross-linked with 1% DVB; 100 – 200 mesh; 1.20 mmol g^{-1}, 0.20 g, 0.24 mmol) was swollen in dry CH_2Cl_2 (2 mL) for 45 min and washed twice with dry DMF (2 mL) and dry DCM (2 mL). The first monomer **3.15** was loaded on the resin with the following protocol; 0.67 equiv of **3.15** (68.0 mg, 0.26 mmol) and 2.6 equiv of DIPEA (110 µL, 0.64 mmol) were dissolved in dry CH_2Cl_2 (2 mL) and the solution was added onto the resin. The resulting mixture was shaken on a shaker platform for 90 min at room temperature, and then rinsed with CH_2Cl_2 (3 × 1 min) and DMF (3 × 1 min). To terminate the excess of reactive positions, the resin was incubated with 2 mL of a capping solution; DCM/MeOH/DIPEA (17:2:1) and the reaction was shaken for 15 more min. Then, the solvents were removed by suction, and the resin washed with DCM (3 × 1 min) and DMF (3 × 1 min). The Fmoc-deprotection treatment was carried out with Piperidine/DMF (1:4) (2 x 1 min, 2 x 5 min) and the subsequent bromoacetylation reactions were accomplished by reaction the oligomer with a solution of bromoacetic acid (0.222 g, 1.60 mmol) and DIC (0.272 mL, 1.76 mmol) in DMF (3.00 mL) on a shaker platform 40 min at room temperature. To the bromoacetylated

resin methoxyethlamine (0.138 mL, 1.60 mmol) in dry DMF (2 mL) was added. The mixture was left on a shaker platform for 30 min at room temperature, then the resin was washed with DMF (3 × 2.0 mL). The resin was then incubated with a solution of monomer **3.15** (0.272 g, 0.64 mmol), HATU (0.236 g, 0.62 mmol), DIPEA (0.222 mL, 1.28 mmol) in dry DMF (2 mL) on a shaker platform for 1 h, followed by extensive washes with DMF (3 × 3.0 mL), DCM (3 × 3.0 mL) and DMF (3 × 3.0 mL). Chloranil test was performed and once the coupling was complete the Fmoc group was deprotected with piperidine as described above and the resin washed again to prepare it for the bromoacetylation/amination reactions. The synthesis proceded until the desired oligomer length was obtained. The oligomer on the resin was then cleaved in 4.0 mL of 20% HFIP in DCM (v/v). The cleavage was performed on a shaker platform for 30 min at room temperature and the resin was then filtered away. The resin was treated again with 4.0 mL of 20% HFIP in DCM (v/v) for 5 min, washed twice with DCM (3.0 mL), filtered away and the combined filtrates were concentrated *in vacuo.* The final product was dissolved in 50% acetonitrile in HPLC grade water and analyzed by RP-HPLC [purity >90% for oligomer **3.20**; conditions: 5 → 100% A in 30 min for the all oligomers (A, 0.1% TFA in acetonitrile, B, 0.1% TFA in water); flow: 1 mL min− 1, 220 nm]. The linear oligomer was subjected to the cyclization reaction without further purification.

3.20: 91% (crude residue); HRMS (ES): $[M+H]^+$, *m/z* found 919.5248 $C_{42}H_{75}N_6O_{16}^+$ requires 919.5234. t_R : 15.1 min (see general information for the conditions).

Linear peptoid 3.21 (“monomer” approach)

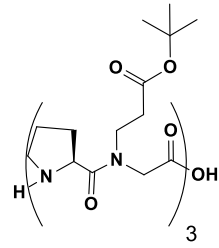

3.21

Linear peptoid **3.21** was synthesized using the standard manual Fmoc solid-phase peptide synthesis protocol. 2-chlorotrityl chloride resin (Fluka; 2,α-dichlorobenzhydryl-polystyrene crosslinked with 1% DVB; 100-200 mesh; 1.50 mmol g^{-1}, 0.70 g, 1.05 mmol) was swelled in dry DCM (2.0 mL) for 45 min and washed twice in dry DCM (2.0 mL). Monomer **3.15** (0.716 g, 1.68 mmol) in dry DCM (2.0 mL) and DIPEA (1.17 mL, 6.72 mmol) were added on a shaker platform for 1.5 h at room temperature, followed by washing with dry DCM (3.0 mL) then with a mixture of DCM/MeOH/DIPEA (17:2:1) (2 × 3.0 mL) and finally with DMF (3 × 3.0 mL). Resin loaded with the first *N*-Fmoc *N*-alkylated glycine was incubated twice with 20% piperidine/DMF (v/v, 3.0 mL) on a shaker platform (2 x 1 min, 2 x 5 min), followed by extensive washes with DMF (3 × 3.0 mL), DCM (3 × 3.0 mL) and DMF (3 × 3.0 mL). After loading of the first monomer all subsequent addition of monomer **3.15**, Fmoc deprotection steps and coupling of Fmoc-Pro-OH were performed as follow, until the desired oligomer length was obtained. The resin was incubated with a solution of monomer **3.15** (1.34 g, 3.15 mmol), or Fmoc-Pro-OH (1.06 g, 3.15 mmol) in the presence of HATU (1.16 g, 3.04 mmol) and DIPEA (1.10 mL, 6.30 mmol) in DMF dry (7 mL) on a shaker platform for 1 h and 2 h for the coupling of the second and third Fmoc-Pro-OH, followed by extensive washes with DMF (3 × 3.0 mL), DCM (3 × 3.0 mL) and

DMF (3 × 3.0 mL). Chloranil test was performed and once the coupling was complete the Fmoc group was deprotected with piperidine as described above and the resin washed again to prepare it for the next coupling. The oligomer-resin was cleaved in 7.0 mL of 20% HFIP in DCM (v/v). The cleavage was performed on a shaker platform for 30 min at room temperature the resin was then filtered away. The resin was treated again with 7.0 mL of 20% HFIP in DCM (v/v) for 5 min, washed twice with DCM (3.0 mL), filtered away and the combined filtrates were concentrated *in vacuo*. A small amount of the the final product was dissolved in 50% ACN in HPLC grade water and analysed by RP-HPLC for analytical pourposes [purity >90% for oligomer **3.21**; conditions: 5 → 100% A in 30 min for the all oligomers (A, 0.1% TFA in acetonitrile, B, 0.1% TFA in water); flow: 1 mL min− 1, 220 nm]. The linear oligomer was subjected to the cyclization reaction without further purification.

3.21: 47% (crude residue); ESI-MS (positive, m/z): 879.7 *m/z* (100, $[M + H]^+$). t_R: 13.4 min (see general information for the conditions).

Compounds 3.24 and 3.25

A solution of the linear oligomers **3.20** and **3.21** (0.200 mmol), previously co-evaporated three times with toluene, was prepared under nitrogen in dry DMF (7.00 mL). The mixture was dropwise added to a stirred solution of HATU (0.304 g, 0.800 mmol) and DIPEA (217 µL, 1.24 mmol) in dry DMF (60.0 mL) by a syringe pump in 4 h, at room temperature in anhydrous atmosphere. After 18 h the resulting mixture was concentrated *in vacuo*, diluted with CH_2Cl_2 (20.0 mL), and washed with a solution of HCl (0.01 M, 10.0 mL). The water layer was further extracted with CH_2Cl_2 (2 × 20.0 mL) and the combined organic phases were washed two times with a

solution of HCl (0.01 M, 10.0 mL) and once with water (10.0 mL), dried over anhydrous $MgSO_4$, filtered and concentrated *in vacuo.* The cyclic products were dissolved in 50% acetonitrile and HPLC grade water and analyzed by RP-HPLC [purity >95% for oligomers **3.24** and **3.25**, conditions: 5% – 100% A in 30 min for the two cyclopeptoids (A, 0.1% TFA in acetonitrile, B, 0.1% TFA in water); flow: 1 mL min^{-1}, 220 nm]. The crude residues **3.24** and **3.25** were purified by HPLC on a C_{18} reversed-phase preparative column, conditions: 20%-100% B in 30 min and 25%-100% B in 30 min respectively [A: 0.1% TFA in water, B: 0.1% TFA in acetonitrile], flow: 2.0 mL/min, 220 nm. The samples were dried in a falcon tube under low pressure and analyzed by RP-HPLC [purity >95% for oligomers **3.24** and **3.25**, conditions: 5% – 100% A in 30 min for the two cyclopeptoids (A, 0.1% TFA in acetonitrile, B, 0.1% TFA in water).

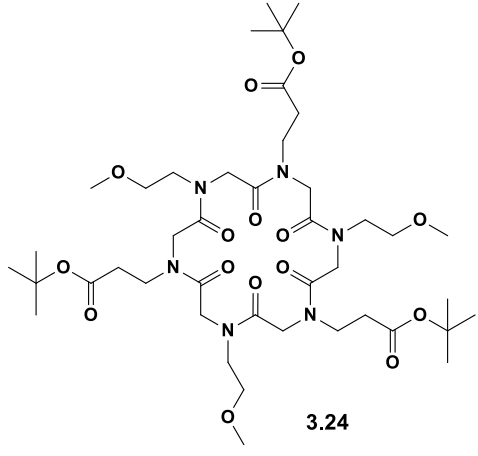

3.24

Compound **3.24**: 61%; t_R: 13.3 min (see general information for the conditions).

^{1}H NMR: (400.13 MHz, $CDCl_3$, complex mixture of conformers) δ: 3.94-4.65 (12H, b m, NC$\underline{H}_2$CO), 3.25-3.70 (33H, b m, C$\underline{H}_2$C$\underline{H}_2$COO*t*Bu and C$\underline{H}_2$C$\underline{H}_2$OC$\underline{H}_3$), 1.43-1.46 (54H, b s,

C(C<u>*H*</u>$_3$)$_3$); ^{13}C NMR (100.03 MHz, $CDCl_3$, complex mixture of conformers) δ: 171.8, 171.7, 171.6, 171.2, 171.0, 170.9, 170.6, 170.5, 170.2, 169.9, 169.6, 169.5, 169.2, 168.7, 168.1, 81.4, 81.0, 80.7, 80.5, 71.5, 71.2, 70.6, 70.4, 70.2, 69.5, 68.7, 59.0, 58.7, 58.3, 52.9, 50.7, 50.3, 49.8, 49.3, 49.0, 48.7, 48.4, 47.5, 46.0, 45.4, 45.2, 44.8, 44.4, 43.9, 34.3, 34.2, 33.7, 28.3, 28.1, 27.9, 27.7.

HRMS (ES) $[M+H]^+$, *m/z* found 901.5138. $C_{42}H_{73}N_6O_5^+$ requires 901.5128.

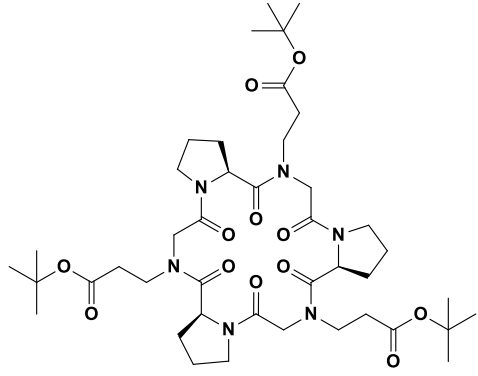

3.25

Compound **3.25**: 70%; t_R: 14.9 min (see general information for the conditions).

^{1}H NMR: (400.13 MHz, CD_3CN:$CDCl_3$=9:1, complex mixture of conformers) δ: 4.30-5.30 (9H, b m, $NCH_2CH_2CH_2C\underline{H}$ and $NC\underline{H}_2CO$), 3.32-3.93 (12H, b m, $NC\underline{H}_2CH_2CH_2CH$ and $C\underline{H}_2CH_2COO$*t*Bu), 1.66-3.01 (18H, b m, $NCH_2C\underline{H}_2C\underline{H}_2CH$ and $CH_2C\underline{H}_2COO$*t*Bu, overlapped with the signal of CD_2HCN), 1.34-1.55 (27H, b s, C(C<u>*H*</u>$_3$)$_3$). ^{13}C-NMR (100 MHz, CD_3CN:$CDCl_3$=9:1, complex mixture of conformers) δ:174.80, 173.90, 173.65, 173.50, 173.19, 173.02, 172.11, 171.98, 171.88, 171.70, 171.52, 169.77, 169.28, 169.05, 168.83, 163.99, 160.41, 160.01, 159.65, 159.28, 120.93, 118.28, 115.19, 82.24, 82.17, 82.16, 82.14, 81.79, 81.56, 81.22, 81.17, 80.98, 79.23, 79.10, 78.90, 78.58, 59.58, 59.44, 59.29,

59.20, 59.17, 57.65, 57.25, 52.77, 52.14, 51.74, 51.41 50.50, 49.73, 49.49, 49.34, 48.56, 48.43, 48.08, 47.45, 47.37, 47.23, 46.44, 46.34, 46.18, 45.93, 37.03, 36.35, 35.50, 34.75, 34.60, 34.41, 33.95, 32.60, 32.43, 32.13, 31.70, 30.91, 30.67, 30.45, 30.30, 30.01, 29.45, 28.30, 25.79, 25.68, 25.65.

ESI-MS (positive, m/z): 847.5 *m/z* (100, $[M + H]^+$).

Compounds 3.10 and 3.11

Cyclopeptoids **3.24** and **3.25** (0.079 mmol) were dissolved in 2.0 mL of TFA/*m*-cresol (95:5), stirred for one hour and concentrated under a flux of nitrogen to one third of the volume. The mixtures were then slowly added to 20.0 mL of stirred cold diethyl ether. The white precipitates were centrifuged and washed twice with cold ether (10.0 mL). The white solids were dried in an Eppendorf vial to give **3.10** and **3.11**, which were used in the complexation with gadolinium without further purification. A small portion of cyclic peptoids was dissolved in 50% acetonitrile in HPLC grade water and analyzed by RP-HPLC. [purity >95% for oligomers **3.10** and **3.**11, conditions: 5%-100% B in 30 min [A: 0.1% TFA in water, B: 0.1% TFA in acetonitrile].

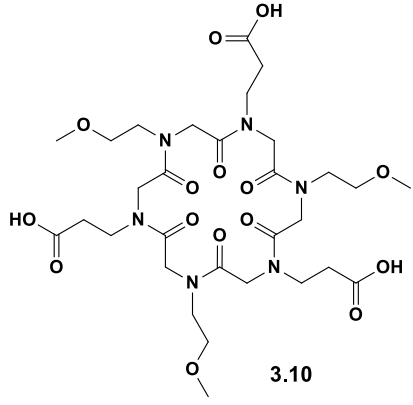

3.10

Compound **3.10**: 64%; t_R: 8.2 min (see general information for the conditions).

^{1}H NMR (300.1 MHz, CD_3CN/CD_3OD, 9:1, complex mixture of rotamers) δ: 4.75-3.66 (12H, m, NC<u>H_2</u>CO), 3.65-3.24 (33H, complex signal, C<u>H_2</u>C<u>H_2</u>OC<u>H_3</u>, C<u>H_2</u>C<u>H_2</u>COOH); ^{13}C NMR: (75.5 MHz, CD_3CN/CD_3OD, 40:15, complex mixture of rotamers) δ: 171.3, 171.2, 171.1, 170.8, 170.7, 170.4, 170.1, 170.0, 169.7, 71.5, 71.4, 71.3, 71.1, 70.8, 59.5, 59.2, 59.0, 58.8, 51.4, 51.2, 50.8, 50.6, 50.3, 47.0, 46.4, 46.3, 46.0, 45.8, 45.5, 45.3, 45.2, 44.7, 43.8, 34.2, 33.9, 33.7, 33.4, 33.1.

HRMS (ES) $[M+H]^+$, m/z found 733.3241. $C_30H_{49}N_6O_{15}^+$ requires 733.3250.

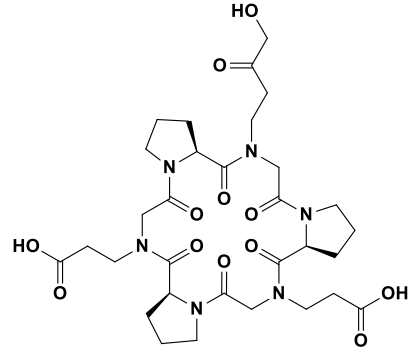

3.11

Compound **3.11**: 33%; t_R: 6.7 min (see general information for the conditions).

^{1}H NMR (400 MHz, MeOD , rt, complex mixture of conformers) δ: 5.77-4.24 (9H, b m, $NCH_2CH_2CH_2C$<u>H</u> and NC<u>H_2</u>CO water overlapped signals), 4.21-3.06 (12H, b m, NC<u>H_2</u>CH_2CH_2CH and C<u>H_2</u>CH_2COOH), 3.04-1.42 (18H, b m, NCH_2C<u>H_2</u>C<u>H_2</u>CH and CH_2C<u>H_2</u>COOH). ^{13}C-NMR (100 MHz, MeOD, complex mixture of conformers) δ: 175.70,175.52, 174.86, 174.72, 174.31, 172.14, 170.34, 170.03, 169.49, 169.38, 169.10,168.89, 118.27, 79.41, 66.89, 59.92, 59.55, 59.20, 58.39, 57.79, 52.69, 52.43, 52.13, 34.01,

33.47, 33.00, 32.81, 32.76, 30.82, 30.69, 30.17, 26.64, 26.12, 26.01, 23.74, 23.35.

ESI-MS (positive, m/z): 679.4 *m/z* (100, $[M + H]^+$).

7.3.2. Complexation Of The Cyclic Peptoids In The Presence Of Sodium Picrate

In an NMR tube, to a 4.0 mM solution of **3.24**, **3.25**, **3.10** and **3.11** in $CD_3CN:CDCl_3$ 9:1 (0.5 mL), 6.0 equivalents of sodium picrate were added (3.0 mg, 12.0 µmol). After the addition the suspension was vigorously stirred for 5 minutes and the ^1H NMR spectrum was recorded.

Compound Na-3.24

^1H NMR: (400.13 MHz, $CD_3CN:CDCl_3$ 9:1, 4.0 mM solution) δ: 8.74 (~6H, s, picrate), 4.68 (3H, d, *J* 17.0 Hz, -OCCH<u>H</u>N), 4.64 (3H, d, *J* 17.0 Hz, -OCCH<u>H</u>N), 3.89 (3H, d, *J* 17.0 Hz, -OCC<u>H</u>HN), 3.81 (3H, d, *J* 17.0 Hz, -OCC<u>H</u>HN), 3.70-3.47 (18H, m, C<u>H</u>$_2$CH$_2$CO and C<u>H</u>$_2$C<u>H</u>$_2$OCH$_3$), 3.32 (9H, s, CH$_2$CH$_2$OC<u>H</u>$_3$), 2.54 (6H, t, *J* 6.0 Hz, CH$_2$C<u>H</u>$_2$COO*t*-Bu), 1.44 (27H, s, C(C<u>H</u>$_3$)$_3$). ^{13}C NMR (75.5 MHz, $CD_3CN:CDCl_3$ 9:1) δ: 172.1, 171.0, 170.4, 163.1 (picrate), 143.0 (picrate), 128.4 (picrate), 127.4 (picrate), 82.1, 71.4, 59.7, 50.9, 50.6, 50.1, 45.8, 35.2, 28.7.

ESI-MS(positive, *m/z*): 923,(100, $[M+Na]^+$).

Compound Na-3.25

^1H NMR: (400.13 MHz, $CD_3CN:CDCl_3$ 9:1, 4.0 mM solution) δ: 4.65 (1H, t, *J* 7.68, NCH$_2$CH$_2$CH$_2$C<u>*H*</u>), 4.44 (1H, d, *J* 17.0, NC<u>*H*</u>$_2$CO), 3.78 (1H, m, *J* 6.92, C<u>*H*</u>$_2$CH$_2$COO*t*Bu), 3.73 (1H, d, *J* 17.0, NC<u>*H*</u>$_2$CO), 3.63-3.44 (3H, m, C<u>*H*</u>$_2$CH$_2$COO*t*Bu e NC<u>*H*</u>$_2$CH$_2$CH$_2$CH), 2.59 (1.90H, m, *J* 6.92, CH$_2$C<u>*H*</u>$_2$COO*t*Bu), 2.34 (1H, m, NCH$_2$CH$_2$C<u>*H*</u>$_2$CH, overlapped with the water signal), 1.97 (2H, m

overlapped with the CD_2HCN signal, $NCH_2C\underline{H_2}CH_2CH$), 1.76 (1.02 H, m, *J* 6.98, $NCH_2CH_2C\underline{H_2}CH$), 1.42 (9H, s, $C(C\underline{H_3})_3$).

ESI-MS(positive, *m/z*): 883.5,(100, $[M+Na]^+$).

Compound Na-3.10

^1H NMR: (300.1 MHz, CD_3CN:$CDCl_3$ 9:1) δ: 8.68 (~6H, s, picrate), 4.83 (3H, d, *J* 18.0 Hz, -OCCH<u>H</u>N), 4.64 (3H, d, *J* 18.0 Hz, -OCCH<u>H</u>N), 3.84 (3H, d, *J* 18.0 Hz, -OCC<u>H</u>HN), 3.77 (3H, d, *J* 18.0 Hz, -OCC<u>H</u>HN), 3.60-3.50 (18H, m, $C\underline{H_2}CH_2COOH$ and $C\underline{H_2}C\underline{H_2}OCH_3$), 3.30 (9H, s, $CH_2CH_2OC\underline{H_3}$), 2.61 (6H, br s, $CH_2C\underline{H_2}COOH$, overlapped with the water signal).

ESI-MS(positive, *m/z*): 755, (100, $[M+Na]^+$).

Compound Na-3.11

^1H-NMR: (600 MHz, CD_3CN:$CDCl_3$ 9:1, 4.0 mM solution) δ: 4.79 (1H, t, *J* 7.68, $NCH_2CH_2CH_2C\underline{H}$), 4.47 (1H, d, *J* 16.9, $NC\underline{H_2}CO$), 3.83 (1H, m, *J* 6.74, $C\underline{H_2}CH_2COOH$), 3.76 (1H, d, *J* 16.9, $NC\underline{H_2}CO$), 3.61-3.51 (3H, m, $C\underline{H_2}CH_2COOH$ and $NC\underline{H_2}CH_2CH_2CH$), 2.68 (2H, t, *J* 6.74, $CH_2C\underline{H_2}COOH$), 2.37 (1H, m, *J* 6.74, $NCH_2CH_2C\underline{H_2}CH$), 2.05-1.94 (2H, m overlapped with CD_2HCN signal, $NCH_2C\underline{H_2}CH_2CH$), 1.80 (1H, m, $NCH_2CH_2C\underline{H_2}CH$, *J* 6.74). ^{13}C-NMR (150 MHz, CD_3CN:$CDCl_3$ 9:1) δ: 174.2, 162.6, 59.0, 51.5, 47.4, 46.2, 33.9, 29.4, 25.4.

ESI-MS(positive, *m/z*): 715.3,(100, $[M+Na]^+$).

7.4 COMPOUNDS FROM CHAPTER 4

7.4.1. Synthesis and Characterization of Peptoidic Scaffolds

General procedure for sub-monomer solid-phase synthesis of the linear peptoids 4.30–4.38

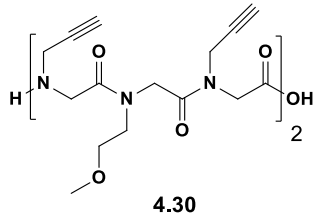

4.30

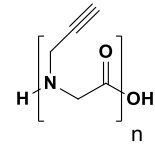

4.31, n=4
4.32, n=5
4.33, n=6
4.34, n=8
4.35, n=10
4.36, n=12
4.37, n=14
4.38, n=16

Linear peptoid oligomers **4.30**–**4.38** were synthesized using a submonomer solid-phase approach. In a typical synthesis 2-chlorotrityl chloride resin (α-dichlorobenzhydryl-polystyrene cross-linked with 1% DVB; 100 – 200 mesh; 1.5 mmol g^{-1}, 0.30 g, 0.45 mmol) was swelled in dry CH_2Cl_2 (3 mL) for 45 min and washed twice with dry DMF (3 mL). The first submonomer was attached onto the resin by adding bromoacetic acid (100 mg, 0.72 mmol) in dry CH_2Cl_2 (3 mL) and DIPEA (392 µL, 2.20 mmol) on a shaker platform for 60 min at room temperature, followed by washing with dry CH_2Cl_2 (3 × 1 min) and then with DMF (3 × 1 min). A DMF solution of the commercially available propargyl amine (1 M, 3.0 mL), or methoxyethyl amine (1 M, 3.0 mL) needed for the synthesis of **4.30**, was added to the bromoacetylated resin. The mixture was left on a shaker platform for 30 min at room temperature, then the resin was washed with DMF (3 × 1 min), CH_2Cl_2 (3 × 1 min) and then again with DMF (3 × 1 min). Subsequent bromoacetylation reactions were accomplished by reacting the aminated oligomer with a solution of bromoacetic acid (625 mg, 4.50 mmol) and DIC (766 µL, 5.00 mmol)

in dry DMF (3 mL) for 40 min at room temperature. The filtrated resin was washed with DMF (3 × 1min), CH_2Cl_2 (3 × 1 min), DMF (3 × 1 min) and treated again with the amine under the same conditions reported above. This cycle of reactions was iterated until the desired chain length was accomplished and the target oligomer obtained. The cleavage was performed by treating twice the resin, previously washed with CH_2Cl_2 (3 × 1 min), with a solution of HFIP in CH_2Cl_2 (20% v/v, 6 mL) on a shaker platform at room temperature for 30 min and 5 min, respectively. The resin was then filtered away and the combined filtrates were concentrated *in vacuo*. The final products were dissolved in 50% acetonitrile in HPLC grade water and analyzed by RP-HPLC [purity >95% for oligomers **4.30**-**4.33**, 82% for oligomer **4.34**, 72% for oligomer **4.35,** 70% for oligomer **4.36**, 65% for oligomer **4.37**, 60% for oligomer **4.38**; conditions: 5 → 100% A in 30 min for the all oligomers (A, 0.1% TFA in acetonitrile, B, 0.1% TFA in water); flow: 1 mL min^{-1}, 220 nm]. The linear oligomers were subjected to the cyclization reaction without further purification.

4.30: 70% (crude residue); ESI-MS (positive, m/z): 669.05 $[M + H]^+$; t_R : 9.01 min;

4.31: quant. (crude residue); ESI-MS (positive, m/z): 399.1 $[M + H]^+$; t_R : 3.70 min;

4.32: quant. (crude residue); ESI-MS (positive, m/z): 494.1 $[M + H]^+$; t_R: 4.04 min;

4.33: 70% (crude residue); ESI-MS (positive, m/z): 589.2 $[M + H]^+$; t_R : 7.0 min;

4.34: 80% (crude residue); ESI-MS (positive, m/z): 779.0 $[M + H]^+$; t_R : 7.7 min;

4.35: 66% (crude residue); ESI-MS (positive, m/z): 969.4 $[M + H]^+$; t_R: 10.1 min;

4.36: 70% (crude residue); ESI-MS (positive, *m/z*): 1160.7 (60, $[M + H]^+$) and 1182.2 (100, $[M+Na]^+$); t_R : 10.1 min

4.37: 80% (crude residue); ESI-MS (positive, *m/z*): 1350.5 (100, $[M + H]^+$); 1372.6 (22, $[M+Na]^+$) and 1388.5 (15, $[M + K]^+$); t_R : 11.1 min;

4.38: 66% (crude residue); ESI-MS (positive, *m/z*): 1541.3 (100, $[M + H]^+$) and 1563.3 (100, $[M+Na]^+$) t_R: 11.9 min;

Procedure for sub-monomer solid-phase synthesis of the linear peptoid 4.68

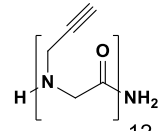

4.68

Peptoid oligomer **4.68** was synthesized on a Fmoc-Rink-Amide resin (aminomethyl-polystyrene cross-linked with 1% DVB; 100 – 200 mesh) using the submonomer methodology. 50 mg of Rink amide resin at a loading level of 0.59 mmol/g was swollen in DMF for 40 minutes. Fmoc deprotection of the resin was performed by 20% piperidine in DMF, followed by multiple washing steps using DMF (3 × 1 min), CH_2Cl_2 (3 × 1 min) and then again DMF (3 × 1 min). Washing were performed between each step described below. Fmoc cleavage was followed by bromoacetylation, in which approximately 15 eq bromoacetic acid (1.0 M in DMF, 8.5 mL/g resin) and 18 eq of diisopropylcarbodiimide (1.7 mL/g resin) were added, followed by 30 min agitation. 15 equivalents of propargyl amine (1.0 M in DMF, 8.5 mL/g resin) were added and the amine displacement step was effected by 20 min agitation. The bromoacetylation and the propargyl amine displacement steps were repeated until the peptoid oligomer was completely synthesized. **4.68** was cleaved from the resin, previously washed with CH_2Cl_2 (3

× 1 min), by a treatment with a solution of TFA (50% v/v) and 1,3 dimethoxybenzene (DMB) (4% v/v) in CH_2Cl_2 (1.0 mL) on a shaker platform at room temperature for 20 min. The resin was then extensively washed with DCM and filtered away. The cleavage cocktail was evaporated and the peptoid oligomer **4.68** was precipitated in cold diethyl ether (20 mL). The final product was dissolved in 50% acetonitrile in HPLC grade water and analyzed by RP-HPLC [purity 90%; conditions: 5 → 100% A in 30 min (A, 0.1% TFA in acetonitrile, B, 0.1% TFA in water); flow: 1 mL min^{-1}, 220 nm].

4.68: 66%; white amorphous solid; ESI-MS (positive, *m/z*): 602.1 (100, $[M + 2 Na]^{2+}$); 1159.1 (65, $[M + H]^+$) and 1181.1 (44, $[M + Na]^+$); t_R : 9.9 min;

^{1}H-NMR: (600 MHz, CD_3OD, mixture of rotamers) δ: 5.59-4.60 (bs, water overlapped, $COCH_2N$ and NCH_2CCH), 4.28-3.98 (bs, 40 H, $COCH_2N$ and NCH_2CCH), 2.93 (bs, 4 H, NCH_2CCH), 2.74 (bs, 8 H, NCH_2CCH). ^{13}C-NMR: (150 MHz, CD_3OD, mixture of rotamers, broad signals) δ: 170.9, 170.6, 170.4, 170.2, 169.8, 79.7, 78.8, 78.5, 75.7, 75.4, 75.1, 74.8, 74.3, 48.3, 38.7, 37.6, 37.5, 37.4, 37.3, 37.1.

General procedure for the cyclization reactions: synthesis of compounds 4.16-4.24

A solution of the linear peptoids precursors of **4.30** – **4.38** (0.30 mmol), previously co-evaporated three times with toluene, was prepared under nitrogen in dry DMF (20 mL). The mixture was added drop wise to a stirred solution of HATU (465 mg, 1.22 mmol) and DIPEA (330 µL, 1.90 mmol) in dry DMF (82 mL) by a syringe pump in 12 h, at room temperature in anhydrous atmosphere. After 65 h the resulting mixture was concentrated *in vacuo*, diluted with CH_2Cl_2 (100 mL), and washed with a solution of HCl (1.0 M, 50 mL). The

mixture was extracted with CH_2Cl_2 (2 × 100 mL) and the combined organic phases were washed with water (150 mL), dried over anhydrous $MgSO_4$, filtered and concentrated *in vacuo*. The cyclic products were dissolved in 50% acetonitrile in HPLC grade water and analyzed by RP-HPLC [purity 81% for oligomer **4.21**, >95% for the others, conditions: 5% – 100% A in 30 min for all cyclic compounds (A, 0.1% TFA in acetonitrile, B, 0.1% TFA in water); flow: 1 mL min^{-1}, 220 nm]. The crude residues **4.16** and **4.19** were purified by precipitation in hot acetonitrile, **4.17** by precipitation in ethyl acetate, **4.18** by precipitation in acetonitrile/H_2O 1:1 + 0.1%TFA , **4.20** by precipitation in hot acetonitrile 0.1% TFA, **4.21** by RP-HPLC on a C_{18} reversed-phase semi-preparative column, t_R : 10.9 min, conditions: 25% – 100% A in 30 min [(A, 0.1% TFA in acetonitrile, B, 0.1% TFA in water); flow: 2 mL min^{-1}, 220 nm], **4.22, 4.23** and **4.24** were purified by flash chromatography over demetalated silica gel (CH_2Cl_2/CH_3OH, from 100/0 to 95/05).

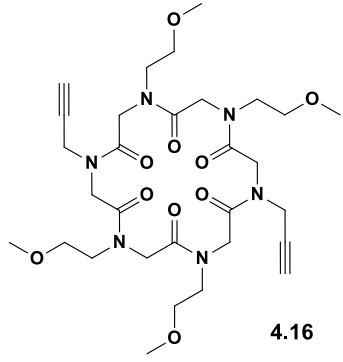

4.16

Compound **4.16**: 31%; white amorphous solid; ESI-MS (positive, *m/z*): 651.20 (100, $[M + H]^+$), t_R: 10.4 min;

^{1}H NMR: (400 MHz,$CDCl_3$, mixture of rotamers) δ: 5.13-3.89 (12H, m, COC*H*$_2$N); 3.78-3.07(32H, m, NC*H*$_2$$CH_2OCH_3$, NCH_2C*H*$_2$$OCH_3$, NCH_2CH_2OC*H*$_3$, NC*H*$_2$CCH); 2.43-2.10 (2H, m, NCH_2CC*H*); ^{13}C NMR: (100 MHz, $CDCl_3$, mixture of rotamers, broad

signals) δ: 170.9, 170.6, 169.8, 169.6, 169.5, 169.4, 169.2, 169.1, 168.8, 168.7, 168.6, 168.4, 168.0, 167.9, 167.8, 167.7, 78.7, 78.7, 73.8, 73.6, 73.1, 73.0, 72.8, 72.7, 72.4, 72.3, 72.1, 72.0, 71.8, 71.6, 71.5, 71.0, 70.6, 70.5, 70.3, 70.2, 70.0, 69.7, 69.5, .68.8, 68.6, 59.3, 59.1, 59.0, 58.7, 58.5, 58.4, 58.3, 58.2, 52.0, 51.0, 20.8, 50.6, 50.3, 50.2, 50.0, 79.9, 49.8, 49.6, 49.5, 49.2, 49.0, 48.9, 48.8, 48.6, 48.5, 48.2, 48.0, 47.9, 47.8, 47.7, 47.6, 47.6, 47.5, 47.4, 47.3, 47.3, 47.2, 47.1, 47.0, 46.8, 46.6, 46.4, 46.2, 46.0, 45.8, 45.7, 45.6, 43.5, 43.2, 42.6, 37.5, 37.4, 37.3, 37.2, 36.9, 36.8, 36.6, 36.2, 36.0, 35.8, 35.7, 35.5, 35.4, 35.3, 31.8.

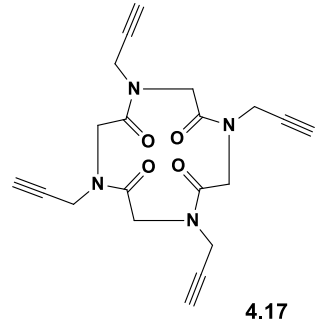

4.17

Compound **4.17**: 35%; white amorphous solid; ESI-MS (positive, *m/z*): 381.4 (100, $[M + H]^+$), t_R: 4.07 min;

^{1}H NMR: (600 MHz,$CDCl_3$) δ: 5.26 (2H, d, *J* 14.1 Hz COC*H*$_2$N); 4.94 (2H, dd, *J* 17.1 Hz, *J* 1.28 Hz NC*H*$_2$CCH); 4.37 (2H, d, *J* 18.1 Hz COC*H*$_2$N); 4.31 (2H, d, *J* 18.1 Hz COC*H*$_2$N); 4.07 (2H, dd, *J* 17.1 Hz, *J* 1.28 Hz NC*H*$_2$CCH); 3.84 (2H, dd, *J* 19.1 Hz, *J* 2.45 Hz NC*H*$_2$CCH); 3.74 (2H, dd, *J* 19.1 Hz, *J* 2.45 Hz NC*H*$_2$CCH); 3.59 (2H, d, *J* 14.1 Hz COC*H*$_2$N); 3.39 (2H, t, *J* 1.28 Hz NCH_2CC*H*); 2.27 (2H, t, *J* 2.45 Hz NCH_2CC*H*); ^{13}C NMR: (150 MHz, DMSO) δ: 169.26 (*C*OCH_2N), 168.08 (*C*OCH_2N), 79.91 (NCH_2*C*CH), 78.62 (NCH_2*C*CH); 77.19 (NCH_2C*C*H); 76.04 (NCH_2C*C*H); 48.58 (CO*C*H_2N); 48.40 (CO*C*H_2N); 37.43 (N*C*H_2CCH); 36.08 (N*C*H_2CCH).

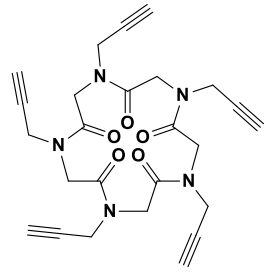

4.18

Compound **4.18**: 20%; white amorphous solid; ESI-MS (positive, *m/z*): 497.97 (100, $[M + Na]^+$), t_R: 5.40 min;

^{1}H NMR: (300 MHz, $CDCl_3$, mixture of rotamers) δ: 5.04 – 3.41 (20 H, m, COC*H*$_2$N, NC*H*$_2$CCH); 2.51 (1 H, bt, NCH$_2$CC*H*); 2.40 (1 H, bt, NCH$_2$CC*H*); 2.33 (1 H, bt, NCH$_2$CC*H*); 2.24 (1 H, bt, NCH$_2$CC*H*); 2.15 (1 H, bt, NCH$_2$CC*H*); ^{13}C NMR: (75 MHz, $CDCl_3$, mixture of rotamers, broad signals) δ: 169.8, 169.0, 168.4, 167.7, 166.8, 78.3 (overlapped with the solvent signal), 74.3, 73.5, 73.2, 72.3, 71.7, 48.8, 46.7, 47.1, 46.0, 38.9, 36.0, 35.6, 34.5, 35.1, 34.8.

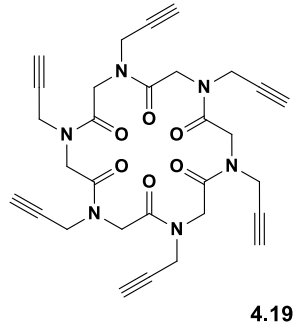

4.19

Compound **4.19**: 31%; white amorphous solid; ESI-MS (positive, *m/z*): 593.2 m/z (100, $[M + Na]^+$), t_R: 8.6 min;

^{1}H NMR: (400 MHz, DMSO, mixture of rotamers) δ: 5.60 – 2.90 (m, 30 H, COC*H*$_2$N, NC*H*$_2$CCH, NCH$_2$CC*H*, water-overlapped signals). ^{13}C NMR: (100 MHz, DMSO, mixture of rotamers, broad

signals) δ: 170.7, 169.8, 169.5, 169.3, 169.2, 169.0, 168.9, 168.8, 168.6, 168.4, 168.2, 167.9 , 167.8, 167.7, 167.1, 79.5, 79.4, 79.3, 79.1, 79.0, 78.8, 78.7, 78.5, 78.4, 78.3, 78.2, 78.0, 77.9, 76.3, 76.2, 76.1, 75.9, 75.7, 75.6, 75.4, 75.2, 75.1, 74.7, 74.5, 49.4, 49.3, 49.0, 48.4, 48.3, 47.9, 47.7, 47.6, 47.4, 47.3, 47.0, 46.8, 46.7, 37.2, 36.8, 36.6, 36.4, 36.2, 36.0, 35.7, 35.3, 35.1, 34.7, 34.5, 34.4.

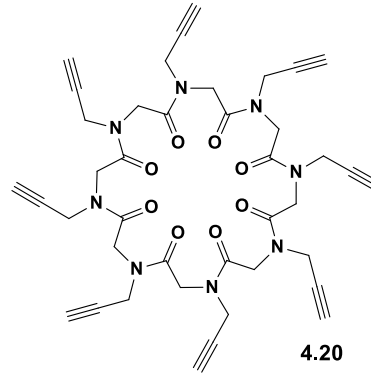

4.20

Compound **4.20**: 32%; white amorphous solid; ESI-MS (positive, m/z): 761.3 m/z (100, $[M + H]^+$), 783.3 m/z (64, $[M + Na]^+$); t_R: 9.7 min;

^{1}H NMR: (400 MHz, $CDCl_3$, mixture of rotamers) δ: 4.97 (4 H, m, COC*H*$_2$N,), 4.75 (1H, d, *J* 16.8 Hz, COC*H*$_2$N), 4.61 – 3.83 (23 H, m, COC*H*$_2$N and NCH$_2$CC*H*), 3.71 (3 H, m, COC*H*$_2$N), 3.34 (1H, d, *J* 16.8 Hz COC*H*$_2$N,), 2.46 (2 H, t, *J* 2.1 Hz, NCH$_2$CC*H*), 2.39 (2 H, t, *J* 2.3 Hz, NCH$_2$CC*H*), 2.32 (2 H, t, *J* 2.5 Hz, NCH$_2$CC*H*), 2.22 (2 H, t, *J* 2.4 Hz, NCH$_2$CC*H*); ^{13}C NMR: (100 MHz, $CDCl_3$, mixture of rotamers) δ : 169.0, 168.4, 168.2, 167.0, 78.3, 78.1, 77.2, 76.7, 74.6, 74.2, 73.6, 73.3, 49.4, 48.6, 46.7, 46.5, 38.6, 38.1, 36.5, 35.8.

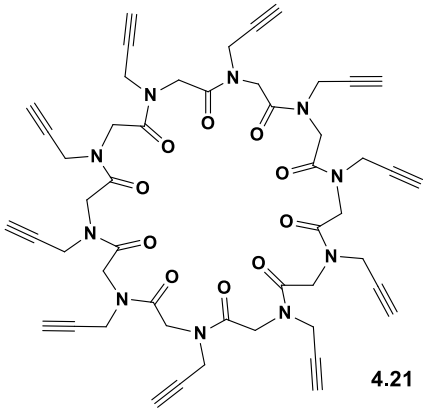

4.21

Compound **4.21**: 12%, by HPLC; pale yellow amorphous solid; ESI-MS (positive, m/z): 951.3 m/z (40, $[M + H]^+$), 973.3 m/z (100, $[M + Na]^+$); t_R : 10.9 min;

^{1}H NMR: (400 MHz, $CDCl_3$, mixture of rotamers) δ: 4.74 – 3.77 (37 H, m, COC<u>*H*</u>$_2$N and NC<u>*H*</u>$_2$CCH), 3.33 (3 H, bs, NC<u>*H*</u>$_2$CCH), 2.49 – 2.00 (10 H, m, NCH_2CC<u>*H*</u>); ^{13}C NMR: (100 MHz, $CDCl_3$, mixture of rotamers, broad signals) δ: 169.6 , 169.4, 169.1, 168.7, 168.5, 168.2, 168.1, 167.9, 167.7, 167.4, 167.1, 78.2, 78.0, 77.8, 77.6, 74.8, 74.6, 74.4, 74.2, 74.0, 73.8, 73.7, 73.5, 73.3, 73.2, 73.1, 72.8, 49.0, 48.8, 48.5, 48.2, 47.9, 47.7, 47.5, 47.1, 46.7, 46.4, 46.2, 38.7, 38.6, 38.3, 38.1, 38.0, 37.8, 37.6, 37.4, 37.2, 37.0, 36.8, 36.6, 36.4, 36.2, 36.0, 35.8, 35.6.

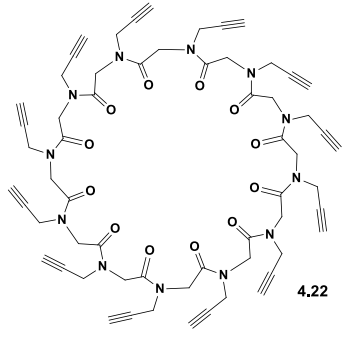

4.22

Compound **4.22**: 10%; white amorphous solid; ESI-MS (positive, *m/z*): 1163.2 $[M + Na]^+$; t_R : 11.2 min;

^{1}H NMR: (300 MHz, $CDCl_3$, mixture of rotamers) δ: 4.59 – 3.38 (48 H, bs, COC*H*$_2$N and NC*H*$_2$CCH), 2.46-2.12 (12 H, m, NCH_2CCH). ^{13}C NMR: (100 MHz, $CDCl_3$, mixture of rotamers, broad signals) δ: 168.07, 80.3, 73.9, 73.3, 46.6, 46.4, 37.6, 37.5, 37.3, 37.2, 37.0, 36.7, 36.6, 35.9.

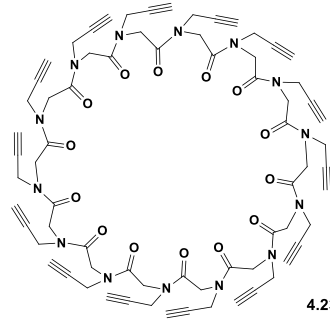

4.23

Compound **4.23**: 8%; white amorphous solid; ESI-MS (positive, *m/z*): 685.3 $[M + K + H]^{2+}$; t_R: 12.1 min;

^{1}H NMR: (600 MHz, CD_3CN, mixture of rotamers) δ: 4.48 (7 H, bs, COC*H*$_2$N and NC*H*$_2$CCH), 4.33-4.02 (49 H, bs, COC*H*$_2$N and NC*H*$_2$CCH), 2.73 (6 H, bs, NCH_2CCH), 2.56 (8 H, bs, NCH_2CCH). ^{13}C NMR: (150 MHz, CD_3CN, mixture of rotamers, broad signals) δ: 170.8, 170.6, 170.4, 170.2, 170.1, 170.0, 169.9, 169.8, 169.7, 169.5, 169.4, 169.3, 169.2, 169.1, 169.0, 168.8, 168.7, 168.5, 168.3, 79.4, 78.9, 78.6, 75.4, 74.8, 74.2, 48.3, 39.5, 38.5, 37.3.

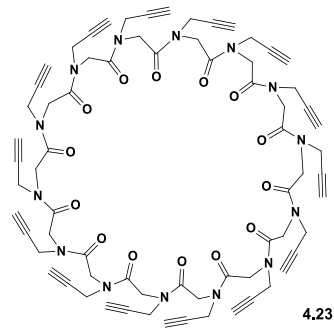

4.23

Compound **4.24**: 5%; white amorphous solid; ESI-MS (positive, *m/z*): 761.2 (100, $[M + 2 H]^{2+}$) and 783.9 (33, $[M + 2 Na]^{2+}$), t_R : 12.8 min;

^{1}H NMR: (600 MHz, CD_3CN, mixture of rotamers) δ: 4.47 (12 H, bs, COC*H*$_2$N and NC*H*$_2$CCH), 4.30-4.05 (52 H, bs, COC*H*$_2$N and NC*H*$_2$CCH), 2.77-2.69 (6 H, bs, NCH_2CCH), 2.56-2.54 (10 H, bs, NCH_2CCH). ^{13}C NMR: (150 MHz, CD_3CN, mixture of rotamers, broad signals) δ: 169.3, 79.4, 78.6, 78.6, 75.4, 74.3, 48.3, 39.5, 38.6, 37.4

7.4.2. Synthesis And Characterization Of Cyclopeptoid Based Iminosugar Click Clusters

General procedure for the synthesis of cyclopeptoid based iminosugar click clusters 4.44a, 4.44b, 4.46a-4.48a, 4.46b-4.48b, 4.54-4.59 and 4.66.

Cyclopeptoid **4.16**, or **4.19**-**4.24** (typically 5 to 15 mg) and ligand **4.43a**, **4.43b** or **4.53** (1.1 equiv/alkyne moiety) were placed in a microwave vial and dissolved in DMF (typically 0.5 to 1 mL). To this solution, a bright yellow suspension of $CuSO_4 \cdot 5H_2O$ (10 mol %/alkyne moiety) and sodium ascorbate (20 mol %/alkyne moiety) in water (typically 0.1 to 0.2 mL) were added. The mixture was stirred and heated under microwave irradiation for 3 h at 80 °C. The mixture was concentrated, diluted in a 9:1:1 (v/v/v) mixture of MeCN/water/

30 wt %-NH_4OH and filtrated with the same eluent (25 mL) over a small pad of SiO_2 (typically 1 cm thick). The filtrate was concentrated and then filtrated again on another pad of SiO_2 (typically 1 cm wide and 2 cm thick). To recover clean unclicked ligand, this was eluted with AcOEt/PE 4:6 (25 mL), and then with MeCN/water 8:2 (25 mL). Iminosugar click clusters **4.44a**, **4.44b**, **4.46a-4.48a, 4.46b-4.48b, 4.54-4.59 and 4.66** were obtained as pale brown translucent wax after concentration.

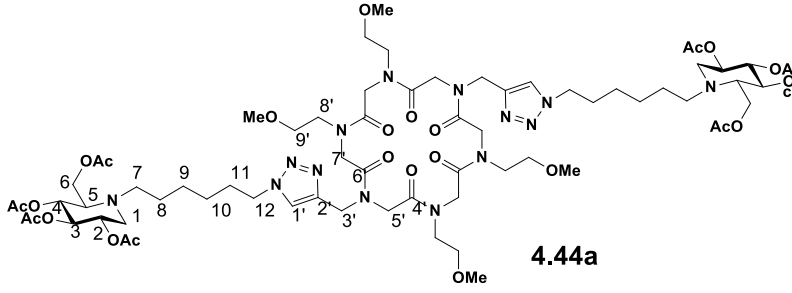

4.44a

Compound **4.44a**: $[\alpha]_D^{20}$ = 0 (c 0.5, $CHCl_3$);^{1}H-NMR ($CD_3CN/CDCl_3$ 9:1 + 1.9 eq Na picrate, 400 MHz) δ 7.76 (s, 2H; H-1'), 5.06-4.94 (m, 4H; H-3 and H-4), 4.92 (d, *J* 16.7 Hz, 2H; H-3 or H-5), 4.85 (td, *J* 9.7, 5.2 Hz, 2H; H-2), 4.76 (d, *J* 16.5 Hz, 2H; H-3' or H-5'), 4.67 (d, *J* 16.7 Hz, 4H; H-7'), 4.46 (d, *J* 16.5 Hz, 2H; H-3' or H-5'), 4.35 (t, *J* 7.1 Hz, 4H; H-12), 4.15 (dd, *J* 12.7, 2.1 Hz, 2H; H-6a), 4.10 (dd, *J* 12.8, 3.2 Hz, 2H; H-6b), 3.96 (d, *J* 16.7 Hz, 2H; H-3' or H-5'), 3.84 (dd, *J* 16.8, 6.2 Hz, 4H; H-7'), 3.70-3.22 (m, 28H; H-8', H-9' and MeO), 3.15 (dd, *J* 11.5, 4.8 Hz, 2H; H-1a), 2.80-2.65 (m, 2H; H-7a), 2.69 (d, *J* 8.8 Hz, 2H; H-5), 2.59-2.47 (m, 2H; H-7b), 2.36 (t, *J* 11.0 Hz, 2H; H-1b), 2.05-1.93 (m, 24H; Ac), 1.87 (m, 4H; H-11), 1.43 (m, 4H; H-8), 1.31 ppm (m, 8H; H-9 and H-10); ^{13}C-NMR ($CD_3CN/CDCl_3$ 9:1, 100 MHz) δ 171.9, 171.8, 171.6, 171.4 (C=O Ac), 171.0-170.5 (C-4' and C-6'), 143.2 (C-2'), 124.1 (C-1'), 75.2 (C-2),

71.6-70.9 (C-8' and C-9'), 70.4, 70.2 (C-3 and C-4), 62.1 (C-5), 60.5 (C-6), 59.3 (MeO), 53.4 (C-1), 52.2 (C-7), 51.6-50.3 (C-7'), 50.8 (C-12), 49.7, 44.9 (C-3' and C-5'), 30.9, 27.2, 26.8, 25.3 (C-8 to C-11), 21.1 ppm (CH3 Ac); IR (neat) 1743 (strong, C=O acetate), 1670 cm-1 (strong, C=O amide); HRMS (ESI) m/z calcd for C70H111N14O26 [M + H]+ 1563.7788; found 1563.7690.

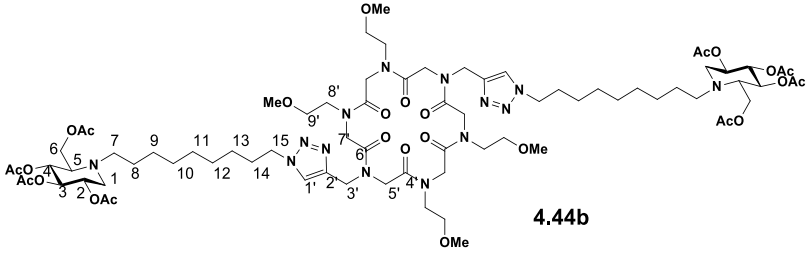

4.44b

Compound **4.44b**: $[\alpha]_D^{20}$ = +3.5 (c 1, $CHCl_3$); ^{1}H-NMR ($CD_3CN/CDCl_3$ 9:1 + 1.8 eq Na picrate, 400 MHz) δ 7.75 (s, 2H; H-1'), 5.05-4.92 (m, 4H; H-3 and H-4), 4.90 (d, *J* 16.9 Hz, 2H; H-3' or H-5'), 4.83 (td, *J* 9.7, 4.9 Hz, 2H; H-2), 4.73 (d, *J* 16.3 Hz, 2H; H-3' or H-5'), 4.65 (d, *J* 16.9 Hz, 4H; H-7'), 4.46 (d, *J* 16.3 Hz, 2H; H-3' or H-5'), 4.33 (t, *J* 7.1 Hz, 4H; H-15), 4.14 (d, *J* 12.9, 1.9 Hz, 2H; H-6a), 4.09 (dd, *J* 12.9, 3.0 Hz, 2H; H-6b), 3.95 (d, *J* 16.9 Hz, 2H; H-3' or H-5'), 3.83 (dd, *J* 16.9, 5.9 Hz, 4H; H-7'), 3.61-3.25 (m, 28H; H-8', H-9' and MeO), 3.13 (dd, *J* 11.3, 5.0 Hz, 2H; H-1a), 2.77-2.64 (m, 2H; H-7a), 2.69 (d, *J* 8.5 Hz, 2H; H-5), 2.59-2.47 (m, 2H; H-7b), 2.37 (t, *J* 11.3 Hz, 2H; H-1b), 2.04-1.91 (m, 24H; Ac), 1.85 (m, 4H; H-14), 1.41 (m, 4H; H-8), 1.28 ppm (m, 20H; H-9, H-10, H-11, H-12 and H-13); ^{13}C-NMR ($CD_3CN/CDCl_3$ 9:1, 100 MHz) δ 171.9, 171.8, 171.6, 171.4 (C=O Ac), 171.1-170.6 (C-4' and C-6'), 143.2 (C-2'), 124.0 (C-1'), 75.3 (C-2), 71.9-70.9 (C-8' and C-9'), 70.5, 70.2 (C-3 and C-4), 62.1 (C-5), 60.5 (C-6), 59.3 (MeO), 53.4 (C-1), 52.4 (C-7), 51.8-50.2 (C-7'), 51.0 (C-15), 49.7, 45.0 (C-3' and C-5'), 31.0, 30.13, 30.07, 29.7,

27.8, 27.0, 25.5 (C-8 to C-14), 21.1 ppm (CH3 Ac); IR (neat) 1745 (strong, C=O acetate), 1670 cm-1 (strong, C=O amide); HRMS (ESI) m/z calcd for C76H122N14O26Na [M + Na]+ 1669.8547; found 1669.8459. MS (MALDI) m/z calcd for C76H123N14O26 [M + H]+ 1647.873; found 1647.999.

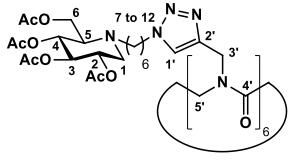

4.46a

Compound **4.46a**: $[\alpha]_D^{18}$ =+6.2 (*c* 1, $CHCl_3$); ^1H NMR ($CD_3CN/CDCl_3$ 9:1 + 11 equiv sodium picrate, 400 MHz) δ 7.76 (6H, s, H-1'), 4.97 (12H, m, *J* 10.3 Hz, H-3, H-4), 4.85 (6H, d, *J* 16.3 Hz, H-3' or H-5'), 4.83 (6H, td, *J* 9.8, 5.3 Hz, H-2), 4.71 (6H; d, *J* 16.3 Hz, H-3' or H-5'), 4.45 (6H, d, *J* 16.3 Hz, H-3' or H-5'), 4.32 (12H, t, *J* 7.0 Hz, H-12), 4.10 (12H, dd, *J* 19.4, 13.0 Hz, H-6), 3.97 (6H, d, *J* 16.3 Hz, H-3' or H-5'), 3.11 (6H, dd, *J* 11.1, 5.3 Hz, H-1a), 2.70 (6H, m, H-7a), 2.68 (6H, d, *J* 8.8 Hz, H-5), 2.51 (6H, m, H-7b), 2.35 (6H, dd, *J* 12.7, 11.1 Hz, H-1b), 1.95 (72H, s, AcO), 1.85 (12H, m, H-11), 1.40 (12H, m, H-8), 1.28 (24H, m, H-9, H-10) ppm; ^{13}C NMR ($CD_3CN/CDCl_3$ 9:1, 100 MHz) δ 171.4, 170.94, 170.88, 170.6, 170.6–168.9, 144.4–142.8, 124.7–123.8, 75.3, 70.5, 70.2, 62.1, 60.5, 53.4, 52.3, 50.8, 50.3–48.5, 44.9–42.6, 30.9, 27.3, 27.0, 25.2, 21.1 ppm; HRMS–ESI (*m/z*): $[M + 2H]^{2+}$ calcd for $C_{150}H_{224}N_{30}O_{54}$ 1654.7847; found: 1654.7827.

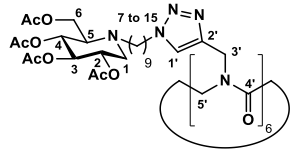

4.46b

Compound **4.46b**: $[\alpha]_D^{20}$ = +5.8 (*c* 1, $CHCl_3$); ^{1}H NMR ($CD_3CN/CDCl_3$ 9:1 + 9 eq. sodium picrate, 400 MHz): δ 7.76 (s, 6H; H-1'), 4.97 (m, *J* 10.3 Hz, 12H; H-3, H-4), 4.85 (d, *J* 16.3 Hz, 6H; H-3' or H-5'), 4.83 (dt, *J* 12.7, 5.6 Hz, 6H; H-2), 4.71 (d, *J* 16.3 Hz, 6H; H-3' or H-5'), 4.45 (d, *J* 16.3 Hz, 6H; H-3' or H-5'), 4.32 (t, *J* 7.0 Hz, 12H; H-15), 4.10 (dd, *J* 19.4, 13.0 Hz, 12H; H-6), 3.97 (d, *J* 16.3 Hz, 6H; H-3' or H-5'), 3.11 (dd, *J* 11.1, 5.3 Hz, 6H; H-1a), 2.70 (m, 6H; H-7a), 2.68 (d, *J* 8.8 Hz, 6H; H-5), 2.51 (m, 6H; H-7b), 2.35 (dd, *J* 12.7, 11.1 Hz, 6H; H-1b), 1.95 (s, 72H; AcO), 1.85 (m, 12H; H-14), 1.40 (m, 12H; H-8), 1.28 ppm (m, 60H; H-9 to H-13); ^{13}C-NMR ($CD_3CN/CDCl_3$ 9:1, 100 MHz): δ 171.4, 170.94, 170.88, 170.6, 144.4-142.8, 124.7-123.8, 75.3, 70.5, 70.2, 62.1, 60.5, 53.4, 52.5, 51.1-50.6, 30.9, 30.2, 30.1, 29.7, 27.9, 27.2, 25.3, 21.1 ppm; HRMS (ESI): m/z calcd for $C_{168}H_{261}N_{30}O_{54}$ $[M + 3H]^{3+}$ 1187.6194; found 1187.6215.

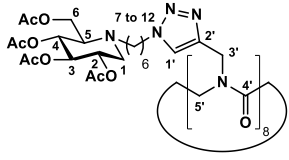

4.47a

Compound **4.47a**: $[\alpha]_D^{24}$ = +5.1 (*c* 1, $CHCl_3$); ^{1}H-NMR ($CD_3CN/CDCl_3$ 9:1, 400 MHz): δ 7.78-76.8 (m, 8H; H-1'), 5.26-5.10 (m, 4H; H-3' or H-5'), 4.98 (m, 16H; H-3 and H-4), 4.95-3.83 (m, 28H; H-3' and H-5'), 4.84 (m, 8H; H-2), 4.33 (m, 16H; H-12), 4.12 (s, 16H; H-6), 3.11 (m, 8H; H-1a), 2.69 (m, 16H; H-5 and H-7a), 2.55 (m, 8H; H-7b), 2.37 (m, 8H; H-1b), 1.99 (s, 96H; AcO), 1.88 (m, 16H; H-11), 1.42 (br s, 16H; H-8), 1.31 ppm (br s, 32H; H-9 and H-10); ^{13}C-NMR ($CD_3CN/CDCl_3$ 9:1, 100 MHz): δ 171.2, 170.83, 170.79, 170.7, 170.5, 169.8, 169.7, 167.5, 144.1, 143.2, 124.2, 124.1, 124.0, 123.8, 75.2, 70.3, 70.1, 61.9, 60.4, 53.3, 52.2, 50.7, 50.0, 49.2, 48.8, 47.9,

44.4, 43.5, 42.55, 30.7, 27.1, 26.9, 25.1, 21.0 ppm; HRMS (ESI): m/z calcd for $C_{200}H_{299}N_{40}O_{72}$ [M + 3H]$^{3+}$ 1471.0316; found 1471.0329.

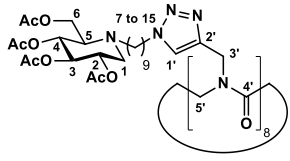

4.47b

Compound **4.47b**: $[\alpha]_D^{21}$ = +5.9 (*c* 1, $CHCl_3$); ^{1}H-NMR ($CD_3CN/CDCl_3$ 9:1, 400 MHz): δ 7.78-76.8 (m, 8H; H-1'), 5.26-5.10 (m, 4H; H-3' or H-5'), 4.99 (m, 16H; H-3 and H-4), 4.95-3.83 (m, 28H; H-3' and H-5'), 4.85 (td, *J* 9.7, 5.1 Hz, 8H; H-2), 4.33 (m, 16H; H-15), 4.13 (s, 16H; H-6), 3.14 (dd, *J* 11.7, 4.8 Hz, 8H; H-1a), 2.69 (m, 16H; H-5 and H-7a), 2.55 (m, 8H; H-7b), 2.37 (dd, *J* 11.9, 10.3 Hz, 8H; H-1b), 1.99 (s, 96H; AcO), 1.88 (m, 16H; H-14), 1.42 (br s, 16H; H-8), 1.31 ppm (br s, 80H; H-9 to H-13); ^{13}C-NMR ($CD_3CN/CDCl_3$ 9:1, 100 MHz): δ 171.2, 170.83, 170.76, 170.7, 170.5, 169.8, 169.7, 167.5, 144.1, 143.14, 143.07, 124.17, 124.05, 123.94, 123.8, 75.2, 70.3, 70.1, 61.9, 60.4, 53.3, 52.2, 50.7, 50.0, 49.2, 48.8, 47.9, 44.4, 43.5, 42.55, 30.8, 30.0, 29.6, 27.7, 27.1, 25.3, 21.0 ppm; HRMS (ESI): m/z calcd for $C_{224}H_{345}N_{40}O_{72}Na$ [M + H + Na]$^{2+}$ 2385.2226; found 2385.2264.

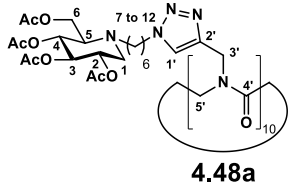

4.48a

Compound **4.48a**: $[\alpha]_D^{20}$ = +4.5 (*c* 1, $CHCl_3$); ^{1}H-NMR ($CD_3CN/CDCl_3$ 9:1, 400 MHz): δ 8.05-7.64 (m, 10H; H-1'), 5.58-3.48 (br m, 40H; H-3' and H-5'), 4.98 (m, 20H; H-3 and H-4), 4.84 (m, 10H; H-2), 4.34 (br s, 20H; H-12), 4.12 (m, 20H; H-6), 3.12 (br s, 10H; H-

1a), 2.69 (m, 20H; H-5 and H-7a), 2.56 (m, 10H; H-7b), 2.37 (m, 10H; H-1b), 1.99 (s, 120H; AcO), 1.87 (m, 20H; H-11), 1.51-1.15 ppm (m, 60H; H-8 to H-10); ^{13}C-NMR ($CD_3CN/CDCl_3$ 9:1, 75.5 MHz): δ 171.9, 171.4, 171.3, 171.1, 171.0-169.2, 145.0-143.3, 125.6-124.1, 75.7, 70.9, 70.7, 62.5, 61.0, 53.9, 52.8, 51.4, 50.4-48.9, 45.2-42.3, 31.4, 27.8, 27.5, 25.8, 21.6 ppm; HRMS (ESI): m/z calcd for $C_{250}H_{372}N_{50}O_{90}$ $[M + 2H]^{2+}$ 2757.3029; found 2757.3300.

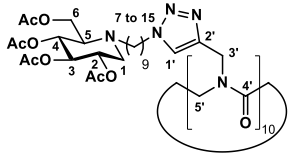

4.48b

Compound **4.48b**: $[\alpha]_D^{21} = +6.5$ (*c* 1, $CHCl_3$); ^{1}H-NMR ($CDCl_3$, 400 MHz): δ 8.14-7.44 (m, 10H; H-1'), 5.86-3.30 (br m, 40H; H-3' and H-5'), 5.04 (m, 20H; H-3 and H-4), 4.93 (m, 10H; H-2), 4.33 (br s, 20H; H-15), 4.14 (s, 20H; H-6), 3.18 (m, 10H; H-1a), 2.71 (m, 10H; H-7a), 2.62 (d, *J* 8.8Hz, 10H; H-5), 2.54 (m, 10H; H-7b), 2.31 (dd, *J* 11.6, 9.9 Hz, 10H; H-1b), 2.04 (m, 120H; AcO), 1.89 (m, 20H; H-14), 1.51-1.05 ppm (m, 120H; H-8 to H-13); ^{13}C-NMR ($CD_3CN/CDCl_3$ 9:1, 100 MHz): δ 171.4, 170.9, 170.8, 170.6, 170.2-168.9, 144.4-142.2, 125.0-123.5, 75.3, 70.4, 70.2, 62.0, 60.5, 53.4, 52.5, 50.9, 50.4-47.0, 45.3-41.5, 31.0, 30.2, 30.1, 29.7, 27.9, 27.2, 25.4, 21.1 ppm; MS (MALDI-TOF): m/z calcd for average mass of $C_{280}H_{430}N_{50}O_{90}Na$ $[M + Na]^+$ 5959.1; found 5958.7.

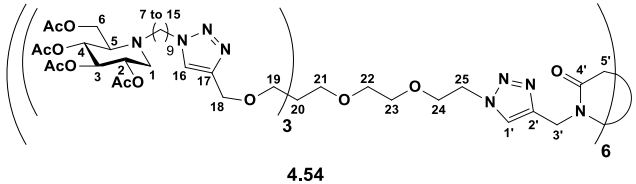

4.54

Compound **4.54**: $[\alpha]_D^{20} = +4.2$ (*c* 1, $CHCl_3$); ^{1}H-NMR ($CDCl_3$, 500 MHz) δ 8.28-7.43 (m, 6H; H-1'), 7.56 (s, 18H; H-16), 5.07-4.96

(m, 36H; H-3 and H-4), 4.96-4.89 (m, 18H; H-2), 4.83-3.71 (br m, 24H; H-3' and H-5'), 4.50 (m, 48H; H-18 and H-25), 4.27 (m, 36H; H-15), 4.11 (s, 36H; H-6), 3.94-3.79 (m, 12H; H-24), 3.58-3.31 (m, 72H; H-19, H-21, H-22 and H-23), 3.15 (dd, *J* 11.2, 5.1 Hz, 18H; H-1a), 2.73-2.64 (m, 18H; H-7a), 2.60 (d, *J* 8.7 Hz, 18H; H-5), 2.56-2.48 (m, 18H; H-7b), 2.29 (dd, *J* 11.2, 10.4 Hz, 18H; H-1b), 2.07-1.92 (m, 216H; C(O)CH_3), 1.85 (m, 36H; H-14), 1.45-1.10 ppm (m, 216H; H-8, H-9, H-10, H-11, H-12 and H-13); ^{13}C-NMR ($CDCl_3$, 125 MHz) δ 171.0, 170.4, 170.1, 169.8 (C(O)CH_3), 169.5-167.0 (C-4'), 145.2 (C-17), 143.9-141.3 (C-2'), 125.3-123.6 (C-1'), 122.6 (C-16), 74.7 (C-2), 71.1, 71.0, 70.2, 69.9 (C-21 to C-24), 69.52, 59.46 (C-3 and C-4), 69.2 (C-18), 65.1 (C-19), 61.4 (C-5), 59.5 (C-6), 53.0 (C-1), 51.9 (C-7), 50.3 (C-15 and C-25), 49.4-47.1 (C-3' or C-5'), 45.4 (C-20), 44.3-41.0 (C-3' or C-5'), 30.5, 29.5, 29.1, 27.3, 26.6, 24.6 (C-8 to C-14), 20.95, 20.93, 20.82, 20.76 ppm (C(O)CH_3); IR (neat) 1744 (strong, C=O acetate), 1672 cm^{-1} (strong, C=O amide); HRMS (ESI) average *m/z* calcd for $C_{552}H_{870}N_{96}O_{180}$ $[M + 6H]^{6+}$ 1955.2008; found 1955.2005; MS (MALDI) *m/z* calcd for $C_{552}H_{864}N_{96}O_{180}Na$ $[M + Na]^+$ 11748.32; found 11751.97.

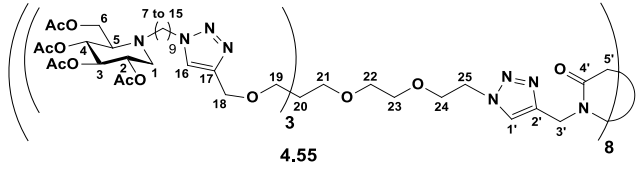

4.55

Compound **4.55:** $[\alpha]_D^{20} = +4.1$ (*c* 1, $CHCl_3$); ^{1}H-NMR ($CDCl_3$, 500 MHz) δ 7.90-7.39 (m, 32H; H-16 and H-1'), 5.08-4.96 (m, 48H; H-3 and H-4), 4.92 (m 24H; H-2), 4.75-3.72 (br m, 32H; H-3' and H-5'), 4.56-4.42 (m, 64H; H-18 and H-25), 4.33-4.22 (m, 48H; H-15), 4.12 (s, 48H; H-6), 3.91-3.77 (m, 16H; H-24), 3.61-3.27 (m, 96H; H-19, H-21, H-22 and H-23), 3.15 (dd, *J* 11.2, 4.9 Hz, 24H; H-1a), 2.74-2.64 (m, 24H; H-7a), 2.60 (d, *J* 8.9 Hz, 24H; H-5), 2.57-2.47 (m, 24H;

H-7b), 2.30 (dd, *J* 11.2, 10.3 Hz, 24H; H-1b), 2.07-1.93 (m, 288H; C(O)CH_3), 1.85 (m, 48H; H-14), 1.45-1.12 ppm (m, 288H; H-8, H-9, H-10, H-11, H-12 and H-13); ^{13}C-NMR ($CDCl_3$, 125 MHz) δ 171.0, 170.4, 170.1, 169.8 (C(O)CH_3), 169.3-165.0 (C-4'), 145.2 (C-17), 144.0-141.4 (C-2'), 124.9-123.4 (C-1'), 122.6 (C-16), 74.7 (C-2), 71.1, 70.9, 70.3, 69.9 (C-21 to C-24), 69.55, 69.49 (C-3 and C-4), 69.3 (C-18), 65.1 (C-19), 61.4 (C-5), 59.5 (C-6), 53.0 (C-1), 51.9 (C-7), 50.3 (C-15 and C-25), 50.0-46.8 (C-3' or C-5'), 45.4 (C-20), 44.2-41.3 (C-3' or C-5'), 30.5, 29.5, 29.1, 27.3, 26.6, 24.6 (C-8 to C-14), 20.96, 20.94, 20.84, 20.77 ppm (C(O)CH_3); IR (neat) 1745 (strong, C=O acetate), 1676 cm^{-1} (strong, C=O amide); HRMS (ESI) average *m/z* calcd for $C_{736}H_{1164}N_{128}O_{240}$ $[M + 12H]^{12+}$ 1303.7751; found 1303.7710; MS (MALDI) *m/z* calcd for $C_{736}H_{1152}N_{128}O_{240}Na$ $[M + Na]^+$ 15656.8; found 15647.2.

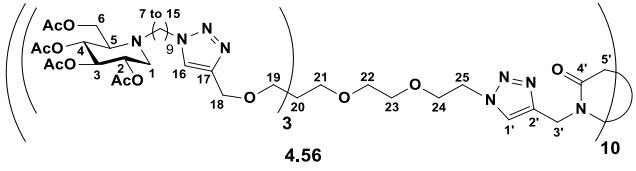

4.56

Compound **4.56**: $[\alpha]_D^{20} = +4.3$ (*c* 1, $CHCl_3$); **1**H-NMR ($CDCl_3$, 500 MHz) δ 8.14-7.40 (m, 40H; H-16 and H-1'), 5.10-4.97 (m, 60H; H-3 and H-4), 4.93 (m, 30H; H-2), 4.73-3.72 (br m, 56H; H-3' and H-5'), 4.60-4.37 (m, 80H; H-18 and H-25), 4.29 (t, *J* 7.1 Hz, 60H; H-15), 4.12 (s, 60H; H-6), 3.92-3.74 (m, 20H; H-24), 3.61-3.30 (m, 120H; H-19, H-21, H-22 and H-23), 3.16 (dd, *J* 11.4, 5.0 Hz, 30H; H-1a), 2.75-2.65 (m, 30H; H-7a), 2.61 (d, *J* 8.9 Hz, 30H; H-5), 2.58-2.48 (m, 30H; H-7b), 2.30 (t, *J* 10.7 Hz, 30H; H-1b), 2.07-1.93 (m, 360H; C(O)CH_3), 1.85 (m, 60H; H-14), 1.49-1.11 ppm (m, 360H; H-8, H-9, H-10, H-11, H-12 and H-13); ^{13}C-NMR ($CDCl_3$, 125 MHz) δ 171.0, 170.4, 170.1, 169.8 (C(O)CH_3), 169.9-166.5 (C-4'), 145.3 (C-17), 144.0-141.0 (C-2'), 125.2-123.2 (C-1'), 122.5 (C-16), 74.7 (C-2), 71.1, 71.0, 70.3,

69.9 (C-21 to C-24), 69.6, 69.5 (C-3 and C-4), 69.3 (C-18), 65.1 (C-19), 61.4 (C-5), 59.5 (C-6), 53.0 (C-1), 51.9 (C-7), 60.4 (C-15 and C-25), 49.2-47.7 (C-3' or C-5'), 45.4 (C-20), 44.6-40.9 (C-3' or C-5'), 30.5, 29.5, 29.0, 27.3, 26.6, 24.6 (C-8 to C-14), 20.98, 20.96, 20.86, 20.79 ppm (C(O)$\underline{C}H_3$); IR (neat) 1744 (strong, C=O acetate), 1676 cm^{-1} (strong, C=O amide); HRMS (ESI) average *m/z* calcd for $C_{920}H_{1452}N_{160}O_{300}Na$ + HCOOH [M + 12H + Na + HCOOH]$^{13+}$ 1508.5584; found 1508.9507; MS (MALDI) *m/z* calcd for $C_{920}H_{1440}N_{160}O_{300}Na$ [M + Na + HCOOH]$^{+}$ 19565.20; found 19575.83.

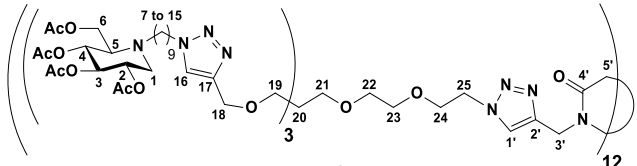

4.57

Compound **4.57**: $[\alpha]_D^{20} = +3.1$ (*c* 1, $CHCl_3$); ^{1}H-NMR ($CDCl_3$, 400 MHz) δ 8.07-7.46 (m, 48H; H-16 and H-1'), 5.10-4.84 (m, 108H; H-2, H-3 and H-4), 4.80-3.72 (br m, 48H; H-3' and H-5'), 4.50 (m, 96H; H-18 and H-25), 4.28 (m, 72H; H-15), 4.12 (s, 72H; H-6), 3.86 (br s, 24H; H-24), 3.62-3.26 (m, 144H; H-19, H-21, H-22 and H-23), 3.15 (dd, *J* 11.2, 4.8 Hz, 36H; H-1a), 2.68 (m, 36H; H-7a), 2.60 (d, *J* 8.7 Hz, 36H; H-5), 2.52 (m, 36H; H-7b), 2.29 (dd, *J* 11.2, 10.3 Hz, 36H; H-1b), 2.11-1.90 (several singlets, 432H; C(O)CH_3), 1.85 (m, 72H; H-14), 1.50-1.07 ppm (m, 432H; H-8 to H-13); ^{13}C-NMR ($CDCl_3$, 100 MHz) δ 170.9, 170.4, 170.0, 169.8 ($\underline{C}$(O)CH_3), 169.9-166.5 (C-4'), 145.2 (C-17), 144.0-141.0 (C-2'), 125.2-123.2 (C-1'), 122.6 (C-16), 74.8 (C-2), 71.1, 71.0, 70.2, 69.9 (C-21 to C-24), 69.6, 69.5 (C-3 and C-4), 69.3 (C-18), 65.1 (C-19), 61.5 (C-5), 59.6 (C-6), 53.0 (C-1), 51.9 (C-7), 50.3 (C-15 and C-25), 49.5-47.5 (C-3' or C-5'), 45.4 (C-20), 44.5-40.5 (C-3' or C-5'), 30.5, 29.5, 29.1, 27.3, 26.6, 24.8 (C-8 to C-14), 20.93, 20.82, 20.8 ppm (C(O)$\underline{C}H_3$); IR (neat) 1743

(strong, C=O acetate), 1673 cm^{-1} (strong, C=O amide); MS (ESI) average *m/z* calcd for $C_{1104}H_{1740}N_{192}O_{360}$ $[M + 12H]^{12+}$ 1955.22; found 1955.22.

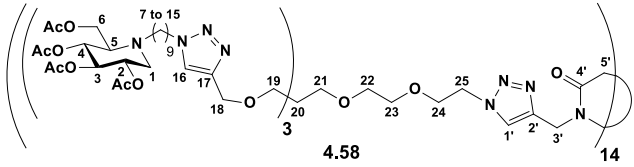

Compound **4.58**: $[\alpha]_D^{20}$= +2.1 (*c* 1, CH_3OH); ^{1}H-NMR ($CDCl_3$, 400 MHz) δ 8.10-7.45 (m, 56H, H-16, H-1'), 5.12-5.00 (m, 84H, H-4, H-3), 5.00-4.93 (m, 42H, H-2), 4.83-3.68 (br m, 56H; H-3' and H-5'), 4.52 (m, 112H, H-18, H-25), 4.34-4.26 (m, 84H, H-15), 4.16 (s, 84H, H-6), 3.91 (br s, 28H, H-24), 3.65-3.32 (m, 168H, H-19, H-21, H-22 and H-23), 3.20 (dd, *J* 11.0, 4.5 Hz, 42H, H-1a), 2.80-2.53 (m, 126H, H-5, H-7), 2.32 (dd, *J* 11.0, 10.5 Hz, 42H, H-1b), 2.08-1.97 (several singlets, 504H, $C(O)CH_3$), 1.87 (m, 84H, H-14), 1.49-1.12 (m, 504H, H-8 to H-13) ppm ; ^{13}C-NMR ($CDCl_3$, 100 MHz) δ 170.9, 170.4, 170.1, 169.8 ($\underline{C}(O)CH_3$), 169.9-168.5 (C-4'), 145.3 (C-17), 144-142.0 (C-2'), 125.4-123.5 (C-1'), 122.7 (C-16), 74.8 (C-2), 71.2, 71.0, 70.3, 70.0 (C-21 to C-24), 69.6, 69.5 (C-3 and C-4), 69.3 (C-18), 65.1 (C-19), 61.5 (C-5), 59.6 (C-6), 53.0 (C-1), 51.9 (C-7), 50.4 (C-15 and C-25), 49.5-47.5 (C-3' or C-5'), 45.5 (C-20), 44.5-40.5 (C-3' or C-5'), 30.5, 29.6, 29.2, 27.3, 26.7, 24.8 (C-8 to C-14), 20.98, 20.96, 20.86, 20.80 ($C(O)\underline{C}H_3$) ppm ; IR (neat) 1743 (strong, C=O acetate), 1673 (strong, C=O amide) cm^{-1} ; MS (ESI) average *m/z* calcd for $C_{1288}H_{2028}N_{224}O_{420}$ $[M + 12H]^{12+}$ 2280.96; found 2280.53 ; MS (MALDI) *m/z* calcd for $C_{1288}H_{2016}KN_{224}O_{420}$ $[M + K]^+$ 27398.2; found 27396.0.

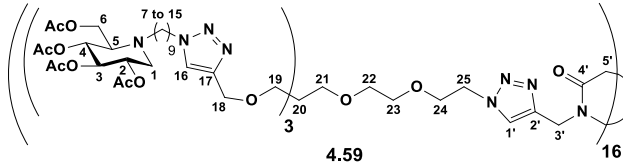

4.59

Compound **4.59**: $[\alpha]_D^{20}$ = +3.0 (*c* 1, $CHCl_3$); ^{1}H-NMR ($CDCl_3$, 400 MHz) δ 8.09-7.52 (m, 64H; H-16 and H-1'), 5.13-4.86 (m, 144H; H-2, H-3 and H-4), 4.85-3.68 (br m, 64H; H-3' and H-5'), 4.50 (m, 128H; H-18 and H-25), 4.29 (m, 96H; H-15), 4.13 (s, 96H; H-6), 3.88 (br s, 32H; H-24), 3.65-3.25 (m, 192H; H-19, H-21, H-22 and H-23), 3.17 (dd, *J* 11.3, 4.8 Hz, 48H; H-1a), 2.70 (m, 48H; H-7a), 2.62 (d, *J* 8.9 Hz, 48H; H-5), 2.54 (m, 48H; H-7b), 2.31 (dd, *J* 11.3, 10.5 Hz, 48H; H-1b), 2.10-1.92 (several singlets, 576H; C(O)CH_3), 1.86 (m, 96H; H-14), 150-1.09 ppm (m, 576H; H-8 to H-13); ^{13}C-NMR ($CDCl_3$, 100 MHz) δ 170.9, 170.4, 170.1, 169.8 (C(O)CH_3), 169.9-166.5 (C-4'), 145.2 (C-17), 144.0-141.0 (C-2'), 125.2-123.2 (C-1'), 122.7 (C-16), 74.8 (C-2), 71.1, 71.0, 70.2, 70.0 (C-21 to C-24), 69.6, 69.5 (C-3 and C-4), 69.3 (C-18), 65.1 (C-19), 61.5 (C-5), 59.6 (C-6), 53.0 (C-1), 51.9 (C-7), 50.3 (C-15 and C-25), 49.5-47.5 (C-3' or C-5'), 45.5 (C-20), 44.5-40.5 (C-3' or C-5'), 30.5, 29.6, 29.2, 27.3, 26.7, 24.8 (C-8 to C-14), 20.98, 20.95, 20.85, 20.79 ppm (C(O)CH_3); IR (neat) 1743 (strong, C=O acetate), 1672 cm^{-1} (strong, C=O amide); MS (MALDI) *m/z* calcd for $C_{1472}H_{2305}N_{256}O_{480}$ $[M + H]^+$ 31268.5; found 31265.0.

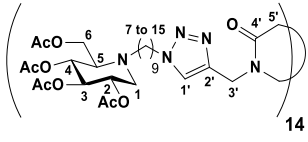

4.66

Compound **4.66**: $[\alpha]_D^{20}$ = +2.5 (*c* 1, CH_3OH); ^{1}H-NMR ($CDCl_3$, 400 MHz) δ 8.15-7.53 (m, 14H; H-1'), 5.10-4.99 (m, 28H; H-3 and H-4), 4.99-4.90 (m, 14H; H-2), 4.83-3.72 (br m, 56H; H-3' and

H-5'), 4.33 (br s, 28H; H-15), 4.15 (br s, 28H; H-6), 3.22-3.14 (m, 14H; H-1a), 2.78-2.65 (m, 14H; H-7a), 2.65-2.60 (m, 14H; H-5), 2.59-2.50 (m, 14H; H-7b), 2.32 (t, *J* 10.8 Hz, 14H; H-1b), 2.09-1.96 (m, 168H; C(O)CH_3), 1.93-1.84 (m, 28H; H-14), 1.38-1.13 ppm (m, 168H; H-8 to H-13); ^{13}C-NMR ($CDCl_3$, 75 MHz) δ 170.9, 170.4, 170.0, 169.8 (C(O)-CH_3), 169.5-168.0 (C-4'), 144.8-141.5 (C-2'), 124.9-122.6 (C-1'), 74.9 (C-3), 69.8, 69.6 (C-4 and C-2), 61.7 (C-5), 59.8 (C-6), 53.1 (C-1), 52.0 (C-7), 50.6 (C-15), 30.4 (C-14), 29.8, 29.6, 29.2, 27.4, 26.8 (from C-9 to C-13), 25.0 (C-8), 21.0, 20.9, 20.84, 20.78 (C(O)CH_3) ppm; IR (neat) 1745 (strong, C=O acetate), 1673 cm^{-1} (strong, C=O amide); HRMS (ESI) average *m/z* calcd for $C_{392}H_{606}N_{70}O_{126}$ $[M + 4H]^{4+}$ 2078.6075; found 2078.6117.

General procedure for the synthesis of deprotected cyclopeptoid-based iminosugar click clusters 4.45a, 4.45b, 4.49a-4.51a, 4.49b-4.51b, 4.60-4.65, and 4.67.

Acetate-protected iminosugar click clusters **4.44a**, **4.44b**, or **4.46a-4.48a, 4.46b-4.48b, 4.54-4.59,** and **4.66** were dissolved in a 1:1 mixture of water/MeOH (typically 600 µL/µmol). To the resulting mixture, Amberlite IRA400 (OH^-) (5.5n g/mmol of substrate; n = number of acetate groups) was added. The suspension was gently stirred overnight at 40 °C and the mixture was filtrated. Then the filtrate was concentrated to give deprotected iminosugar click clusters **4.45** and **4.49-4.51** in quantitative yields.

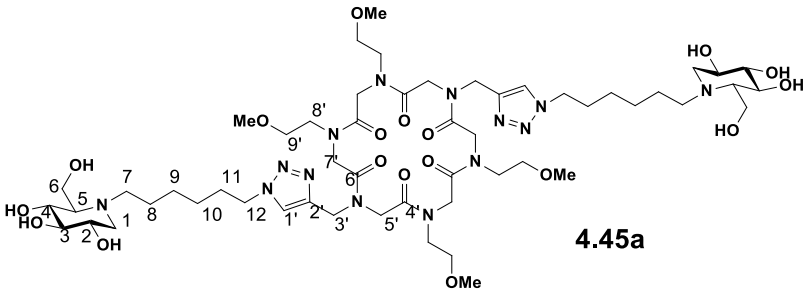

4.45a

Compound **4.45a**: $[\alpha]_D^{20}$ = -7.8 (c 1, MeOH); ^{1}H-NMR (CD_3OD, 400 MHz) δ 8.18-7.78 (m, 2H; H-1'), 5.10-3.08 (m, 52H; H-2, H-4, H-12, H-3', H-5', H-7', H-8', H-9' and MeO), 3.86 (m, 4H; H-6), 3.16 (m, 2H; H-3), 2.98 (dd, *J* 11.0, 4.4 Hz, 2H; H-1a), 2.80 (m, 2H; H-7a), 2.56 (m, 2H; H-7b), 2.16 (t, *J* 11.0 Hz, 2H; H-1b), 2.11 (d, *J* 10.7 Hz, 2H; H-5), 1.93 (m, 4H; H-11), 1.51 (m, 4H; H-8), 1.36 ppm (m, 8H; H-9 and H-10);^{13}C-NMR (CD_3OD, 100 MHz) δ 174.0-171.0 (C-4' and C-6'), 146.2-143.3 (C-2'), 125.0 (C-1'), 80.8 (C-3), 72.2 (C-4), 72.6-70.9 (C-8' and C-9'), 70.9 (C-2), 67.6 (C-5), 59.8 (C-6), 59.5 (MeO), 57.9 (C-1), 53.7 (C-7), 51.4 (C-12), 51.2-49.6, 45.6-43.9 (C-3', C-5' and C-7'), 31.4, 28.1, 27.5, 25.3 ppm (C-8 to C-11); IR (neat) 3376 (broad, O-H), 1651 cm-1 (strong, C=O amide); MS (MALDI) m/z calcd for C54H94N14O18Na [M + H]+ 1227.694; found 1227.729.

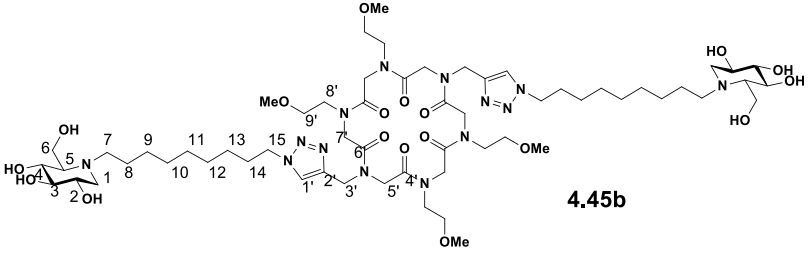

4.45b

Compound **4.45b**: $[\alpha]_D^{20}$ = -6 (c 1, MeOH); ^{1}H-NMR (CD_3OD, 400 MHz) δ 8.15-7.77 (m, 2H; H-1'), 5.04-3.10 (m, 52H; H-

2, H-4, H-15, H-3', H-5', H-7', H-8', H-9' and MeO), 3.86 (m, 4H; H-6), 3.15 (m, 2H; H-3), 3.00 (dd, *J* 10.8, 4.9 Hz, 2H; H-1a), 2.80 (m, 2H; H-7a), 2.57 (m, 2H; H-7b), 2.18 (t, *J* 10.8 Hz, 2H; H-1b), 2.11 (d, *J* 9.4 Hz, 2H; H-5), 1.91 (m, 4H; H-14), 1.50 (m, 4H; H-8), 1.35 ppm (m, 20H; H-9, H-10, H-11, H-12 and H-13); ^{13}C-NMR (CD_3OD, 100 MHz) δ 174.6-169.3 (C-4' and C-6'), 146.0-143.5 (C-2'), 125.0 (C-1'), 80.6 (C-3), 72.0 (C-4), 71.8, 70.9 (C-8' and C-9'), 70.7 (C-2), 67.4 (C-5), 59.5 (C-6), 59.7-58.7 (MeO), 57.7 (C-1), 53.8 (C-7), 51.3 (C-15), 51.9-49.5, 45.5-43.5 (C-3', C-5' and C-7'), 31.3, 30.5, 30.0, 28.5, 27.4, 25.1 ppm (C-8 to C-14); IR (neat) 3401 (broad, O-H), 1660 cm-1 (strong, C=O amide); HRMS (ESI) m/z calcd for C60H107N14O18 [M + H] + 1311.7882; found 1311.7881.

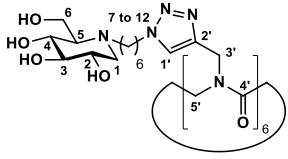

4.49a

Compound **4.49a**: $[\alpha]_D^{20}$ = -28.0 (*c* 0.1, H_2O/DMSO 1:1 + 0.1% TFA); ^{1}H NMR (D_2O + 0.1% TFA, 500 MHz) δ 8.21–7.60 (m, 6H, H-1'), 5.20–3.72 (br m, 12H, H-3' and H-5'), 4.35 (s, 12H, H-12), 3.85 (s, 12H, H-6), 3.59 (s, 6H, H-2), 3.43 (s, 6H, H-4), 3.31 (s, 6H, H-3), 3.16 (s, 6H, H-1a), 2.91 (s, 6H, H-7a), 2.78 (s, 6H, H-7b), 2.56 (s, 12H, H-1b and H-5), 1.84 (s, 12H, H-11), 1.51 (s, 12H, H-8), 1.25 (s, 24H, H-9 and H-10) ppm; ^{13}C NMR (D_2O + 0.1% TFA, 125 MHz) δ 173.4–169.3, 145.6–142.8, 127.4–124.6, 78.9, 70.4, 69.3, 66.8, 57.5, 55.9, 53.9, 51.9, 51.5–49.3, 46.3–43.3, 30.9, 27.3, 26.8, 24.0 ppm; HRMS–ESI (m/z): $[M + 2H]^{2+}$ calcd for C102H174N30O30 1150.6579; found: 1150.6626

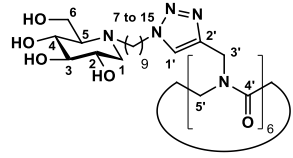

4.49b

Compound **4.49b**: $[\alpha]_D^{20}$ = -14.0 (*c* 0.0625, H_2O/DMSO 1:1 + 0.1% TFA); ^{1}H-NMR (D_2O/CD_3OD 1:1, 400 MHz): δ 8.13-7.68 (m, 6H; H-1'), 5.09-3.89 (br m, 12H; H-3' and H-5'), 4.36 (s, 12H; H-15), 3.80 (dd, *J* 19.6, 12.8 Hz, 12H; H-6), 3.47 (td, *J* 9.2, 5.0 Hz, 6H; H-2), 3.32 (t, *J* 9.6 Hz, 6H; H-4), 3.16 (t, *J* 9.4 Hz, 6H; H-3), 2.93 (dd, *J* 10.6, 5.0 Hz, 6H; H-1a), 2.67 (s, 6H; H-7a), 2.56 (s, 6H; H-7b), 2.20 (dd, *J* 10.6, 9.2 Hz, 6H; H-1b), 2.13 (d, *J* 9.6 Hz, 6H; H-5), 1.83 (s, 12H; H-14), 1.40 (s, 12H; H-8), 1.23 ppm (s, 60H; H-9 to H-13); ^{13}C-NMR (D_2O + 0.1% TFA, 125 MHz): δ 173.5-169.4, 144.6-142.7, 127.1-124.7, 77.5, 68.7, 67.8, 66.7, 55.2, 54.8, 54.7, 52.2, 51.7-48.8, 46.4-43.2, 31.0, 30.2-28.9, 27.7-26.4, 24.8 ppm; HRMS (ESI): m/z calcd for $C_{120}H_{212}N_{30}O_{30}$ $[M + 2H]^{2+}$ 1276.7987; found 1276.7991.

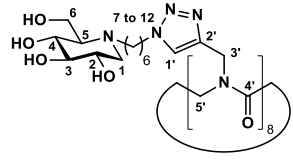

4.50a

Compound **4.50a:** $[\alpha]_D^{20}$ = -9.6 (*c* 1, H_2O); ^{1}H-NMR (D_2O/CD_3OD 1:1, 400 MHz): δ 8.05-7.77 (m, 8H; H-1'), 5.11-4.02 (br m, 32H; H-3' and H-5'), 4.37 (m, 16H; H-12), 3.77 (m, 16H; H-6), 3.47 (br s, 8H; H-2), 3.31 (m, 8H; H-4), 3.16 (m, 8H; H-3), 2.91 (br s, 8H; H-1a), 2.66 (br s, 8H; H-7a), 2.53 (br s, 8H, H-7b), 2.14 (m, 16H; H-1b and H-5), 1.85 (br s, 16H; H-11), 1.39 (br s, 16H; H-8), 1.25 ppm (m, 32H; H-9 and H-10); ^{13}C-NMR (D_2O/CD_3OD 1:1, 100 MHz): δ 171.7, 171.4, 170.9, 170.3, 169.3, 144.2, 144.1, 143.5, 143.3, 125.5, 79.8, 71.4, 70.9, 70.2, 66.5, 59.1, 56.9, 53.3, 51.5, 50.9-49.8, 44.7-

43.2, 30.7, 27.6, 26.9, 24.0 ppm; MS (MALDI-TOF): m/z calcd for $C_{136}H_{233}N_{40}O_{40}$ $[M + H]^+$ 3066.7; found 3066.8.

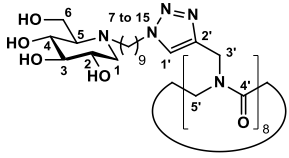

4.50b

Compound **4.50b:** $[\alpha]_D^{20}$ == -10.0 (*c* 1, MeOH); ^{1}H-NMR (CD_3OD, 400 MHz): δ 8.11-7.80 (m, 8H; H-1'), 5.25-3.99 (br m, 32H; H-3' and H-5'), 4.40 (m, 16H; H-15), 3.84 (s, 16H; H-6), 3.49 (td, *J* 9.5, 4.5 Hz, 8H; H-2), 3.36 (t, *J* 9.0 Hz, 8H; H-4), 3.16 (t, *J* 9.0 Hz, 8H; H-3), 2.98 (dd, *J* 9.8, 4.4 Hz, 8H; H-1a), 2.75 (m, 8H; H-7a), 2.57 (m, 8H; H-7b), 2.18 (t, *J* 10.7 Hz, 8H; H-1b), 2.12 (d, *J* 10.9 Hz, 8H; H-5), 1.89 (br s, 16H; H-14), 1.47 (br s, 16H; H-8), 1.31 ppm (m, 80H; H-9 to H-13); ^{13}C-NMR (CD_3OD, 100 MHz): δ 172.0, 171.2, 170.6, 169.3, 144.7, 144.5, 143.9, 143.6, 125.4, 125.33, 125.29, 125.23, 80.6, 72.1, 70.8, 67.3, 59.6, 57.7, 53.9, 51.6, 51.0-49.6, 44.6, 44.3, 44.0, 43.7, 31.4, 30.6, 30.2, 28.7, 27.6, 25.1 ppm; MS (MALDI-TOF): m/z calcd for $C_{160}H_{281}N_{40}O_{40}$ $[M + H]^+$ 3403.1; found 3403.3.

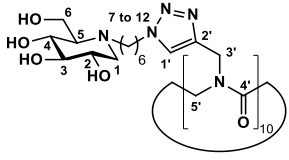

4.51a

Compound **4.51a:** $[\alpha]_D^{20}$ = -10.2 (*c* 1, H_2O); ^{1}H-NMR (D_2O, 500 MHz): δ 8.15-7.62 (m, 10H; H-1'), 5.69-3.85 (br m, 40H; H-3' and H-5'), 4.35 (m, 20H; H-12), 3.76 (m, 20H; H-6), 3.47 (m, 10H; H-2), 3.30 (m, 10H; H-4), 3.17 (m, 10H; H-3), 2.90 (m, 10H; H-1a), 2.61 (m, 10H; H-7a), 2.50 (m, 10H; H-7b), 2.15 (m, 20H; H-1b and H-5), 1.80 (m, 20H; H-11), 1.35 (m, 20H; H-8), 1.18 ppm (m, 40H; H-9 and H-10); ^{13}C-NMR (D_2O, 125 MHz): δ 171.5-167.7, 143.5-141.1, 124.6,

78.3, 70.0, 68.8, 65.0, 57.5, 55.3, 51.9, 50.4, 49.3-47.0, 43.9-41.5, 29.4, 26.1, 25.5, 22.5 ppm; HRMS (ESI): m/z calcd for $C_{170}H_{292}N_{50}O_{50}$ $[M + 2H]^{2+}$ 1917.0916; found 1917.1349.

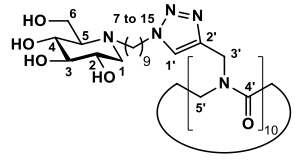

4.51b

Compound **4.51b:** $[\alpha]_D^{20}$ = -6.5 (*c* 0.5, MeOH/H_2O 1:1); ^{1}H-NMR (D_2O/CD_3OD 1:1, 400 MHz): δ 8.16-7.71 (m, 10H; H-1'), 5.64-4.03 (br m, 40H; H-3' and H-5'), 4.37 (m, 20H; H-15), 3.82 (m, 20H; H-6), 3.50 (t, *J* 9.7, 4.7 Hz, 10H; H-2), 3.35 (t, *J* 9.7 Hz, 10H; H-4), 3.18 (t, *J* 9.4 Hz, 10H; H-3), 2.96 (d, *J* 9.4 Hz, 10H; H-1a), 2.70 (m, 10H; H-7a), 2.59 (m, 10H; H-7b), 2.22 (t, *J* 11.1 Hz, 10H; H-1b), 2.16 (d, *J* 9.5 Hz, 10H; H-5), 1.86 (m, 20H; H-14), 1.43 ppm (m, 20H; H-8), 1.24 (m, 100H; H-9 to H-13); ^{13}C-NMR (CD_3CN/CD_3OD 1:1, 100 MHz): δ 172.4-168.4, 144.7-141.6, 124.7, 79.6, 71.1, 69.9, 66.3, 58.7, 56.8, 53.1, 51.1, 50.3, 59.0, 44.1-42.0, 30.6, 29.9, 29.4, 28.0, 26.9, 24.0 ppm; MS (MALDI-TOF): m/z calcd for $C_{200}H_{351}N_{50}O_{50}$ $[M + H]^+$ 4253.7; found 4254.1.

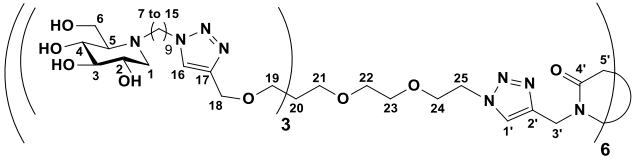

4.60

Compound **4.60:** $[\alpha]_D^{20}$ = -10.0 (*c* 1, MeOH); ^{1}H-NMR (CD_3OD, 500 MHz) δ 8.20-7.78 (m, 6H; H-1'), 7.94 (s, 18H; H-16), 4.62-4.42 (m, 48H; H-18 and H-25), 4.36 (s, 36H; H-15), 3.94-3.76 (m, 48H; H-6 and H-24), 3.58-3.28 (m, 108H; H-2, H-4, H-19, H-21, H-22 and H-23), 3.19 (t, *J* 9.2 Hz, 18H; H-3), 2.98 (dd, *J* 11.0, 4.9 Hz, 18H; H-1a), 2.80-2.68 (m, 18H; H-7a), 2.65-2.53 (m, 18H; H-7b),

2.22 (t, *J* 11.0 Hz, 18H; H-1b), 2.16 (d, *J* 9.8 Hz, 18H; H-5), 1.85 (s, 36H; H-14), 1.45 (s, 36H; H-8), 1.25 ppm (s, 180H; H-9 to H-13); ^{13}C-NMR (CD_3OD/D_2O 2.75:1, 125 MHz) δ 174.1-168.2 (C-4'), 146.0 (C-17), 145.0-142.8 (C-2'), 125.8 (C-1'), 125.3 (C-16), 80.2 (C-3), 72.0 (C-21 or C-22 or C-23 or C-24), 71.7 (C-4), 71.2 (C-21 or C-22 or C-23 or C-24), 70.7 (C-21 or C-22 or C-23 or C-24), 70.5 (C-2), 70.3 (C-21 or C-22 or C-23 or C-24), 69.9 (C-18), 66.9 (C-5), 65.3 (C-19), 59.3 (C-6), 57.4 (C-1), 53.7 (C-7), 51.5 (C-15 and C-25), 46.4 (C-20), 45.8-43.8 (C-3' or C-5'), 31.3 (C-14), 30.5, 30.0, 28.6, 27.4 (C-9 to C-13), 24.6 ppm (C-8); IR (neat) 3343 (broad, O-H), 1668 cm^{-1} (strong, C=O amide); HRMS (ESI) average *m/z* calcd for $C_{408}H_{726}N_{96}O_{108}$ $[M + 6H]^{6+}$ 1450.740; found 1450.722; MS (MALDI) *m/z* calcd for $C_{408}H_{721}N_{96}O_{108}$ $[M + H]^+$ 8699.7; found 8700.1.

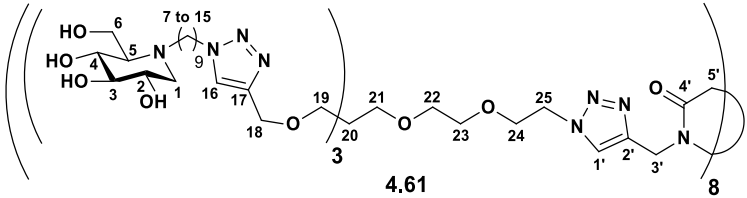

4.61

Compound **4.61**: $[\alpha]_D^{20}$ = -10.0 (*c* 1, MeOH); ^{1}H-NMR (CD_3OD/D_2O 2.25:1, 500 MHz) δ 8.20-7.73 (m, 32H; H-16 and H-1'), 4.60-4.40 (m, 64H; H-18 and H-25), 4.40-4.24 (m, 48H; H-15), 3.97-3.74 (m, 64H; H-6 and H-24), 3.59-3.25 (m, 144H; H-2, H-4, H-19, H-21, H-22 and H-23), 3.19 (t, *J* 9.3 Hz, 24H; H-3), 2.97 (dd, *J* 11.1, 4.7 Hz, 24H; H-1a), 2.80-2.66 (m, 24H; H-7a), 2.66-2.52 (m, 24H; H-7b), 2.22 (t, *J* 11.1 Hz, 24H; H-1b), 2.15 (d, *J* 9.7 Hz, 24H; H-5), 1.84 (m, 48H; H-14), 1.44 (m, 48H; H-8), 1.36-1.08 ppm (m, 240H; H-9 to H-13); ^{13}C-NMR (CD_3OD/D_2O 2.25:1, 125 MHz) δ 172.4-168.4 (C-4'), 145.9 (C-17), 144.7-142.7 (C-2'), 125.9 (C-1'), 125.3 (C-16), 80.2 (C-3), 72.0 (C-21 or C-22 or C-23 or C-24), 71.7 (C-4), 71.2 (C-21 or C-22 or C-23 or C-24), 70.7 (C-21 or C-22 or C-23 or C-24), 70.5 (C-

2), 70.3 (C-21 or C-22 or C-23 or C-24), 69.9 (C-18), 66.9 (C-5), 65.3 (C-19), 59.2 (C-6), 57.3 (C-1), 53.7 (C-7), 51.5 (C-15 and C-25), 46.4 (C-20), 45.0-43.2 (C-3' or C-5'), 31.3 (C-14), 30.5, 30.0, 28.6, 27.4 (C-9 to C-13), 24.6 ppm (C-8); IR (neat) 3351 (broad, O-H), 1674 cm^{-1} (strong, C=O amide); HRMS (ESI) average *m/z* calcd for $C_{544}H_{969}N_{128}O_{144}$ $[M + 9H]^{9+}$ 1289.584; found 1289.598; MS (MALDI) *m/z* calcd for $C_{544}H_{961}N_{128}O_{144}$ $[M + H]^{+}$ 11599.25; found 11601.85.

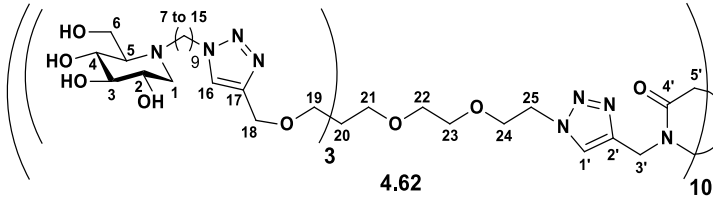

Compound **4.62**: $[\alpha]_D^{20} =$ -10.0 (*c* 1, MeOH); ^{1}H-NMR (CD_3OD/D_2O 2.25:1, 500 MHz) δ 8.22-7.85 (m, 40H; H-16 and H-1'), 4.63-4.41 (m, 80H; H-18 and H-25), 4.41-4.25 (m, 60H; H-15), 3.98-.372 (m, 80H; H-6 and H-24), 3.60-3.25 (m, 180H; H-2, H-4, H-19, H-21, H-22 and H-23), 3.20 (t, *J* 9.1 Hz, 30H; H-3), 3.04-2.90 (m, 30H; H-1a), 2.80-2.67 (m, 30H; H-7a), 2.65-2.52 (m, 30H; H-7b), 2.23 (t, *J* 11.0 Hz, 30H; H-1b), 2.16 (d, *J* 9.5 Hz, 30H; H-5), 1.83 (m, 60H; H-14), 1.44 (m, 60H; H-8), 1.24 ppm (m, 300H; H-9, H-10, H-11, H-12 and H-13); ^{13}C-NMR (CD_3OD/D_2O 2.25:1, 125 MHz) δ 172.1-169.4 (C-4'), 145.9 (C-17), 144.6-142.9 (C-2'), 126.0 (C-1'), 125.2 (C-16), 80.1 (C-3), 72.0 (C-21 or C-22 or C-23 or C-24), 71.6 (C-4), 71.2 (C-21 or C-22 or C-23 or C-24), 70.6 (C-21 or C-22 or C-23 or C-24), 70.4 (C-2), 70.3 (C-21 or C-22 or C-23 or C-24), 69.9 (C-18), 66.8 (C-5), 65.3 (C-19), 59.2 (C-6), 57.3 (C-1), 53.7 (C-7), 51.5 (C-15 and C-25), 46.4 (C-20), 45.1-42.5 (C-3' and C-5'), 31.3 (C-14), 30.5, 30.0, 28.5, 27.4 (C-9 to C-13), 24.6 ppm (C-8); IR (neat) 3350 (broad, O-H), 1677 cm^{-1} (strong, C=O amide); MS (MALDI) *m/z* calcd for $C_{680}H_{1201}N_{160}O_{180}$ $[M + H]^{+}$ 14498.8; found 14503.1.

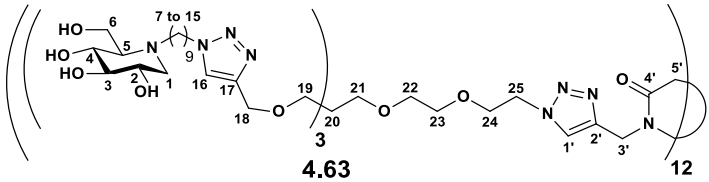

4.63

Compound **4.63** :$[\alpha]_D^{20}$ = -4.8 (*c* 0.47, MeOH/H_2O 75/10); ^{1}H-NMR (CD_3OD, 400 MHz) δ 8.16-7.85 (m, 48H; H-16 and H-1'), 4.57-4.42 (m, 96H; H-18 and H-25), 4.39-4.29 (m, 72H; H-15), 3.92-3.76 (m, 96H; H-6 and H-24), 3.58-3.24 (m, 216H; H-2, H-4, H-19, H-21, H-22 and H-23), 3.19 (t, *J* 9.0 Hz, 36H; H-3), 3.02-2.90 (m, 36H; H-1a), 2.80-2.66 (m, 36H; H-7a), 2.65-2.50 (m, 36H; H-7b), 2.21 (t, *J* 11.2 Hz, 36H; H-1b), 2.15 (d, *J* 10.6 Hz, 36H; H-5), 1.87-1.76 (m, 72H; H-14), 1.49-1.36 (m, 72H; H-8), 1.32-1.15 ppm (m, 360H; H-9, H-10, H-11, H-12 and H-13); ^{13}C-NMR (CD_3OD, 100 MHz) δ 172.1-169.4 (C-4'), 145.9 (C-17), 125.0 (C-16), 80.0 (C-3), 71.9 (C-21 or C-22 or C-23 or C-24), 71.5 (C-4), 71.0 (C-21 or C-22 or C-23 or C-24), 70.3 (C-2), 70.1 (C-21 or C-22 or C-23 or C-24), 69.8 (C-18), 66.7 (C-5), 65.1 (C-19), 59.1 (C-6), 57.2 (C-1), 53.7 (C-7), 51.3 (C-15 and C-25), 46.2 (C-20), 31.1 (C-14), 30.3, 29.8, 28.4, 27.2 (C-9 to C-13), 24.5 (C-8) ppm; IR (neat) 3335 (broad, O-H), 1671 cm^{-1} (strong, C=O amide); MS (ESI) average *m/z* calcd for $C_{816}H_{1449}N_{92}O_{216}$ $[M + 9H]^{9+}$ 1934.1; found 1934.1; MS (MALDI) *m/z* calcd for $C_{816}H_{1441}N_{192}O_{216}$ $[M + H]^+$; 17398.369, found 17398.151.

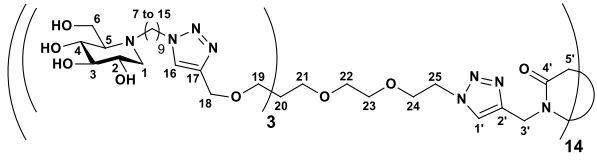

4.64

Compound **4.64:** $[\alpha]_D^{20}$ = -4.3 (*c* 0.345, MeOH/H_2O 75/10); ^{1}H-NMR (CD_3OD, 400 MHz) δ 8.16-7.85 (m, 56H; H-16 and H-1'), 4.52-4.43 (m, 112H; H-18 and H-25), 4.39-4.31 (m, 84H; H-15), 3.92-

3.77 (m, 112H; H-6 and H-24), 3.58-3.04 (m, 294 H; H-2, H-3, H-4, H-19, H-21, H-22 and H-23) 3.02-2.94 (dd, *J* 10.5, 5.0 Hz, 42H; H-1a), 2.82-2.68 (m, 42H; H-7a), 2.62-2.51 (m, 42H; H-7b), 2.21 (t, *J* 10.5 Hz, 42H; H-1b), 2.12 (d, *J* 9.6 Hz, 42H; H-5), 1.88-1.79 (m, 84H; H-14), 1.50-1.39 (m, 84H; H-8), 1.37-1.20 ppm (m, 420H; H-9, H-10, H-11, H-12 and H-13); ^{13}C-NMR (CD_3OD, 100 MHz) δ 172.1-169.4 (C-4'), 146.0 (C-17), 144.6-142.9 (C-2'), 126.5-125.7 (C-1'), 125.0 (C-16), 80.4 (C-3), 72.1 (C-21 or C-22 or C-23 or C-24), 71.9 (C-4), 71.2 (C-21 or C-22 or C-23 or C-24), 70.6 (C-2), 70.5 (C-21, C-22, C-23 or C-24), 69.9 (C-18), 67.1 (C-5), 65.4 (C-19), 59.4 (C-6), 57.6 (C-1), 53.7 (C-7), 51.4 (C-15 and C-25), 46.5 (C-20), 45.1-42.5 (C-3' and C-5'), 31.4 (C-14), 30.6, 30.1, 28.6, 27.5 (C-9 to C-13), 24.3 ppm (C-8); IR (neat) 3351 (broad, O-H), 1671 cm^{-1} (strong, C=O amide); MS (MALDI) *m/z* calcd for $C_{952}H_{1681}N_{224}O_{252}$ $[M + H]^+$ 20297.929; found 20289.064.

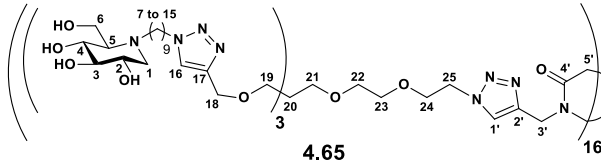

4.65

Compound **4.65:** $[\alpha]_D^{20}$ = -6.2 (*c* 0.487, MeOH/H_2O 75/10); ^{1}H-NMR (CD_3OD, 400 MHz) δ 8.22-7.85 (m, 64H; H-16 and H-1'), 4.56-4.41 (m, 128H; H-18 and H-25), 4.39-4.30 (m, 96H; H-15), 3.92-3.76 (m, 128H; H-6 and H-24), 3.58-3.07 (m, 336H; H-2, H-3, H-4, H-19, H-21, H-22 and H-23), 3.02-2.94 (dd, *J* 10.8, 4.2 Hz, 48H; H-1a), 2.81-2.66 (m, 48H; H-7a), 2.63-2.51 (m, 48H; H-7b), 2.21 (t, *J* 10.8 Hz, 48H; H-1b), 2.12 (d, *J* 9.8 Hz, 48H; H-5), 1.90-1.77 (m, 96H; H-14), 1.52-1.37 (m, 96H; H-8), 1.37-1.20 ppm (m, 480H; H-9, H-10, H-11, H-12 and H-13); ^{13}C-NMR (CD_3OD, 100 MHz) δ 145.9 (C-17), 125.0 (C-16), 80.2 (C-3), 70.3 (C-21 or C-22 or C-23 or C-24), 70.0 (C-18), 66.9 (C-5), 65.4 (C-19), 59.3 (C-6), 57.4 (C-1), 53.7 (C-7),

51.5 (C-15 and C-25), 46.4 (C-20), 31.3 (C-14), 30.5, 30.0, 28.5, 27.4 (C-9 to C-13), 24.7 ppm (C-8); IR (neat) 3351 (broad, O-H), 1671 cm^{-1} (strong, C=O amide); MS (ESI) average *m/z* calcd for $C_{1088}H_{1932}N_{256}O_{288}$ $[M + 12H]^{12+}$ 1934.0; found 1934.0; MS (MALDI) *m/z* calcd for $C_{1088}H_{1921}N_{256}O_{288}$ $[M + H]^{+}$ 23197.49; found 23196.22.

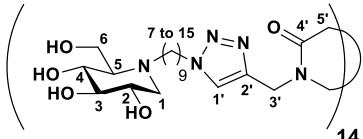

4.67

Compound **4.67**: ^{1}H-NMR ($CDCl_3$, 400 MHz) δ 8.15-7.81 (m, 14H; H-1'), 4.49-4.18 (m, 28H; H-15), 3.90-3.77 (m, 28H; H-6), 3.50 (td, *J* 9.9 and 4.2 Hz, 14H, H-2), 3.36 (t, *J* 9.9 Hz, 14H, H-4), 3.17 (t, *J* 9.9Hz, 14H, H-3), 2.97 (dd, *J* 10.9 and 4.2 Hz, 14H, H-1a), 2.81-2.67 (m, 14H, H-7a), 2.63-2.50 (m, 14H, H-7b), 2.19 (t, *J* 9.9 Hz, 14H, H-1b), 2.13 (d, *J* 9.9, 14H, H-5), 1.99-1.72 (m, 28H, H-14), 1.52-1.39 (m, 28H, H-8), 1.36-1.15 (m, 140H, from H-9 to H-13) ppm; ^{13}C-NMR ($CDCl_3$, 100 MHz) δ 125.4 (C-1'), 80.3 (C-3), 71.8 (C-4), 70.5 (C-2), 67.0 (C-5), 59.4 (C-6), 57.4 (C-1), 53.7 (C-7), 51.5 (C-15), 44.6-42.4 (C-3' or C-5'), 31.2 (C-14), 30.5, 30.0, 28.5, 27.4 (from C-9 to C-13), 24.8 (C-8) ppm; IR (neat) : 3348 (broad, O-H), 1655 cm^{-1} (strong, C=O amide); HRMS (ESI) m/z calcd for $C_{280}H_{497}N_{70}O_{70}$ $[M + 7H]^{7+}$ 851.535; found 851.971 and $C_{280}H_{496}N_{70}O_{70}$ $[M + 6H]^{6+}$ 993.290; found 993.965.

7.5 COMPOUNDS FROM CHAPTER 5

7.5.1. Synthesis and Characterization of Peptoidic Scaffolds

General procedure for sub-monomer solid-phase synthesis of the linear peptoids 5.15–5.19

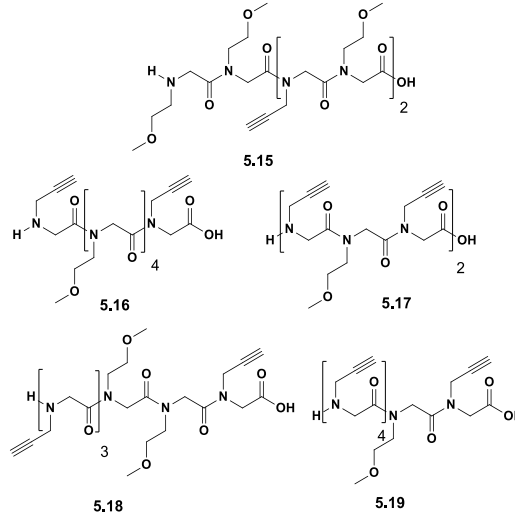

Linear peptoid oligomers **5.15-5.19** were synthesized using a submonomer solid-phase approach. In a typical synthesis 2-chlorotrityl chloride resin (α-dichlorobenzhydryl-polystyrene cross-linked with 1% DVB; 100 – 200 mesh; 0.89 mmol g^{-1}, 0.400 g, 0.356 mmol was swelled in dry CH_2Cl_2 (3 mL) for 45 min and washed twice with dry DMF (3 mL). The first submonomer was attached onto the resin by adding bromoacetic acid (79.7 mg, 0.57 mmol) in dry CH_2Cl_2 (3.0 mL) and DIPEA (310 µL, 1.78 mmol) on a shaker platform for 60 min at room temperature, followed by washing with dry CH_2Cl_2 (3 × 1 min) and then with DMF (3 × 1 min). A DMF solution of the commercially available propargyl amine (228 µl, 3.56 mmol), or methoxyethyl amine (307 µl, 3.56 mmol) was added to the bromoacetylated resin. The mixture was left on a shaker platform for 30 min at room temperature, then the resin was washed with DMF (3 × 1 min), CH_2Cl_2 (3 × 1 min) and then again with DMF (3 × 1 min). Subsequent bromoacetylation reactions were accomplished by reacting the aminated oligomer with a solution of bromoacetic acid (494 mg, 3.56 mmol) and DIC (607 µL, 3.91 mmol) in dry DMF (3.0

mL) for 40 min at room temperature. The filtrated resin was washed with DMF (3 × 1min), CH_2Cl_2 (3 × 1 min), DMF (3 × 1 min) and treated again with the amine under the same conditions reported above. This cycle of reactions was iterated until the desired chain length was accomplished and the target oligomer obtained. The cleavage was performed by treating twice the resin, previously washed with CH_2Cl_2 (3 × 1 min), with a solution of HFIP in CH_2Cl_2 (20% v/v, 6 mL) on a shaker platform at room temperature for 30 min and 5 min, respectively. The resin was then filtered away and the combined filtrates were concentrated *in vacuo*. The final products were dissolved in 50% acetonitrile in HPLC grade water and analyzed by RP-HPLC [purity 82% for oligomer **5.15**, 85% for oligomer **5.16**, >95% for oligomer **5.17**, 76% for oligomer **5.18**, >95% for oligomer **5.19**; conditions: 5 → 100% A in 30 min for the all oligomers (A, 0.1% TFA in acetonitrile, B, 0.1% TFA in water); flow: 1 mL min^{-1}, 220 nm]. The linear oligomers were subjected to the cyclization reaction without further purification.

5.15: 78% (crude residue); ESI-MS (positive, *m/z*): 669.4 $[M + H]^+$; t_R : 8.4 min;

5.16: 59%. (crude residue); ESI-MS (positive, *m/z*): 669.4 $[M + H]^+$; 691.9 $[M + Na]^+$; t_R : 8.5 min;

5.17: 98% (crude residue); ESI-MS (positive, *m/z*): 629.2 $[M + H]^+$; t_R: 7.4 min;

5.18: 90% (crude residue); ESI-MS (positive, *m/z*): 591.3 $[M + H]^+$; 613.5 $[M + Na]^+$; 629.4 $[M + K]^+$ t_R : 7.6 min;

5.19: 95% (crude residue); ESI-MS (positive, *m/z*): 629.2 $[M + H]^+$; t_R : 7.6 min;

General procedure for the cyclization reactions: synthesis of compounds 5.5-5.9

A solution of the linear peptoids precursors of **5.15** – **5.19** (0.348 mmol), previously co-evaporated three times with toluene, was prepared under nitrogen in dry DMF (20.0 mL). The mixture was added drop wise to a stirred solution of HATU (528 mg, 1.39 mmol) and DIPEA (376 µL, 2.16 mmol) in dry DMF (82.0 mL) by a syringe pump in 12 h, at room temperature in anhydrous atmosphere. After 24 h the the resulting mixture was concentrated *in vacuo*, diluted with CH_2Cl_2 (100 mL), and washed with a solution of HCl (1.0 M, 50 mL). The mixture was extracted with CH_2Cl_2 (2 × 100 mL) and the combined organic phases were washed with water (150 mL), dried over anhydrous $MgSO_4$, filtered and concentrated *in vacuo*. The cyclic products were dissolved in 50% acetonitrile in HPLC grade water and analyzed by RP-HPLC [purity >95% for oligomer **5.5-5.9**, conditions: 5% – 100% A in 30 min for all cyclic compounds (A, 0.1% TFA in acetonitrile, B, 0.1% TFA in water); flow: 1 mL min^{-1}, 220 nm]. The crude residues **5.5**-**5.9** were purified by precipitation in hot acetonitrile.

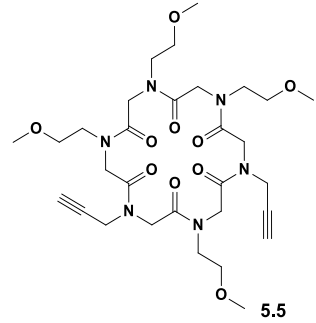

5.5

Compound **5.5**: 56%; white amorphous solid; ESI-MS (positive, *m/z*): 651.9 (100, $[M + H]^+$), 673.9 (100, $[M + Na]^+$); t_R: 10.1 min;

^{1}H NMR: (600 MHz,CD_3CN + 2% D_2O, mixture of rotamers) δ: 4.54-3.86 (12H, m, $COC\underline{H}_2N$); 3.57-3.22 (34H, m, $NC\underline{H}_2CH_2OCH_3$, $NCH_2C\underline{H}_2OCH_3$, $NCH_2CH_2OC\underline{H}_3$, $NC\underline{H}_2CCH$); 2.75-2.40 (2H, m,

$NCH_2CC\underline{H}$ overlapped with water signal); ^{13}C NMR: (150 MHz, $CDCl_3$, mixture of rotamers, broad signals) δ: 171.8, 171.6, 171.2, 171.0, 170.8, 170.6, 170.3, 170.0, 80.0, 79.9, 79.7, 79.5, 75.1, 74.7, 73.9, 73.6, 73.2, 71.4, 71.3, 71.2, 70.9, 70.8, 70.7, 70.6, 70.3, 70.1, 69.1, 59.5, 59.4, 59.3, 59.2, 58.9, 58.8, 58.5, 58.2, 51.0, 50.8, 50.7, 50.3, 50.1, 49.9, 49.5, 49.4, 49.2, 49.0, 48.9, 48.8, 48.5, 48.2, 48.1, 47.7, 47.2, 46.9, 38.8, 37.6, 37.5, 37.4, 37.1, 37.0, 36.9.

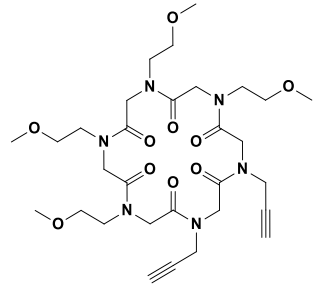

5.6

Compound **5.6**: 56%; white amorphous solid; ESI-MS (positive, *m/z*): 651.9 (77, $[M + H]^+$), 673.9 (100, $[M + Na]^+$); t_R: 10.1 min;

^1H NMR: (600 MHz,CD_3CN + 2% D_2O, mixture of rotamers) δ: 4.56-3.79 (12H, m, $COC\underline{H}_2N$); 3.56-3.23 (34H, m, $NC\underline{H}_2CH_2OCH_3$, $NCH_2C\underline{H}_2OCH_3$, $NCH_2CH_2OC\underline{H}_3$, $NC\underline{H}_2CCH$); 2.75-2.40 (2H, m, $NCH_2CC\underline{H}$ overlapped with water signal); ^{13}C NMR: (150 MHz, $CDCl_3$, mixture of rotamers, broad signals) δ: 170.9, 170.4, 79.8, 73.8, 73.5, 73.0, 71.4, 71.2, 70.9, 70.7, 70.6, 59.5, 59.4, 59.2, 58.9, 50.7, 49.8, 49.4, 49.3, 49.1, 48.5, 48.4, 48.3, 48.0, 37.5, 37.4.

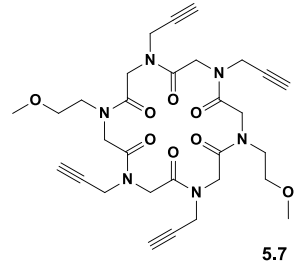

5.7

Compound **5.7**: 37%; white amorphous solid; ESI-MS (positive, *m/z*): 611.1 (100, $[M + H]^+$), 633.4 (94, [M + Na]+) and 649.1 (30, [M + K]+), t_R: 8.5 min;

^{1}H NMR: (600 MHz,DMSO, mixture of rotamers) δ: 4.80-3.77 (12H, m, COC*H*$_2$N), 3.76-3.36 (8H,m, NC*H*$_2$CCH), 3.35-3.27 (4H,m, NC*H*$_2$CH$_2$OCH$_3$), 3.26-3.02 (14H, m, NCH$_2$C*H*$_2$OCH$_3$, NCH$_2$CH$_2$OC*H*$_3$, and NCH$_2$CC*H*); ^{13}C NMR: (150 MHz, DMSO, mixture of rotamers, broad signals) δ: 171.5, 171.0, 170.9, 170.5, 169.6, 169.5, 169.1, 81.1, 80.9, 80.7, 80.6, 80.4, 80.0, 77.2, 77.1, 77.0, 76.7, 76.3, 76.2, 76.1, 76.0, 75.8, 71.9, 71.7, 71.6, 71.3, 71.2, 70.9, 70.8, 70.5, 60.1, 60.0, 59.9, 59.8, 59.7, 59.5, 59.3, 50.7, 50.4, 50.1, 49.9, 49.6, 49.4, 49.0, 48.9, 48.8, 48.6, 48.1, 47.8, 38.0, 37.6, 37.0, 37.2, 36.0, 35.6.

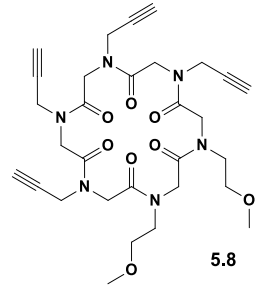

5.8

Compound **5.8**: 57%; white amorphous solid; ESI-MS (positive, *m/z*): 611.1 (100, $[M + H]^+$), 633.4 (40, [M + Na]+); t_R: 8.6 min;

^{1}H NMR: (400 MHz, CD_3CN, mixture of rotamers) δ: 4.53-3.86 (16H, m, $COCH_2N$ and $NCH_2CH_2OCH_3$), 3.58-3.24 (18H, m, $NCH_2CH_2OCH_3$, $NCH_2CH_2OCH_3$ and NCH_2CCH), 2.40-2.70 (4H,m, NCH_2CCH); ^{13}C NMR: (100 MHz, CD_3CN, mixture of rotamers, broad signals) δ: 170.3, 169.8, 79.2, 74.6, 73.9, 73.5, 73.3, 70.9, 70.2, 59.1, 58.9, 58.5, 58.2, 50.3, 49.5, 49.1, 48.9, 48.1, 48.0, 37.3, 37.1, 37.0, 36.6.

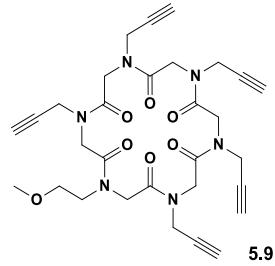

5.9

Compound **5.9**: 86%; white amorphous solid; ESI-MS (positive, *m/z*): 591.3 (100, $[M + H]^+$), 613.3 (70, [M + Na]+); t_R: 8.3 min;

^{1}H NMR: (400 MHz, CD_3CN + 2% D_2O, mixture of rotamers) δ: 4.54-3.86 (14H, m, $COCH_2N$ and $NCH_2CH_2OCH_3$), 3.65-3.20 (15H, m, $NCH_2CH_2OCH_3$, $NCH_2CH_2OCH_3$, $NCH_2CH_2OCH_3$ and NCH_2CCH), 2.70-2.50 (5H,m, NCH_2CCH overlapped with water signal); ^{13}C NMR: (100 MHz, CD_3CN + 2% D_2O, mixture of rotamers, broad signals) δ: 171.1, 170.9, 170.3, 169.9, 169.8, 169.6, 169.4, 169.2, 169.1, 79.4, 79.1, 78.6, 78.2, 78.0, 77.5, 74.7, 74.3, 74.0, 73.7, 73.6, 73.5, 73.4, 73.1, 72.8, 71.0, 70.2, 59.2, 59.0, 58.7, 49.7, 49.3, 49.0, 48.9, 48.8, 48.7, 48.5, 48.3, 48.1, 47.8, 47.5, 37.3, 37.2, 37.0, 36.7, 36.5.

7.5.2. Single Crystal X-Ray Diffraction

Compound 4.16

Compound **4.16** was dissolved in hot acetonitrile and crystallized by slowly cooling the acetonitrile solution.

Diffraction data were collected at 100 K with a Rigaku AFC7S diffractometer equipped with an CCD Mercury detector using Mo *K*α radiation. Crystals were mounted using Mitegen loops. Data reduction was performed with the crystallographic package CrystalClear. The structure was solved by direct methods using the program SIR2011 and refined by means of full matrix least-squares based on F^2 using the program SHELXL97. All non-hydrogen atoms were refined anisotropically, hydrogen atoms were positioned geometrically and included in structure factors calculations but not refined.

	4.16
Formula	$C_{30}H_{46}N_6O_{10}\cdot 4\ CH_3CN$
Formula weight	650.33
System	triclinic
Space group	*P* -1
a (Å)	8.575(6)
b (Å)	9.743(6)
c (Å)	14.182(7)
β (°)	74.68(8)
V (Å^3)	1102.14

Compound 4.19

Compound **4.19** was dissolved in hot acetonitrile and crystallized by slowly cooling the acetonitrile solution, yielding prismatic crystals.

Diffraction data were collected at 100 K with a ID13 diffractometer at ESRF (Grenoble, France). Crystals were mounted using Mitegen loops. Data reduction was performed with the crystallographic

package SADABS. The structure was solved by direct methods using the program SIR2011 and refined by means of full matrix least-squares based on F^2 using the program SHELXL97. All non-hydrogen atoms were refined anisotropically, hydrogen atoms were positioned geometrically and included in structure factors calculations but not refined.

	4.19
Formula	$C_{30}H_{30}N_6O_6 \cdot 2\ CH_3CN$
Formula weight	570.22
System	monoclinic
Space group	$P\ 2_1/c$
a (Å)	11.717(6)
b (Å)	17.333(9)
c (Å)	8.824(5)
β (°)	106.290(6)
V (Å^3)	1720.13
Z	2

Compound 5.7

Compound **5.7** was dissolved in hot acetonitrile and crystallized by slowly cooling the acetonitrile solution, yielding white blocky and flat-plate crystals.

Diffraction data were collected at 100 K with a Bruker Smart diffractometer equipped with an APEXII CCD detector using Mo *K*α radiation. Crystals were mounted using Mitegen loops.

Data reduction was performed with the crystallographic package APEX. The structure was solved by direct methods using the program SHELXS and refined by means of full matrix least-squares

based on F^2 using the program SHELXL97. The software X-Seed was used as GUI. All non-hydrogen atoms were refined anisotropically, hydrogen atoms were positioned geometrically and included in structure factors calculations but not refined.

	5.7
Formula	$C_{30}H_{38}N_6O_8 \cdot 2\ CH_3CN$
Formula weight	692.77
System	monoclinic
Space group	$P\ 2_1/c$
a (Å)	9.773(5)
b (Å)	20.961(10)
c (Å)	8.500(4)
β (°)	90.990(7)
V (Å^3)	1740.9(14)
Z	2
D_X (gcm^{-3})	1.322
μ (mm^{-1})	0.096
F_{000}	736.0
R ($I>2\sigma_I$)	0.0465 (2958)
$_wR_2$ (all)	0.1173 (3594)
N. of param.	226
GooF	1.057
ρ_{min}, ρ_{max} (eÅ^{-3})	-0.26, 0.27

BIBLIOGRAPHY

1. (a) E., J., Ariëns, *TIPS* **1979,** *1*, 11-15; (b) Farmer, P. S., Ariëns, E. J. , *TIPS* **1982**, 362-365.

2. Simon, R. J., Kania, R. S., Zuckermann, R. N., Huebner, V. D., Jewell, D. A., Banville, S., Ng, S., Wang, L., Rosenberg, S., Marlowe, C. K., Spellmeyer, D. C., Tan, R., Frankel, A. D., Santi, D. V., Cohen, F. E., Bartlett, P. A., *Proc. Natl. Acad. Sci.* **1992,** *82*, 9367-9371.

3. Zuckermann, R. N., Kerr, J. M., Kent, S. B. H., Moost, W. H., *J. Am. Chem. Soc* **1992,** *114*, 10646-10647

4. Armand, P., Kirshenbaum, K., Falicov, A., Dunbrack Jr, R. L., Dill, K. A., Zuckermann, R. N., Cohen, F. E., Chiral N-substituted glycines can form stable helical conformations. *Folding and Design* **1997,** *2* (6), 369-375.

5. (a) Kirshenbaum, K., Barron, A. E., Goldsmith,R. A., Armand, P., Bradley, E. K., Truong, K. T. V., Dill, K. A., Cohen, F. E., Zuckermann, R. N., *PNAS* **1998,** *95* (8), 4303-4308; (b) Wu, C. W., Sanborn, T. J., Zuckermann, R. N., Barron, A. E., *Journal of the American Chemical Society* **2001,** *123* (13), 2958-63; (c) Wu, C. W., Sanborn, T. J., Huang, K., Zuckermann, R. N., Barron, A. E., *Journal of the American Chemical Society* **2001,** *123* (28), 6778-6784; (d) Wu, C. W., Kirshenbaum, K., Sanborn, Tracy J., Patch, James A., Huang, Kai., Dill, Ken A., Zuckermann, Ronald N., Barron, A. E, *Journal of the American Chemical Society* **2003,** *125* (44), 13525-13530.

6. (a) Gorske, B. C., Bastian, B. L., Geske, G. D., Blackwell, H. E., *Journal of the American Chemical Society* **2007,** *129* (29), 8928-8929; (b) Shah, N. H., Butterfoss, G. L., Nguyen, K., Yoo, B., Bonneau, R., Rabenstein, D. L., Kirshenbaum, K., *Journal of the American Chemical Society* **2008,** *130* (49), 16622-16632; (c) Roy, O., Caumes, C., Esvan, Y., Didierjean, C., Faure, S.,Taillefumier, C., *Organic letters* **2013,** *15* (9), 2246-2249; (d) Renfrew, P. D., Craven, T. W., Butterfoss, G. L., Kirshenbaum, K., Bonneau, R., *Journal of the American Chemical Society* **2014,** *136* (24), 8772-8782.

7. Crapster, J. A., Stringer, J. R., Guzei, I. A., Blackwell, H. E., *Biopolymers* **2011,** *96* (5), 604-616.

8. Jordan, P. A., Paul, B., Butterfoss, G. L., Renfrew, P. D., Bonneau, R., Kirshenbaum, K., *Peptide Science* **2011,** *96* (5), 617-626.

9. Huang, K., Wu, C., W., Sanborn, T., J., Patch, J., A., Kirshenbaum, K., Zuckermann, R. N., Barron, A. E., Radhakrishnan, I., *Journal of the American Chemical Society* **2006,** *128* (5), 1733-1738.

10. Shin, S. B. Y., Yoo, B.,Todaro, L. J., Kirshenbaum, K., *J. Am. Chem. Soc.* **2007,** *129*, 3218-3225.

11. Horton, D. A., Bourne, G. T., Smythe, M. L., *Mol Divers* **2000,** *5* (4), 289-304.

12. (a) Fairlie, D. P., Abbenante, G., March, D. R. , *Curr. Med. Chem* **1995,** *2*, 654; (b) Reyes, S. J., Burgess, K. , *Tetrahedron: Asymmetry* **2005,** *16*, 1061; (c) Columbo, G., Curnis, F., De Mori, G. M. S, Gasparri, A., Longoni, C., Sacci, A., Longhi, R., Corti, A., *J. Biol. Chem.* **2002,** *277*, 47891; (d) Jackson, D. Y., King, D. S., Chmielewski, J., Singh, S., Schultz, P. G. , *J. Am. Chem. Soc.* **1991,** *113*, 9391; (e) Blackwell, H. E., Grubbs, R. H., *Angew. Chem., Int. Ed.* **1998,** *37*, 3281; (f) Schafmeister, C. E., Po, J., Verdine, G. L. , *J. Am. Chem. Soc.* **2000,** *122*, 5891; (g) Chapman, R. N., Dimartino, G., Arora, P. S. , *J. Am. Chem. Soc.* **2004,** *126*, 12252.

13. (a) Blankenstein, J., Zhu, J. , *Eur. J. Org. Chem.* **2005,** *2005*, 1949; (b) Yuan, L., Feng, W., Yamato, K., Sanford, A. R., Xu, D., Guo, H., Gong, B., *J. Am. Chem. Soc.* **2004,** *126*, 11120.

14. Tedesco, C., Erra, L., Izzo, I., De Riccardis, F., *CrystEngComm* **2014,** *16*, 3667-3687.

15. Butterfoss, G. L., Yoo, B., Jaworski, J., N., Chorny, Y., Dill, K. A., Zuckermann, R. N., Bonneau, N., Kirshenbaum, K., Voelz, V. A., *PNAS* **2012,** *109* (36).

16. Culf, A. S., Čuperlović-Culf, M., Léger, D. A., Decken, A., *Org. Lett.* **2014,** *16*, 2780 − 2783.

17. Maulucci, N., Izzo, I., Bifulco, G., Aliberti, A., De Cola, C., Comegna, D., Gaeta, C., Napolitano, A., Pizza, C., Tedesco, C., Flot, D., De Riccardis, F. , *Chem. Comm.* **2008**, 3927–3929.

18. (a) Maayan, G., *European Journal of Organic Chemistry* **2009,** *2009* (33), 5699-5710; (b) Lee, B.-C., Chu, T. K., Dill, K. A., Zuckermann, R. N. , .*J. Am. Chem. Soc.* **2008,** *130*, 8847-8855

19. (a) De Cola, C., Licen, S., Comegna, D., Cafaro, E., Bifulco, G., Izzo, I., Tecilla, P., De Riccardis, F. , *Org. Biomol. Chem.* **2009,** *7*, 2851–2854; (b) Della Sala, G., Nardone, B., De Riccardis, F., Izzo, I., *Organic & Biomolecular Chemistry* **2013,** *11* (5), 726-731; (c) De Cola, C., Fiorillo, G., Meli, A., Aime, S., Gianolio, E., Izzo, I., De Riccardis, F. , *Org. Biomol. Chem.* **2014,** *12*, 424–431; (d) Izzo, I., Ianniello, G., De Cola, C., Nardone, B., Erra, L., Vaughan, G., Tedesco, C., De Riccardis, F. , *Org. Lett.* **2013,** *15*, 598–601.

20. Schettini, R., Nardone, B., De Riccardis, F., Della Sala, G.; Izzo, I. , *Eur. J. Org. Chem.* **2014**, 7793–7797.

21. (a) Fowler, S. A., Blackwell, H. E., *Org. Biomol. Chem.* **2009,** *7*, 1508–1524; (b) Chongsiriwatana, N. P., Patch, J. A.,Czyzewski, A. M., Dohm, M. T., Ivankin, A., Gidalevitz, D., Zuckermann, R. N., Barron, A. E., *Proc Natl Acad Sci U S A* **2008,** *105* (8), 2794-9.

22. (a) Maayan, G., Ward, M. D., Kirshenbaum, K., *Proceedings of the National Academy of Sciences of the United States of America* **2009,** *106* (33), 13679-13684; (b) Prathap, K. j. J., Maayan, G., *Chemical Communications* **2015,** *51* (55), 11096-11099.

23. (a) Comegna, D., Benincasa, M., Gennaro, R., Izzo, I., De Riccardis, F., *Bioorganic & Medicinal Chemistry* **2010,** *18* (5), 2010-2018; (b) Huang, M., Shin, S. B. Y., Benson, M. A.,Torres, V. J., Kirshenbaum, K., *ChemMedChem* **2012,** *7*, 114-122.

24. Huang, M. L., Benson, M. A., Shin, S. B. Y., Torres, V. J., Kirshenbaum, K., *European Journal of Organic Chemistry* **2013,** *2013* (17), 3560-3566.

25. Smith, P. T., Huang, M. L., Kirshenbaum, K., *Biopolymers* **2014,** *103* (4), 227-236.

26. Zuckermann, R. N., Martin, E. J., Spellmeyer, D. C.,Stauber, G. B., Shoemaker, K. R., Kerr, J. M., Figliozzi, G. M., Goff, D. A., Siani, M. A., Simon, R., Banville, S. C., Brown, E. G., Wang, L., Richter, L. S., Moos, W. H., *J. Med. Chem.* **1994,** *37*, 2678–2685.

27. Park, S., Kwon, Y., *ACS Combinatorial Science* **2015,** *17* (3), 196-201.

28. *Gao, Y. K., T.*, *ACS Comb. Sci.* **2015,** *17*, 190.

29. Seo, J., Lee, B. C., Zuckermann, R. N., Peptoids-Synthesis,; Characterization, a. N. I. C. B.; Ducheyne, P., Healy, K. E., Hutmacher, D. W., Grainger, D. W.,; Kirkpatrick, C. J., Eds.; Elsevier: 2011; Vol. 2, pp 53 − 76., *Comprehensive Biomaterials*.

30. Hille, *Ion Channels of Excitable Membranes*. third ed. Sinauer Associates, I., Ed. Sunderland, MA, **2001**.

31. Gouaux, E., MacKinnon, R., *Science* **2005,** *310*, 1461-1465.

32. Gokel, G., W., Carasel, I., A. , *Chem. Soc. Rev.* **2007,** *36*, 378-389.

33. Matile, S., Jentzsch, A., V., Montenegro, J., Fin, A., ***Chem. Soc. Rev.*** **2011,** *40*, 2453–2474.

34. (a) Rao, S., Si, K., J., Yap, L., W., Xiang, Y, Cheng, W., *ACS Nano* **2015**, Ahead of Print; (b) Ko, S., K., Kim, S., K., Share, A., Lynch, V., M., Park, J., Namkung, W., Rossom, W., V., Busschaert, N., Gale, P., A., Sessler, J., L., Shin, S., I., *Nature Chemistry* **2014,** *6*, 885-892; (c) Gadsby, D., C., *Nature* **2004,** *427*, 795-797.

35. Dutzler., R., *Current Opinion in Structural Biology* **2006,** *16*, 439-446.

36. Kelkar, D., A., Chattopadhyay, A., *Biochimica et Biophysica Acta* **2007,** *1768*, 2011-2025.

37. MacKinnon, R., *Angew. Chem.* **2004,** *43*, 4265-4277.

38. Cragg, P., *Science Progress* **2002,** *85*, 219-241.

39. Gokel, G., W., et al., *Bioorg. Med. Chem.* **2004,** *12*, 1291–1304.

40. De Riccardis, F., Izzo, I., Montesarchio, D., Tecilla, P., *Accounts of Chemical Research* **2013,** *46* (12), 2781–2790.

41. Lalgee, L., J., Grierson, L., Fairman, R., A., Jaggernauth, G., E., Schulte, A., Benz, R., Winterhalter, M., *Biochimica et Biophysica Acta* **2014,** *1838*, 1247–1254.

42. Fyles, T., M., *Chem. Soc. Rev.* **2007,** *36*, 335–347.

43. Murakami, Y., Kikuchi, J., Hisaeda, Y., Hayashida, O., *Chem. Rev.* **1996,** *96*, 721-758.

44. Takeuchiw, T., Matile, S., *Chem. Commun.* **2013,** *49*, 19-29.

45. (a) Fernandez-Lopez, S., Hui-Sun, K., Choi, E. C., Delgado, M., Granja, J. R., Khasanov A., Kraehenbuehl, K., Long, G., Weinberger, D. A., Wilcoxen, K. M., Ghadiri, M. R., *Nature* **2001,** *412*, 452–455; (b) Montenegro, J., Ghadiri, M. R., Granja, J., R., *Accounts of Chemical Research* **2013,** *46* (12), 2955-2965; (c) Yu, Z., Li, J., Zhu, J., Zhu, M., Jiang, F., Zhang, J., Li, Z., Zhong, M., Kaye, J., B., Du, J., Shen, B., J. , *Mater. Chem. B* **2014,** *2*, 3809–3818; (d) El Ghoul, Y., Renia, R., Faye, I., Rassou, S., Badi, N., Bennevault-Celton, V., Huin, C., Guégan, P., *Chem. Commun.* **2013,** *49*, 11647-11649.

46. Riley, K. E., Merz, K., M., *The Journal of Physical Chemistry A* **2007,** *111* (9), 1688-1694.

47. Sakai, N., Mareda, J., Matile, S., , *Mol. BioSyst.* **2007,** *3*, 658–666.

48. Maayan, G. W., M., D.; Kirshenbaum, K.; , *Chem. Commun.* **2009**, 56–58.

49. (a) Rasmussen, J. E., Boccia, M. M., Nielsen, J., Taillefumier, C., Faure, S., Hjelmgaard, T. , *Tetrahedron Lett.* **2014,** *55*, 5940–5943; (b) Hjelmgaard, T., Roy, O., Nauton, L., El-Ghozzi, M., Avignant, D., Didierjean, C., Taillefumier C., Faure, S., *Chem. Commun.* **2014,** *22*, 3564–3567; (c) Hjelmgaard, T., Nielsen, J., *Eur. J. Org. Chem.* **2013**, 3574–3589; (d) Hjelmgaard, T., Faure, S., De Santis, E., Staerk, D., Alexander, B. D., Edwards, A. A., Taillefumier, C., Nielsen, J., *Tetrahedron Lett.* **2012,** *68*, 4444–4454; (e) Hjelmgaard, T., Faure, S., Staerk, D., Taillefumier C., Nielsen, J., *Org. Biomol. Chem.* **2011,** *9*, 6832–6843; (f) Hjelmgaard, T., Plesner, M., Dissing, M. M., Andersen, J. M., Frydenvang, K., Nielsen, J., *Eur. J. Org. Chem.* **2014**, 3971–3975.

50. (a) Hjelmgaard, T., Faure, S., Staerk, D., Taillefumier C., Nielsen, J. , *Eur. J. Org. Chem.* **2011**, 4121–4132; (b) Combs, D. J., Lokey, R. S., *Tetrahedron Lett.* **2007,** *48*, 2679–2682.

51. Axén, A., Andersson, H., Lindeberg, G., Rönnholm, H., Kortesmaa, J., Demaegdt, H., Vauquelin, G., Karlén, A., Hallberg, M., *J. Pept. Sci.* **2007,** *13*, 434-444.

52. (a) Gea, A., Farcy, N., Roqué i Rossell, N., Martins, J. C., De Clercq, P. J., Madder, A., *Eur. J. Org. Chem.* **2006**, 4135–4146; (b) Nevill, C. R., Jakubowski, Jr. J. A., Fuchs, P. L., *Biomed. Chem. Lett.* **1991,** *1*, 83–86.

53. Westaway, S., M.; Brown, S., L.; Fell, S., C., M.; Johnson, C., N.; MacPherson, D., T.; Mitchell, D., J.; Myatt, J., W.; Stanway, S., J.; Seal, J., T.; Stemp, G.; Thompson, M.; Lawless, K.; McKay, F.; Muir, A., I.; Barford, J., M.; Mahmood, S., R.; Matthews, K., L.; Mohamed, S.; Smith, B., B.; Stevens, A., J.; Bolton, V., J.; Jarvie, E., M.; Sanger, G., *J. Med. Chem.* **2009,** *52*, 1180–1189.

54. Sakai, N., Matile, S., *J. Phys. Org. Chem.* **2006,** *19*, 452–460.

55. Izzo, I., Licen, S., Maulucci, N., Autore, G., Marzocco, S., Tecilla, P., De Riccardis, F., *Chem. Commun.* **2008**, 2986–2988.

56. Runge, V., M., *Clinical MRI*. 1st Ed. ed.; Saunders: **2002**.

57. Freedman, J., D.; Lusic, H.; Wiewiorski, M.; Farley, M.; Snyder, B., D.; Grinstaff, M., W.; , *Chem. Commun.* **2015,** *51*, 11166-11169.

58. (a) Amouroux, G., Pan, J., Jenni, S., Zhang, C., Zhang, Z., Hundal-Jabal, N., Colpo, N., Liu, Z., Bénard, F., Lin, K., *Mol. Pharmaceutics* **2015,** *12*, 2879-2888; (b) Baker, J., H., E., McPhee, K., C., Moosvi, F., Saatchi, K., Häfeli, U., O., Minchinton, A. I., Reinsberg, S., A., *Contrast Media Mol. Imaging* **2015**; (c) Ye, D., Shuhendler, A., J., Pandit, P., Brewer, K., D.,Tee, S., S., Cui, L.,Tikhomirov, G., Rutt, B., Rao, J., *Chem. Sci.* **2014, *5***, 3845-3852; (d) Gianolio, E., Cabella, C., Colombo Serra , S., Valbusa, G., Arena, F., Maiocchi, A., Miragoli, L., Tedoldi, F., Uggeri, F., Visigalli, M., Bardini, P., Aime, S., *J. Biol. Inorg. Chem.* **2014,** *19*, 715-726; (e) Zhou, Z., Qutaish, M., Han, Z., Schur, R., M., Liu, Y., Wilson, D., L., Lu, Z., *Nat Commun* **2015,** *6*.

59. Bort, G. C., S.; Borderies, H.; Kebsi, A.; Ballet, S.; Louin, G.; Port, M.; Ferroud, C., *European Journal of Medicinal Chemistry* **2014,** *87*, 843-861.

60. (a) Leung, A., H., Jin, J., Wang, S., Lei, H., Wong, W., T., *Bioconjugate Chem.* **2014,** *25*, 1112-1123; (b) Caravan, P., Ellison, J., McMurry, T., J., Lauffer, R., B.,, *Chem. Rev.* **1999,** *99*, 2293-2352; (c) Lauffer, R., B., *Chem. Rev.* **1987,** *87*, 901-927

61. Henderson, R., G. , *Journal of the Royal Society of Medicine* **1983,** *76*, 206-212.

62. Pykett, I. L., *Sci. Am.* **1982,** *246* (78).

63. Werner, E., J., Datta, A., Jocher, C., J., Raymond, K., N., *Angewandte Chemie International Edition* **2008,** *47* (45), 8568-8580.

64. Aime, S., Geninatti Crich, S., Gianolio, E, Giovenzana, G., B.,Tei, L., Terreno, E., *Coordination Chemistry Reviews* **2006,** *250*, 1562-1579.

65. Aime, S., Botta, M., Fasano, M., Terreno, E., *Chemical Society Reviews* **1998,** ***27***, 19-29.

66. Verwilst, P., Park, S., Yoon, B., Kim, J., S., *Chem. Soc. Rev.* **2015,** *44*, 1791-1806.

67. (a) Baker, J. H. E., McPhee, K. C., Moosvi, F., Saatchi, K., Häfeli, U. O., Minchinton, A. I., Reinsberg, S. A., *Contrast Media & Molecular Imaging* **2015**; (b) Luo, K., Liu, G., She, W., Wang, Q., Wang, G., He, B., Ai, H., Gong, Q., Song, B., Gu, Z., *Biomaterials* **2011,** *32* (31), 7951-7960.

68. Loukopoulos, E., Griffiths, K., Akien, G., Kourkoumelis, N., Abdul-Sada, A., Kostakis, G., *Inorganics* **2015,** *3* (4), 448-466.

69. Vaccaro, M., Mangiapia, G., Paduano, L., Gianolio, E., Accardo, A., Tesauro, D., Morelli, G., *ChemPhysChem* **2007,** *8* (17), 2526-2538.

70. (a) Bonnet, C., S., Fries, P.,l H., Crouzy, S., Sénèque, O., Cisnetti, F., Boturyn, D., Dumy, P., Delangle, P., *Chemistry – A European Journal* **2009,** *15* (29), 7083-7093; (b) Caravan, P.,

Greenwood, J., M., Welch, J., T., Franklin, S., J., *Chemical Communications* **2003,** (20), 2574-2575.

71. (a) Kölmel, D. K., Rudat, B., Schepers, U. Bräse, S., *European Journal of Organic Chemistry* **2013,** *2013* (14), 2761-2765; (b) De León-Rodríguez, L. M., Lubag, A., Udugamasooriya, D. G., Proneth, B., Brekken, R. A., Sun, X., Kodadek, T., Sherry, D. A., *Journal of the American Chemical Society* **2010,** *132* (37), 12829-12831.

72. Fulton, D., A., Elemento, E., M., Aime, S., Chaabane, L., Botta, M., Parker, D., *Chemical Communications* **2006,** (10), 1064-1066.

73. Caravan, P., *Accounts of Chemical Research* **2009,** *42* (7), 851-862.

74. Miller, S. M., Simon, R.J., Ng, S., Zuckermann, R.N., Kerr, J.M. & Moos, W.H. , *Bioorg. Med. Chem. Lett.* **1994,** *4*, 2657-2662.

75. Gellerman, G., Elgavi, A., Salitra, Y., Kramer, M. , *J. Peptide Res.* **2001,** *57*, 277 – 291.

76. (a) Kajimoto, T., Node, M., *Current Topics in Medicinal Chemistry* **2009,** *9*, 13-33; (b) Davies, G. J., Gloster, T. M., Henrissat, B., *Current Opinion in Structural Biology* **2005,** *15* (6), 637-645; (c) Vocadlo, D. J., Davies, G. J., *Current Opinion in Chemical Biology* **2008,** *12* (5), 539-555.

77. Gerber-Lemaire, S., Juillerat-Jeanneret, L., *Mini-Reviews in Medicinal Chemistry* **2006,** *6*, 1043-1052.

78. (a) Bernacki, R. J., Niedbala, M. J., Korytnyk, W., *Cancer metastasis reviews* **1985,** *4* (1), 81-101; (b) Herscovics, A., *Biochimica et Biophysica Acta (BBA) - General Subjects* **1999,** *1473* (1), 96-107.

79. (a) Rye, C. S., Withers, S. G., *Current Opinion in Chemical Biology* **2000,** *4* (5), 573-580; (b) Vasella, A., Davies, G. J., Böhm, M., *Current Opinion in Chemical Biology* **2002,** *6* (5), 619-629.

80. Gloster, T. M., Davies, G., J., *Organic & Biomolecular Chemistry* **2010,** *8* (2), 305-320.

81. Pauling, L., *Chem. Eng. News* **1946,** *24*, 1375–1377.

82. Inouye, S., Tsuroka, T., Nida, T., *J. Antibiot.* **1966,** *19*, 288–292.

83. Yagi, M., Kouno, T., Aoyagi, Y., Murai, H., *Nippon Nogei Kagaku Kaishi* **1976,** *50*, 571–572.

84. Katsilambros, N., Philippides, P., Toskas, T., Protopapas, J., Frangaki, D., Marangos, M., Siskoudis, P., Anastasopoulou, K., Xefteri, H., Hillebrand, I., *Arzneimittelforschung* **1986,** *36*, 1136–1138.

85. Platt, F., M., Neises, G., R., Dwek, R., A., Butters, T., D., *J. Biol. Chem.* **1994,** *269*, 8362–8365.

86. Birault, V., Solari, R., Hanrahan, J., Thomas, D. Y. , *Curr. Opin. Chem. Biol.* **2013,** *17*, 353–360.

87. Butters, T., D., *Curr. Opin. Chem. Biol.* **2007,** *11*, 412-418.

88. Kolter, T., Sandhoff, K. , *Biochim. Biophys. Acta* **2006,** *1758*, 2057-2079.

89. Wraith, J. E., *J. Inherit. Metab. Dis.* **2006,** *29*, 442-447.

90. Butters, T. D., Dwek, R. A., Platt, F. M. , *Chem. Rev.* **2000,** *100*, 4683-4696.

91. Lubamba, B., Dhooghe, B., Noel, S., Leal, T. , *Clin. Biochem.* **2012,** *45*, 1132-1144.

92. Becq, F., Mall, M. A., Sheppard, D. N. , Conese, M., Zegarra-Moran, O., *J. Cystic Fibrosis* **2011,** *10*, S129–S145.

93. (a) Asano, N., Ikeda, K., Yasuda, K., Kizu, H., Kameda, Y., Kato, A., Okamato, T., Ishii, S., Compain, P., Martin, O. R., Fan, J.-Q., *Glycoconj J* **1999,** *16* (4-5), 2-175; (b) Oulaıdi, F., Front-Deschamps, S., Gallienne, E., Lesellier, E., Ikeda, K., Asano, N., Compain, P., Martin, O., R., *ChemMedChem* **2011,** *6*, 353-361; (c) Compain, P., Martin, O., R., Boucheron, C., Godin, G., Yu, L., Ikeda, K., Asano, N., *ChemBioChem* **2006,** *7*, 1356-1359; (d) Compain, P., *Synlett.* **2014,** *25*, 1215-1240; (e) Schönemann, W., Gallienne, E., Compain, P., Ikeda, K., Asano, N., Martin, O., N., *Bioorg. Med.*

Chem. **2010,** *18*, 2645-2650; (f) Yu., L., Ikeda, K., Kato, A., Adachi, I., Godin, G., Compain, P., Martin, O., Asano, N., *Bioorg. Med. Chem.* **2006,** *14*, 7736-7744.

94. Decroocq, C., Joosten, A., Sergent, R., Mena Barragán, T., Ortiz Mellet, C., Compain, P. , *ChemBioChem* **2013,** *14*, 2038–2049.

95. Compain, P., Bodlenner, A., *ChemBioChem* **2014,** *15* (9), 1239-1251.

96. Kiessling, L., L., Gestwicki, J., E., Strong, L., E., *Angewandte Chemie International Edition* **2006,** *45* (15), 2348-2368.

97. Compain, P., Decroocq, C., Iehl, J., Holler, M., Hazelard, D., Mena Barragán, T., Ortiz Mellet, C., Nierengarten, J., *Angewandte Chemie International Edition* **2010,** *49* (33), 5753-5756.

98. (a) Decroocq, C., Rodriguez-Lucena, D.Russo, V., Mena Barragan, T., Ortiz Mellet, C., Compain, P., *Chem. Eur. J.* **2011,** *17* (49), 13825-31; (b) Joosten, A., Schneider, J., P. Lepage, M., L., Tarnus, C., Bodlenner, A., Compain, P., *European Journal of Organic Chemistry* **2014,** *2014* (9), 1866-1872.

99. Brissonet, Y., Ortiz Mellet, C., Morandat, S., Garcia-Moreno, M. I., Deniaud, D., Matthews, S. E., Vidal, S., Sestak, S., El Kirat, K., Gouin, S. G. , *J. Am. Chem. Soc* **2013,** *135*, 18427–18435.

100. (a) Singhamahapatra, A., Sahoo, L., Loganathan, D., *J. Org. Chem.* **2013,** *78*, 10329 − 10336; (b) Fürniss, D., Mack, T., Hahn, F., Vollrath, S. B. L., Koroniak, K., Schepers, U., Bräse, S., *Beilstein Journal of Organic Chemistry* **2013,** *9*, 56-63; (c) Khan, S. N., Kim, A., Grubbs, R.H., Kwon, Y., *Organic Letters* **2012,** *14* (12), 2952-2955; (d) Ahn, M., Murugan, R. N., Nan, Y. H., Cheong, C., Sohn, H., Kim, E., Hwang, E., Ryu, E. K., Kang, S. W., Shin, S. Y., Bang, J. K., *Bioorganic & Medicinal Chemistry Letters* **2011,** *21* (20), 6148-6153; (e) Norgren, A. S., Budke, C., Majer, Z., Heggemann, C., Koop, T., Sewald, N., *Synthesis* **2009,** *3* (488–494); (f) Seo, J., Michaelian, N., Owens, S. C., Dashner, S. T., Wong, A. J., Barron, A. E., Carrasco, M. R., *Org. Lett.* **2009,** *11* (22), 5210-5213; (g) Burger, K., Boettcher, C., Radics, G., Hennig, L., *Tetrahedron Letters* **2001,** *42*, 3061–3063; (h) Marcaurelle, A. L., Bertozzi, R. C. , *Chem. Eur. J.* **1999,** *5* (5), 1384-1390; (i) Dechantsrciter, M. A., Burkhart, F., Kessler, H., *Tetrahedron Letters* **1998,** *39*, 253-254 ; (j) Kim, J. M., Roy, R., *Tetrahedron Letters* **1997** *38* (20), 3487-3490; (k) Kim, J. M., Roy, R.,, *Carbohydrate Research* **1997,** *298*, 173-179.

101. (a) Caumes, C., Gillon, E., Legeret, B., Taillefumier, C., Imberty, A., Faure, S., *Chemical Communications* **2015,** *51* (61), 12301-12304; (b) Cecioni, S., Faure, S., Darbost, U., Bonnamour, I., Parrot-Lopez, H., Roy, O., Taillefumier, C., Wimmerov, M., Praly, J., Imberty, A., Vidal, S., *Chem. Eur. J.* **2011,** *17*, 2146 – 2159; (c) Comegna, D., De Riccardis, F., *Org. Lett.* **2009,** *11* (17), 3898-3901.

102. (a) Himo, F., Lovell, T., Hilgraf, R., Rostovtsev, V. V., Noodleman, L., Sharpless, K. B., Fokin, V. V., *J. Am. Chem. Soc.* **2005,** *127*, 210-216; (b) Appukkuttan, P., Dehaen, W., Fokin, V. V., Van der Eycken, E., *Organic letters* **2004,** *6* (23), 4223-5.

103. Holub, J. M., Jang, H., Kirshenbaum, K., *Org Biomol Chem* **2006,** *4* (8), 1497-502.

104. (a) Wu, C. W., Sanborn, T. J., Zuckermann, R. N., Barron, A. E., *J. Am. Chem. Soc.* **2001,** *123*, 2958 - 2963; (b) Kirshenbaum, K. B., A. E.; Armand, P.; Goldsmith, R.; Bradley, E.; Cohen, F. E.; Dill, K. A.; Zuckermann, R. N. , *Proc. Natl. Acad. Sci., U.S.A.* **1998,** *95*, 4303 - 4308; (c) Murphy, J. E. U., T.; Hamer, J. D.; Cohen, F. E.; Dwarki, V.; Zuckermann, R. N. , *Proc. Natl. Acad. Sci. U.S.A.* **1998,** *95*, 1517 - 1522.

105. Malesevic, M., Strijowski, U., Bachle, D., Sewald, N. , *J. Biotechnol.* **2004,** *112*, 73-77.

106. Joosten, A., Decroocq, C., de Sousa, J., Schneider, J., Etamé, E., Bodlenner, A., Butters, T. D., Compain, P., *ChemBioChem* **2014,** *15*, 309–319.

107. Lepage, M. L., Meli, A., Bodlenner, A., Tarnus, C., De Riccardis, F., Izzo, I., Compain, P., *Beilstein journal of organic chemistry* **2014,** *10*, 1406-1412.

108. Culf, A. S., Ouellette, R. J. , *Molecules* **2010,** *15*, 5282-5335.

109. Sui, Q., Borchardt, D., Rabenstein, D. L., *J. Am. Chem. Soc.* **2007,** *129*, 12042-12048.

110. Armand, P., Kirshenbaum, K., Goldsmith, R. A., Farr-Jones, S., Barron, A. E., Truong, K. T. V., Dill, K. A., Mierke, D. F., Cohen, F. E., Zuckermann, R. N., Bradley, E. K., *Proceedings of the National Academy of Sciences* **1998,** *95* (8), 4309-4314.

111. Vollrath, S. B. L., Chunhua, H., Bräse, S., Kirshenbaum, K., *ChemComm* **2013,** *49*, 2317-2319.

112. (a) Desiraju, G. R., *Crystal Engineering: The Design of Organic Solids*. Elsevier: Amsterdam, **1989**; (b) Desiraju, G. R., *Chem. Commun.* **1997**, 1475–1482; (c) Nangia, A., Desiraju, G. R., In *Design of Organic Solids*, Weber, E., Ed. Springer-Verlag: Berlin, **1998**; pp 57-95.

113. Hirshfeld, L., F. , *Theor. Chim. Acta* **1977,** *44* (2), 129-138

114. (a) McKinnon, J., J. Spackman, M. A., Mitchell, A., S., *Acta Cryst.* **2004,** *B60*, 627-668; (b) Spackman, M., Jayatilaka, D., *CrystEngComm.* **2009,** *11*, 19-32; (c) Spackman, M. A., *Phys.Scr.* **2013,** *87* (4); (d) Spackman., M. A., McKinnon, J. J. , *Cryst.Eng.Comm* **2002,** *4* (66), 378-392.

115. Wolff, S. K., Grimwood, D. J., McKinnon, J. J., Turner, M. J., Jayatilaka, D., Spackman, M. A., University of Western Australia, **2012**.

116. Desiraju, G. R., *Journal of the American Chemical Society* **2013,** *135* (27), 9952-9967.

117. Ricciardulli, A. G., Autoassemblaggio di ciclopeptoidi allo stato solido. *Tesi di laurea magistrale* **Anno accademico 2013-2014**.

118. Gallo, G., Verso il controllo dell'assemblaggio allo stato solido di ciclopeptoidi. *Tesi di laurea triennale* **Anno Accademico 2013-2014**.

APPENDIX

Continuous Flow Chemistry. Application of Diazomethane for Synthesis in Drug Discovery.

The following work has been performed at the Global Discovery Chemistry laboratories of NIBR (Novartis Institutes for Biomedical Research) in Basel (Switzerland) and it is protected by the industrial secret. For that reason, I am going to explain the methodology studied during my research stay and I am using generic molecular structures to elucidate its application.

A.1 INTRODUCTION

Synthetic chemistry achieved a central role in all areas of Science, driven by remarkable improvements in the development of new reactions, reagents and catalysts as well as ever more powerful analytical tools.[1]

Despite the sheer complexity of methods to address the challenge of chemical transformations, most equipment to usually run reactions consists in standardized glassware such as round-bottomed flasks or reaction vessels.[2] Indeed, batch reactors offer several advantages for synthesis in chemistry laboratories; they are easy to handle and allow a practical follow-up of the reaction proceeding in them.[1b] Hence, there is no point in simply replacing such versatile batch mode, unless a clear benefit can been obtained.[3]

New chemical processing techniques are required when a high level of control over a certain reaction is needed.

In this context, microreactors and continuous flow technologies are emerging in the portfolio of the synthetic chemist's devices.

Continuously flowing microreactors, featured by small dimensions of the order of less than 1000 μm, offer a high surface-to-volume ratio that allows for rapid and homogeneous mixing.[4] Such efficient mixing provides an homogeneous mass transport in the reactor and guarantees an optimal thermal management, which is necessary either to avoid runaway reactions, that could lead to explosion, either to gain kinetic and thermodynamic control when two different pathways are possible.[5] Hence, reactions can be carried out quickly with increases in both yields and selectivity and added efficiency and safety.

Furthermore, the small volumes of reactive material used by microreactors at any one time, enable to run reactions with highly toxic or explosive intermediates.[6] Such hazardous reagents would also be less problematic since they are flowing in a contained environment, so avoiding any direct contact with the worker.

Another benefit of continuous flow synthesis is that such processes are suitable for automation, since solutions of starting materials and reagents are fed by pumps and their flow rate are controlled by a computer.[1b] Consequently, once the reaction conditions are optimized, these can be easily transferred from laboratory reactors to production scales.[7] Overall higher safety standards and a fast, reliable and directly scalable chemical process are so achieved, making continuous flow reactors a new and powerful tool for laboratory synthesis and for production in chemical and pharmaceutical industries.

A.1.1 Diazomethane As A Powerful Toll In Organic Synthesis

One of the most interesting and versatile reagents in synthetic chemistry is diazomethane, as it can perform a plethora of reactions under mild conditions (**Scheme A.1**).[9]

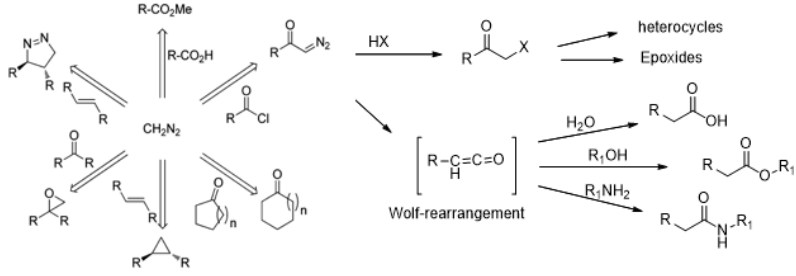

Scheme A. 1. Synthetic applications of diazomethane.

However, its hazardous properties such as explosiveness, toxicity, and carcinogenicity are well-known, and make its use in laboratory or pilot-plant scale quite problematic.[10] In the laboratory, special techniques and safety precautions are needed, such as dedicated glassware carefully fire-polished or explosion protection. For industrial-scale production of diazomethane, the equipment necessary for its safe handling is elaborate and expensive. Furthermore, diazomethane not only has to be prepared, conveniently generated through the reaction of a suitable precursor with bases, but also separated and purified for the subsequent reaction, and routine separation processes like distillation are not certainly appropriate for a toxic gas.

The use of continuous flow microreactors offers a solution to these safety issues, providing a total reaction system in which the toxic and explosive reagent is first self-generated and then separated within, to be reacted for the formation of the desired product. Being

always contained in-line, diazomethane is so readily accessible for both laboratory and industrial applications.

A.2 AIM OF THE WORK

A.2.1. Introduction

Herein, we describe a convenient procedure for the preparation on lab-scale of a vast platform of organic compounds using diazomethane by means of a reliable and robust flow-chemistry system (**Figure A.1**). They will serve as model examples to elucidate the several advantages of the method and to explore the selectivity of diazomethane in terms of chemoselectivity and regioselectivity.

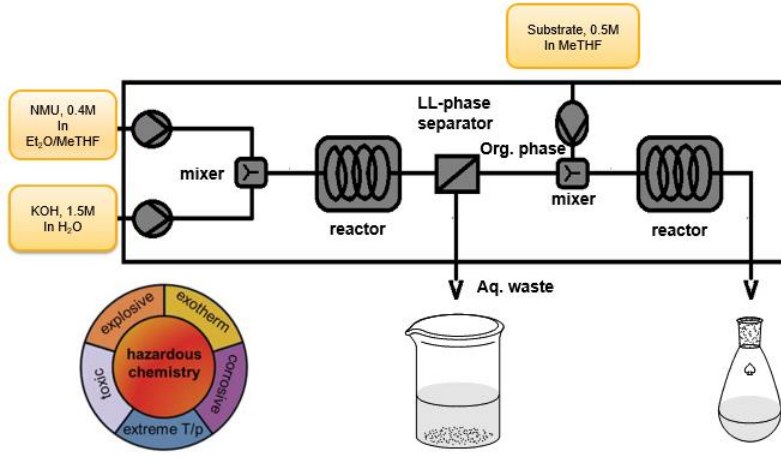

Figure A. 1. Diazomethane-flow generator.

A.2.2 Results and Discussion

In-flow generation of diazomethane has been applied for the methylation of carboxylic acids into methyl esters and for the cyclopropanation of double bonds.

Continuous flow esterification is a very elegant process, where diazomethane is generated and reacted *in-situ* with carboxylic acids to give clean, quantitative and instantaneous reactions.[9a]

For the continuous flow process we developed, two connected reactors were used. In the first one, diazomethane was produced from a feed containing *N*-methyl-*N*-nitroso urea (NMU) 0.45 M in 2-MeTHF/Et_2O 1:1 and a second feed of potassium hydroxide (1.5 equiv relative to NMU) 1.5 M in water. The two streams were pumped with flow rates of 4.31 ml min^{-1} and 1.94 ml min^{-1} respectively, mixed, and reacted in a PFA (Perfluoroalcoxy alkane) coiled tube reactor of 5 mL (0.8 min residence time) cooled at 10°C. Diazomethane was formed and pumped from the outlet of the first reactor, where a back pressure regulator (BPR, 8.0 bar) was attached to ensure a stable flow rate, to a phase separator equipped with a semipermeable, microporous and hydrophobic membrane. The diazomethane in the organic solvent crossed the membrane, whereas the aqueous phase was retained and discarded into an acetic acid quench solution to decompose any unconsumed diazomethane. After the separation of the organic solution, this was mixed in a standard T-mixer with a third stream containing the carboxylic acid dissolved in 2-MeTHF (0.5 M), at a flow rate ranging from 2.33 ml min^{-1} to 1.55 ml min^{-1} depending on the substrate. The combined streams then entered the second reactor, which consisted of a 5 mL PFA coil at room temperature, and the product mixture from the outer tube was collected in a flask into a quenching solution of acetic acid and analyzed by LC-MS. Applying the parameters stated above, the residence time for the methylation process was set from ≈ 0.8 min to ≈1.1 min depending on the case.

To check the efficiency of diazomethane formation and its separation by the membrane under these general reaction

conditions, a set of preliminary experiments was carried out converting the *m*-nitrobenzoic acid to the corresponding ester, which is known to take place quantitatively and instantaneously. This enabled us not only to evaluate the setting of the parameters, but also the concentration of the outcoming diazomethane, which was estimated ≈ 0.3 M. With these features in mind, we optimized the reaction stoichiometry in flow and on small scale for all the substrates studied in this work.

In the preliminary screenings performed on small scale, the number of equivalents of diazomethane relative to the starting material was varied from time to time, ranging from 1.0 to 2.0 equivalents. Transferring such conditions on large scale, it was possible to get full conversion of the carboxylic acids into esters.

Scheme A.2 shows the general reaction scheme for the conversion of a carboxylic acid into the corresponding methyl ester.

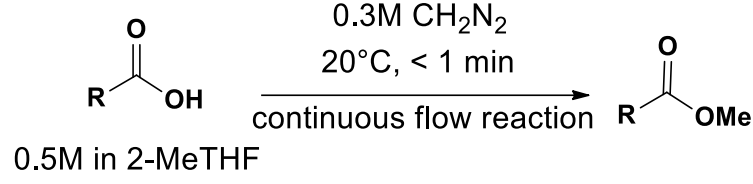

Scheme A. 2. In-flow methylation of carboxylic acids.

The major advantage of such process is the formation of up to 10 grams of the desired product within 30 minutes, and no work-up is subsequently needed in most of the cases. Otherwise, the extraction procedure is enough to isolate the desired products. Esters were obtained in quantitative yields, with rates of 138 mg min^{-1} up to 400 mg min^{-1}, highlighting the terrific and impressive efficiency of such process.

It is noteworthy that carboxylic acid substrates containing functional groups sensitive to diazomethane, such as primary

amines, primary alcohols or double bonds, yielded methyl esters via a chemoselective reaction. Such control was achieved by adjusting the number of equivalents of diazomethane with respect to the starting material and the reaction time.

For example, when the system examined bore a carboxylic acid together with a primary alcohol (**A.1**, **Scheme A.3**), using DAM in ≈ 1.0 equivalent led to the complete conversion to the ester **A.2** within 1 minute. The dimethylated compound **A.3** was obtained in the presence of an excess DAM. Ranging from 3.0 to 10 equivalents of diazomethane and monitoring the progress of the reaction over the time, the conversion to **A.3** showed to have a comparable rate within the first hour, reaching the 30%. After this point, the reaction slowed down, until it stopped in 4 hours with a conversion of 55%. This result shows that a large excess of diazomethane is not beneficial for the reaction, since it decomposes over the time anyhow.

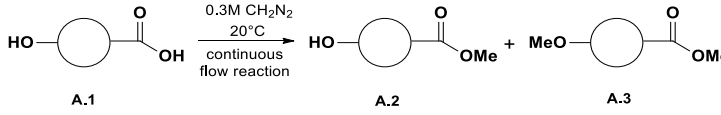

Scheme A. 3. Chemoselective methylation with diazomethane.

However, when we tested substrates with more acidic alcoholic functions, we recovered 6% of the demethylated product even under a treatment with 1.0 equivalent of diazomethane within 1-minute reaction time.

This outcome is perfectly consistent with the proposed mechanism of methylation with diazomethane (**Scheme A.2**), which implies a correlation between the acidity of the reacting species and the rate of alkylation.[11] Indeed it was suggested that the diazomethane is first protonated to give the methyldiazonium ion which then reacts with the nucleophile to give the methylation product.

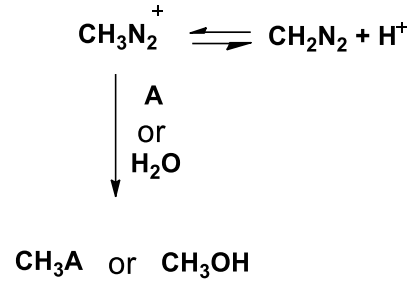

Scheme A.2. Mechanism of diazomethane alkylation

When applied to our system, the hydroxyl group protonates CH_2N_2 to $CH_3N_2^+$, which then reacts with the alkoxyde to give the ether. This explains why if the substrate is not acidic enough, the protonation of diazomethane is reversible and, after a while, it reaches the equilibrium with the starting material. Furthermore, in case the nucleophile attack is not fast, the methyldiazonium ion would react more rapidly with the traces of water that are eventually in the reaction medium, leading to the formation of methanol and the consumption of diazomethane.

To further investigate the selectivity in the methylation reactions with diazomethane, we studied more complex substrates, which allowed also for the exploration of the regiochemistry.

We considered carboxylic acids bearing two alcoholic functions with different reactivity and a disubstituted alkene (**Scheme A.4**). To focus on the methylation of the hydroxyl functions, we performed first the esterification of the carboxylic acid that, under a treatment with 1.0 equivalent of diazomethane within 1-minute reaction time, yielded exclusively **A.5**.

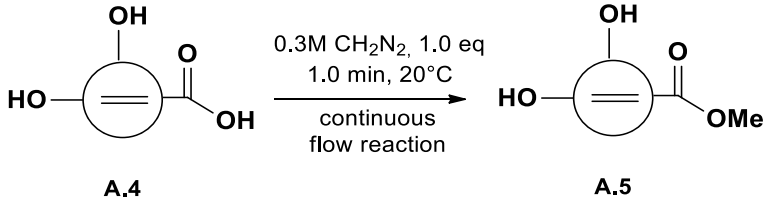

A.4 A.5

Scheme A. 4. Chemoselective methylation with diazomethane.

A.5 was treated with 2.0, 5.0, 10, 15 and 20 equivalents of DAM for 30 minutes (**Scheme A.5**). Within 10 equivalents, the more reactive hydroxyl function was converted into the corresponding methyl ether **A.6** in 60%. We also recovered 24% of the dimethylated compound **A.7** and 16% of unreacted ester **A.5**. Increasing the amount of diazomethane to 15 and 20 equivalents led to the progressive increase of side reactions and decreased the methylation of the –OH groups. Possible [3+2] cycloaddition could occur under such conditions, as demonstrated by a LC-MS peak whose mass matched the one of compound **A.8.**

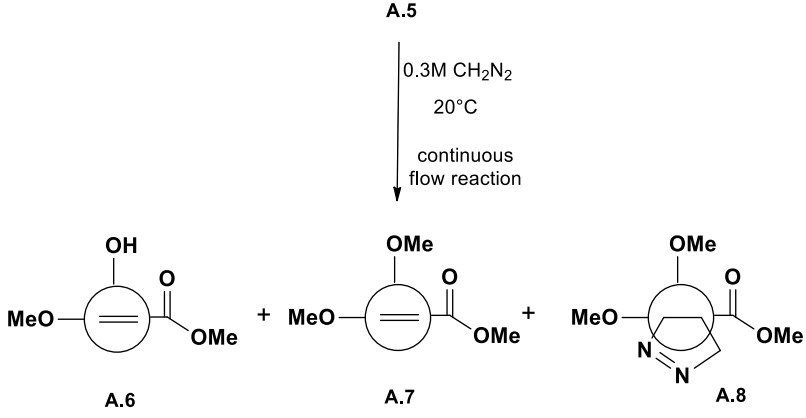

A.6 A.7 A.8

Scheme A. 5. Chemo- and regioselectivity studies for methylation with DAM.

The outcome of such studies points out that a certain reaction control is possible playing around with the equivalents of

diazomethane and the reaction time, so that a high chemoselectivity towards the carboxylic acids, and a discrete regioselectivity between the hydroxyl groups were observed.

To expand the portfolio of selective methylation by diazomethane, we took into account the catalytic cyclopropanation.

The cyclopropanation of double bonds is one of the most widely used reactions in organic synthesis, that subtly alter the structure of a given scaffold achieving higher rigidity and peculiar electronic properties through the incorporation of the cyclopropane ring.[15] Such modification could affect its biological activities and for this reason cyclopropanation represents a key-step in drug discovery.

Herein, the reaction of diazomethane with olefinic substrates assisted by transition metal complexes has been studied for the cyclopropanation of double bonds.

Rhodium (II) and palladium (II) complexes have been tested as catalysts since they have emerged as the most usual and efficient agents for the reliable methylation of olefins by diazomethane.[12]

Diazomethane was always generated by a continuous flow process and subsequently used in the catalytic in-batch transformations. The development of such user-friendly reaction protocol allowed us to study a plethora of substrates with different electronical and structural features, ranging from α,β-unsaturated carbonyl compounds to endo- and exocyclic double bonds.

α,β-unsaturated carbonyl compounds are electron-deficient activated alkenes that readily undergo cyclopropanation especially when palladium(II) salts are the catalysts of choice.[13]

A.9 (**Scheme A.6**) was the starting point of our study, considering different reaction conditions in order to get the highest conversion to the cyclopropane derivative **A.10.**

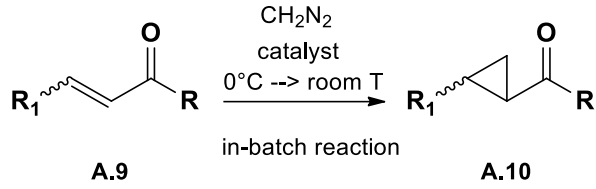

A.9 A.10

Scheme A. 6. Catalytic cyclopropanation of double bond with DAM.

Palladium (II) acetate, bis(benzonitrile) palladium(II) chloride, bis(triphenylphosphine) palladium(II) chloride and rhodium(II) acetate dimer were tested as catalysts. The only metal which formed cyclopropane in significant conversion was palladium. Furthermore, in a control experiment it was demonstrated that diazomethane alone gave no reaction over a several hour period at 0°C, showing that a catalyst is needed for the reaction to proceed.

Addition of 1-2 equivalents of diazomethane to a chilled (0°C) solution of the olefin and 1-2 mol% $Pd(OAc)_2$ led to modest conversions, as monitored by LC-MS. In each case, the reaction stopped within 1 hour.

Keeping the amount of diazomethane constant to 4 equivalents and varying the catalyst loading from 0.5 to 1.5 mol% gave an increased conversion, that however dropped down again when $Pd(OAc)_2$ was used in 2 mol% and 4 mol%. Consequently, we envisioned that, depending on the relative amount of catalyst and diazomethane, the former might give unreactive adducts with CH_2N_2 or otherwise become deactivated after a certain time. Indeed, in the course of these studies, we have noticed the reduction of palladium (II) acetate to palladium (0) with the precipitation of palladium-black in the reaction mixture. This species exits the catalytic cycle and so it is no longer catalytically active. Hence, the right balance between the catalyst loading and the amount of diazomethane has to be

chosen, in order to avoid the deactivation of $Pd(OAc)_2$ in the very first stages of the reaction.

To broaden our knowledge regarding the selectivity of diazomethane, we reconsidered the compound **A.5** previously obtained, but this time we focused on the difference between the O- and the C-methylation (**Scheme A.7**).

Keeping the catalyst-loading constant at 2 mol%, the amount of diazomethane ranged from 2.0 to 6.0 equivalents. LC-MS analysis showed 30% of starting material left when the reaction was performed with 2.0 equivalents, while full conversion was gained with 4.0 and 6.0 equivalents. However, the highest excess of diazomethane also led to the side products of dimethylation and trimethylation (14% and 13% respectively).

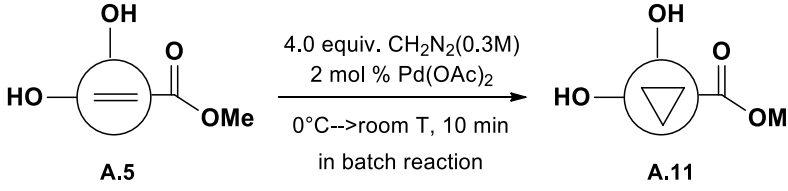

Scheme A. 7. Chemoselective cyclopropanation with DAM.

We therefore performed the scale-up as indicated in the **Scheme A.7**, recovering 79% conversion of the starting material into the cyclopropane ring but no undesired side products.

This example shows that the rate of cyclopropanation is faster than the O-methylation, enabling a chemoselective reaction, which involves exclusively the double bond even in presence of an excess of diazomethane.

It is reported that the success of palladium catalyzed cyclopropanation reactions is strongly dependent on features of the employed alkene.[14] Electronic and steric effects influence the

outcome of the reaction so much that excellent to extremely disappointing results can be obtained. Electron poor alkenes display good reactivity while electron rich alkenes usually give only low conversion. Terminal and strained alkenes are also good substrates, while the reactivity systematically drops with an increase of its substitution degree. For example, endo- double bonds like in cycloalkenes do not react with the system diazomethane/palladium (II) acetate, unless they are extremely strained like norbonene derivatives.[14, 15]

We investigated the response of **A.12** (**Scheme A.8**) to the cyclopropanation treatment.

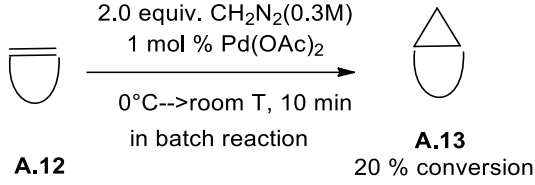

Scheme A. 8. Cyclopropanation of endocyclic double bond.

Attempts to carry out the reaction were almost unsuccessful, giving just a partial conversion to the cyclopropane derivative. Roughly 20% conversion was always recovered after the treatments with 2, 4 and 6 equivalents of diazomethane either with 1 mol% and 2 mol% of palladium (II) acetate at 0°C for 5 minutes. Applying a huge excess of diazomethane and a higher catalyst loading (3-5 mol%) also led to the same result. **A.12** proved to have the same reactivity even under tris(dibenzylideneacetone) dipalladium(0) catalysis.

The results collected so far show that such substrate stops reacting after a while, reaching a maximum conversion, no matter the reaction conditions.

With this clue in mind, we thought that reiterated treatments with diazomethane and fresh catalyst might have been useful to push **A.12** to full conversion.

Hence, six portions of diazomethane (2 equivalents each) were added in series to a cooled solution (0°C) of the olefin and 1mol % of palladium (II) acetate. Each time the former catalyst was filtered and the fresh one was added. The mixture was allowed to stir for 10 minutes and assayed by LC-MS, and then the next 2 equivalents of diazomethane were added, until no more starting material was detected. The reaction mixture was finally filtrated over celite, concentrated and silica gel chromatography was performed to give **A.13**.

We managed to completely convert **A.12** into the corresponding cyclopropane derivative, even if quite strong reaction conditions are needed.

Non functionalized terminal alkene also undergo cyclopropanation with high yield. Consequently, carbene transfer to alkenyl substituted cycloalkenes occurs highly regioselective.

According to this, we were able to selectively insert the cyclopropyl moiety into the terminal alkene of **A.14** in the presence of an endocyclic double bond (**Scheme A.9**).

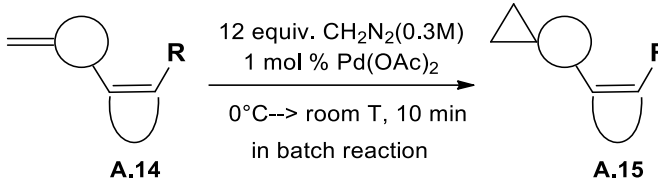

Scheme A. 9. Regioselective cyclopropanation of double bond.

A.14 underwent cyclopropanation with diazomethane and $Pd(OAc)_2$ without further purifications. From the initial screening it was clear that harsh reaction conditions were needed, requiring a

huge excess of diazomethane. Indeed, with 8 equivalents and $Pd(OAc)_2$ 2 mol% the conversion observed was 26%, while performing reiterated treatments with 4 equivalents and $Pd(OAc)_2$ 1 mol% the conversion after the third addition was still 44%. Hence, 12 equivalents of diazomethane were added to an ice-bath cooled solution of **A.14** 0.5M in 2-MeTHF and $Pd(OAc)_2$ 1 mol%, resulting in the complete conversion of the starting material into **A.15**.

It is well known that diazomethane can act as a 1,3-dipole taking an important role in the vast area of [3+2]-cycloaddition chemistry. Depending on the substitution pattern of the alkene, some of these cycloadducts are stable enough to be isolated. Others can instead rearrange or eliminate nitrogen to form cyclopropane.

Methylation of **A.14** in the absence of catalyst with 5.0 equivalents of diazomethane led to the respective **A.16** in essentially quantitative conversion (Scheme **A.10**).

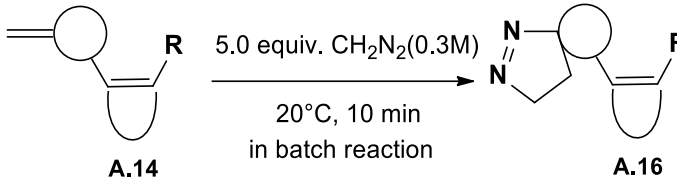

Scheme A. 10. Regioselective [3+2] cycloaddition with diazomethane.

Again, the reaction resulted completely regioselective. Furthermore, also the cycloaddition of the 1,3-dipoled occurred in a regioselective fashion into the exo-double bond.

A.3 CONCLUSION

We have studied the chemistry of diazomethane, a powerful C1 building block in the vast scenario of organic synthesis.

The in-flow technology, applied on lab-scale for its safe generation and handling, enabled us to explore the reactivity of

diazomethane towards carboxylic acids, hydroxyl groups and double bonds.

We remarked several advantages related to its use, giving clean and fast reactions and increasing the productivity defined as the amount of compound synthesized in a certain reference time.

Furthermore, we considered chemoselectivity and regioselectivity of the methylation reactions with diazomethane. The more acid is the functional group, the faster the methylation, while Pd (II) catalyzed cyclopropanation occurs preferentially on terminal and electron poor alkenes. Thus, diazomethane reactions display good to high chemoselectivity and regioselectivity, which can also be controlled by tuning the equivalents of reagents and the reaction time.

A.4 BIBLIOGRAPHY

1. (a) Kündig, Science, **2006**, 314, 430; (b) Yoshida, J.-i., Takahashi, Y., Nagaki, A., Chem. Commun., **2013**, 49, 9896-9904.

2. Wegner, J., Ceylan, S., Kirschning, A., Chem. Commun., **2011**, 47, 4583-4592

3. Ley, S., V., Baxendale, I., R., Proc. of the Beilstien Symposium on Systems Chemistry, Bozen, Italy ISBN 978-8325-2188-2, **2009**, 65-85

4. Wiles, C.; Watts, P.; Eur. J. Org. Chem., **2008**, 1655-1671

5. Mason, B. P., Price, K.. E., Steinbacher, J. L., Bogdan, A. R., McQuade, D. T., Chem. Rev., **2007**, 107, 2300-2318

6. O'Brien, M.; Baxendale, I., R.; Ley, S., V.; Org. Lett., **2010**, 12, 1596-1598

7. Baxendale, I., R., Brocken, L., Mallia, C., J., Green Process Synth, **2013**, 2, 211-230

9. (a) Mastronardi, F., Gutmann, B., Kappe, O., C., Org. Lett, **2013**, 15, 21, 5590-5593; (b) Struempel, M., Ondruschka, B., Daute, R., stark, A., Green Chem., **2008**, 10, 41-43

10. (a) Maurya, R., A., Park, C., P., Lee, J., H., Kim, D.-P., Angew. Chem. Int. Ed., **2011**, 50, 5952-5955; (b) Rossi, E., Woehl, P., Maggini, M., Org. Process Res. Dev., **2012**, 16, 1146-1149

11. (a) Kreevoy, M., M.; Thomas, S. J.; J. Org. Chem. **1977**, 42, 3979-3981; (b) Lei, Y., X.; Rappoport, Z.; J. Org. Chem. **2002**, 67, 6971-6978

12. (a) Daquini, C.; Rescifina, A.; Spatafora, C.; Tringali, C.; Eur.J.Org.Chem, **2009**, 6289-6300; (b) Tymtsunik, A., V.; Bilenko, V., A.; Ivon, Y., M.; Grygorenko, O., O.; Komarov, I.; Tetrahedron Letters, **2012**, 53, 3847-3849

13. Reiser, O., **2002**, Cyclopropanation and Other Reactions of Palladium-Carbene (and Carbyne) Complexes, in Handbook of

Organopalladium Chemistry for Organic Synthesis (ed E.-i. Negishi), John Wiley & Sons, Inc., New York, USA

14. Denmark, S., E.; Stavenger, R., A.; Faucher, A-M.; Edwards, J., P.; J. Org. Chem, **1997**, 62, 3375-3389

15. Kottwitz, J. ; Vorbrüggen, H.; Synthesis, **1975**; 10, 636-637

ACKNOWLEDGMENTS

Scrivere la mia tesi di dottorato è stato un vero piacere. Parlare di Chimica in queste pagine mi ha fatto sentire non solo una piccola scienziata, ma anche un po' scrittrice, con il compito di catturare il lettore e trascinarlo nell'affascinante microcosmo peptoidico. Tuttavia, è con ancor più grande gioia che scrivo questa pagina, in cui voglio ringraziare tutte le persone che ho incrociato durante il mio percorso, quelle che mi hanno inspirato e coloro che sono sempre stati al mio fianco.

Mamma, Papà e Lisa, voi siete la mia stella polare, e anche se le Scienze mi porteranno lontana da voi, sappiate che il mio cuore batterà sempre a casa, lì dove siete voi. Lisa, grazie per i consigli grafici e la copertina. Sei la mia designer preferita!

Irene e Francesco, qui non vi ringrazio come tutor, ma come amici e mentori. Avere il vostro supporto, la vostra spinta, i vostri incoraggiamenti, è stato fondamentale. Siete stati di esempio, ispirazione e modello per me, ed oggi gioiamo insieme di questo risultato. Consiglia, grazie per avermi introdotto nel magico mondo dei cristalli. Il tuo entusiasmo è stato il seme di una bellissima e ricca esperienza. Rosaria, mia collega fidata, amica sincera e compagna di lab, sei una persona speciale e ti ringrazio per essermi stata sempre vicino, condividendo le gioie e i dolori, le risate e le lacrime che solo il lab conosce. Gerardo, con te ho iniziato questo percorso ben dieci anni fa, ma da allora niente è cambiato! Grazie di cuore. Stefano, le nostre prese in giro hanno reso tutto più divertente. Grazie. Carmen, grazie per i consigli di scienza e di vita, e per la tua simpatia, compagnia e disponibilità. Gruppo pranzo-Proci o Porci?!- unico ed insostituibile! Grazie per le numerose pause pranzo e feste pranzo passate insieme. È bello ingrassare insieme!

Thanks to all the people I met during my time abroad.

Dott. Luigi La Vecchia and Dott. Hansjoerg Lehmann, thanks for hosting me in your labs. It was a pleasure working with you and learning from you. Dott. Luca Arista, grazie per le lunghissime chiacchierate, i caffè e i numerosissimi consigli. Mi hai fatto crescere tanto! Maria Teresa, grazie per essere stata sempre al mio fianco durante il mio periodo basilese, tra uno svizzerismo e un altro. Sono stata fortunata ad incontrarti! Himanshu, thanks for being such a good friend during my time in Southafrica. I will never forget it! Vincent, thanks for the introduction to crystallography and south African lifestyle. Mathieu, it was a pleasure to work by your side in the sweet world of sugar chemistry. Thanks for what you taught me. Gracias a el Prof. Fernando Albericio y a su “IRB crew”, que me enseñaron la quìmica de los peptidos, cuando aùn estaba en mi master. Esto fuè el principio, pues muchas gracias! Y allì yo encontrè tambien los amigos que nunca voy a olvidar: Silvia Cavalli, Silvia Vilpry y Giulio. Vilpri, aùn tenemos pendientes unos viajes!!!!

I might consider you as one of the amazing people I met abroad, so I will thank you here. Then you turned to be my special person, and I am so grateful for that. Thanks for being such a great player in our team, MM!

Infine, non smetterò mai di ringraziare i miei nonni, che mi hanno reso la persona che oggi raggiunge questo traguardo. Tu, nonna, mi hai insegnato a leggere e a scrivere, che altro aggiungere? E tu, nonno, non hai mai smesso di credere in me, e hai sempre celebrato ogni mio passo in avanti verso questa meta. Siete stati semplicemente meravigliosi.

Grazie di cuore a tutti. Questo giorno è la nostra vittoria!